2023-07

Pressure Response During Gas Diffusion in Tight Porous Media

Zhu, Guanying

UNIVERSITY OF CALGARY

Pressure Response During Gas Diffusion in Tight Porous Media

by

Guanying Zhu

A THESIS
SUBMITTED TO THE FACULTY OF GRADUATE STUDIES
IN PARTIAL FULFILMENT OF THE REQUIREMENTS FOR THE
DEGREE OF MASTER OF SCIENCE

GRADUATE PROGRAM IN CHEMICAL ENGINEERING

CALGARY, ALBERTA

JULY, 2023

Abstract

In this thesis, the pressure change during countercurrent diffusion in the cyclic gas injection process was investigated. It briefly introduces the situation of climate change and the importance for considering Carbon Capture Utilization and Storage (CCUS) in the application of Enhance Gas Recovery. A real core and two compartments were used to represent the relationship in the system of fractures, porous media, and the gas reservoir. Three kinds of experiments, including single gas flooding in the core system, coupled gases diffusion without core in the system, and the most important one, coupled gases diffusion in different cores were carried out. The experimental system consists of two compartments and one core holder with the core samples in the middle. The initial conditions at the two sides of the core were set as an isobaric, both at around 40 psi (gauge pressure) to eliminate the convection effect and observing the pressure change caused by diffusion solely. Nitrogen, carbon dioxide and methane were used in different combinations to see the binary behavior in Scioto Sandstone and Torrey Sandstone. The general pressure trend for single gas flow in the cores is always decreasing at the very beginning and reaches a plateau due to the unsteady flow in the system. The binary gas behavior in no-core countercurrent diffusion is dominated by the heavier component. The binary gas behavior in the two sandstones is controlled by molecular weight at the beginning stage, but later it combines surface diffusion and sorption, rendering a more complex general behavior. The pore size also plays an important role if the pore diameter is comparable with the mean free path of the gas molecules. The response curve changes by varying the pore diameter and the critical surface area.

Key Words: Countercurrent Diffusion, Surface Diffusion, Sorption, Cyclic Gas Injection

Acknowledgments

As I near the end of my academic journey at the University of Calgary, I want to take a moment to express my deepest gratitude for the opportunities and experiences that have shaped my time here. It has been an incredible journey, and I couldn't have done it without the support and guidance of so many incredible individuals. First and foremost, I would like to express my sincere appreciation to my supervisor Dr. Apostolos Kantzas for his unwavering support, encouragement, and patience throughout my thesis project. Your guidance and mentorship have been invaluable, and I am truly grateful for everything you have done to help me succeed. During my graduate studies, I gained a lot of help from Dr. Kantzas. He ignited the spark of my interest in the exploration in porous media phenomena and the shale gas. I want to thank Dr. Kantzas very much. He is always willing to help and provide critical information and suggestions for research activities. He is more than a supervisor but much like a father. And, I want to thank the help of the FUR group, and PERM. Inc for providing equipment and materials for doing the experiments. During the experiment, the FUR research group members helped me a lot. They include but are not limited to Sajjad Esmaeili, Sepideh Maaref, Saeid Khasi and so on. They helped me construct the equipment and fix problems during the experiments. Without their help, I could not successfully reach my target smoothly. Furthermore, I would like to thank the faculty and staff of the University of Calgary for providing me with a world-class education and fostering an environment of academic excellence. I am grateful for the many opportunities I have had to engage with and learn from so many brilliant scholars, and for the resources and facilities that have enabled me to pursue my research interests. Other than this, my parents offered me unconditional support during my graduate study. Even though we have separated for more than 3 years due to COVID, I still miss them every day, and I can feel different aspects of their love. Thanks to everyone I met in these three years. That would become the best memory in my life.

No matter where I am, in China or the west, I will keep all the memory in mind. It's not only my journey, but your journey.

The Master of Science degree is not only an academic qualification, and not a terminal point of academic life, but also an attitude towards academic life. Humans always want to find the laws of nature. During this exploration, we may fail (for the most part), and we may be under stress. As long as we are still alive, we cannot stop our footsteps on the journey to the truth. Sometimes it is called science. I like a Sci-Fi work by a Chinese author very much – The Three Body Problem, by Liu Cixin. He described a very interesting situation for the science we humans have now: If there is a higher level of civilization in the universe, much cleverer and more advanced than humans, what humans are to them is just like what a turkey is to human. We thought we know the mechanism of physics and the truth from God, just like, the turkeys are fed every day at 12 o'clock, and the "turkey scientist" find a law in their world: The food will automatically come every day at 12. But the next day, food doesn't come, and they all die. Because that day is Thanksgiving Day. We are little bugs or worms in the eyes of advanced civilization, easy to eliminate. But acridids do not vanish from the world, maybe even no less than humans appear in this world, even though humans don't like them. The bugs have their own world, and science. We can see those acridids are still flying in the world. What I did in the master's does not even touch the boundary of human science. We are trapped by the unknown. As long as we have the courage to explore, we will defeat the scare of the unknown. What I learned from this period is not only the way to explore, but also the mindset of how to explore. I am not afraid of continuing to go forward.

Table of Contents

LIST OF TABLES

LIST OF FIGURES AND ILLUSTRATIONS

LIST OF SYMBOLS

Symbol	Meaning
A	Cross-section area
$a_t{}'$	Darcy flow term
B_g	Gas volume coefficient
b	Slippage factor
b'	Non-Darcy flow term
c	Density of binary mixture
c_g	Gas compressibility factor
C	Concentration
d	Gas molecular diameter/average diameter/characteristic length/pore diameter
D	Core diameter
D'	Additional skin factor
D_a	Bimolecular diffusion coefficient
D_{AB}	Diffusion coefficient of clear fluids
D_{AB}^*	Effective diffusion coefficient
D_d	Molecular diffusion coefficient
D_k/D_{ik}	Knudsen diffusion coefficient
D_s	Surface diffusion coefficient
D_T	Configurational diffusion coefficient
D_Z	Molecular bulk diffusion coefficient
D_0	Diffusion coefficient of infinite dilution solution
E_T/E_S	Diffusion activation energy
J	Molar mass flux
k	Boltzmann Constant
K	Permeability
K_g	Gas tested permeability
K_L	Intrinsic permeability (liquid test)
K_n	Knudsen number
K_∞	Intrinsic permeability/fluid permeability
l	Length of the core
L	Length in axial direction
m	Gas mass
M_i/M/M_g	Molecular weight
n	Molecular density

N_A	Avogadro's Constant
N_i	Components' molar diffusion flux densities
p	Absolute gas pressure
P	pressure
P_{atm}	Atmosphere pressure
$\overline{P}$	Average pressure
P_e	Peclet number
P_a	Outlet pressure
P_{ave}	Average Pore Pressure
P_i	Inlet pressure
P_{RT}	Real-time pressure
P_{SC}	Pressure at standard condition
P_{total}	Total pressure
Q	Flow rate
Q_{atm}	Bulk flow rate at atmosphere pressure
Q_{SC}	Volumetric velocity
q_{sc}	Production rate of gas well at ground pressure
r	Radial distance
r_K	Radius of particle/component
R	Ideal gas constant
r_p/r	Pore radius
S	Skin factor
S_a	General skin factor
S_g	Saturation of gas
t	time
T	temperature
T_{SC}	Temperature at standard condition
u	Velocity field
u_x, u_y, u_z	Velocity in x, y, z direction
v	Average solution velocity
V	Gas Seepage velocity
V'	Gas Volume
x	Distance at x direction
X_A	Mole fraction of component A
Z	Compressibility factor
Z_{SC}	Compressibility at standard condition
∇	Nabla operator

τ	tortuosity
α	Longitudinal dispersity
β	First velocity coefficient
λ	Mean free path
η	Pressure transmitting coefficient
ϕ	porosity
μ	viscosity
μ_i	Viscosity at initial reservoir pressure
μ_α	Phase viscosity
φ_{AB}	Lennard-Jones potential
σ_{AB}	Collision diameter
ϵ_{AB}	Maximum energy of attraction between two molecules
$\Omega_{D\ AB}$	Collision integral for diffusion
ρ	Gas density
ψ	Pseudo pressure
ψ_e	Pseudo pressure at reservoir edge
ψ_i	Pseudo pressure at initial condition
ψ_{wf}	Pseudo pressure at well bottom

1. Introduction

1.1 Background Overview

The demand for energy across the world is still increasing since the end of World War II last century and will continue for even decades. The world-famous energy companies, such as Exxon Mobil (Exxon Mobil Energy Outlook, 2022[1]) and BP (BP Energy Outlook, 2023[2]) had made their latest forecasts on the energy consumption and production in different regions and the whole world. We can acknowledge from their data that the general trend of energy consumption keeps going up. The developed world, such as Europe Union and North America will decrease the demand for energy (all potential users, absolute usage) after achieving carbon peak in recent ten years, whereas the energy demand in developing countries like India, China, Southeast Asia, and Africa would keep increasing for a long time. In the traditional fossil fuel energy, the time when reaching the carbon peak coincides with the maximum consumption point of oil, which means the demand for oil will decrease after a smooth increase until the peak. Natural gas, as the cleanest petroleum format in the industry, will soar with the energy transition action taken by different countries, which is good news for the developing world. On the other hand, some renewable energy technologies applied in recent years, such as geothermal energy, hydrogen energy, wind energy and solar energy, will stimulate their consumption after lowering the cost of the infrastructure. This is to say, before the 2050s, humans and industry still cannot get rid of fossil fuels completely. Therefore, the "Net Zero" concept has been proposed by some countries and is recognized by IPCC (Intergovernmental Panel on Climate Change, 2019[3]). The realization of carbon neutral is by using carbon capture and carbon storage to compensate the emission of carbon in the atmosphere created by the burning or petrochemical process of fossil fuels. The estimation from BP is more optimistic. They thought the energy market will be shared by fossil fuels and renewable energy by almost the same percentage. The most optimistic reckoning of the market shows the traditional energy would be overwhelmed

by renewable energy. Meanwhile, the energy outlooks from both BP and Exxon Mobil admit the same viewpoint: as the industrialization of the developing countries continues, the energy consumption of these new emerged economy bodies would continuously increase, will reach their peak at different times, but mostly will achieve it in the middle of 21 century. At the same time, those developing countries have realized the importance of lowering carbon emissions in their industrialization process. Therefore, BP thought those countries would lower their emission amount and the consumption of fossil fuels after reaching the carbon peak, and then achieve net zero by their own carbon-lowering programs. The trend of the whole world of carbon emissions is decreasing. Therefore, in the current situation, using natural gas is a very competitive choice when substituting more pollutive coal and oil. The requirement for the natural gas would grow fast, especially for large economy bodies with great populations such as China and India. The increasing demand for energy and the pressure of environmental protection provide natural gas with a unique competitive role in the energy market. Notice, the Net Zero concept applied here is not a thermodynamics concept, but a "What if" situation, which states that the efforts we need to apply by reducing 95% of carbon emission compared to the level of 2019. However, the conventional natural gas reservoirs are depleted and are much harder to find. A new onshore conventional natural gas reservoir in geology is an almost impossible thing. At the early 21st century, North America was the first to focus on unconventional natural gas exploitation (Stevens, 2012[5]; Gong, 2020[6]; O'Sullivan and Paltsev, 2012[7]). Non-traditional natural gas reservoirs represented by shale gas, coalbed gas and tight sandstone gas have entered people's view and raised their interest. Those reservoirs originally thought to be lacking exploration value and were often ignored are now becoming the new direction for development and exploration (Wang, 2018[8]; Kinnaman, 2011[9]). As engineers and geologists get more information and deeply understand the behaviors of unconventional reservoirs, the chance of making use of them is booming. Many companies in the United States have achieved their goal in such reservoirs (Wang and Li, 2017[10]; Melikoglu, 2014[11]). In this case, shale gas can be a potential substitute for oil and coal before renewable energy is fully popularized (Burnham et al., 2011[12]).

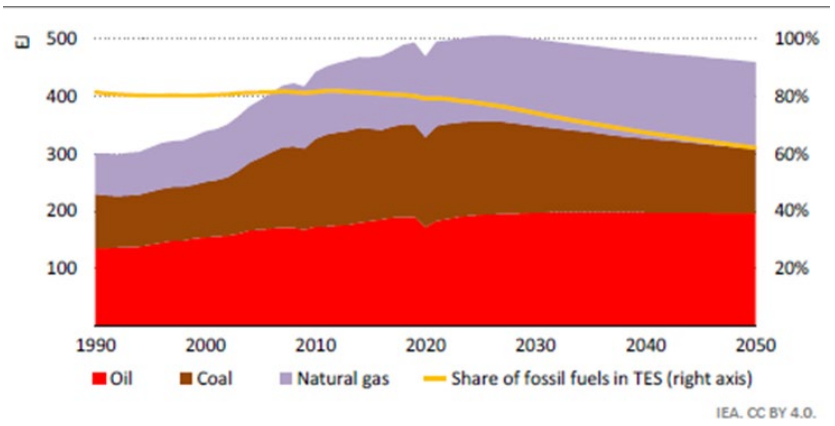

Figure 1 Fossil Fuel Demand in the Stated Policies Scenario, 1990-2050 (IEA World Energy Outlook[4])

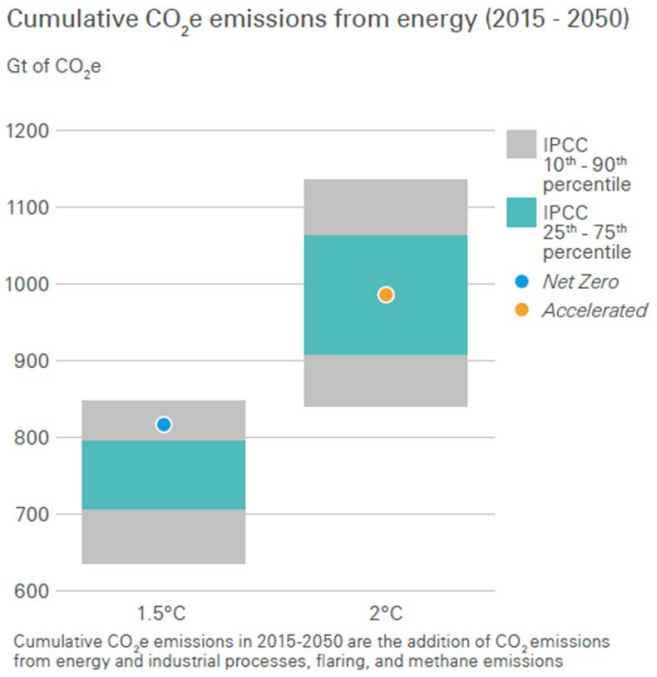

Figure 2 Cumulative CO_2 Emissions from Energy (BP Energy Outlook, 2023[2])

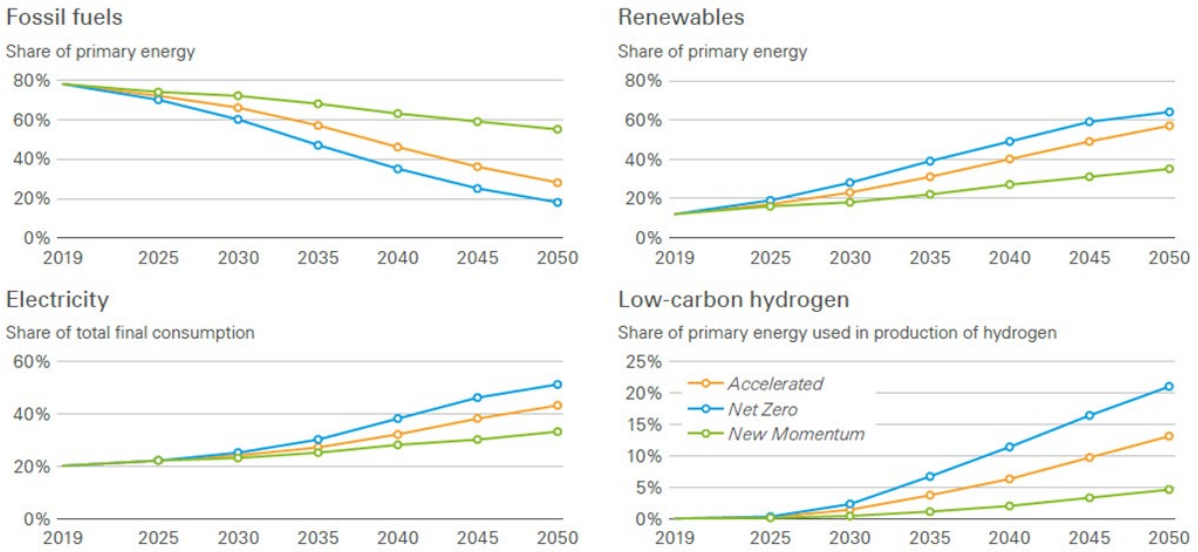

Figure 3 The future of global energy is dominated by four trends: declining role for hydrocarbons, rapid expansion in renewables, increasing electrification, and growing use of low-carbon hydrogen (BP Energy Outlook, 2023[2])

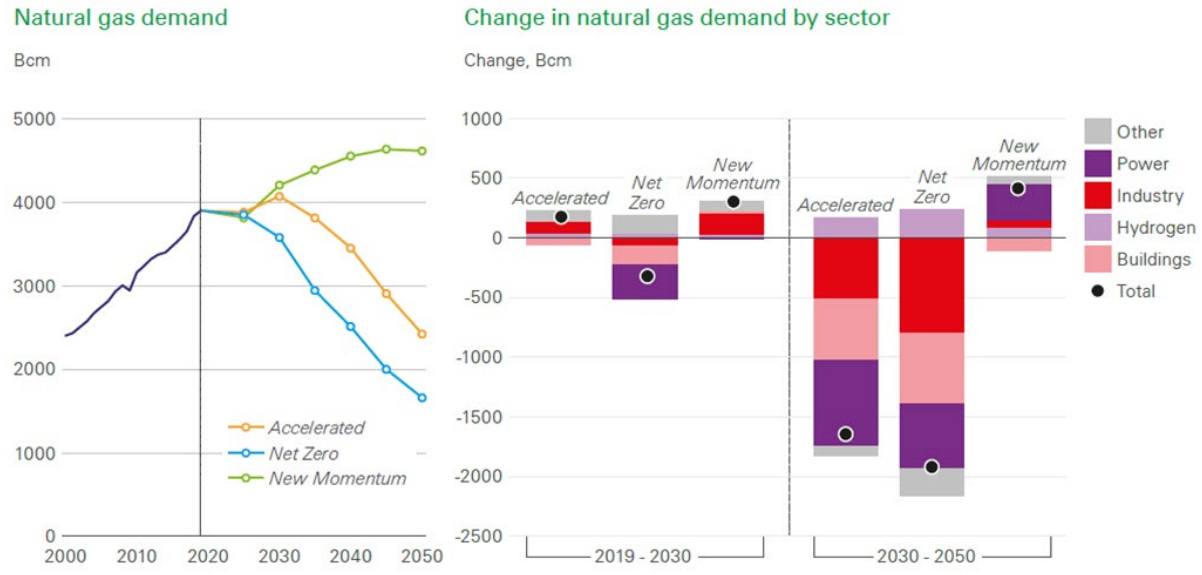

Figure 4 Prospects for natural gas depend on the speed of the energy transition (BP Energy Outlook, 2023[2])

ExxonMobil *Outlook for Energy*

Last update: 10 January 2023

Energy demand (quadrillion BTUs, unless otherwise noted)									Average annual change 2021 2050	% change 2021 2050	Share of total	
Energy by Regions	**2000**	**2010**	**2020**	**2021**	**2025**	**2030**	**2040**	**2050**			**2021**	**2050**
World	404	511	548	572	592	616	639	658	0.5%	15%	100%	100%
OECD	220	224	205	213	212	210	201	193	-0.3%	-9%	37%	29%
Non OECD	184	286	344	360	380	406	439	465	0.9%	29%	63%	71%
Africa	22	29	34	35	38	43	51	58	1.8%	67%	6%	9%
Asia Pacific	121	198	243	253	268	285	302	315	0.8%	25%	44%	48%
China	45	100	132	138	146	153	152	154	0.4%	12%	24%	23%
India	17	26	36	38	41	48	58	66	1.9%	73%	7%	10%
Europe	77	80	70	72	72	70	65	64	-0.4%	-12%	13%	10%
European Union	61	64	54	56	55	52	48	47	-0.6%	-17%	10%	7%
Latin America	19	25	25	26	27	29	33	35	1.0%	33%	5%	5%
Middle East	17	28	33	35	38	41	45	48	1.1%	39%	6%	7%
North America	111	109	103	109	109	110	106	101	-0.2%	-7%	19%	15%
United States	94	91	85	89	90	90	85	80	-0.4%	-11%	16%	12%
Russia/Caspian	37	42	41	43	40	39	38	36	-0.6%	-15%	7%	6%
Energy by type - World												
Primary	404	511	548	572	592	616	639	658	0.5%	15%	100%	100%
Liquids	147	166	165	175	185	191	199	200	0.5%	**15%**	**31%**	**30%**
Oil	147	164	161	171	180	185	187	183	0.2%	7%	30%	28%
Gas	89	116	137	143	149	158	169	178	0.8%	25%	25%	27%
Coal	91	140	141	144	139	134	110	88	-1.7%	-39%	25%	13%
Nuclear	27	29	27	29	31	35	40	44	1.4%	49%	5%	7%
Biomass/Waste	39	44	50	51	51	53	54	54	0.2%	5%	9%	8%
Hydro	9	12	14	14	15	16	18	19	1.0%	35%	3%	3%
Geothermal	2	2	4	4	5	5	6	7	1.9%	71%	1%	1%
Biofuels	0	2	4	4	5	6	12	17	5.1%	320%	1%	3%
Wind	0	1	6	7	9	14	24	36	6.0%	446%	1%	6%
Solar	0	1	4	5	7	11	20	32	6.6%	538%	1%	5%
End-use sectors - World												
Residential and commercial												
Total	94	107	116	119	123	128	134	138	0.5%	16%	100%	100%
Oil	13	11	11	11	11	10	9	9	-0.8%	-20%	9%	6%
Gas	21	24	27	28	29	29	28	26	-0.3%	-8%	24%	19%
Biomass/Waste	28	28	28	28	27	27	26	24	-0.5%	-12%	23%	18%
Electricity	23	32	39	41	45	50	60	68	1.8%	67%	34%	49%
Other	10	11	11	12	12	11	11	11	-0.3%	-9%	10%	8%
Transportation												
Total	77	95	99	108	119	128	136	144	1.0%	33%	100%	100%
Oil	76	91	91	100	110	114	110	102	0.1%	2%	92%	71%
Biofuels	0	2	4	4	5	6	12	17	5.1%	320%	4%	12%
Gas	0	1	2	2	3	3	5	7	3.6%	182%	2%	5%
Other	1	1	2	2	2	4	10	18	8.5%	959%	2%	12%
Industrial												
Total	144	195	215	221	225	234	249	259	0.5%	17%	100%	100%
Oil	45	51	52	53	54	57	65	70	1.0%	33%	24%	27%
Gas	37	44	54	56	59	62	67	70	0.8%	25%	25%	27%
Coal	26	51	48	47	44	42	38	32	-1.4%	-33%	21%	12%
Electricity	22	31	40	43	46	51	58	67	1.6%	58%	19%	26%
Other	14	18	21	22	22	22	21	19	-0.5%	-13%	10%	7%
Power generation - World												
Primary	145	189	212	223	232	246	259	280	0.8%	26%	100%	100%
Oil	14	10	7	7	5	4	3	2	-3.7%	-66%	3%	1%
Gas	31	46	53	56	59	63	69	75	1.0%	34%	25%	27%
Coal	61	84	89	94	93	90	70	55	-1.8%	-41%	42%	20%
Nuclear	27	29	27	29	31	35	40	44	1.4%	49%	13%	16%
Hydro	9	12	14	14	15	16	18	19	1.0%	35%	7%	7%
Wind	0	1	6	7	9	14	24	36	6.0%	446%	3%	13%
Solar	0	0	3	3	5	9	17	28	7.6%	735%	2%	10%
Other Renewables	4	7	12	12	13	15	17	20	1.6%	59%	6%	7%
Electricity demand												
World	13223	18594	23551	24856	27324	30859	36836	43900	2.0%	77%	100%	100%

Figure 5 Exxon Mobil Energy Outlook for Energy Demand (Exxon Mobile Energy Outlook, 2022[1])

Shale gas was stored inside the shale rocks. Shale is composed of very fine particles, whose diameter is usually less than 4 micrometers (John, 2002[13]). Generally, we can sort the unconventional reservoirs into three parts: coalbed, shales and tight sandstone. It may contain mud and organic matter inside the granular space. There are nanoscale pores in the organic matter in shales (A.Sakhaee-Pour and Bryant, 2014[15]). In this case, the sandstone is made of granular material having diameter between 62.5 to 2000 micrometers (the composition can change in different sediments). Just like sandstones can have different compositions, such as quartz, feldspar, rock fragments, clay, etc., shale stone (better to be called mudstone) can have various components in the reservoir, such as clay, quartz, feldspar, or even heavy minerals. Tight sandstones mainly refer to those that have permeability less than 0.1 Millidarcy. The formation of tight sandstone underwent sedimentation, diagenesis, and tectonism in later times. The main and dominant procedures are the first two. The sedimentary rocks have all gone through a diagenesis process. Some sedimentary rocks have become denser, and some have become looser. In the process of reservoir densification, sedimentation, diagenesis and even tectonism play an important role in reservoir densification and reservoir improvement (Naik, 2012). Under the same conditions of sedimentary facies or sedimentation, compaction, cementation (Spencer, 1985[16]), dissolution and metasomatism play a controlling role in the porosity and permeability of the reservoir. A tight sandstone reservoir is characterized by tight lithology, low porosity and permeability, and high irreducible water saturation. Compared with the pore types of conventional sandstone reservoirs, the residual intergranular primary pores of tight sandstone are less retained, but the secondary pores account for a higher percentage of the total pores (Clarkson et al., 2012[17]). The secondary pores are formed during the dissolution of unstable minerals. In tight sandstone reservoirs, the reservoir space is mainly composed of intergranular pores, dissolution pores and microfractures. The pore throat structure characteristics of sandstones with different permeability levels are significantly different (Aguilera, 2010[18]). For tight sandstones, nano pore throats and capillary pore throats are the main channels of fluid seepage, and their pore throat structure characteristics determine that the resistance of natural gas or gas-water flowing in such rocks is much higher than

that in conventional or medium-high permeability sandstones. Some scholars suggest that all reservoirs with different pressure, depth, and temperature can be defined as tight gas reservoirs (Curtis, 2002[13]), no need to have a specific definition. Holditch (Holditch, 2006[14]) gave a new definition for tight reservoirs: reservoirs that cannot be produced at economic flow rates nor recover economic volumes of natural gas unless the wells are stimulated by a large hydraulic fracture treatment or produced by use of a horizontal wellbore or multilateral wellbores. In this article, we do not separate the definition of shale gas or tight gas. For convenience, when we are talking about the name of shale (gas) and tight sandstone (gas), we will give them a unified name "tight (gas)" in this thesis. We give a resource triangle below to show how their considerable reserves compare with conventional gas reservoirs, which holds great potential for exploration.

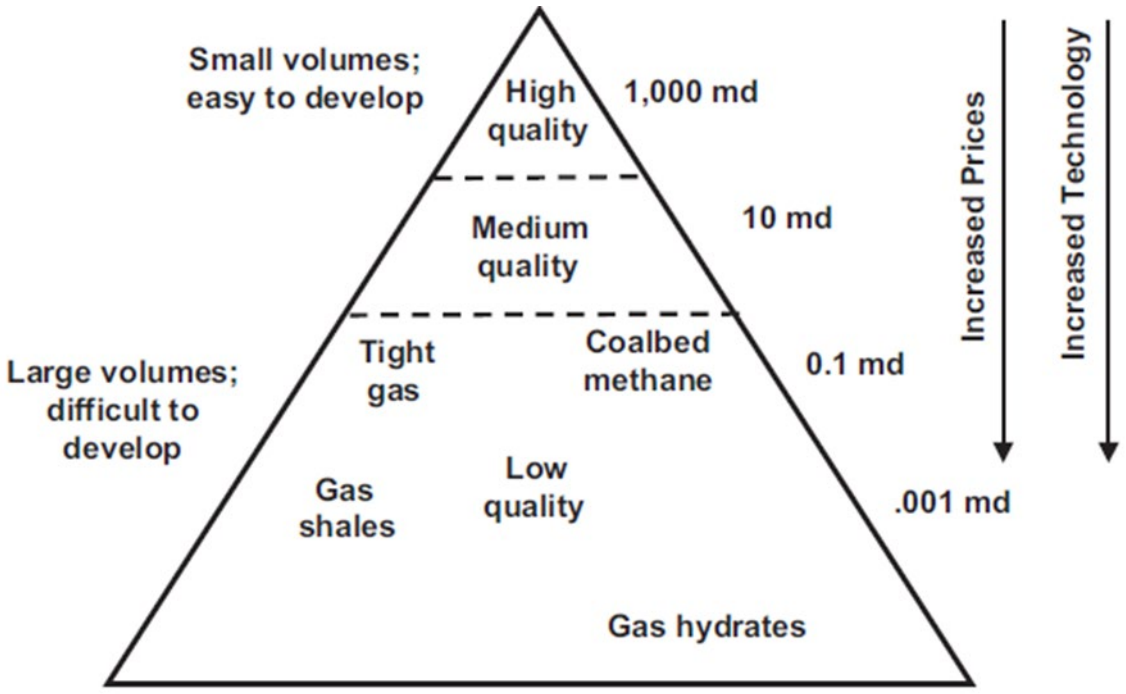

Figure 6 The resource tringle shows the potential of the reserve for unconventional resources are more than conventional one (Holditch, 2006[14])

Shale gas is biogenic or thermogenic natural gas that accumulates in organic-rich shale or

mudstone in adsorbed and free state, and also includes natural gas in thin interbeds such as sandstone and siltstone in shale formation. The main component of shale gas is methane and has little carbon dioxide and nitrogen in it since the generation of the gas was in a hypoxic environment and had no contact with the air. The storage space of shale gas mainly includes matrix, pores and natural fractures. Shale gas is mainly stored in dark shale or high carbon shale. The amount of adsorbed gas, which contributes 20%-85% gas storage in total reservation, is closely related to the concentration of organic matter. The variation of adsorbed gas content is mainly affected by rock composition, organic matter content, reservoir pressure, fracture development, etc. The biggest difference between conventional gas reservoirs and shale gas reservoirs is that shale gas reservoirs are characterized by low porosity, low permeability (in nano Darcy scale) and rich in nano pores. The micro-nano scale pores are the fundamental storage space for shale gas. The generation and migration of hydrocarbons in shale can be explained by traditional petroleum migration theory. Organic matter is deposited in the source rock and converted into oil and gas in geological period. Then hydrocarbon migration occurs until there is stratigraphic structure to trap it and prevent its further movement. The rock that eventually stores hydrocarbons is called reservoir rock. The caprock of the reservoir is usually shale, with extremely low permeability, which does not allow further migration of oil and gas. In shale gas reservoirs, shale gas is formed from source rock (i.e., shale), but it does not migrate due to the extremely low permeability of the source rock. It is a typical self-generating and self-storing gas bearing system with source-reservoir integration. This explains why there are organic matters in shale gas reservoirs. In some shales rich in organic matter, organic matter or kerogen can account for up to 40% of the reservoir volume. During exploitation process, the gas adsorbed on the pore wall gradually desorbed into free gas and is stored in the matrix pores. The free gas in the matrix pores and the adsorbed gas after desorption will flow to the low-pressure zone or diffuse to the low concentration zone. Finally, gas will flow through hydraulic fractures and gets produced by the wells. The gas migration mechanism in shale matrix is more complex than that in conventional reservoirs, covering different transport mechanisms such as viscous flow, Darcy flow, sorption, slippage flow and diffusion. In the storage mode of

shale gas, it is similar to traditional reservoirs in that it also has free gas in the middle part of pores and sorption gas in organic matter and pore wall. The storage form of shale gas will affect the migration mechanism of gas in the matrix, and the heterogeneity of shale matrix makes gas storage and transportation more complex. In this case, it is hard to forecast the production rate of shale gas reservoir. Methane can be stored in a free state in intercrystallite pores and natural fractures, adsorbed on the surface of organic matter and clay particles, or dissolved in kerogen and asphalt. After hydraulic fracturing, the gas production rate increases significantly in the short term by increasing large scale fracture across the reservoir and thus increase the permeability but decreases rapidly in the later period. This is because the gas in shale gas reservoirs mainly exists in micro-scale or nano-scale pores. Therefore, the desorption of shale gas and its flow in micro-nanopore determine the production cycle of shale gas in nanopores, the traditional Darcy's law is no longer applicable, and the classical seepage theory needs to be further extended and rewritten. Darcy's law is suitable for those laminar flow or low velocity flow. The gas transport behavior and the calculation of permeability should include both bulk transport and gas adsorption and desorption (Zhang et al., 2018[20]; Wu et al., 2014[21]; Shabro et al., 2011[22]; Hu et al., 2013[23]; Yang and Fu., 2012[24]; Fu et al., 2012[25]; Yang, 2018[26]).

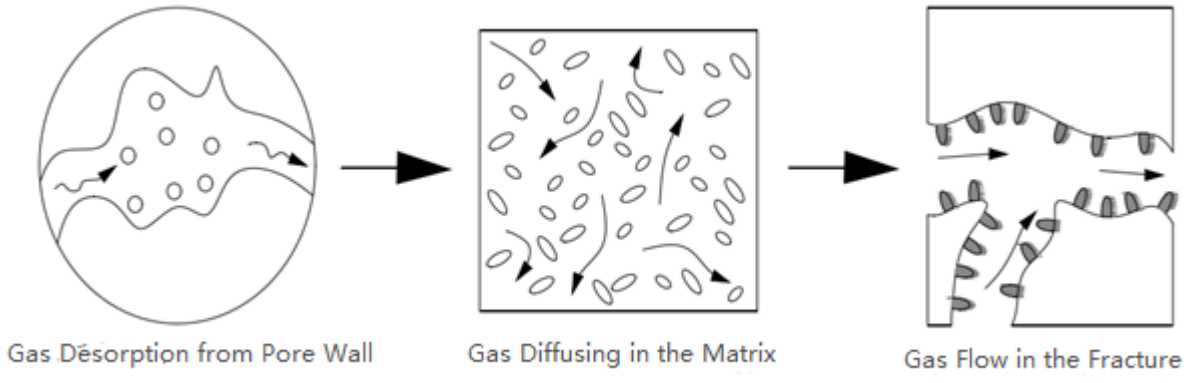

Figure 7 Gas Transport Mechanism in Reservoir During Exploration (Moridis et al., 2010[27])

Shale reservoirs and ultra-tight sandstone reservoirs have much lower porosity and permeability, which is totally different from conventional ones. The micro-structure could affect the adsorption, desorption, diffusion and even flow regimes inside the pores. Originally, the shale layers were often seen as the cover layer of the reservoir. This impermeable feature provides outstanding protection and preservation for the gas and oil in the pores. Shale can be seen as a cover layer and restoration layer at the same time. After the fracturing methods were improved, the potential value of the shale and tight sandstone is under reassessment. There are three kinds of status of shale gas existing in the reservoir: Free gas, adsorbed gas and dissolved gas. The first two contribute the most percentage of the gas. The dissolved gas mainly exists in the liquid hydrocarbons, asphaltenes, kerogen or residual water. For the adsorption process, the gas would get into the pores in the matrix by diffusion and/or convection, and then attached to the pore walls by Van der Waals force. Desorption is an opposite process. Micropores are the storage and adsorption place for gases. The mesopores provide both tunnels and adsorption and diffusion control for the gases (Dong, 2019[28]; Bing, 2018[29]; Law et al., 1986[30]).

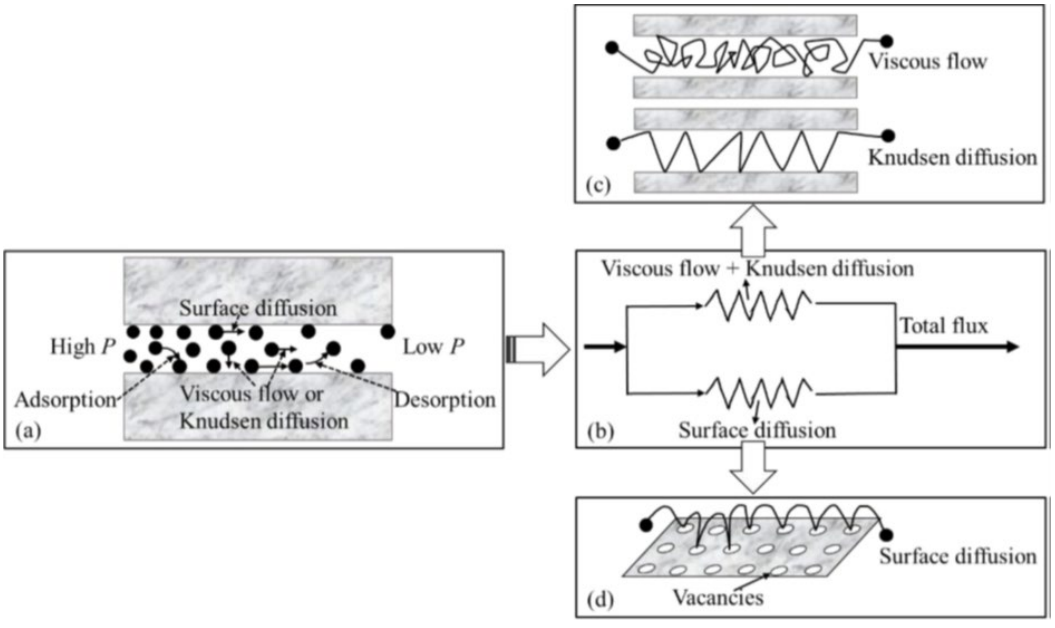

Figure 8 Gas Transport Mechanism in Nanopores (Wu et al., 2016[31])

Table 1 Pore Size Classification Criteria[28]

Pore Scale	Size
Micropores	Less than 2 nm
Mesopores	2 to 50 nm
Macropores	Larger than 50 nm

There are two things to be clear here: The first one is, the terminology of "sorption". Sorption can be seen as the gas molecules are attached to the pore walls. It has two forms: adsorption and absorption. Adsorption is a physical (or we can call it physical adsorption) process where the gas molecules are attached to the pore walls with Van der Waals forces in a low stability mode. It can create a single layer or multi-layer of adsorbed gas on the pore wall. The physical adsorption is usually non-selective, which means any gas can adsorbed on the porous media and it can happen at low pressure and low temperature condition. Whereas absorption is much like a chemical reaction due to the share, exchange, or movement of electrons between gas and solid molecules. The interaction of absorption is higher than that of adsorption, which needs more energy to form chemical bond to be adsorbed at the special point (Li et al., 2014[32]; Zhou, 2021[33]). The second one is, the use of "diffusion of shale gas". This phrase is not accurate in chemical engineering. Diffusion is a concept based on concentration and chemical potential. For a mixture, there is no concentration for mixture itself, just like air. The concentration concept is only for the component

in the mixture. To be accurate, we need to figure out the specific gas type we want to explore and talk about the diffusion of certain gas (Li and Zhu, 2015[34]).

Now let us put the focus on the environment. At present, the gases that can produce greenhouse effect in the atmosphere include carbon dioxide, methane, hydrofluorocarbons, perfluorocarbons and sulfur hexafluoride, etc. Among them, carbon dioxide contributes the most to the global warming effect. According to statistics data, the global temperature has increased by about 1 ℃ in the past 100 years, and the temperature will continue to rise. This 1 ℃ seems harmless in mathematical meaning, but it presented the average global temperature has been elevated. This means we will get higher temperatures in both summer and winter and across the globe. The greenhouse effect will lead to a series of hazards such as glacier melting, sea level rising, frequent occurrence of extreme climate, land drought and desertification, and accelerated extinction of biological species. Carbon capture and storage (CCS), or Carbon capture, utilization, and storage (CCUS, IEA[35]), is a technology to collect the carbon dioxide emitted by human beings and store it in various ways to avoid its emission into the atmosphere (Vega and Kovscek., 2010[37]; Melzer, 2012[36]). This technology is considered to be the most economical and feasible way to reduce greenhouse gas emissions on a large scale in the future. CO_2 storage can generally be divided into geological storage, Earth surface storage and marine storage (Hasan et al., 2015[38]). Among them, surface storage and marine storage technologies are not mature and have great impact on the environment. Therefore, CO_2 geological storage is the main choice for CO_2 storage at present. CO_2 geological storage refers to the permanent storage of CO_2 by injecting the collected CO_2 into the closed underground rock mass through the physical and chemical capture mechanism to achieve the purpose of reducing the emission of CO_2 into the atmosphere. Generally, the injection of carbon dioxide will be combined with Enhanced Oil/Gas Recovery (EOR/EGR) process. The carbon dioxide will enter the formation in liquid or supercritical state after high-pressure compression, and the residual methane and even heavy hydrocarbons in the reservoir will be replaced by competitive adsorption. Geological bodies suitable for CO_2 geological storage mainly include deep non-exploitable coalbeds, deep brine beds, abandoned oil/gas reservoirs and shale reservoirs. In

this case, injecting CO_2 into coalbeds or abandoned oil/gas reservoirs can not only achieve the geological storage of CO_2, but also improve the production of coalbed methane and oil/gas (Liu et al., 2017[39]; Bachu, 2016[40]). The cost of capture, transportation and injection of carbon dioxide is the highest among all the procedures. Therefore, it is very important to select the appropriate formation and gas source. And the final result will vary greatly with the change of formation properties and the selection of injection parameters. In the CCUS project of the oil reservoir, the minimum miscible pressure of the reservoir and oil density are important influencing factors, and the reservoir pressure and porosity have little influence. The mechanism behind this still needs to be explored (Liu et al., 2017[41]).

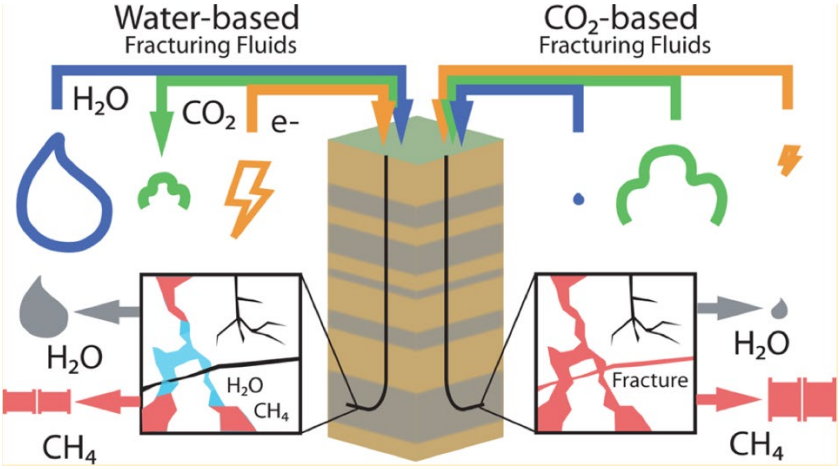

Figure 9 Comparison of hydraulic fracturing and Supercritical CO_2 fracturing (Rodney et al., 2016[42])

The most applicable methods of exploration of shale gas are using horizontal wells and multi-stage fracturing. This creates a flow tunnel for the free methane inside the pores to flow into the fractures from the matrix. Some scholars also suggested in-situ combustion, which means burning the kerogen in the shale reservoirs can effectively increase the permeability of the shale. This could be a good replacement for water fracturing (Chapiro and Bruining, 2015[43]).

For the fracturing, at first, the production rate could be high, since most gas is free gas in the matrix. As the pressure declines from the highest point, the adsorbed gas gradually desorbs from the matrix and combined with existing free gas, can be transported by pressure difference across the matrix and the fracture. But the desorption process could be achieved only in low pressure circumstances, which contradicts the requirements of maintaining high pressure in the reservoir to make sure the flow keeps stable. Therefore, the natural decay method would not contribute to the higher recovery rate for the reservoir. The injection of carbon dioxide could solve this problem (Ettehadtavakkol et al., 2014[44]; Núñez-López and Moskal., 2019[45]; Gozalpour et al., 2015[46]). Carbon dioxide has been used in the petroleum industry for more than 50 years. With gas sources near the reservoir, engineers use pumps to inject carbon dioxide into the pores to drive the residual oil and gas out of the reservoir. When the carbon dioxide is injected into the reservoir, under such a condition, it automatically becomes supercritical. Using carbon dioxide as fracturing fluid is a more ideal choice than water. First, it will not have water-block phenomena in the porous media, which means there is no damage to the formations. And when the fracturing ends, we just change the pressure to make it become gas again and then it will flow to the surface. Or it can be stored underground to reduce the carbon in the atmosphere. With supercritical carbo dioxide, the consumption of water is far more reduced and has the same effect of using water. More environment friendly, more efficient, less cost are the advantages of using supercritical carbon dioxide. What's more, when using it for flooding the reservoir, the affinity between the supercritical carbon dioxide and the rock will efficiently drive the residual oil out of pores dominated by competitive adsorption (Du et al., 2019[47]; Hou et al., 2018[48]; Hajj et al., 2013[49]; Rodeny et al., 2016[50])

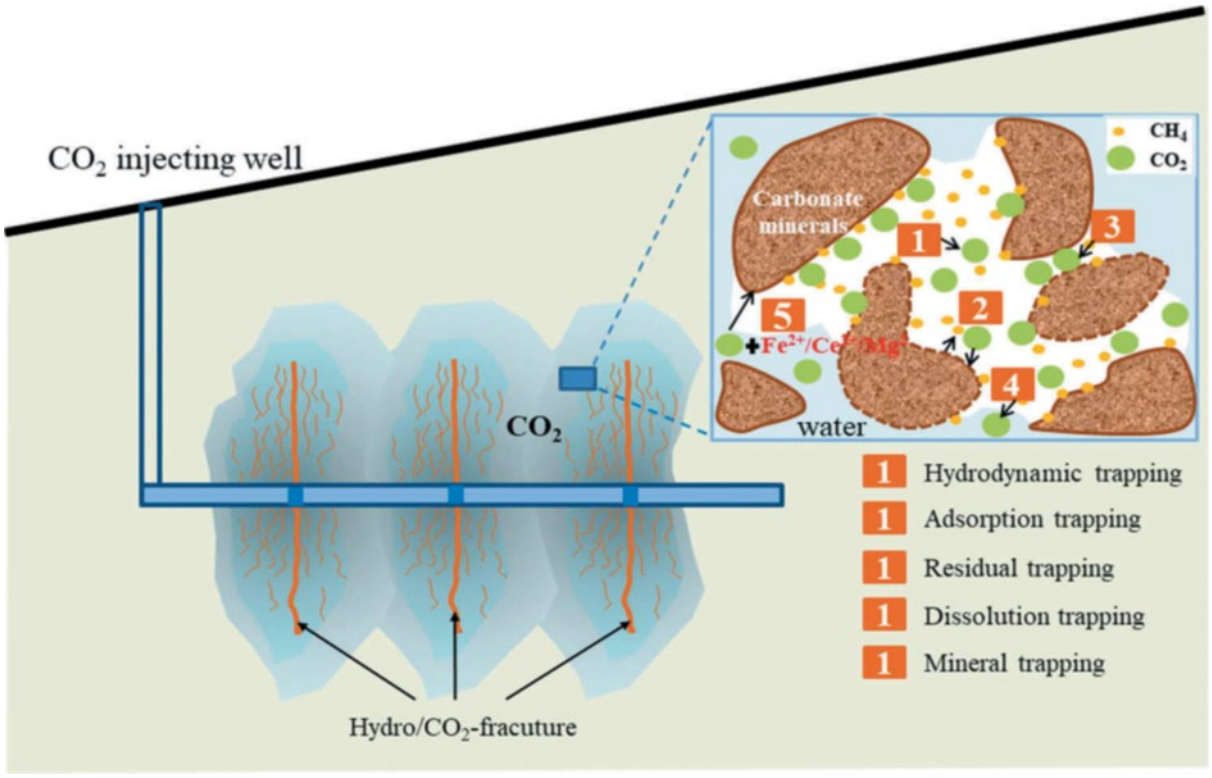

Figure 10 CO_2 Trapping Mechanism in the Reservoir (Wang et al., 2015[52])

Syah et al. (Syah et al., 2021[51]) carried an experiment to study the effect of injection of supercritical carbon dioxide in tight reservoirs. They found that the lower the permeability is, the higher displacement efficiency it would be due to the smaller pore structure inside the core and the competitive adsorption with methane. With the decrease of water saturation in the cores, the less supercritical carbon dioxide dissolved in the water, and thus more carbon dioxide was stored inside the porous media.

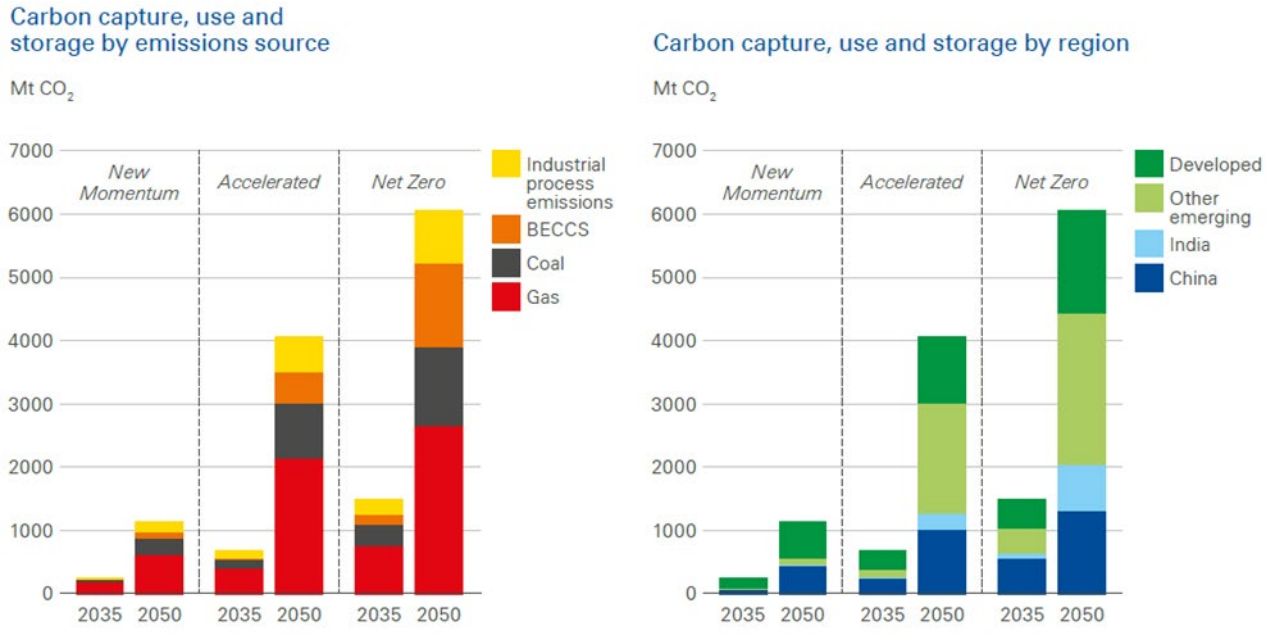

Figure 11 Carbon capture, use and storage plays a central role in enabling deep decarbonization pathways. (BP Energy Outlook, 2023[2])

From the outlook of BP, we can see the major contribution of CCUS are from emerging economy bodies and developing countries. The CCUS projects require the exploitation of oil and gas reaching a high level before carrying out CCUS. This means the combination of utilizing and storage of carbon could be achievable in the following energy consumption era.

Cyclic Gas Injection is considered to be an efficient and effective way of increasing production after the fracturing of the shale gas reservoirs. During the stimulation process, supercritical carbon dioxide and liquid carbon dioxide can be injected to create fractures instead of water. This means two situations: First, carbon dioxide can be injected from the ground in gas state. And it will become a supercritical state or liquid state under the pressure and temperature of reservoirs. Or engineers can pressurize the carbon dioxide at the ground, and make it become liquid or supercritical state at the ground, and then inject it to the reservoir. During the gas injection process,

nitrogen and carbon dioxide are usually considered. The choice of nitrogen is due to the lower price and easily available in the fields. Whereas carbon dioxide is very expensive compared to nitrogen, and it's a perfect competitive source of gas injection. Usually, the fracturing of using carbon dioxide can be sorted into two kinds: CO_2 foam fracturing and dry CO_2 fracturing (Zhou et al., 2013[53]; Liu et al., 2021[54]).

Zhou (Zhou, 2021[33]) studied the huff-n-puff process by injecting carbon dioxide into shale sample saturated with methane in the Yanchang oilfield. They found the adsorption amount of both methane and carbon dioxide would increase with the reservoir pressure but decrease with the rising temperature. The diffusion coefficient of carbon dioxide is positively proportional to the pressure and temperature, which is opposite to that of methane. As the injection pressure increases, the diffusion coefficient of carbon dioxide increases, and the diffusion coefficient of methane decreases. The reason of the decrease of diffusion coefficient due to the pressure increase can be attributed to several reasons: First, the matrix would expand due to the adsorption, which will lower the permeability of the shale matrix and thus create additional resistance to the flow of gases. Second, the attraction between free gas and the surface of micropores is going down due to more gas molecules are adsorbed on the surface, which will also create resistance to diffusion. This creates both positive and negative sides for the recovery process: If the final purpose is to gain methane, the injection pressure should be kept as low as possible. But if we want to storage carbon dioxide underground, the injection pressure should be kept high. But this is also related to the status of carbon dioxide and the soak period time. When the carbon dioxide is in the gas state, the longer the soak period, the more methane we can get from the production well (less carbon dioxide were storage inside the porous media). However, under supercritical conditions, the longer the soak period, the less methane, and more carbon dioxide one will get from the production well.

Louk et al. (Louk et al., 2017[55]) carried a small project injecting 500 tons of carbon dioxide into shale reservoir from a vertical well and then carry huff-n-puff to see the enhanced recovery performance of CO_2 in Chattanooga, Central Appalachia of United States. They found under high

flow rates and low injection pressure, the injectivity of carbon dioxide is considerable. The status of carbon dioxide when injection is still gas. After injected into the reservoir, according to the pressure monitor data, it becomes liquid or supercritical status. During the soaking period, however, the data from the observation wells showed that there was no communication between the injection well and the observation wells. No more carbon dioxide in the total component or the tracer were found in the samples from the monitoring wells. This may be due to the ultra-low permeability of the shale itself. But they also found the storage of carbon dioxide near the injection well region was successful. At the flowback stage, more than 40 percent of carbon dioxide was obtained again in 17 months. But the hydrocarbon production rate was over 8 times higher than the time before carrying out the huff-n-puff. Another thing worth mentioning was the production amount of heavier hydrocarbon like ethane or butane was strongly related to the concentration of carbon dioxide. While methane production rate was negatively proportional to the concentration of carbon dioxide. At the beginning of the flowback stage, the partial pressure of carbon dioxide was high, which means heavier hydrocarbon would be produced during this time and was more beneficial. Later, as the concentration of carbon dioxide decreased, more methane was gained.

As we mentioned before, carbon dioxide and methane can have competitive adsorption in the shale matrix. In order to get the methane, we can inject carbon dioxide into the reservoir. The injection pressure is equal or a little bit higher than the reservoir pressure. As methane is continuously taken out from the matrix and carbon dioxide enters the matrix, the concentration of methane in the fractures decreasing and the carbon dioxide concentration in matrix decreasing too due to it adsorbed onto the matrix, which lowers the concentration of it in the free gas phase. In this case, the viscous flow or Darcy's flow contributes a negligible part to the total mass transfer. Diffusion would be the dominate mechanism between the matrix and fractures. In this thesis, we are going to discuss the impact of diffusion behavior across the porous media (tight matrix), especially the pressure response at the two side of the porous media to see the effect of cyclic gas injection.

1.2 Basic Theory & Literature Review

1.2.1 Rationale

Before we further explore the mechanism happening during the cyclic gas injection in the porous media, we need to know the existing theory of microscale mass transfer in porous media. We introduce three important mechanisms. They are advection, dispersion, and diffusion. The mass transfer of diffusion can be reflected in Gibbs energy. The gradient of pressure, temperature, and electron potential can all impact diffusion (Tosun, 2019[56]).

1.2.1.1 Advection (Thirumaleshwar, 2006[57])

Advection is a transport process in which a fluid or a substance is transported by the bulk motion of a fluid. It occurs when a fluid, such as gas or water, flows over a surface or through a medium, carrying particles or heat with it, and occurs only in fluid. The properties of that substance are carried with it. Advection can transfer various quantities, such as heat, mass, momentum, and pollutants. The advection operator can be expressed in Cartesian coordinates:

$$u \cdot \nabla = u_x \frac{\partial}{\partial x} + u_y \frac{\partial}{\partial y} + u_z \frac{\partial}{\partial z} \tag{1.1}$$

Where $u = (u_x, u_y, u_z)$ is the velocity field, and ∇ is nabla operator.

The specific properties of the transported quantity, such as its concentration, temperature, or velocity, can be affected by other physical processes that occur concurrently with advection, such as diffusion, turbulence, or chemical reactions. Here we have slight differences between the definition of advection and convection. Generally, natural convection is caused by the density

gradient, which is attributed to the temperature difference during the fluid flow. And advection or forced convection is caused by the fluid velocity and then makes some material have a movement. The later one is caused by external force like a pump.

1.2.1.2 Dispersion

Dispersion typically refers to the process by which small particles of one substance are evenly distributed throughout another substance. The requirement of the existence of this phenomenon is the presence of advection. In general, hydrodynamic dispersion can be divided into two parts: molecular diffusion and mechanical dispersion. Diffusion will be discussed in the next part. The mechanical dispersion can further be divided into two sorts: longitudinal dispersion and transverse dispersion. There is a dimensionless number that can describe the flow in the system: Peclet Number. It defined as the ratio of convection to diffusion as follows:

$$P_e = \frac{vd}{D_d} \tag{1.2}$$

Whereas *v* is average solution velocity in cm/s, *d* is average diameter of particles in cm (sometimes this is called Characteristic Length), D_d is molecular diffusion coefficient in cm^2/s. The picture below shows the Peclet Number dominate range.

Mechanical dispersion is a general concept that includes all velocity changes that can introduce the mixing of solvent or dilution and is related with the solvent. It is dominated by both the carrying fluid velocity and the porous media characteristics. The change in velocity can be attributed to ① the irregular distribute of the velocity at the cross-section, i.e. the velocity at the center of pores is higher than that at the pore wall; ②the distribution of pore sizes (the velocity increases faster in smaller pores), and finally ③the tortuosity of flow channel. The magnitude of mechanical dispersion depends on the heterogeneity and the system size. The dispersion behavior can be

expressed by the advection-dispersion equation below:

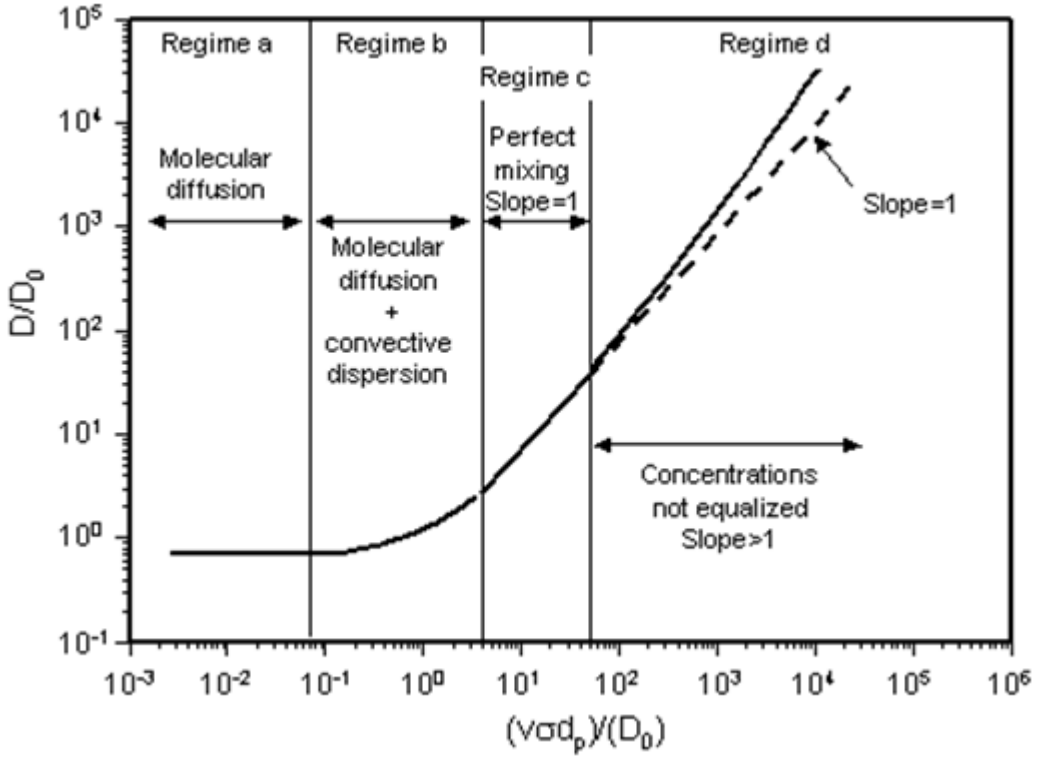

Figure 12 Dependence of Dispersion Coefficient on Peclet Number in Different Flow Regimes. The Scales on the Axes Depend on Porous Medium and Other Factors(Perkins and Johnston, 1963[132])

$$\frac{\partial C}{\partial t} = -v\frac{\partial C}{\partial x} + D_d\frac{\partial^2 C}{\partial x^2} \tag{1.3}$$

In this equation, C means concentration, t is time, v is velocity, x is distance. The term $-v\frac{\partial C}{\partial x}$ represents advection, and term $D_d\frac{\partial^2 C}{\partial x^2}$ represents dispersion. In mechanical dispersion, longitudinal dispersion is more important than transverse dispersion. Therefore, the dispersion can be expressed by only longitudinal dispersion coefficient D_d. It has the form:

$$D_d = D_a\tau + \alpha v \tag{1.4}$$

Here, D_a is bimolecular diffusion coefficient, τ is tortuosity coefficient between 0 to 1, α is longitudinal dispersity, v is average gas linear velocity. Term αv represents the mechanical dispersion. And term $D_a\tau$ represents the contribution from the diffusion related with solvent, and this term is also called effective diffusion coefficient. In porous media, the effective diffusion coefficient is different from the actual diffusion coefficient. This is because the effective diffusion cross section is smaller than that of the free fluid, and the distance from one point to another in the porous material is also smaller than the distance that the molecule must move between these two points. Molecules must move within the solid parts of this material. In this case, the actual concentration gradient is less than the apparent concentration gradient. Under ideal conditions, longitudinal dispersity is strongly correlated to the heterogeneity of the porous media and is not sensitive to the solvent. But this is actually not correct, because we should also consider other mass transfer mechanisms occurring at the same time. Dispersion is a function of solvent velocity, *v*. If we look at the equation of longitudinal dispersity, we can easily find the mechanical dispersion part is positively proportional to the velocity, whereas the diffusion part has no relation with velocity. In this case, the total *D* would decrease with the lowering of the velocity. But if the velocity is too low, the solute will stay longer in the system, which will cause diffusion, adsorption or dissolution to happen, and also increase the apparent dispersion. The magnitude of dispersity is a function of solute, which means substance has lower molecular weight has more chance to disperse. As a result of this, a broader range of dispersion would happen. But the magnitude of dispersity would not increase. If the velocity is high enough, the contribution of diffusion can be neglected. In this case, the Peclet number is just corelated with the characteristics of porous media and do not interfere by solute, and could be transformed to a new expression irrelated to velocity, which gives:

$$P_e = \frac{vd}{D_d} = \frac{vd}{\alpha v} = \frac{d}{\alpha} \tag{1.5}$$

1.2.1.3 Diffusion

Diffusion is the movement of molecules from a region of higher concentration to a region of lower concentration down the concentration gradient[143], and it will transfer momentum between specific molecules and other molecules or walls. When the velocity of a specific kind of molecule is different from the total system, which we call reference velocity, we can say this kind of substance is diffusing. The flux created by this substance is called diffusion flux. The velocity it has under the reference coordinate frame is the diffusion velocity. If this momentum transfer only happens within molecules, this is called molecular diffusion. If the momentum transfer happens only between molecules and walls, then it is called Knudsen diffusion. For a binary system or multicomponent system, if one substance has concentration gradient, then it will create a net flux from high concentration region to low concentration region. Different molecules will have different fluxes, which will all contribute to the total flux. In a binary system, the summation of all diffusion fluxes is zero. They are equal in number but different in direction. Diffusion means a material separation between diffusing substance and total mixture due to the velocity difference. In this case, flux relating to the diffusion velocity is called separation flux, and flux that carries different substances but in same velocity is called non-separation flux. In an isobaric system, the total molecular concentration gradient would quickly dissipate with the establishment of non-separation flux contradictory to the lighter molecular flux direction. For a given substance in the system, the diffusion flux of it, or we can say the resistance caused by the collapse of this kind of molecules and other kinds of molecules is dominated by two factors: ① number of molecules of specific component in unit area and ② number of molecules of other component in unit area. If the pressure increase, the concentration of each substance would increase, and thus the diffusion flux of given substance would increase, because factor ① increases at first and then decreases

but factor ② does not change much. Therefore, the pressure cannot affect the diffusion flux. The molecules are continuously bombarding the pore wall when considering the diffusion in porous media. Usually, the pore wall is not flat, thus the specular collision cannot happen. There is no conservation of momentum along the normal direction of the wall.

For gas flow regimes in porous media, an important parameter used to classify them is the Knudsen number. It is defined as the ratio of the mean free path of the gas molecules λ to the pore diameter d, written as:

$$K_n = \frac{\lambda}{d} \tag{1.6}$$

The chart below shows the corresponding regime to specific range of Knudsen number:

Table 2 Classification of Knudsen Number

K_n range	Flow regime
K_n<0.001	Darcy flow
0.001<K_n<0.01	Slippage flow
0.01<K_n<0.1	Fick's diffusion
0.1<K_n<10	Transition diffusion

K_n>10	Knudsen diffusion

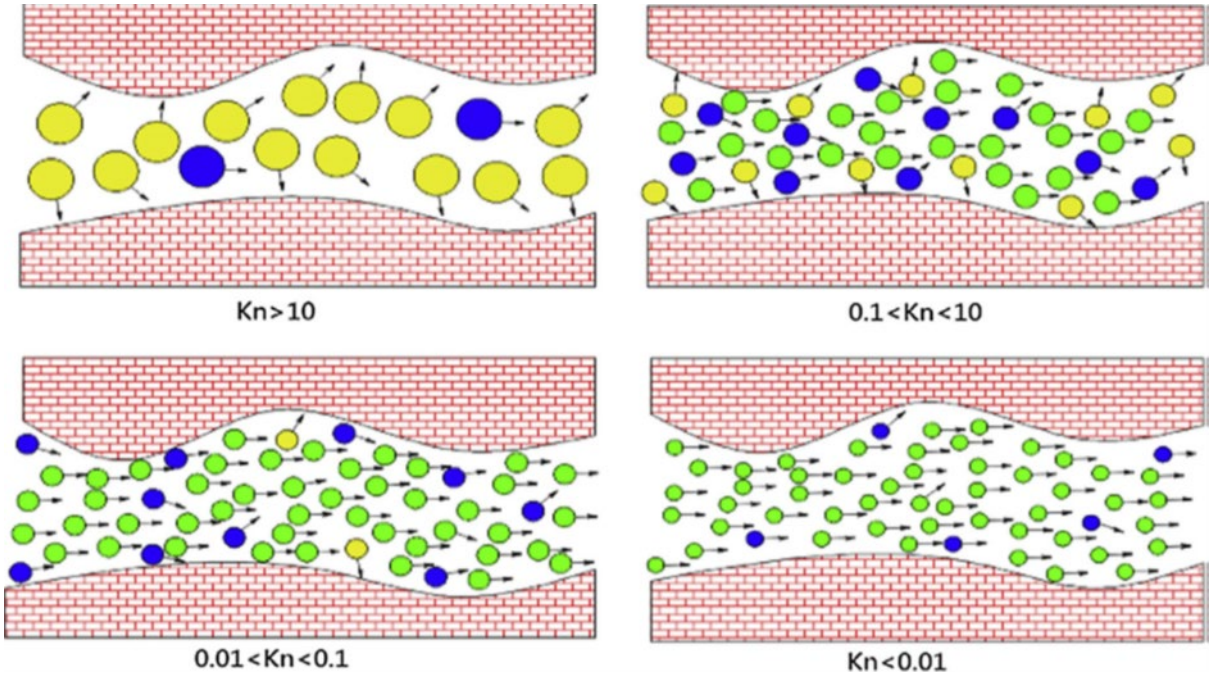

Figure 13 Schematic diagram of shale gas transport mechanism with different flow regimes (Song et al., 2016[58])

The different color dots in Figure 13 show different molecules in porous media. Yellow ones represent those hitting the wall and cannot flow out. Blue ones mean those entering the pores but do not collide with others and can flow out. Green ones mean those collide with each other/with the wall and finally can flow out. If the mean free path is much smaller than the pore diameter and the radius of solid particles, it means that there are many gas molecules surrounding a single solid particle. The gas molecules would collide with each other or with solid particles. First, the relative speeds of gas molecules to the solid particles are the same without external force exerting in the system. Once the pressure gradient is established, the concentration gradient would form. At this

time, the solid particles in the high concentration area would be bombarded by gas molecules more severely than in the low concentration area. If the solid particles want to stay still, an external force must be exerted on them. Therefore, the momentum of gas molecules would transfer to solid particles. Some of the gas molecules are bounced back at an arbitrary angle into the bulk phase, i.e., diffuse reflection. The reflected molecules are continuously colliding with other nearby molecules, thus the momentum at the flow direction (pressure gradient direction) is dropping. This resistance will continue until the gas molecules boundary layer reaches the same velocity as the solid particles. This collision is called viscous collision, and the corresponding flow regime is called viscous flow. The resistance depends on the characteristics of the fluid and the pore wall, as well as the flow rate.

The gas diffusion velocity is controlled by two factors: the collision between gas molecules and the collision between gas molecules with the pore wall. When the mean free path is close to the pore diameter, the interaction between the bounced back molecules and those molecules inside the bulk phase is not complete. The velocity of boundary layer is not zero but becomes stable. This flow regime is between Knudsen diffusion and Fick's diffusion, and it is called transition flow.

If the pore size is close to the molecule size, then it is called configurational diffusion. Configurational diffusion is a process in materials science where the atoms or molecules in a solid material rearrange themselves by exchanging positions with one another, in order to reach a lower-energy configuration. This rearrangement process is driven by thermal energy, and it can occur at temperatures below the melting point of the material. In configurational diffusion, the rearrangement of atoms or molecules is a result of the diffusion of point defects, such as vacancies or interstitials, through the material. These point defects can move through the crystal lattice and affect the positions of neighboring atoms, leading to a rearrangement of the material's atomic structure. The chart below shows the magnitude of diffusion coefficient for different diffusion mechanisms:

Table 1 Gas Diffusion Type in Porous Media[33]

Diffusion Type	Diffusion Coefficient Equation	Magnitude of Diffusion Coefficient
Configurational Diffusion	$D_T = D_0 \exp\left(-\frac{E_T}{RT}\right)$	D_T<$10^{-9}\ m^2/s$
Surface Diffusion	$D_S = D_0 \exp\left(-\frac{E_S}{RT}\right)$	D_S<$10^{-7}\ m^2/s$
Knudsen Diffusion	$D_K = \frac{2r_p}{3}\sqrt{\frac{8RT}{\pi M}}$	D_K~$10^{-6}\ m^2/s$
Molecular Bulk Diffusion[144]	$D_Z = \frac{kT}{6\pi\mu_\alpha r_K}$	D_Z~$10^{-5}\ to\ 10^{-4}\ m^2/s$

D_0 is the diffusion coefficient of infinite dilution solution, E_T and E_S are diffusion activation energy that can be measured in lab. r_p is pore radius. *M* is the molecular weight. *R* is the ideal gas constant; k is the Boltzmann constant; μ_α is phase viscosity; r_K is the radius of the particle/component. Actually, it is better to assume that these diffusion mechanisms are combined in a certain process, rather than making one of them dominate the whole procedure.

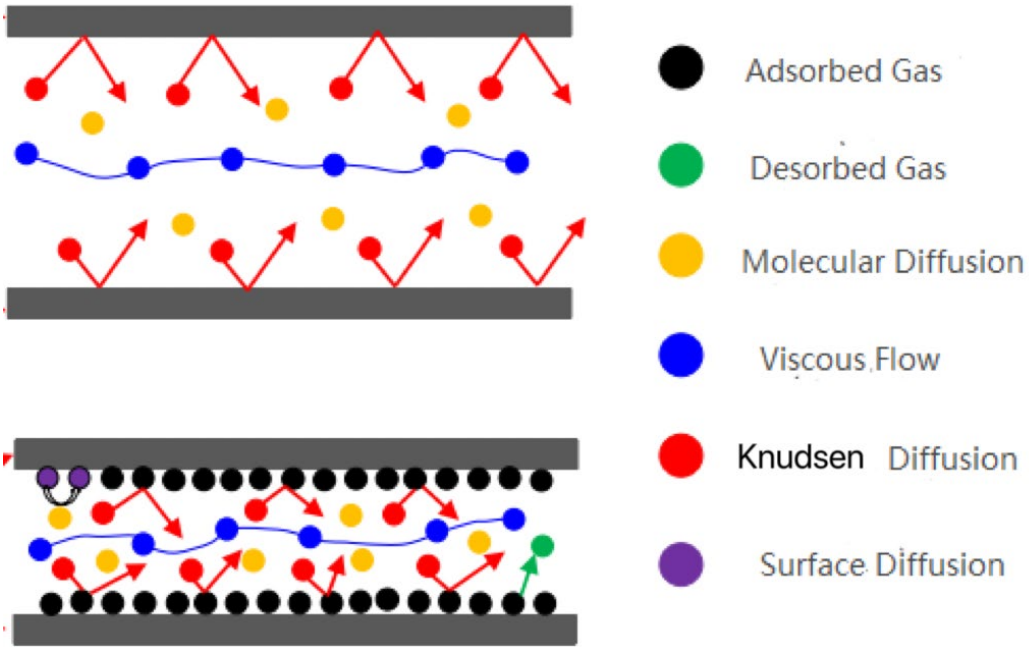

Figure 14 Gas Transport Mechanism in Shale Nano-pores

Another important thing is to estimate the binary diffusion coefficient in a system (Bird, et al., 2002[59]; Marrero and Mason, 1972[60]; Kestin et al., 1984[61]). The equations following are based on nonpolar gases in low pressure, low temperature and low velocity gradient circumstance. The molecules can be taken as rigid spheres. It is based on Lennard-Jones potential. Which gives:

$$\varphi_{AB} = 4\epsilon_{AB}\left[\left(\frac{\sigma_{AB}}{r}\right)^{12} - \left(\frac{\sigma_{AB}}{r}\right)^{6}\right] \tag{1.7}$$

Where σ_{AB} is collision diameter. ϵ_{AB} is the maximum energy of attraction between two molecules. It can be calculated as: $\epsilon_{AB} = \sqrt{\epsilon_A \epsilon_B}$ Then we can estimate the product of the mixture molar density with binary diffusion coefficient cD_{AB} from Chapman-Enskog kinetic theory:

$$cD_{AB} = 2.2646 * 10^{-5}\sqrt{T\left(\frac{1}{M_A} + \frac{1}{M_B}\right)} * \frac{1}{\sigma_{AB}^2 \Omega_{D\,AB}} \tag{1.8}$$

Here c is the molar density of the binary mixture in mol/cm^3. If there are ideal gases, c can be

written as p/RT. M_i is the molecular weight of species i in g/mol. σ_{AB} is binary collision diameter in Å. And σ_{AB} gives: $\sigma_{AB} = 0.5 * (\sigma_A + \sigma_B)$. $\Omega_{D\,AB}$ is collision integral for diffusion, and is the function of reduced temperature, defined as: $T_R = kT/\epsilon_{AB}$. Here k is Boltzmann constant. T is temperature in Kelvin. Now the binary diffusivity has the following form:

$$D_{AB} = 0.0018583\sqrt{T^3\left(\frac{1}{M_A}+\frac{1}{M_B}\right)} * \frac{1}{p\sigma_{AB}^2\Omega_{D\,AB}} \tag{1.9}$$

Here p is pressure in atm. Then we can estimate the binary diffusivity.

The impact of pore structure on the diffusivity in organic matter is also learned by some researchers (Rahmanian et al., 2011[62]; Wan et al., 2015[63]; Mezedur et al., 2012[64]; Qiao et al., 2021[65]; Javadpour et al., 2021[66]). The diffusion mechanisms between the organic pores and the inorganic pores are not the same. They found there is an obvious difference between diffusivity of the rectangular section and the circular section, due to the impact of pore size and pore structure on the Knudsen number. Usually, smaller pore sizes and lower pressure means larger Knudsen number, which means more surface diffusion and Knudsen diffusion in the system. When the pressure decreases, the diffusivity in circular section in organic matter should increase.

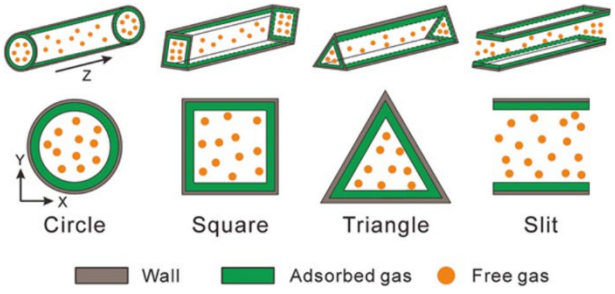

Figure 15 Geometrical Inclusion of the Adsorbed Gas Layer in Flow Constriction of the Organic Nanopore (Javadpour et al., 2021[66])

1.2.1.3.1 Fick's Diffusion

If the conversion of total momentum of the system is achieved during diffusion, then this diffusion is called molecular diffusion, or Fick's Diffusion. In this diffusion regime, the flow resistance created by the collision between molecules will not be affected by the structure of pore wall. The difference between viscous flow and molecular diffusion is that the latter does not lose momentum. Fick's law describes the diffusion behavior and is broadly used. Fick's first law describes the correlation between diffusion flux of gas component and concentration gradient under steady state. Whereas Fick's second law describes the relationship between unsteady diffusion flux and concentration gradient. The following equations about Fick's law is from Ho and Webb's book[145]. The general form of Fick's first law for substance A and B and their molar flux in the system can be expressed as:

$$J_A = -CD_{AB}\nabla X_A \tag{1.10}$$

Where D_{AB} is the diffusion coefficient of clear fluids, X_A is the mole fraction of component A, *C* is the gas concentration. The molar flux is related to molar average velocity. For the diffusion in porous media, we need to introduce porous media factor β, then the diffusion coefficient can be rewritten as:

$$D_{AB}^{*} = \beta D_{AB} \tag{1.11}$$

Where $\beta = \phi * S_g * \tau$. Here D_{AB}^{*} is the effective diffusion coefficient; ϕ is porosity; S_g is the saturation of gas. We take it as 1. This equation implies the porous can have an impact on diffusion speed. τ is tortuosity, which can be written as:

$$\tau = \phi^{\frac{1}{3}} S_g^{\frac{7}{3}} \tag{1.12}$$

Fick's Second law, we can just apply during equimolar counter diffusion. It has the form below:

$$\frac{\partial C_A}{\partial t} = D_{AB}\nabla^2 C_A \tag{1.13}$$

1.2.1.3.2 Knudsen Diffusion

If the mean free path is much larger than the pore size, we can then ignore the collision between gas molecules and just consider the collision between gas molecules and the pore wall particles. The bounced back molecules will not tend to interact with other molecules. In this case, the flow regime is called Knudsen flow, or Knudsen diffusion. The Knudsen flux will be proportional to the pressure of the system and depends on the thermal chaotic velocity. It has the general form for flux of gas *i* as follow:

$$J_{iK} = -D_{iK}\nabla n_i \tag{1.14}$$

Where n_i is molecular density. D_{iK} is Knudsen diffusion coefficient.

Knudsen diffusion would happen when the gas mean free path is close to the pore diameter. Unlike Fick's diffusion, Knudsen diffusion is mainly caused by the collision between gas molecules and the pore walls instead of intermolecular collision. Research shows that Knudsen diffusion and Fick diffusion would dominate the bulk diffusion in shale nanopores, and the former one is always contributing to the flow in shales. Knudsen diffusion is affected by pressure and pore diameter mostly, whereas Fick's diffusion is controlled by molecular sizes and temperature. As the pore diameters decrease, Knudsen diffusion contributes more to the total flux (Zhong et al., 2019[67]; Chen et al., 2017[68]; Kim et al., 2016[69]; Kuila et al., 2013[70]; Li et al., 2021[71]).

1.2.3.3.3 Surface Diffusion

If there is adsorption happening, the gas molecules are adsorbed on the pore wall. The molecules can transfer the momentum to the wall. If the binding energy is appropriate, the molecules can move at the surface of the pore wall. This kind of collision and the movement along the pore wall is called surface diffusion. This is an energy release process. If the molecules can gain a large enough energy at the normal direction, then they can escape the attraction of the pore wall and go back to the bulk again.

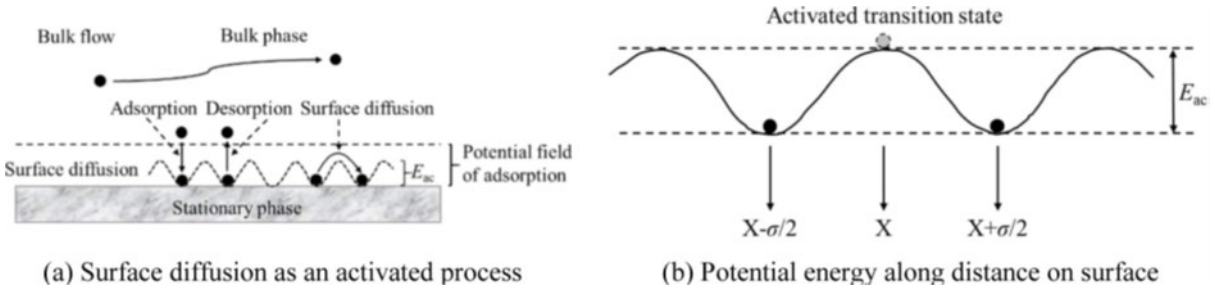

Figure 16 Mechanism of Surface Diffusion (Tsong, 2001[72])

A gas molecule is first adsorbed at a low energy position. When it gains an energy E_{ac} by vibration, it will leap to another adsorption point. The leap velocity is far less than the velocity of exchange between the bulk phase and the adsorption phase. In this case, we can assume that every single adsorption point is in equilibrium. The surface diffusion flux does not always increase with temperature. At high temperatures, the concentration of adsorbed molecules will decrease. As a result, when the motivation energy is higher than E_{ac}, the surface flux and the surface concentration of adsorbed gas would be zero. The surface flux at both high temperatures and low temperatures is small. But it has maximum value. The adsorption layer may change the cross-section of the porous in a great way, which is hard to analyze when considering multiple effects (Wu et al., 2015[73], 2016[74]).

Surface diffusion is investigated by many scholars (Kapoor et al., 1989[75]; Ehrlich and Stolt, 1980[76]; Yang et al., 2016[77]; Qu et al., 2020[78]). Surface diffusion is driven by a concentration gradient, or we can say chemical potential gradient. It not only includes the interaction between the surface and the molecules, but also between Van der Waal forces and electrostatic forces. In general, the surface diffusion would increase with increasing pressure and surface coverage of the adsorbed gas. In most cases, the heavier the molecules are, the less surface diffusion they can have. They found some of the movement of adsorbed gas on the solid surface would only happen in organic matter. This indicated the total gas diffusion was reinforced by the surface diffusion in organic matter. The same atom or molecule can behave differently or have different surface diffusion mechanisms on the same surface due to the different surface structure of the material. They also found the gas diffusivity was negatively affected by the total organic amount, and this relationship was also affected by gas pressure. As the total organic matter increased, higher gas pressure corresponds to a more significant reduction in the diffusivity of homogenized gas, because the diffusivity of gas is controlled by viscous flow under high pressure. The difference between the pore size of organic matter and inorganic matter makes the diffusivity of homogenized gas easily affected by the amount of total organic matter. On the contrary, when the pressure is low, the Knudsen and surface diffusion and slippage flow are more obvious. Therefore, surface diffusion can play a very important role in the diffusion and the gas transition in organic matter. As the pore sizes increased, the surface diffusion contribution decreased. Many researchers show that the surface diffusion coefficient is positively related to the increase of temperature and pressure. And the surface diffusion is an important contributor in the gas flow in micropores and mesopores. This process is often neglected when considering the total mass flux. Surface diffusion is an activation process, but the diffusion activation energy is generally less than the adsorption heat. It will increase with decreasing temperature. As a result of this, when the temperature is higher than the boiling point of the adsorption gases, the surface diffusion can be negligible. The surface diffusion of adsorbed gases could affect the apparent permeability of organic matter by changing the pressure and the pore sizes (Wang et al., 2016[79])

1.2.2 Literature Review

Diffusion is widely present in different industries, such as pollutant control, material design and even architecture. Here we present some of the works led by previous scholars and their results.

In renewable energy applications, electrode designs and the removal of all pollutants research, diffusion depth is a significant factor of determining the quality of the material under these working environments. This concept is always used in Knudsen Diffusion in meso-pores and micro-pores. It means the maximum distance that a molecule can flow inside the pore structure after colliding with the pore wall several times and finally adsorbed on the wall in Knudsen diffusion. This is because in Knudsen diffusion mode, the main collision happens between molecules and the wall of pores instead of inter-molecules. According to Xu et al. (Xu et al., 2022[80]), macro-scale pores are generally providing flow tunnels for the substances to diffuse through the matrix and connect the smaller pores to the outside. Meanwhile, the meso-pores and the micro-pores are mainly the storage place for the adsorbent. In this case, they explore the effect of gas characteristics and pore structures on the diffusion depth when the molecules move from outside of porous media towards micropores. By calculating the adsorption capacity per unit volume of the tested material and the size of the material crystal size, they can get the result of the diffusion depth of the pollutants inside the porous media, which is directly proportional to the cubic root of the ratio of two adsorption capacities of two different crystal structures. Generally, they found that as the temperature (molecular kinetic energy) increases, the diffusion depth also increases due to the higher frequency of collisions between molecules. When considering the mean free path (pressure of the system) and the polarity of the molecules, if these two factors increase, the diffusion depth would decrease. This was because a shorter mean free path would lead to fewer collisions between molecules and the pore walls and the inter-molecules one. And higher polarity would have greater Van der Waals forces between the molecules and the walls, which will tend to adsorb the molecules and prevent them from moving further inside. Their model can estimate the efficiency of the porous media on purifying the air pollution.

Hamdan and Sawalha (Hamdan and Sawalha, 1996[81]) developed a group of PDE to describe the porous media effect on the dusty fluid flow based on Dusty Gas Model (DGM). Without considering the mass transfer coefficient, as well as the diffusion, they used dust-phase continuity equations and liquid-phase momentum equations to define the flow in consolidated and granular porous media. They found both the flow regime and the sorts of porous media could determine the mass transfer between the porous media and dust-phase, and the resistance within the pore of the solids.

Rezaveisi et al. (Rezaveisi et al., 2014[82]) developed a numerical model of gas separation (chromatographic separation) process in shale by considering Knudsen effect and slip effect. They analyzed their model varying different parameters, such as reservoir pressure, reservoir permeability and tortuosity, and the size of the system. Due to different physical and chemical properties of gas molecules, their moving behavior and adsorption process can behave in different ways when moving from shale matrix to the fracture, and thus causing the component change in the wellbore. They concluded that during multicomponent production, gases with lighter molecular weight are more likely to get through the matrix than heavier ones. But their fraction is reducing with increasing reservoir pressure, which is opposite to the heavier components. When the permeability is high and the initial pressure is low, the normalized producing mole fraction of methane decreases quickly than the lower permeability and higher initial pressure situation. And for longer and higher tortuosity of the matrix, the longer time it will take to reach the depletion of the lighter component (methane) and the faster it will be produced when the permeability is fixed. Their model is generally in good agreement with field data.

Long et al. (Long et al., 2021[83]) used Molecular Dynamics simulation and grand canonical Monte Carlo method to study the diffusion and adsorption process of nitrogen, methane, and carbon dioxide in different sizes of porous media (this ranking is also suitable for the loading heat of the three gases). They found the gases loading amount and the adsorption amount of carbon dioxide was the highest, followed by methane and nitrogen. As the pore diameter becomes larger, the

loading amount increased with it, as well as the diffusion coefficient, but the adsorbed amount and the isosteric heat decreased. Due to the adsorption capacity and adsorption energy, as the adsorption amount increased, the adsorption heat of carbon dioxide increased very fast. On the contrary, the adsorption heat of methane and nitrogen decreased fast.

Xu (Xu, 2022[84]) studied the pore shape impact on the advection and diffusion of supercritical methane in the pores. He found the advective and diffusion flux would increase with the pore diameter. The contribution of advection is always higher than diffusion in most pore scales, and the higher the temperature, the more advection contributes.

Remick and Geankoplis. (Remick and Geankoplis, 1973[85]) investigated the binary diffusion (nitrogen and helium) in transition diffusion mode in the glass capillary Wicke-Kallenbach system under isobaric and isothermal conditions. They developed several assumptions and addictive equations in the transition region between Knudsen diffusion and molecular diffusion and designed an experiment to verify their computed results. The fluxes of each gas, effective diffusivities as well as fluxes ratios were measured and compared with the theoretical values by adjusting the total pressure to cover the whole transition zone. Their setting enabled them to flow the nitrogen and helium at steady state as well as taking samples during the experiment (S-1 and S-2). The diffusion cell made up of 644 straight glass capillaries with average length of 0.96 cm and 0.0391 mm in diameter. The result showed the good agreement between the theoretical value and the experimental value of effective diffusivities and the fluxes of the gases. The binary flux ratio generally followed the square root relationship between molar fluxes and molecular weight of each gas. During the lower pressure experiment, the diffusion followed the Knudsen equation and during the higher-pressure experiment, the Stefan-Maxwell equation was in a good match with the experimental data. They also verified the additivity of the momentum transfer of the two above mentioned equations in the middle transition stage.

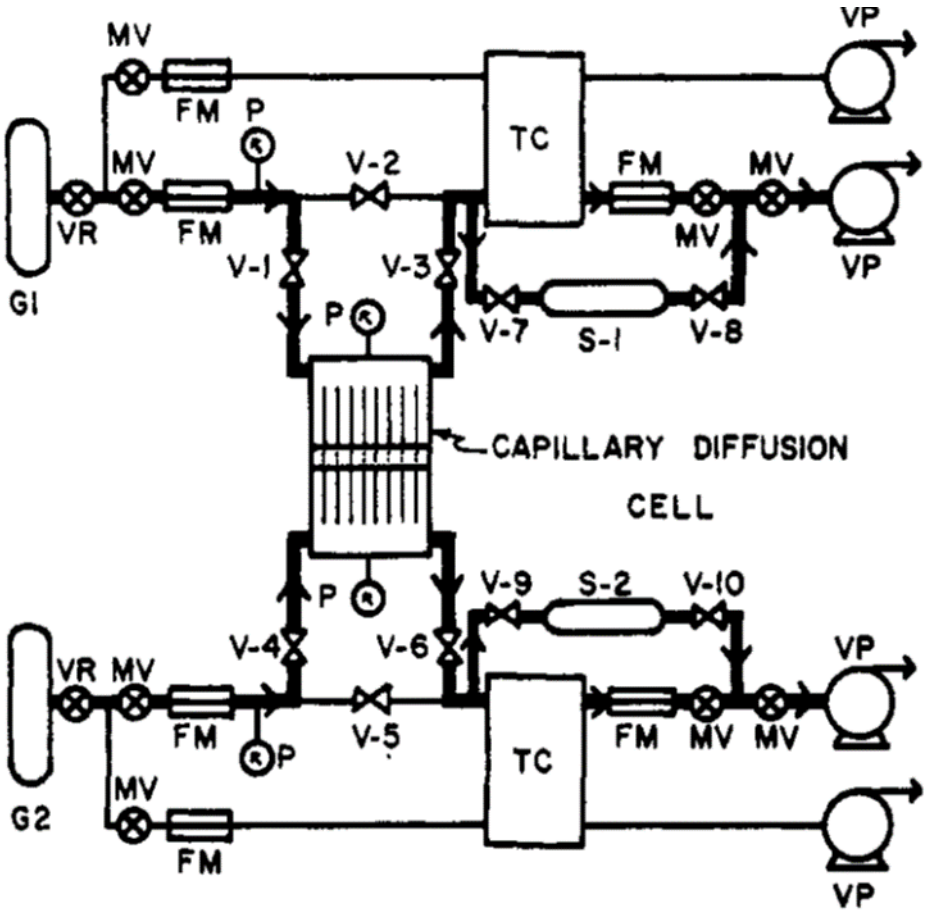

Figure 17 Remick's Experiment Setting (Remick et al., 1973[85])

Novák et al. (Novák et al., 1988[87], 1990[86]) investigated the effect of unsteady-state transport on the two side of α-alumina cylindrical pellets. They used five of these pellets, with 4mm in height and diameter, to represent the porous media. They set the upper cell and the lower cell at the same pressure before starting the experiment and saturated them with the same gas (e.g., helium), and then step changed the gas component of the upper cell with another gas (e.g., nitrogen) at the same pressure (isobaric test). By observing the pressure transducer located at the lower cell, they could easily observe the pressure change at the two sides of the porous media. Except for the gas types, they also looked into the effect of pore structure of the α-alumina (tighter or looser). They concluded that under dynamic transport conditions, the pressure difference is positively

proportional to the molecular difference between two gases and the decreasing trend is inversely proportional to the square root of the molecular weight. The amount of macropores and the volume of lower cell also affect the response time of creating such pressure difference (the bigger the pore, and the smaller the cell volume, the faster the difference would be established).

Based on the experiments carried by Novák et.al, Ehrhardt et al. (Ehrhardt et al., 1988[88]) proposed a responding mathematical model and developed boundary conditions for their model. This unsteady-state multicomponent diffusion process is represented by algorithm of a linear implicit finite-difference scheme. The Stefan-Maxwell theory provides two models for gas diffusion in the porous media due to the different understanding of the characteristics of porous media: the Mean Transport-Pore Model and the Dusty Gas Model. Therefore, after combining the continuity function and the constitutive equation, it had two sets of coefficients. By solving PDE and the sparce matrix, the result is close to the experiment result.

Čapek et al. (Čapek et al., 1997[89]) used the same setting as Novák et al. and developed the corresponding ODE and the boundary conditions. They compared the matching of the Mean Transport Pore Model (MTPM) and the Dusty Gas Model with the real experiment data. Their aim was to acquire the parameters of these two models using four different non-absorbable gases and the industrial catalyst ICI 52-1 in the experiments and accessed the confidence of the parameters under binary or multi-component condition. In this case, they found that the smaller the transport pore was, the more inaccurate of mean pore radius was in the model. And the change of mean of squares of transport pore radii would not affect the pressure response much.

Arnošt and Schneider (Arnošt and Schneider, 1995[90]) developed a set of experiments focusing on multicomponent dynamic gas transport in porous media analyzed by MTPM and DGM separately. In their modified Wicke-Kallenbach cell, they used two sets of α-alumina pellets as the porous solids. The volume ratio of upper chamber to lower chamber is 4:3. And they used a six-way valve to introduce the tracer gas and a four-way valve to push the testing gas into the upper cell in steps.

In this way they tried to understand the impact of cell volume and the dead volume. The difference between their experiments and those of Novák et al. is that the latter group had the lower cell closed and tested only 1 pair of gases each time, as well as their diffusion length for gases was just the height of the α-alumina sample (4 mm). Whereas in the Arnošt and Schneider's experiments, they used a circulation mode at the lower cell, which means the lower cell was not closed. At the same time, they used three gases each time and prolonged diffusion length for the gases (32 mm) to better observe the change of pressure difference and the component. They found that the concentration of the tracer gas was affected by both the molecular weight of carrier gases and the pore structure. The macropores mainly affect the gas transition direction and amount, which is similar to the conclusion of Novák et al. And the simulation results showed a good agreement between the experiment and the mathematical model, which indicated that the components in the triplet component system can have impact on each other by affect the mass flow flux and thus can cause pressure difference under isobaric condition.

Tuchlenski et al. (Tuchlenski et al., 1998[92]) tried to investigate the multicomponent surface diffusion by using Dusty-Gas Model and Maxwell-Stefan equation. They set up a Wicke-Kallenbach cell to carry the experiments similar to Yang's setting to verify the parameters of DGM and the surface diffusivities. They proposed the total molar flux in the system consisting of three parts: Bulk & Knudsen diffusion flux, viscous flux, and surface diffusion flux. They first measured the gas adsorption isotherm at 293 K and 343 K by using the volumetric method. In the diffusion tests, they used six gases, including adsorbable gases and non-adsorbable gases to study their behavior. They measured the permeation rate of the helium, argon and nitrogen, separately, by injecting them into the inner part of the structure region near the symmetrical axis in the picture. These steps can be changed to other adsorbable gas for the diffusion test later at a constant flow rate. Then they measured the pressure change at the inner and outer part of the equipment. Then continued flowing gas through the inner part, which finally went into the atmosphere, and let the inner part have the same pressure as the outer part. Reaching a steady state means the whole system was saturated with gas A first. Then switched the four-way valve to let gas B flow through the

inner part with the same pressure as flowing gas A. This isobaric condition could let the diffusion happen without convection. The pressure between the inner part and the outer part, flow rate and gas compositions were recorded. For binary inert gases transient diffusion, they used argon and helium. Since the molecular weight of helium is smaller, the system which was first saturated with argon would experience an increase of pressure at the outer part after the helium was step introduced into the inner part, until the maximum pressure difference reached, which means during the mobile process of the diffusion, due to the velocity difference of different gases, the accumulation of number difference of gas molecules at the two sides reach a maximum value. And then the pressure would go back close to the initial pressure (14.7 psi) since the argon was diffusing out of the outer part. In the reverse experiment, the principals were the same, but this time, the pressure at the outer part tend to decrease first, and then bounce back to the initial pressure. The maximum value of pressure difference and the time of reaching this value of the two experiments were nearly the same. Therefore, a perfect symmetrical shape occurred.

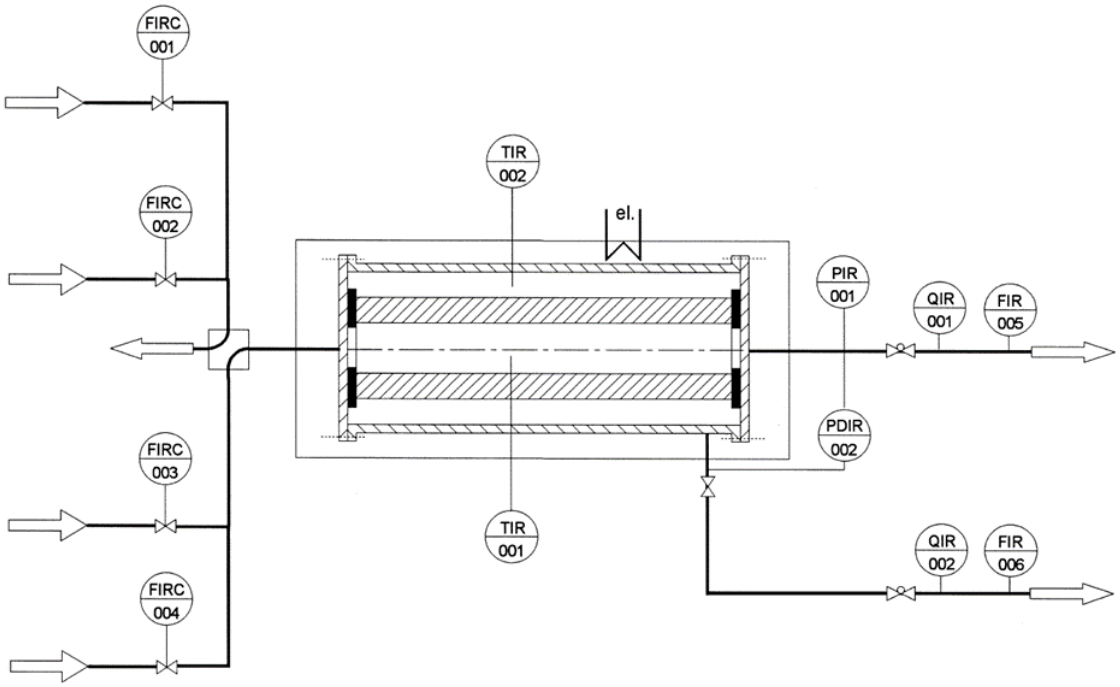

Figure 18 Tuchlenski Experiment Setting[92]

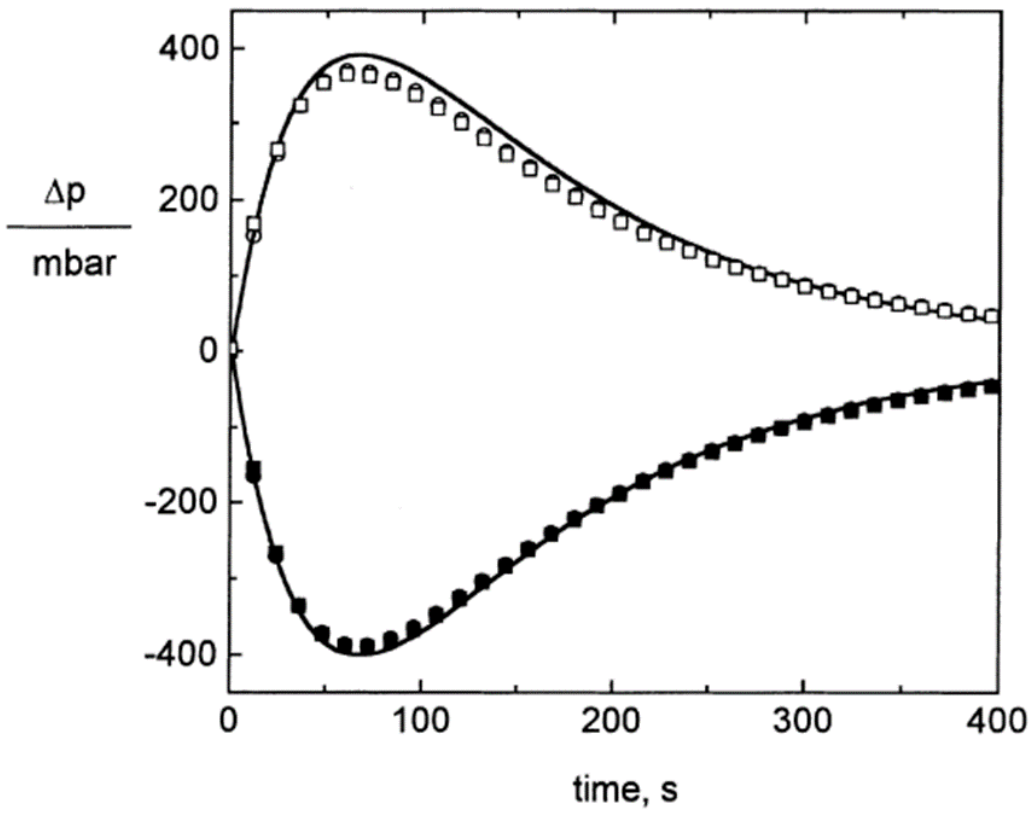

Figure 19 Pressure Response Using Helium & Argon at 293 K. White symbols represent He displacing Ar. Black symbols represent Ar displacing He. These symbols are both experiment data, and the line is the prediction result[92]

Yang et al. (Yang et al., 2005[91]) developed a set of transient diffusion experiments, using a Vycor glass membrane as the porous media to investigate the mass transfer with adsorptive and inert gases. They use DGM to describe the gas phase transport and Maxwell-Stefan equation to describe the adsorbed gases transportation. The modified Wicke-Kallenbach system consists of a concentric structure which is separated into two parts by the Vycor glass membrane in the middle. The whole structure was first saturated with one kind of gas until equilibrium. Then changed the gas flooding in the inner part with another kind of gas by adjusting the four-way valve. They measured the pressure difference between the inner and the outer part. This process can be replaced by both

reversed gases and multicomponent gas mixtures. They found the pressure response is an identical symmetric shape and the maximum pressure difference in both cases (exchange the gas injection order) were the same if only the inert gases were tested (nitrogen & helium pair). The DGM could perfectly describe the pressure transit process. But things could be different when the adsorptive gases are present. In this case the surface diffusion contributes to the total flux and thus the maximum pressure response and the time to reach the maximum pressure difference were different when reversing the gases of testing. This phenomenon could be more obvious if there were two or more adsorptive gases present in the system, which will lead to competitive adsorption on the surface of the porous membrane. The pressure response was strongly affected by the component and the concentration of the gases in the system. At the same time, the DGM and the Maxwell-Stefan equation could not precisely describe the process when the adsorptive gases were present in the system. If argon saturated the system first and then switched to labelled argon (which is heavier), according to their theory, the labelled argon should move slower than argon, therefore the shape should be like the black dots. But since their mass is close to each other, the valley should not as deep as the figure shown.

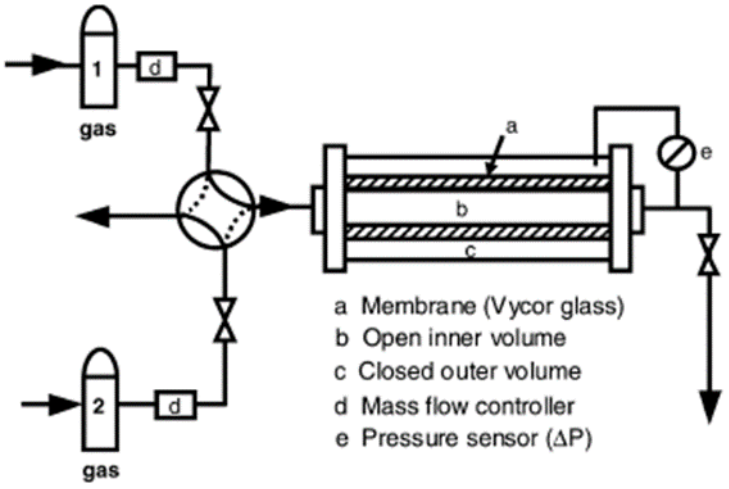

Figure 20 Experiment Setting in Yang's Design (Yang et al., 2005[91])

When using carbon dioxide and helium, the pressure response was different. The system was first equilibrated with carbon dioxide. Then the step changed with helium. The desorption of carbon dioxide made its partial pressure increase, which reduced the diffusion ability through the membrane. In the reverse experiment, helium was introduced first and then followed by carbon dioxide. Since carbon dioxide is an absorbable gas, it accumulates on the surface of the porous media and the helium would not have this behavior. Therefore, the helium flux was compensated by the carbon dioxide flux. In this absorbable-inert gas combination, the maximum pressure response of the two experiments were totally different and the time to reaching this value was slightly different. These pressure response differences, and the time-lag effect can be caused by surface diffusion, and adsorption, respectively. They also developed a series of experiments using various combinations of helium-carbon dioxide and helium-propane to get the surface diffusivity data. And as well as the carbon dioxide-propane 1:1 combination can tell the result of the mixing surface diffusion and adsorption, bulk diffusion, and Knudsen diffusion. We can see the prediction was generally in good match with the experimental data, but lately it deviated from the experiment greatly, which indicated there are still some mechanisms that had not been included in their model.

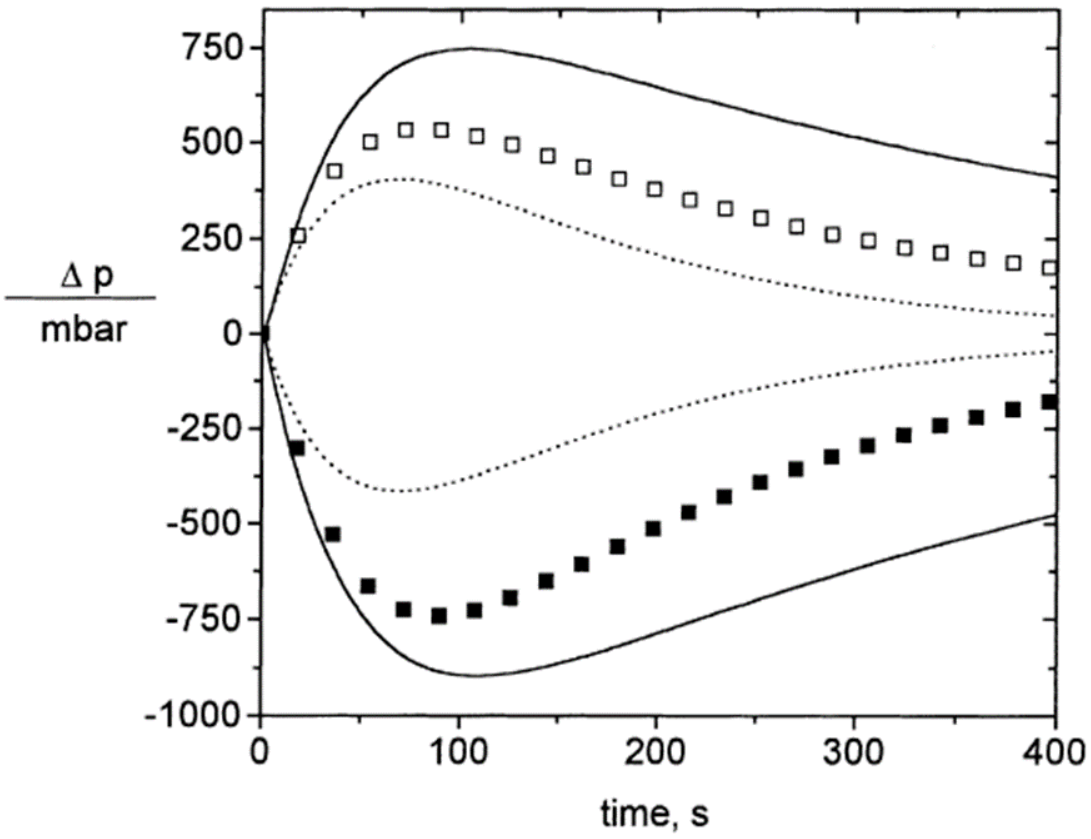

Figure 21 Pressure Response Using Helium & Carbon Dioxide at 293 K. White symbols represent He is displacing CO_2. Black symbols represent CO_2 displacing He. The lines are the prediction result [91].

1.3 Objective of This Thesis

1.3.1 Basic Theory of Previous Setting

Our research is based on Santiago's model and theory (Santiago and Kantzas, 2017[93]). During the transportation of gases in porous media, as the pressure and the permeability varies, different flow regimes, such as Knudsen flow and viscous flow, molecular diffusion, may appear and compete with each other. Different chemicals may be transported in this process and thus chromatographic

separation could appear. This phenomenon could be more apparent if the matrix adsorption plays an important role during the process, especially in the lower and extremely low permeability environments. Then, not only the concentration gradient but also pressure gradient would occur. This is extremely important for the production of condensate gas reservoir and the CCUS process. The flow of shale gases is usually from nanopores to macropores, or even fractures. Understanding the physical properties change in this process could help the engineers analyze the situation and adjust the exploration accordingly.

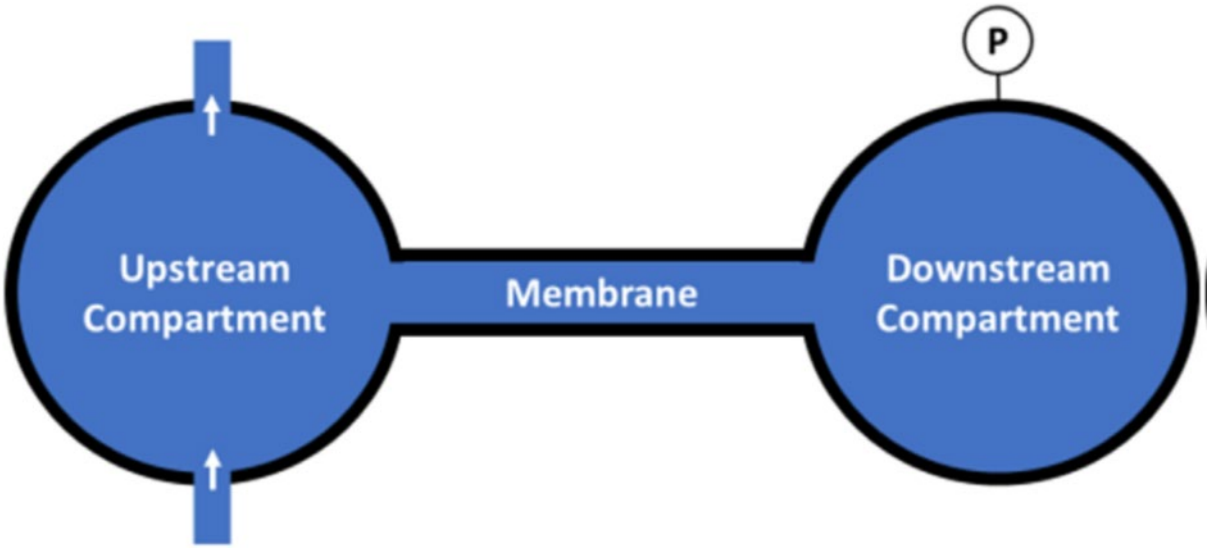

Figure 22 Simplified Diagram in Santiago's Setting [93]

In analyzing the heavier components effect in the diffusion, Santiago and Kantzas used Dusty-Gas Model and Maxwell-Stefan equations to match the history production data and modeling the mass and momentum transfer between molecules and walls and intermolecular behaviors by considering the adsorption and surface diffusion for different transport regimes and reservoir types. By combining Knudsen diffusion and Maxwell-Stefan equations, they developed the diffusion flux for non-adsorbing porous media and adsorbing porous media. In their theoretical experiments steps, the system would saturate with one gas first, with a constant flow rate and composition injected

into the upstream compartment while keeping downstream closed. At time 0, the gas in the upstream is step changed to another gas at the same pressure (actually this is hard to achieve, and this will be explained in section 1.3.2). This introduces a molecular diffusion (no pressure difference at the beginning) then followed by convective force (created by pressure difference as a result of molecular diffusion) due to the different molecular weight and chemical potential between two species. In the helium-argon pairs, the membrane was first saturated with argon. Then at time 0, the argon in the upstream was step changed to helium, which diffuses much faster due to its lower molecular weight. Before reaching the peak, the argon molecules experienced a diffusion barrier and could not diffuse to the upstream part. Then the system would automatically balance the chemical potential in the two compartments. Therefore, the result of this process was the total pressure being equal to the upstream pressure (flowing side), which is the atmospheric pressure. When the pressure difference (calculated by the downstream pressure minus upstream pressure) between the two compartments were shown on the diagram, it started with 0, because the pressures in the two parts were the same, but different in gases. And then as the faster diffusing gas moved more quickly than the heavier gas, there will be a bump as the time increased, and then reach to the maximum value. Then the heavier component would finally reach the lower concentration part, which means the pressure downstream part started to decrease, until it reached the upstream part again, which is represented as 0 on the pressure difference diagram.

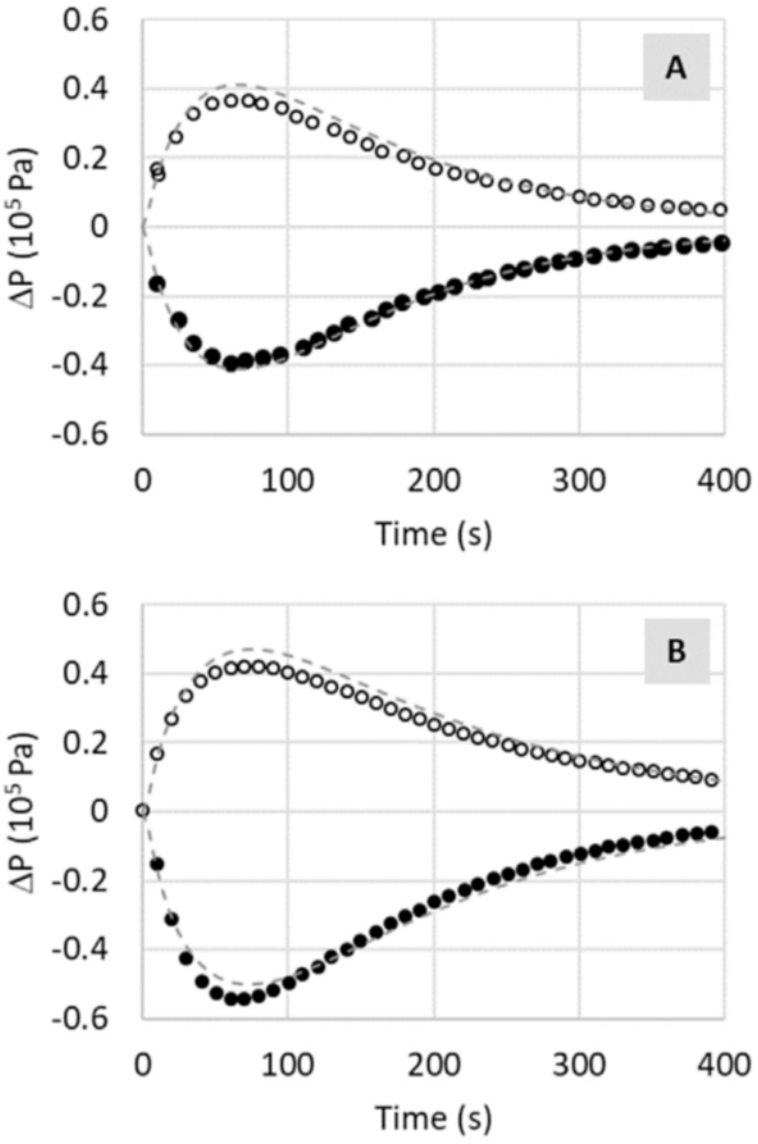

Figure 23 Pressure Response at 293 K. Part A represents the Argon-Helium system. White circles mean helium displacing argon. Black circles mean argon displacing helium. Part B represents the Propane-Helium system. White circles mean helium displacing propane. Black circles are inverted. Dashed lines are simulation result[93].

When the gases were inverted while keeping other conditions the same, something similar happens but in the opposite direction. If the helium was injected into the system at first, then change the

gas in the upstream compartment with argon, the pressure in the downstream would decrease first and then back to the same pressure as the upstream, since the helium will move much quicklier than the argon. Then the pressure difference would be negative. The shape of these two pressure-difference changes were symmetrical because both argon and helium are non-absorbable gases. According to the diagram, the experimental data were in good match with their simulation model for non-adsorbing porous media.

When involving an adsorbable gas, things could be a little different. The system was first saturated with propane both in the membrane and the compartment. Then step change the gas in the upstream with helium. Helium diffuses faster than propane. The positive pressure difference showed again in picture B. But the maximum value was a little bit higher than the multicomponent for non-adsorbing gases. This was because propane was desorbed from the porous media. At the same time, surface diffusion also contributes to this process. And the reverted experiment showed a larger absolute value of pressure difference in negative way, which was caused by the adsorption of propane on the membrane and quickly increase the flow flux at the upstream part. If both sides are saturated with argon, the bump should not exist, since their diffusion speeds are the same. In such a short period, the pressure difference curve should be a flat line and always be zero.

In their simulation process, they monitored the percent of heavier components (C_{4+}) change in the near wellbore region during the gas chromatographic separation to see if there can be condensate blockage that can severely reduce the gas permeability in that region. They looked at the influence of absolute permeability, gas composition and different transport models on the phase envelop change in this process. If not considering adsorption, the chromatographic separation was only determined by Knudsen diffusion, which was nearly negligible for the components change and the pressure change at the outlet. But the adsorption can affect the composition of the gas envelope in a great way due to the drag effect. On the other hand, adsorption and molecular diffusion could also react to the pressure gradient change.

In general, molecular diffusion tends to let the system equilibrate, and Knudsen diffusion tends to let different molecules separate from each other. Molecular diffusion will eliminate the difference of chemical potential of different parts of the system, whereas the Knudsen diffusion will enhance the difference in chemical potential. The absolute permeability can impact the production gases by the molecular sieve mechanism when not considering adsorption. However, when the adsorption was present in the system (e.g., the organic matter), as the carbon number of the compound increased, the affinity of it on the organic matter increased, too. In this case, the variation of permeability plays nearly no role in the component change in the system. When considering the components at the initial condition of the system, the higher the heavier component concentration, the larger the desorption parts playing in the production stage. This pressure difference during isobaric diffusion is also observed by Soukup et al. (Soukup, et al., 2008[94][95]). And this phenomenon caused by the devices (the Wicke–Kallenbach and Graham's diffusion cells) and pore sizes was also explained by them. The larger the pore size, the higher the pressure difference. If the adsorption and surface diffusion are considered, the pressure difference could be more obvious in the binary system (Krishna, 2016[96]; Čapek et al., 1997[97]; Hejtmánek et al., 1998[98], 1999[99]; Van and Krishna, 1995[100]).

Santiago and Kantzas (Santiago and Kantzas, 2018[101]) also investigated the impact of injection mode of gas on the multicomponent gas flow with considering the adsorption. They combined the Dusty-Gas model and the Maxwell-Stefan equation to build their model on the competition of molecular diffusion and Knudsen diffusion. The primary production, flooding and huff-n-puff mode were selected to verify their model. In primary production, gas chromatographic separation happened. The lightest component (methane) escapes the system fastest, which means the heavier components were left inside the porous media. During huff-n-puff mode, the heavier component fraction in the production was investigated by three kinds of gases: nitrogen, methane, and carbon dioxide. Nitrogen could increase the ratio of heavier component due to the partial pressure decrease and then followed by desorption of heavier hydrocarbon. Since nitrogen is inert, it does not interact with the pore-walls and does not absorb on it or the organic matter. Carbon dioxide would have a

competitive adsorption with lighter hydrocarbon (methane, ethane, and propane, etc.). While methane has both competitive adsorption and the partial pressure reducing mechanism advantage in this process. Both these three gases were willing to maintain the reservoir pressure at a high level in order to prevent condensation occurring in the reservoir. Meanwhile in the flooding mode, the displacement front would sweep through the reservoir quickly and efficiently. Both the competitive adsorption and the partial pressure reduction played important roles in the process. Nitrogen forms the front first among the three gases, since it does not interact with the pore walls, but it also had the earliest breakthrough. All in all, the methane had the best performance in huff-n-puff and flooding mode since it had two depletion mechanisms at the same time. Besides, carbon dioxide has the most efficient operation since it has strong competitive adsorption with the hydrocarbons and its front formed slowly, which prolonged the breakthrough time and benefited the sweep efficiency.

Krishna (Krishna, 1993[102]) proposed several important concepts for the diffusion in porous media. He used a simple experiment to prove the traditional Fick's law is not sufficient to describe the diffusion behavior in the binary or ternary gas system. In his setting, two containers having the same volume were separated by a valve at the symmetric center of the structure. Hydrogen, nitrogen, and carbon dioxide were used by adjusting the mole fractions. In container 1, there were 0.50121 hydrogen and 0.49879 nitrogen. Whereas in container 2, there was 0.50086 nitrogen and 0.49914 carbon dioxide. In theory, after the valve was opened at time zero, the gas in the two sides should diffuse from the high concentration side to low concentration side due to the difference in chemical potential. Then the composition and their fraction should be the same in the two containers. It was observed that decreasing of mole fraction of carbon dioxide in container 2 and the mole fraction of hydrogen in container 1 was within the anticipation, as well as the increasing fraction in their opponent container. However, the change of nitrogen is unexpected. Before time *t1*, the behavior is normal: the nitrogen in container 2 decreased and increased in container 1 due to the concentration difference. When they became equal at $t=t1$, it did not stop but continued increasing in container 1 and decreasing in container 2. This uphill diffusion process continued

until *t=t2*. Then the mole fraction behavior was back to normal again. Krishna named three phenomena in total: (1) At *t=t1* as osmotic diffusion. This means the diffusion of certain substances continues disregarding lack of driving force (concentration difference). (2) When *t1<t<t2*, this was called reverse diffusion. This was a process where molecules diffuse against their concentration gradient. (3) When *t=t2*, this was called diffusion barrier. At this point, the diffusion stops despite the large concentration difference between the two sides. This whole process, according to Krishna[102] and Chen & Yang[103], was due to the drag effect between molecules. The driving force of diffusion comes from the concentration gradient established across the system. When the diffusion begins, nitrogen, carbon dioxide, hydrogen will diffuse at the same time but in a different direction. At this time, there are three kinds of force exerting on the nitrogen molecules: Driving force caused by concentration gradient, intermolecular fraction between nitrogen and carbon dioxide, intermolecular fraction between nitrogen and hydrogen. During *t1* to *t2*, the flux of nitrogen was coupled to the driving force of carbon dioxide and hydrogen, even though the driving force for nitrogen became 0 at time *t1*. The driving force of nitrogen was small compared to the frictional drag force exerted by carbon dioxide and hydrogen. And the frictional force of carbon dioxide exerting on nitrogen was larger than that of hydrogen on nitrogen (for the calculation process and result, please see Krishna, 1993[102]). As the concentration difference of nitrogen between two containers increases, the driving force is also increasing. Finally, these three forces become equilibrium at *t2*. Then the whole process is dominated by concentration gradient force again after *t2*. In a binary system, the forces exerted on a single molecule are described by the following diagram. This drag effect is still available in binary system (Chen and Yang, 1992[103]).

1.3.2 Innovation in the Thesis

From previous experiments and simulations, we can find their testing material are either thin catalyst membrane, Vycor membrane or mashed core samples. Several of them focus on the real reservoir conditions with intact cores and temperature-pressure system in the reservoir. Actually, the experimental setting is very important for the application of their conclusions in real conditions.

Therefore, we need to return to the original conditions as much as possible.

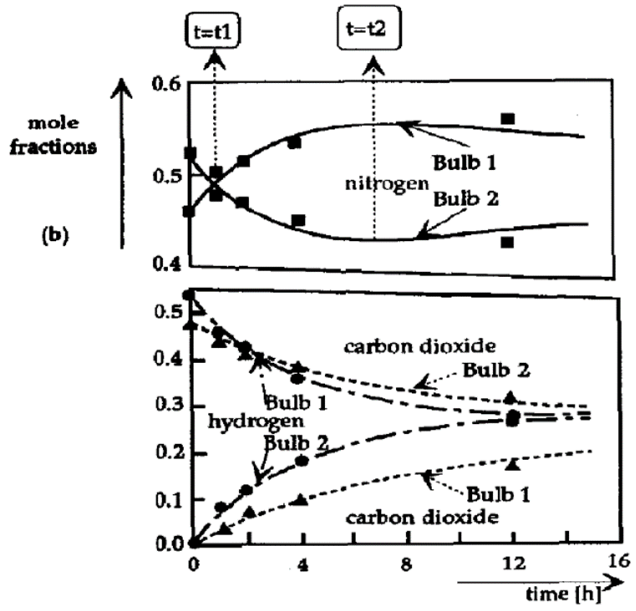

Figure 24 Mole Fraction Change During the Experiment Carried by Krishna[102]

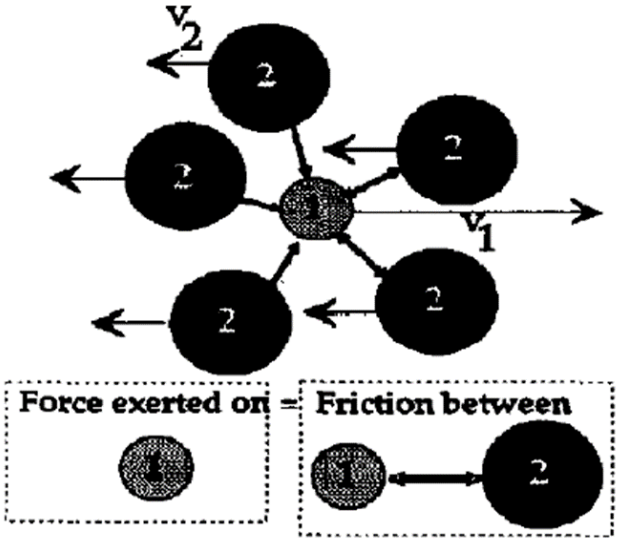

Figure 25 Drag Effect During Binary Diffusion or Multicomponent Diffusion [102]

Table 2 Comparation of Related Experiment Parameter. Notice the N/A means either no data or not applicable in that equipment

Parameter	Name	Šolcová	Novák	Daniel	Pavel	Yang	Axel
Test Material		Methanol Synthesis Catalyst ICI 52-1	α-alumina	α-alumina	ICI 52-1	Vycor Membrane	Vycor Membrane
Temperature		Ambient	Ambient	Ambient	Ambient	N/A	293K/433K

Flow Part Volume	150 cm^3	1.9 ml	0.4 cm^3	19.1 cm^3	4.78 ml	4.78 ml
Closed Part Volume	150 cm^3	8.7 ml	0.3 cm^3	55.2 cm^3	10.4 ml	10.4 ml
Porosity/Pore Diameter	16 nm	0.13-0.6/ 50-240 nm for small ones 640-1870 nm for big ones	N/A	0.623	3.8 nm	0.284/ 4nm
Sample Length	3.8 mm	4 mm	4 mm	0.368 cm	100 mm	100 mm
Sample Diameter	5.5 mm	4mm	N/A	0.54 cm	N/A	N/A
Inner Radius/Outer Radius	N/A	N/A	N/A	N/A	2.85 mm/ 4.05 mm	3.9 mm/ 5mm
Injection Pressure	N/A	N/A	N/A	N/A	N/A	N/A
Outlet Pressure	Atmosphere	Atmosphere	Atmosphere	Atmosphere	Atmosphere	Atmosphere

Flow Rate	150 cm^3/min	20 cm^3/min	N/A	1.34 cm^3/s	N/A	500 ml/min
Gases Being Tested	H_2/N_2/He/Ar	H_2/N_2/He/Ar	H_2/N_2/He/Ar	H_2/N_2/He/Ar	N_2/He/CO_2/C_3H_8/C_4H_{10}	N_2/He/CO_2/C_3H_8/Ar
Sample Numbers	19	12	8	12	N/A	N/A
Equipment	Wicke-Kallenbach	Wicke-Kallenbach	Wicke-Kallenbach	Wicke-Kallenbach	Modified Wicke-Kallenbach	Modified Wicke-Kallenbach

Counter-current diffusion is the basic transport mechanism of our experiments. Previous scholars have studied this phenomenon in their settings. According to Šolcová et al. (Šolcová et al., 2001[124], 2003[125]), the fundamental of this mechanism is based on Graham's law. For n components in porous, it gives:

$$\sum_{i=1}^{n} N_i \sqrt{M_i} = 0 \tag{1.15}$$

Where N_i is components molar diffusion flux densities, and M_i is molecular weight. For an equimolar binary diffusion system, we have:

$$\frac{N_1}{N_2} = -\sqrt{\frac{M_2}{M_1}} \tag{1.16}$$

But in dynamic conditions, Graham's law cannot be used. Both diffusion and convection should be considered. For different molecular weight diffusion, we have $N = \sum N_i$. They found the component change can affect the diffusion flux direction. But in their another experiment, it seems they have a completely opposite conclusion: The transport parameter is only affected by pore structure of the tested material, instead of gas composition, pressure, and temperature.

However, no matter the experiments carried out by Tuchlenski et al. or Novák et al. or others, their experiment setting had some basic problems that can affect the final results. First, they wanted to see the difference between two gases when they are going through the porous media, and they want to observe the diffusion phenomenon solely. In this case, they must maintain pressure at the circulation side (or circulation container) being the same as the pressure at the semi-close side (or closing container). This, however, is hard to realize actually. You have to calibrate the pressure transducers at the two sides and correct them to the same level. But there are not two same transducers in the world. It means we can only reduce the difference between the measurements of the two sides, but not completely eliminate it. Further, this small difference would cause convection because of the pressure difference. If the pressure difference observed is caused by convection or viscous flow, this result will not prove the impact of different gases on diffusion, and thus their conclusions were not convincing. Second, from their result showing the pressure responding due to diffusion through the porous media, the “spike” or the “bump” is not very high (5 psi or higher), but this pressure difference caused by diffusion was high enough compared with their experiment setting (1atm, 14.7 psi). And at the same time, their observation is not very long, usually 200 seconds to 400 seconds. Although their samples were thin enough (4 mm), and the gases may not take such long time to diffuse to the other side. This may be caused by other reasons. The four-way valve was a tool they used to switch between gases. Even though we can assume the pressure at the outlets of the two gas cylinders, e.g., the inlet of the circulation container, were the same (1 atm, gauge pressure), this valve switching behavior can cause a sudden pressure change in the system by changing the flow rate and thus can cause the pressure wave in the system. This is because gases are highly compressive fluids, and their pressures and velocities can change with time and position easily and thus the momentum of the fluid changes quickly. This phenomenon is called hydraulic shock (Zhukovskii, 1900[104]). For example, Zhang et al. (Zhang et al., 2020[105]) carried the research in the effects of instantaneous shut-in of high production gas well on fluid flow in tubing. They concluded that the higher the openness of the valve before closing,

the higher the pressure maximum value they can get after shutting down the well, but the smoother they can get in the pressure variation stage. And the larger the flow rate, the quicker the pressure wave dissipated across the system, and the more severe the pressure changing in the system. Back to the experiment works having done before, in several hundred seconds, the pressure wave may not disappear in the system, although their results seemingly showed the diffusion direction. Therefore, they did not mention whether this pressure change is caused by switching the valve and how they avoid it. Thirdly, the temperature of the gas would change when it flows through a valve or porous media under adiabatic condition. This is called Joule-Thomson effect (Marić, 2005[106]; Perry and Herrmann, 1935[107]). The sudden pressure change could cause temperature change, which could affect the pressure response at the two sides of the porous media. Fourthly, former experiments always used meshed samples or membrane to represent the porous media. This can only make sure the material was the same but not a real reservoir since it destroys the original pore structure. The tortuosity and the pore distribution are all different from the real condition. Therefore, the conclusion from these results may not apply in the reservoir condition.

In this thesis, we used cores from different sites to carry the experiment of countercurrent diffusion across the porous media (cores) with different types of gases. We want to explore over a longer time scale what will happen after the mass transfer is achieved and find out what is the dominant parameter during the process (gas type or characteristic of porous media). We observe the experiment for about 5 days on average, which is much longer compared to the previous membrane tests. We use a real core instead of membrane or crashed shale samples, which keeps the original pore structure and distribution and can reflect the real condition in the reservoir. Due to the limitation of equipment and the conditions in the lab, some of the parameters were not tested. And this will be presented in future work.

For the core we use, there are three aspects that are different from the setting before: length, pressure, and pore diameter. Let us briefly introduce their impact on the target observation.

For the impact of length in the Knudsen diffusion, let us consider if there is a thin board (the thickness can be negligible) separating the gas molecules into two different sides, and there is a small hole on it which is also small compared with the mean free path of a molecule, the net flux per unit area of this hole is dependent on the possibility of the molecules of the inner side escaping to the outside and the molecules of outside coming into the inner side. Since the board is very thin, as long as the molecules is moving towards the hole will pass through it, no matter it hits the edge of the hole or not, which means the ratio of the number of molecules successfully pass it to the number of molecules coming into it is 1. This ratio is called molecular flux effectiveness. However, if the thickness becomes larger, the molecular flux effectiveness would be less than 1. This is because some of the molecules coming into the "tunnel" would have a collision with the wall and bounce back to the inlet or getting trapped inside the tunnel. Furthermore, if the tunnel is longer and more tortuous, this phenomenon would be more obvious. The core itself is a complex combination of flowing tunnel system. Therefore, the real length the molecules fly through is not only the apparent length of the core, but also the tortuosity of the cores.

Now let us analyze the higher-pressure situation. If the pressure is higher for a Knudsen process, while keeping the pressure gradient constant, this means the length of the tunnel is larger. In this case, as we discussed before, the molecular flux effectiveness would decrease, since the mean free path of gas molecules decreases. At the same time, as more molecules are compressed into the same unit space, the chance of collision between molecules becomes higher, which could lead to the increase of molecular flux effectiveness and benefit Fick's diffusion. These contradictory effects should be combined into one harmonious process. According to Cunningham's book[133], as the pressure increase, the total flux is decreasing first, and then increase again.

In total, there are three kinds of flux inside the diffusion system: viscous flux, non-equimolar flux and the diffusive flux. If the system has no pressure difference, the viscous flux is zero. If the system has the same molecular mass in an arbitrary unit region, the non-equimolar flux is zero. If the composition of the system is the same everywhere, the diffusion flux is zero.

In Table 2, we can see most of the experiments are carried out under or near atmosphere (14.7 psi) to better observe the diffusion in the system, because diffusion is more obvious at low pressure conditions. We set the pressure at around 40 psi. Although this is not the reservoir condition, we just want to explore the things happening within lab conditions. And this is also limited by the equipment we have in the lab. If someone wants to explore the situation of Knudsen number at higher pressure, for example, 10 times or 100 times higher than the value used in our experiment, then the mean free path would decrease, and therefore, the Knudsen number will decrease. And there will be no diffusion in the system and it will gradually become Darcy's flow.

The pore size could affect the diffusion mechanism, too. If we keep the total pore space volume and the pore length constant. When the pore size is large enough to let the molecular diffusion happen, the diffusion flux is independent of the pore size. If the pore diameter is small or the pressure is low, the resistance created by the collision between gas molecules and pore walls would occur, which will cause the total flux to decrease. In Knudsen diffusion, the flux is positively proportional to the transport distance, and the Knudsen flux is positively proportional to the pore diameter. If the pore diameter further decreases, say, to the magnitude of molecule sizes, then the configurational diffusion is dominant.

1.3.3 The Organization of the Thesis

In the first chapter, we introduce the background and the meaning of the thesis and introduce some basic theory as we have known. The outstanding previous works are also presented. In chapter 2, we will introduce how we set the experiment and introduce through each setting and explain why we operate them in that way. In chapter 3, we will present all the results we have hitherto, and try to reveal the mechanism behind them. We will combine the wisdom of previous researchers and apply them in our results. In chapter 4, we will give conclusions about what we have in brief and

purpose what we need to do in the future.

2. Experiment Setting

2.1 Equipment Setting

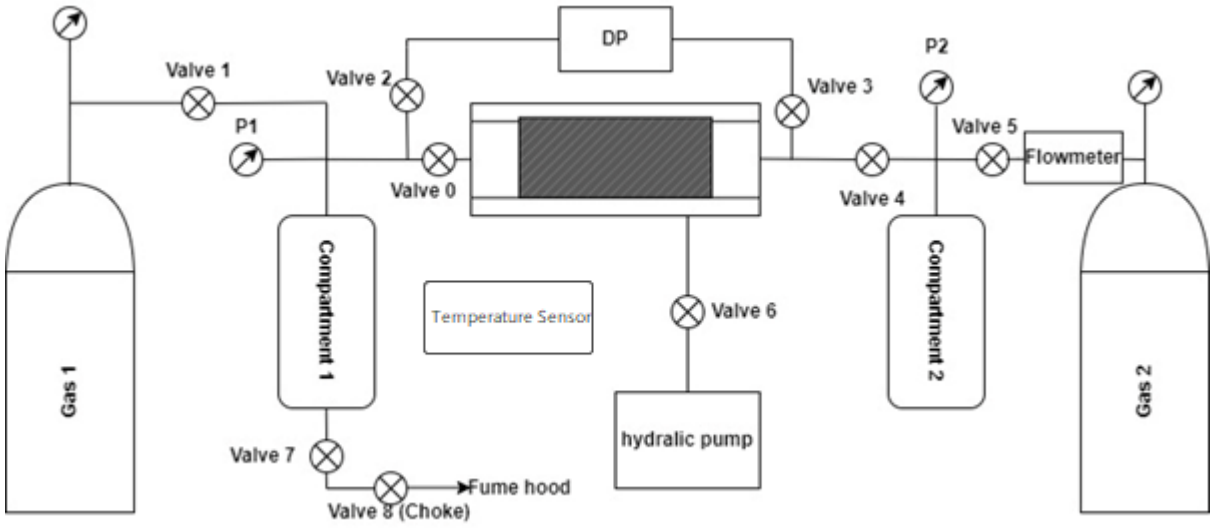

Figure 26 Schematic Setting of Pressure Response During Diffusion

The whole system consists of the following equipment: A 1.5-inch (3.81 cm, in the middle) in diameter Hassler core holder was used to hold the cores where the samples were wedged between the floating plugs attached to the core holder pore line inside a Viton sleeve. The core holder can withstand the maximum pressure up to 3000 psi. The overburden pressure was supplied by the Teledyne Isco, Inc, model 500 D syringe pump and their D-series pump controller. Two gas regulators were installed on each of the gas tanks being used. The gases tested were nitrogen, carbon dioxide and methane, which are supplied by Air Liquide Canada Inc. Their purity was over 99.9%. Two 75 cc stainless steel containers were used to mimic the compartments in Figure 21 mentioned by Santiago. Two pressure transducers were attached on each of the compartments, and whose measuring range is from -8.5 psi to 53 psi with accuracy 0.25%. There were 9 valves in the system. Valve 0 and Valve 7 were ball valves, to achieve the quick shut down or open the system

without delay. The rest were ordinary valves from Swagelok®. Valve 8 was used as a choke to prevent the pressure in compartment 1 decreasing to atmospheric pressure quickly. The openness of Valve 8 was very small. The ball valve structure was showing below:

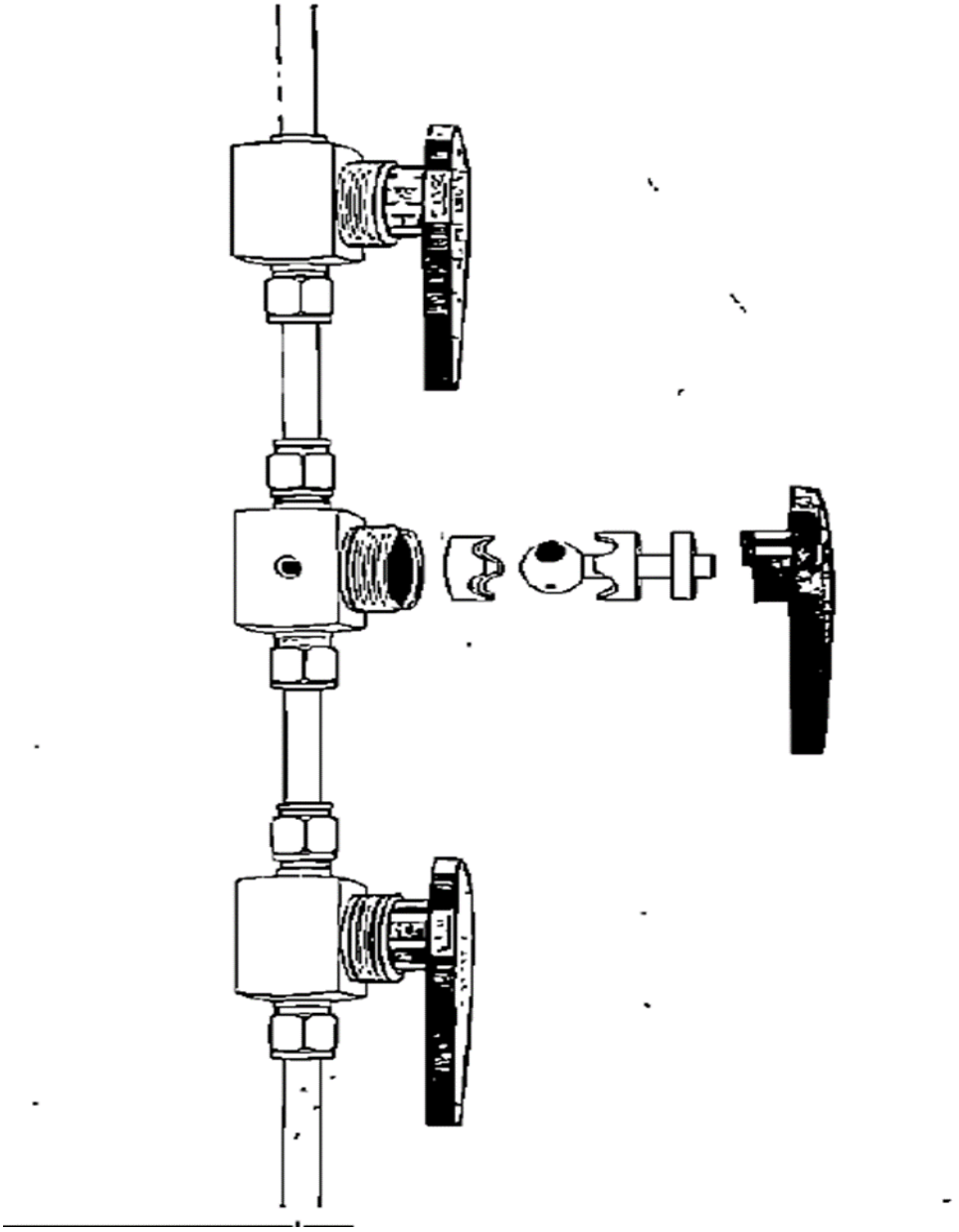

Figure 27 of Ball Valve Schematic (Sigmund, 1976[108])

The differential pressure transducer (Alphaline pressure transmitter) is placed to monitor the pressure difference at the two sides of the core. It can measure from -1.9 psi to 27 psig with accuracy 0.25% of the full range. The lines are 1/8-inch stainless steel 316. A flow meter supplied by OMEGA® Engineering INC. was used to measure the flow rate at gas 2 side. The measured range is 0-2 L/min (using nitrogen). There are also a vacuum pump and J-type temperature sensor. The temperature sensor is used to measure the room temperature and was connected to the computer directly. It was put beside the core holder. Its measure range is 0 to 482 Celsius degrees, with accuracy 0.75% The pressure and temperature data were recorded by "NI-data logger" application developed by PERM. Inc. All the sensors were calibrated based on the instruction provided by the supplier, and according to the ambient circumstances.

2.2 Experimental Conditions

2.2.1 General Setting

The temperature of carrying the experiments was 22-23°C in room temperature, no temperature control or preserve system applied. All the pressure was corrected to 24°C when processing the data to eliminate the impact of temperature based on ideal gas equation of state. To maximize the use of the range of pressure transducers, we set the experiment pressure at around 0.276 MPa (40 psi, gauge pressure). This is because the pressure difference caused by diffusion is too small to be caught at higher pressure by using larger range pressure transducers. And the pressures used by previous works were close to atmospheric pressure, which means the injection pressure should be around 0.1 MPa (14.7 psi).

2.2.2 Core Information

Two cores from different sites were used: Torrey Sandstone and Scioto Sandstone. The pictures

below show their size:

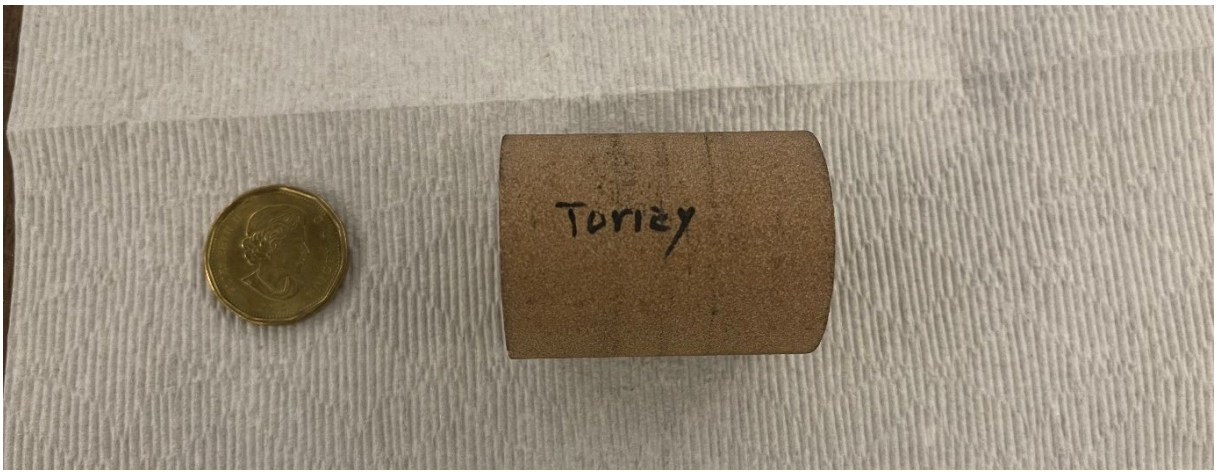

Figure 28 Torrey Sandstone

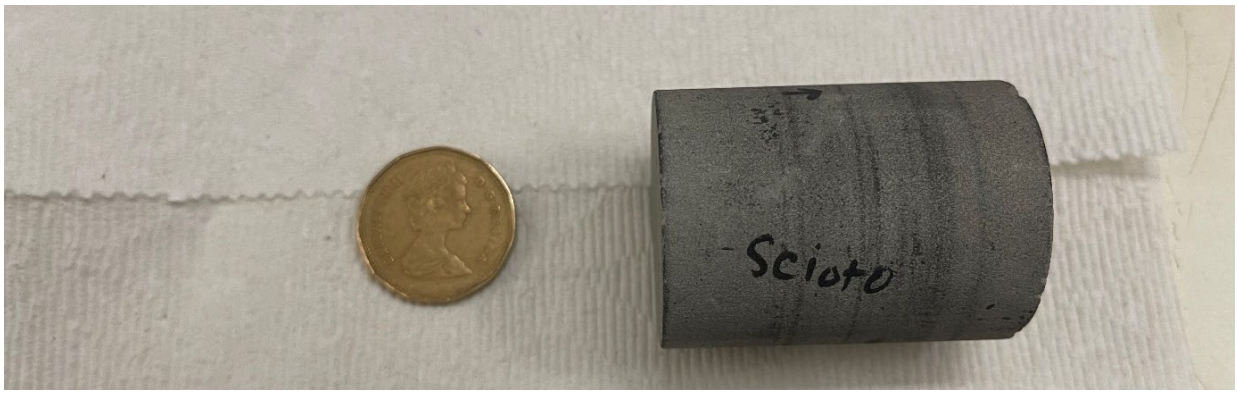

Figure 29 Scioto Sandstone

The core parameters can be summarized in the table following, supplied by PERM. Inc (except the pore radius):

Table 3 Core Information

Parameter	Torrey	Scioto
Length/ mm	50.8	50.82
Diameter/ mm	38.1	38.1
Weight/ g	125.84	126.08
Permeability/ mD	1.91	0.918
Porosity/%	16.62	18.22
Gas Slippage Factor b/ psi	14.16	15.790
Average Pore Radius/μm	0.30	0.20

The average pore radius is estimated by Depuit-Forchheimer equation which gives:

$$r = \sqrt{\frac{8K}{\varphi}} \tag{2.1}$$

Here K is permeability and φ is porosity.

One of the most important factors in petroleum engineering is permeability (Yang, 2018[109]). The permeability measured by gas is nearly the same as using liquid. However, due to the different characteristics of gases and liquids, we should modify Darcy's equation. With fixed pressure difference at two sides of the core, the flow rate should be constant at any intersecting surface (perpendicular to the flow direction). This is because the liquid is taken as incompressible under the lab conditions, especially at low pressure. But gases tell different stories. The volume of gas would change with pressure and temperature in a more drastic way than liquid. Therefore, from the higher-pressure side to the lower-pressure side, the pressure would decrease along this axial direction, which would cause the expanding of the gases and the difference between the inlet flow rate and the outlet flow rate. In this case we need to adopt the differential form of Darcy's Equation as:

$$K = -\frac{Q\mu}{A} \times \frac{dL}{dP} \tag{2.2}$$

Whereas K is the permeability of the core sample. Q is flow rate, which is a variable here when using gases. A is the area of cross section. L is the length in the axial direction. P is the pressure at the measure point. μ is the viscosity of gas. The negative sign here is to make sure the permeability is a positive value and means the pressure would decrease with the increase of the length at axial direction. If we take the flow regime in the core as steady flow, the mass flow rate at any cross-section is constant. According to Boyle's law, we have in ideal gases:

$$Q = \frac{Q_{atm}P_{atm}}{P} \tag{2.3}$$

Whereas Q_{atm} is the bulk flow rate at atmospheric pressure P_{atm}, P is pressure at any point in the system. Therefore, we have:

$$K = -\frac{Q_{atm}P_{atm}\mu}{A} \times \frac{dL}{PdP} \tag{2.4}$$

Then transform the equation and do the integral at both sides, we have:

$$\int_{P_2}^{P_1} KPdP = -\int_0^L \frac{Q_{atm}P_{atm}\mu}{A} dL \tag{2.5}$$

Here we change K to K_g, representing permeability measured by gas in Darcy, we have:

$$K_g = -\frac{2Q_{atm}P_{atm}\mu L}{A\left(P_1^2 - P_2^2\right)} \tag{2.6}$$

With this equation, we can calculate the permeability by using gases. But when we measure the permeability in the lab, things could be different. When adopting average pressure ($\frac{P_1+P_2}{2}$) in the same core, or under the same pressure difference but different gases, the apparent permeability value could vary. This is called the slippage effect. The viscous flow of liquid suggests that the viscosity of fluid would be constant regardless of the change of flow regime, which we can further conclude the velocity of the flow is 0 at the capillary wall. This is because the viscous resistance between solid and liquid is much higher than those between liquids. But the interaction between the gas and solid molecules is weaker than that between liquid and solid, which means that there are still some gas molecules moving at the near wall region. On the other hand, due to the momentum exchange between adjacent layers of gas, the gas molecules at the wall region are forced to move along the flow direction. This will lead to a higher flow rate, compared with liquid test, and thus higher permeability. Gas permeability is affected by many factors, such as gas molecular weight, average pressure, and the pore diameter of the core sample. In this case, we need to introduce Klinkenberg effect:

$$K_g = K_L\left(1 + \frac{b}{\overline{P}}\right) \tag{2.7}$$

Here K_L is liquid permeability in theory, sometimes it is called intrinsic permeability. $\overline{P}$ is the gas average pressure applying on the core which equals to $(P_1 + P_2)/2$. b is gas slippage factor, and its definition is:

$$b = \frac{4C\lambda P_{ave}}{r} \tag{2.8}$$

Here r is capillary radius. C is a constant that can be taken as 1. P_{ave} is average pore pressure. Notice here P_{ave} is different from $\overline{P}$. By definition, pore pressure is the pressure acting on the fluid in the pore space of the formation and is a function of depth. And gas average pressure $\overline{P}$ is the pressure calculation result of the average of inlet gas pressure and outlet gas pressure, which is related to gas. So, these two values are different. So, b is independent of gas pressure. λ is gas molecule mean free path under the corresponding average pressure, which can be defined as:

$$\lambda = \frac{RT}{\sqrt{2}\pi d^2 N_A \overline{P}} = \frac{\mu}{\overline{P}}\sqrt{\frac{\pi RT}{2M}} \tag{2.9}$$

Here R is molar gas constant. T is temperature in Kelvin. d is the diameter of the gas molecule. N_A is Avogadro's number. M is the molar mass of gas. Here λ is the function of average gas pressure.

The average pressure is actually the force on unit area of substance created by the hitting of gas molecules, which depends on the density and the momentum of gas molecules. From the previous equations we know the lower the average pressure, the lower the density of the gases, and the larger the mean free path is, which means the gas molecules are more movable and the slippage effect is more severe. On the other hand, if the average pressure goes to infinity, the permeability will not change any more. This is because the interaction between gases and solids is increasing a lot and the behavior of gas is close to the flow of liquid. Thus, the slippage effect disappears, and the permeability becomes constant.

In the case of the molecular mass and diameter, it will affect the mean free path. The lower the molecular mass, the shorter the diameter is, therefore the larger mean free path we can get. And we can get higher value of b, which means the slippage effect is much clearer. And we can easily figure out the smaller the capillary radius is, the higher the value of b is, and the more slippage effect it would have.

This would happen only when the order of mean free path of the gas molecules is closed or much larger than the pore diameter. Therefore, when using gases to measure the permeability of the porous, we need to make a correction on this value.

Li (Li, 2015[110]) proposed a permeability calculation model based on the Darcy's equation, slip effect and Knudsen diffusion. The equations are given by:

$$u = -\left(\frac{K_\infty}{\mu} + \frac{D_k}{p}\right)\nabla p \tag{2.10}$$

Here u is velocity. K_∞ is intrinsic permeability, or fluid permeability. μ is viscosity. D_k is diffusion coefficient given by $D_k = \frac{K_\infty b}{\mu}$. And p is pressure. After the combination of three mechanisms, we have:

$$Q_{sc} = \frac{T_{sc}Z_{sc}}{TZP_{sc}}\frac{\pi D^2}{4l}\left[D_d(P_i - P_a) + \frac{K_\infty}{\mu}(P_i^2 - P_a^2)\right] \tag{2.11}$$

Here Q_{sc} is volumetric velocity. T_{sc} is temperature at standard state (20°C). T is temperature. Z_{sc} is compressibility factor at standard state. Z is compressibility factor. P_{sc} is gas pressure at standard state. D is the diameter of the core and l is the length of the core. P_i is the inlet pressure. P_a is the outlet pressure.

Some scholars (Liu and Zhang, 2020[111]) found the Knudsen diffusion and the rock mechanical deformation can affect the permeability of the shale. They showed with fixed confining pressure, the permeability would decrease with the pore pressure first due to the Knudsen effect, and then increased again due to the deformation effect. But in the author's opinion (the author of this thesis), Klinkenberg effect may be a mistake. Since people often ignore the change of viscosity of gas in different pressure. The boundary layer theory indicates that the flowing speed of a solid in the gas phase has a limit, and vice versa for gas flow in solid. Therefore, the gas molecules having a non-zero speed at the solid surface is against fluid dynamics[148].

2.2.3 Gases

The characteristics of gases being tested in this experiment are methane, carbon dioxide and nitrogen. Some of their properties will be shown in the chart below:

Table 4 Gas Properties[139]

Gas	Methane	Nitrogen	Carbon Dioxide
Molecular Weight (g/mol)	16.043	28.013	44.010
Kinetic Diameter (nm)	0.38	0.364	0.33
Critical Temperature (K)	190.45	126.15	304.29
Critical Pressure (MPa)	4.5960	3.3999	7.3825
Boiling Point (K)	111.55	77.35	194.65

Dipole Moment (10^{-18}esu·cm)	0	0	0
Quadrupole Moment (10^{-26}esu·cm^2)	0	1.52	4.30
Polarity ($10^{-25}cm^3$)	26.0	17.6	26.5

The self-diffusion coefficient of the carbon dioxide is the largest among the carbon dioxide, nitrogen and methane, because of its strong adsorption capacity and the large molecular mass (Long et al., 2021[83]). Under the experiment conditions, all three gases should be in gas state.

The chart below will show binary diffusion coefficient calculation result based on the Bird et al. book. The temperature is set as room temperature, 300K. Pressure is set as the experiment pressure, 40 psi (2.72 atm).

Table 5 Binary Mixture Parameters[139]

Gas Couples	$D_{AB}(cm^2/s)$	$\sigma_{AB}(\dot{A})$	$\frac{\epsilon_{AB}}{k}(K)$
CH_4-CO_2	0.0614	3.888	165.982
N_2-CO_2	0.0559	3.8315	137.703

N_2-CH_4	0.0801	3.7235	120.295

By comparing the computation result with the experiment data carried by McGivern and Manion.[112], Piszko et al.[113], and Ellis and Holsen[114], the result is trustable and can be used to further analysis.

Huang et al. (Huang et al., 2020[115]) investigated the impact of diffusion on the methane flow in the shale gas in nanopores. In nanoscale or micro-scale pores, the diffusion coefficient of methane would increase with the pore size, which means the methane would diffuse faster in larger pores, but the contribution from diffusion would not change much. Once the pressure difference was introduced into the system, the dominate flow flux in the system converted from diffusion to convective, and the percentage of diffusion in the total flux decreased quickly.

Some scholars (Sander et al., 2020[116]; Long et al., 2021[83]; Liu et al., 2019[117]; Yu et al., 2018[118]; Cui et al., 2004[119]; Shi, 2021[120]) thought the difference between the diffusion coefficients of methane, carbon dioxide and nitrogen are caused by their difference in kinetic diameter, gas-solid behavior, and adsorption heat (enthalpy change). The adsorption heat can indirectly reflect the strength of the interaction between adsorbate and adsorbent. The higher the adsorption heat, the easier for the gas to be adsorbed. The kinetic diameter of carbon dioxide is smaller than that of methane and nitrogen, therefore its adsorption capability is higher than that of methane and nitrogen, and it has the largest diffusion coefficient among the three gases. The kinetic diameter of nitrogen is smaller than methane, but its adsorption capacity on shale is the least. So, in general the diffusion coefficient of nitrogen is smaller than that of methane. The sequence of the diffusion coefficient and the adsorption amount, from high to low, is carbon dioxide, methane, and nitrogen. The most adsorbable gas would quickly diffuse into the shale matrix and was greatly adsorbed, which increases the adsorption rate.

Methane plays an important part in both single gas diffusion and multicomponent diffusion. It is the main component of shale gas. The diffusion coefficient of methane is related to the pore pressure and the pore structure. As the effective stress increases, the diameter of diffusion tunnel for methane decreases. The pressure effect will finally overcome the stress effect and increase the gas production. Under a different pressure level, from atmosphere to in-situ reservoir pressure, as the methane fraction decreases in the mixture of gases, the conductivities of different flow patterns always increase. In a dry shale core, if the pressure goes up, the methane diffusion coefficient would increase too. Fick's diffusion tends to appear in the macropores, and Knudsen diffusion tends to play a more important role in micropores (Sun et al., 2019[121]; Yuan et al., 2014[122]).

Dang (Dang, 2018[123]) built a model for the methane adsorption and diffusion in shale matrix and developed a series of experiments to explore the pore structure and the pressure impact on the adsorption and diffusion process, which means the effective diffusion coefficient of methane would decrease with the increasing of the adsorption amount of methane in the matrix. They found the pore structure is dynamically changing with the adsorption process. The more the methane molecules adsorbed on the organic matter, the less free space left for the other molecules to diffuse, therefore, it is harder for the methane to diffuse further. At the same time, the concentration gradient between shale matrix and its surface is decreasing due to the adsorption, which lowers the driving force based on concentration difference. Under lower pressure conditions, the major adsorption contributor was macro-pores. Under middle pressure level, both the micro pores and macro-pores contribute to the adsorption. Under higher pressure circumstances, micro-pores contribute more to the adsorption. They also built the relationship between adsorption capacity and effective diffusion coefficient under the impact of pressure and sale matrix, which shows the higher the pressure is, the lower the effective diffusion coefficient is. At the same time, the components made up of matrix can greatly affect the diffusion due to its impact on the pore geometry. The pore sizes have positive contribution to the effective diffusion coefficient. Meanwhile, they found the relationship between the diffusion coefficient and the clay mineral content – the higher the content is, the higher the diffusion coefficient. This is because the total volume of micro-pores would

increase and thus connect to each other, which lowers the resistance of the diffusion.

2.3 Experiment Procedure

Before carrying out the experiments, the two cores are placed in an oven with the temperature at 65 Celsius degrees to remove all the moisture inside the core. This heating process is usually longer than one week. Before carrying the experiments, we weigh the core and then put it into oven again and wait for 1 hour and weigh again to confirm the moisture has been moved, if the core weight doesn't change anymore. While we used one of the cores to do the experiment, we left the other one in the oven. After loading the core, the experiments began. Since we do not have needle valve in the lab, we used an ordinary valve and opened it to a very small level to act as a choke in the system (Valve 8) and left it in position for the entire experiment. For all experiments, we did not change the position of Valve 8 to keep the flow rate in the system consistent (please see Appendix, part A). The pressure and temperature data were recorded on a computer as needed. There were totally three kinds of experiments carried. We will introduce the most important, binary countercurrent diffusion first, and then two basic control experiments. The procedures are shown below:

I. Load the core into the core holder. Open Valve 6. Inject the fluid into the sleeve at 2000 psi. Notice the sleeve is just holding the core and apply the overburden pressure (2000 psi) without any fluid touching the core. Valve 6 will always open until the experiment is finished.

II. Use the vacuum pump to vacuum the whole system. At this time, Valve 1, Valve 5 are closed. All other valves are opened. The vacuum pump is attached near valve 8. The Gas cylinders are disconnected from the system at this time.

III. Close vacuum pump. Close Valve 7. Connect the two gas tanks to the system.

IV. Open gas regulator of Gas 2 tank. Open Valve 5. Let Gas 2 flow into Compartment 2. Then open Valve 4 and Valve 0. Let the gas touch the core and flow into Compartment 1. Then fully open Valve 7 finally. Since there is a choke in the system (Valve 8), the pressure in Compartment 1 would not decrease to atmospheric pressure. Apply Snoop at each connection and across the lines.

V. Let the gas flood the system for 3 to 5 minutes by setting the pressure regulator of Gas 2 tank at about 42 psi or higher. Then we open Valve 2 and Valve 3 to connect the differential pressure transducer into the system and measure the pressure difference across the core. Then let the Gas 2 flood the system for at least 24 hours. Since there will be pressure decreasing along the flow direction, we try to let the pressure in Compartment 2 higher than 40 psi and the pressure in Compartment 1 lower than 40 psi to make sure the system pressure will fall to around 40 psi after closing the connection with the outside in step VI. During this process, the pressure in both Compartment 1 and Compartment 2 as well as the DP pressure are recorded as P1 and P2 every 180 seconds. The flow rate read by flow meter is used to calculate the permeability.

VI. After flooding the system for 24 hours, close Valve 5 and Valve 7. Close gas regulator on Gas 2. Let the system become equilibrium (no pressure change after temperature correction) and wait for 24 hours. Record the system pressure as $P_{standard}$.

VII. After 24 hours, close Valve 2 and Valve 0. Open Valve 7 to release the Gas 2 in Compartment 1.

VIII. Vacuum Compartment 1 for 2-4 hours. Then close Valve 7.

IX. Open gas regulator on Gas 1 tank. Open valve 1. Let Gas 1 flow into Compartment 1. Then open Valve 7 to flood Compartment 1 with Gas 1 at pressure as $P_{standard}$.

X. Open Valve 2. Confirm the pressure difference at the two sides of the core equals zero.

XI. Open Valve 0. Take this time as time 0. Record the pressure change in two compartments

(measured by two pressure transducer) as well as the pressure difference measured by differential pressure transducer (DP) every 30 seconds for 1 day. Then record the data every 180 seconds for four to five days (To make sure the computer had enough memory to record the data, we could record the data too frequently. To record the pressure change in short time, we cannot choose a too low frequency to record the data. Therefore, every 180 seconds was chosen as the recording frequency).

XII. When finishing the experiment, release all the gas in the system into the fume hood. Close all the valves after finishing releasing the gas.

In brief, we have two different gases in the system, Gas 1 in Compartment 1, and Gas 2 in the core and Compartment 2, with the same pressure. Gas 1 is always circulating. Gas 2 occupies a fixed volume and cannot get supplement from gas tank. At time 0, we open Valve 0 to let the two gases contact each other. The contact started at Valve 0 as well as the diffusion, and through the core until Compartment 2. Since there is no pressure difference at first, the countercurrent diffusion exists in the system. And then other mechanisms may occur in the system as well.

To prove the pressure response is due to the core, we set two control experiments. One is “coupled gas without core experiment” and another one is “single gas circulation with core.” We introduce “without core experiment” first:

I. Detach two compartments from the system. Keep the choke and the pressure transducers on them. Vacuum them for around 4 hours. Notice here the two compartments were connected to each other directly, with no core holder in between them.

II. Connect two compartments with a line and a valve. Inject Gas 2 into both the compartments, with the valve open. The pressure is setting close to 40 psi.

III. Close the valve between them. Release Gas 2 in Compartment 1. Then vacuum Compartment

1 for 2 hours.

IV. Inject Gas 1 into Compartment 1 after vacuum. Let the pressure inside it close to 40 psi, or as close as to Compartment 2.

V. Open the valve between them. Record the pressure data every second for 3-5 minutes. Then record the pressure data every 180 seconds. Notice here, there was only a tube (about 30 cm in length) connecting two compartments, without core holder.

VI. When the experiment is finished, release all the gas and close all the valves.

Now we introduce "single gas circulation with core."

The first three steps are the same as in the binary diffusion experiment. We use only Gas 1 and inject it into the system. At this time, Valve 5 is closed, and all other valves are opened. After the system becomes stable, we close Valve 0 for a while, up to 4 to 5 hours. Then open valve 0 again and continue the experiment for about 24 hours.

Note that the calibration of the two pressure transducers on the two compartments is not the same. Therefore, even in equilibrium state, they will show different numbers on the screen. Differential pressure is more accurate. Therefore, if we want to use the pressure difference data, we should take the data from DP. If we want to look at the pressure change on a single side, the pressure transducers are trustable. Another thing is we do not have available gas chromatography in the lab. For the gas mixture in the compartment, we can use gas chromatography to detect the components and their ratios inside the volume. Therefore, we tried to analysis the ratio of different gases based on the knowledge of physical chemistry (Perrot, 2008[126]; Holman, 1988[127]; Levine, 2017[128]). According to Dalton's law of partial pressures, the pressure of a mixture of non-reactive ideal gases can be defined as:

$$P_{total} = \sum_{i=1}^{n} P_i = P_1 + P_2 + P_3 + \cdots + P_n \quad (2.12)$$

Where P_1, P_2, …, P_n is the partial pressure of each component. And we have:

$$P_i = P_{total} x_i \tag{2.13}$$

x_i is the mole fraction of the i_{th} component in the total mixture of n components.

Now we know the total pressure of gas mixture in the compartment, the temperature, and gas types. Assuming there are all ideal gases in the system. According to ideal gas equation of state, we have:

$$PV = \frac{m}{M} RT \tag{2.14}$$

M is the molar mass of gas; m is gas mass. T is temperature in Kelvin. R is the ideal gas constant. P is pressure. V is volume. Since all the gases in the compartment have the same temperature and volume, we can further write the ideal gas EOS as:

$$P_{total} = \frac{m_{total}}{M_{total}} RT \tag{2.15}$$

If we have two kinds of gases in the system, we have:

$$P_1 = \frac{m_1}{M_1} RT \tag{2.16}$$

$$P_2 = \frac{m_2}{M_2} RT \tag{2.17}$$

For example, if there are methane (gas 1) and nitrogen (gas 2) in the system, then M_1 is 16, and M_2 is 28. And $P_1 + P_2 = P_{total}$, for example, 40 psi. And then we have:

$$\frac{m_1}{16} RT + \frac{m_2}{28} RT = P_{total} V \tag{2.18}$$

The ratio of m_1 to m_2 then can be known. The general form is:

$$\frac{m_1}{M_1}RT + \frac{m_2}{M_2}RT = P_{total}V \tag{2.19}$$

3. Results and Discussion

3.1 Air Tightness Test

The air tightness test is performed in each single experiment. After saturating the system with one type of gas and closing the inlet and outlet, the system is disconnected from outside. If there is leakage, the pressure of the system would decrease with time after closing the gas source. We chose one of the experiments to show there is no leakage in the system. In the following picture, nitrogen was injected into the Scioto core system. The picture shows the pressure measured by two pressure transducers at two compartments.

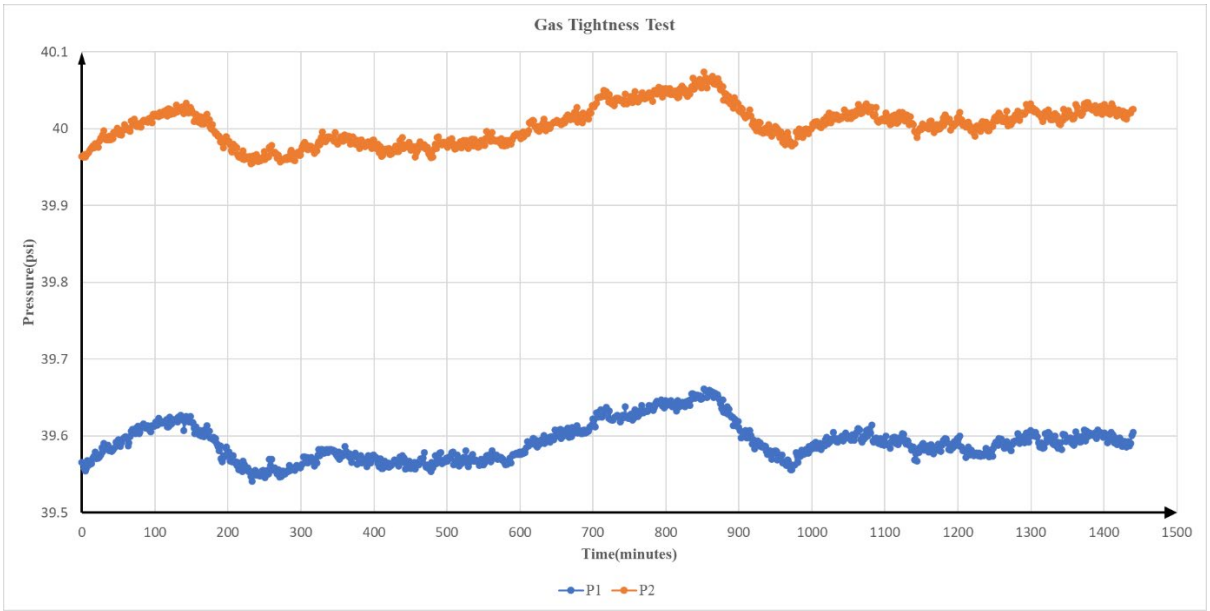

Figure 30 Air Tightness Test

From Figure 30, we can see during the equilibrium stage, the pressure is fluctuating but not decreasing. P1 means the pressure measured at Compartment 1. P2 means pressure measured at Compartment 2. All the pressure data are corrected to 24 degrees Celsius. We cannot exclude the

possibility caused by transducers themselves in the fluctuation in low frequency scale (from 0 to 4 hours, and from 10 to 16 hours), since it showed a 0.1 psi pressure change, although 0.1 psi is small compared to the measure range (the accuracy is 0.125 psi). Therefore, we suppose the fluctuation is related to the transducers, which should be taken as noise. The variation in about 24 hours is very small and doesn't show a trend consistent with a leak in the system. The fluctuation from 0-200 minutes and from 600-950 minutes are small compared to most of the trends observed in the core tests. And here the system can be considered as airtight. This will also show any pressure change, no matter whether it is increasing or decreasing, is due to something else other than the leakage itself. In theory, the two measured pressures should be the same. But the calibration of two pressure transducers is different. Therefore, they are separated on the graph. Later this pressure difference caused by calibration of the pressure would be reduced as much as possible. Here we present it to show the stability of the system when no material flows in or out. The pressure vibrations from 0 to 240 minutes and 600 to 900 minutes are probably due to the transducers.

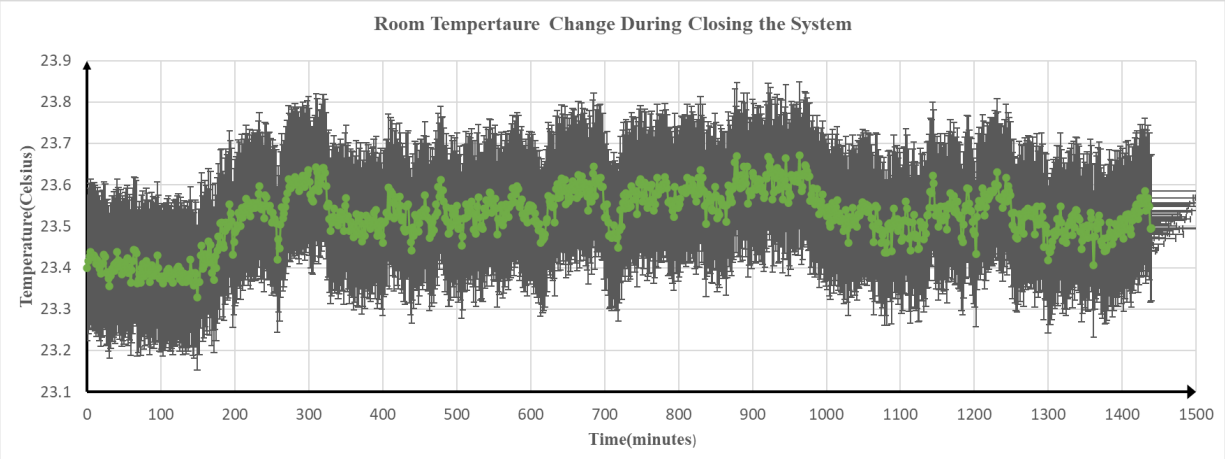

Figure 31 Temperature Change During Gas Tightness Test

The room temperature figure gives a supplement material to illustrate the pressure change in Figure 30 was not the cause of the temperature change. For example, from 600 to 850 minutes, the

temperature was basically stable, but the pressure had 0.1 psi buildup. This indicated that the pressure fluctuation had no relation with the temperature. The grey region represented error bar with 0.75%.

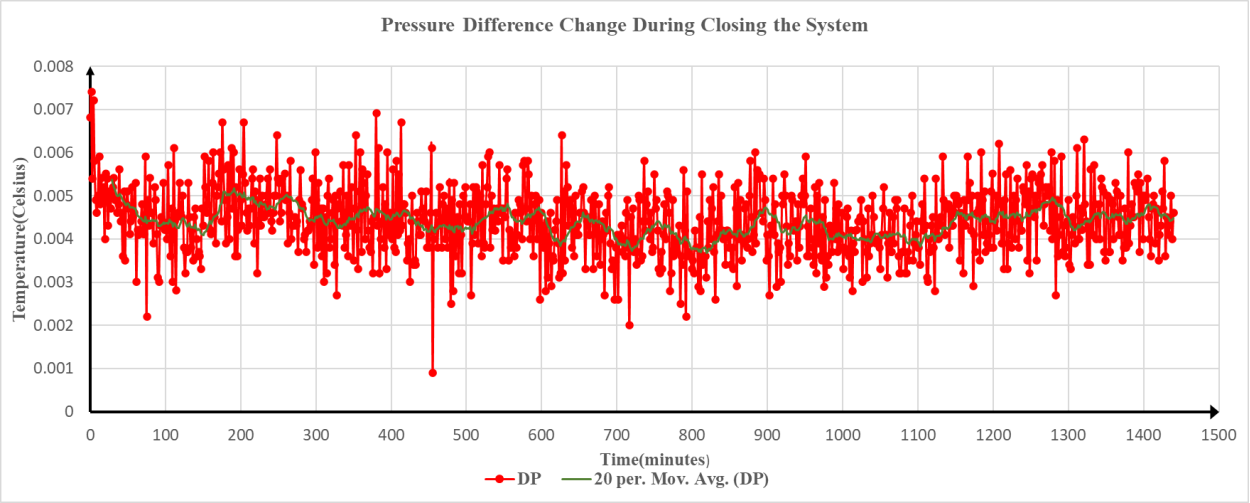

Figure 32 Pressure Difference Change During Closing the System

The pressure difference measured by the differential pressure transducer shows there was no severe pressure fluctuation during the time after closing system. This will eliminate the temperature effect on the pressure. The pressure difference varied within 0.001 psi, which is 0.003% of the whole measure range, and the fluctuation can be taken as noise here. The good sealing of the system is again proved. Generally speaking, the bumps shown in Figure 30 can be taken as noise.

3.2 Single Gas Test with Cores

3.2.1 Nitrogen Test

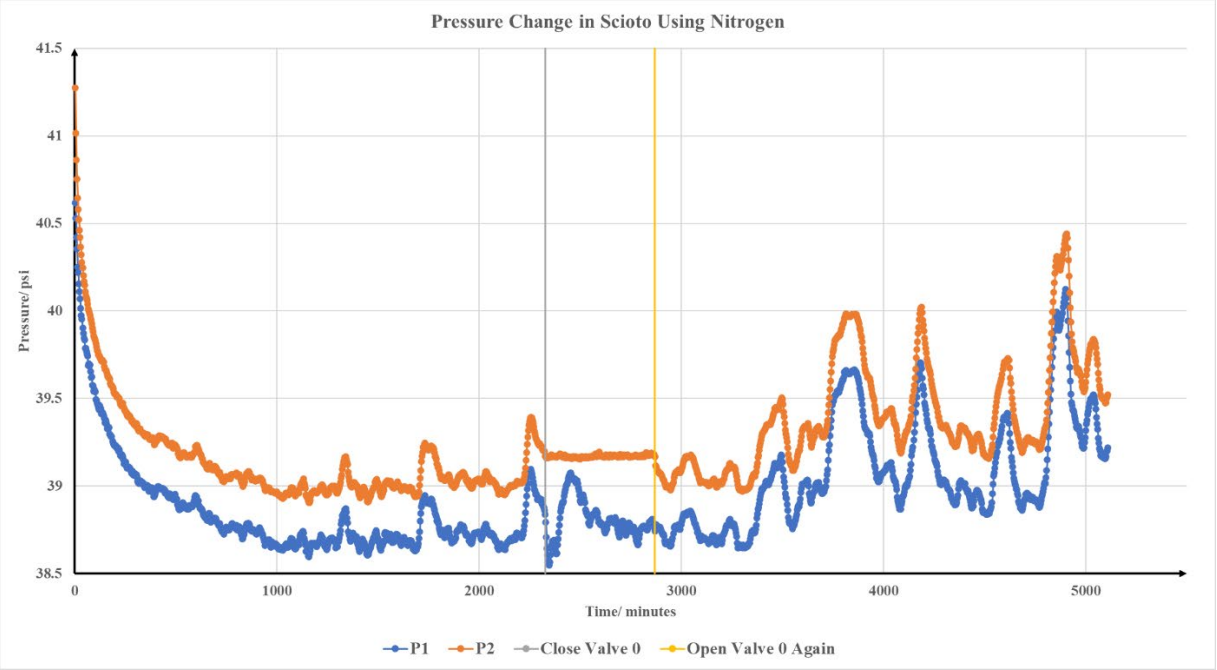

Figure 33 Pressure Change in Scioto Sandstone Using Nitrogen

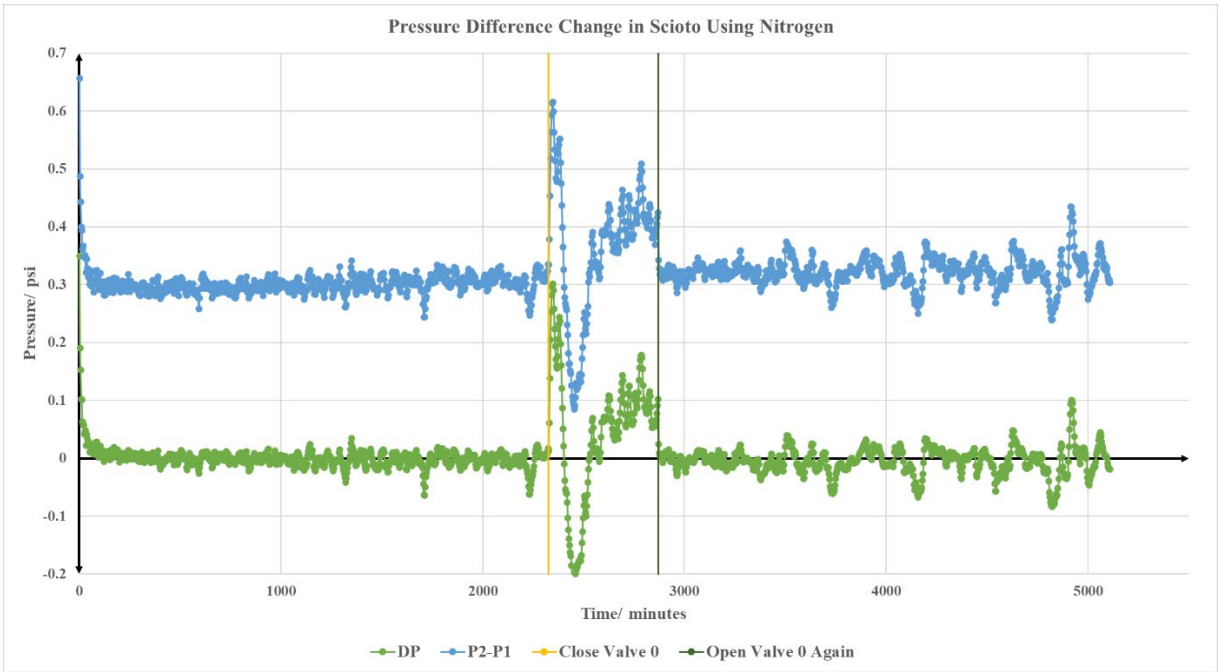

Figure 34 Pressure Difference Change in Scioto Sandstone Using Nitrogen

Here DP is the pressure difference, which is the pressure at the right-hand side of the core minus that at the left-hand side, measured by the differential pressure transducer. This is different from (P2-P1), since what we have mentioned before, the calibrations of the two pressure transducers are not the same. Therefore, the calculation of (P2-P1) is not zero when the system becomes stable. As can be seen in Figure 34, the blue line represents the (P2-P1). It becomes stable at 0.3 psi. This means the difference between the calibrations of two pressure transducers is 0.3 psi. This has also been proven in Figure 33. And this could not be a hysteresis effect, because the pressure data still shows 0.3 psi when we close all the valve and keep the gas in the system. In Figure 33 and 34, we closed Valve 0 for about 500 minutes. During the shutdown, the circulation side is still full of nitrogen and continuously flooding Compartment 1 with nitrogen. Therefore, the pressure in the core and Compartment 2 in this period is constant. If we compared Figure 33 with Figure 30 (data measured by pressure transducers on compartments) and compared Figure 34 with Figure 32 (data

measured by differential pressure transducer), we could find the pressure difference in Figure 32 and 34 both did not have severe fluctuation. Since in Figure 32, it shows a closed system without pressure or substance exchange with outside. Therefore, when there was no gas flow in the system, it will balance the pressure inside itself and had pressure equilibrium everywhere in the system in the end. And in Figure 34, when the flow is stable in the system, the pressure inside the core and Compartment 2 should have the same pressure as Compartment 1, which means the pressure difference between the two sides of the core was also zero. But the pressure fluctuation measured by pressure transducers could be different. First, Figure 30 shows a pressure change in a closed system. Without much temperature change or material exchange with outside, the pressure should be stable. Therefore, we suspect the pressure fluctuation in Figure 30 may be caused by the transducers themselves. But in Figure 33, the pressure transducers were measuring a flowing system, and with the water level in the beaker continuously changing, it will have an impact on the system pressure definitely. Therefore, the fluctuation in Figure 33 was much more severe than in Figure 30. The flat line in Figure 33, from 2400 minutes to 2900 minutes of P2 change, also proved the good air tightness of the system. But the pressure in Compartment 1 is still slowly decreasing, which causes the pressure difference to increase in Figure 34. And when we open valve again, we connect the core with Compartment 1 again, the pressure in the core and Compartment 2 will decrease quickly due to the pressure gradient and the convection following. At the same time, the pressure in Compartment 1 will increase quickly and then decrease. Finally, they have the same pressure again. This process is shown more clearly in Figure 34. As we can see from Figure 33 and 34, at the very beginning, the pressure difference decreased from 0.4 psi to 0 psi in about 100 minutes from time 0, but the pressure in two sides did not become stable until around 1000 minutes. The decreasing trend before 1000 minutes is explained in the appendix, due to the unsteady flow in the system. The gas flows through Compartment 1 under pressure gradient. But before the pressure gradient is established, the gas flow through the choke (Valve 8) will expand its volume and cause a pressure decrease. After the pressure gradient is stable, the flow becomes viscous flow. We also find the pressure difference (reach to 0 psi in 100 minutes in Figure 34) is established

faster than the pressure itself (the slope comes to nearly zero at 1000 minutes in Figure 33). The actual pressure difference measured by the differential pressure transducer (DP) shows zero in most time, which means for single gas separated by the porous medium, there is no diffusion flux between them. There is a significant transient at t = 0, and that analysis of the coupled gas experiments will be attempted for times after the transient has become small compared to the trends induced by diffusion. This will be shown later in part 3.4.

The pressure fluctuation after 1000 minutes in P1 & P2 in Figure 33 is due to the additional part between Valve 8 (choke) and the fume hood. There is a beaker with water in it at this part. A plastic tube after Valve was put into the water in the beaker to see whether there was gas flowing out or not. Sometimes, the tube was put deep into the water (about 3-4 cm). This means the outlet pressure is not exactly the atmosphere pressure but adding the water pressure of that height. Since the beaker is close to fume hood, the water in it continuously evaporates. In this case, the water level is decreasing, and the pressure measured by pressure transducer is not stable. And during the experiment, the water will be added to the beaker, therefore the water level was always changing. But this will not affect the general trend of the pressure decreasing. However, the water at the outlet does not seem to affect the pressure in the two compartments, as can be seen in Figure 33.

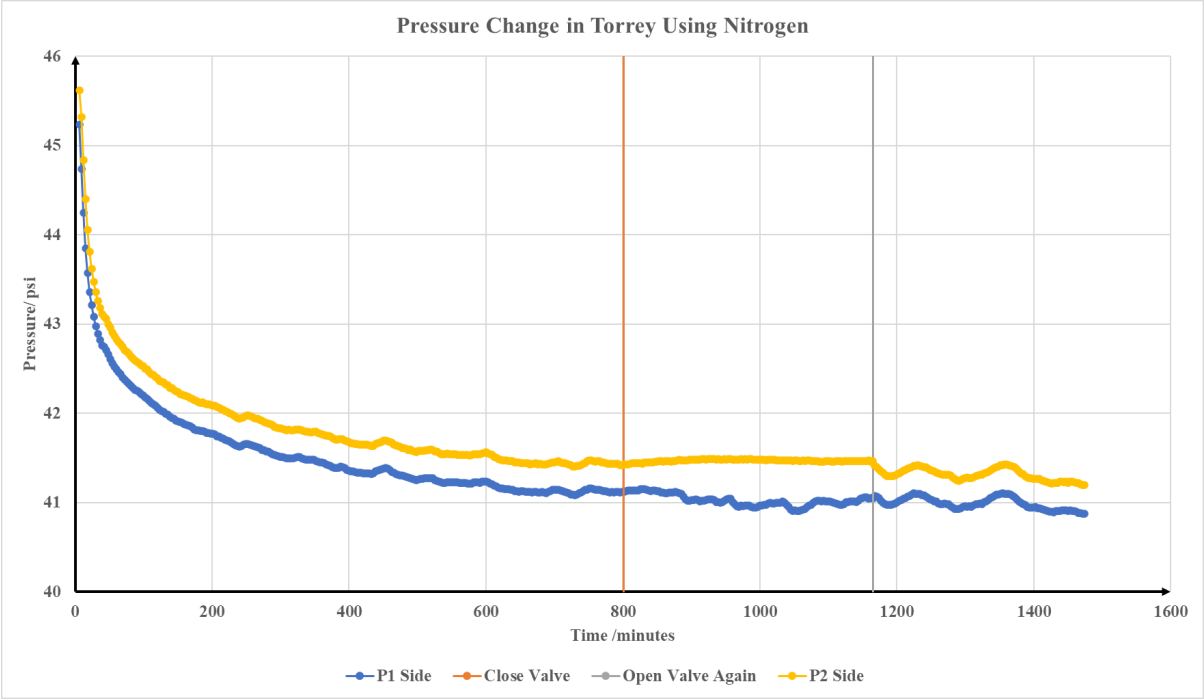

Figure 35 Pressure Change in Torrey Sandstone Using Nitrogen

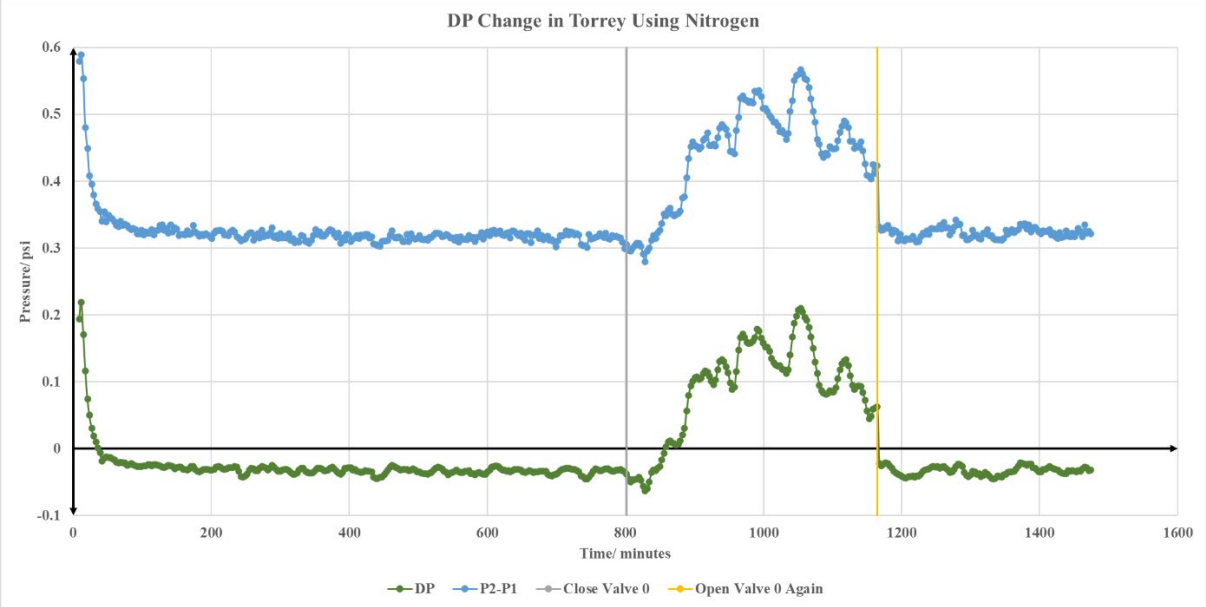

Figure 36 Pressure Difference Change in Torrey Sandstone Using Nitrogen

From Figures 35 and 36, we find the steady state (When DP comes to zero and the slope of pressure comes to or near zero) established in Torrey Sandstone is earlier than that in Scioto Sandstone. This is because Torrey Sandstone has larger permeability, which is a positive contribution to the establishing of steady state. The reason why the green line (showing DP values) here is not zero is due to the calibration of differential pressure transducer. It will show a small value even if there is no pressure difference. This small difference will be eliminated in later experiments.

3.2.2 Carbon Dioxide Test

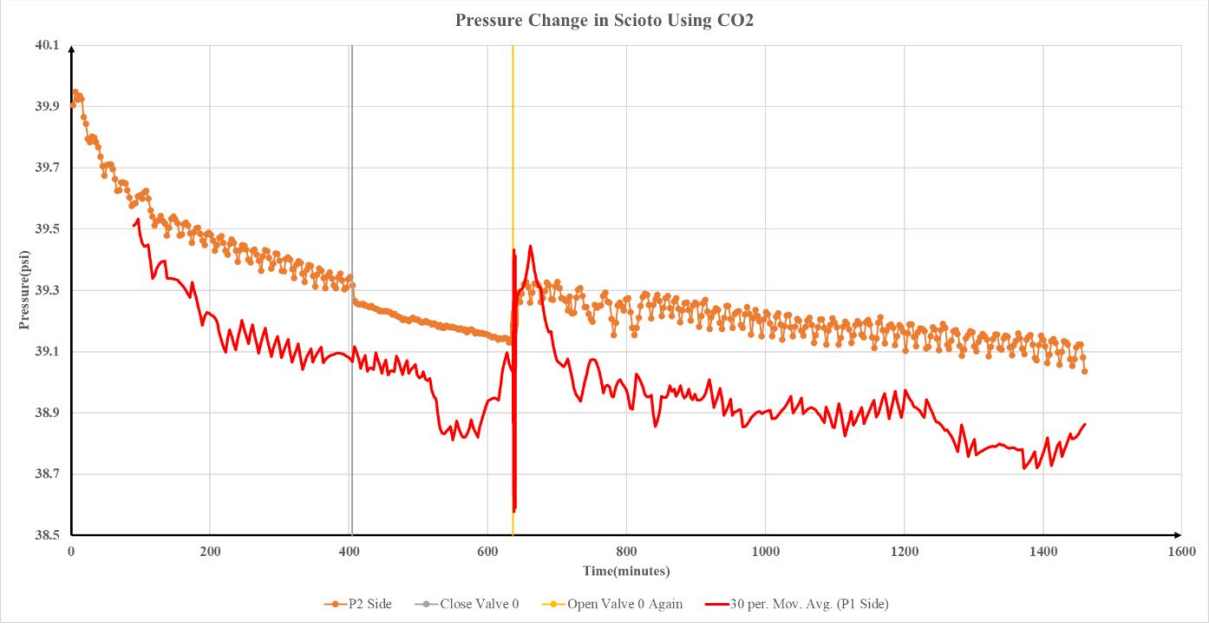

Figure 37 Pressure Change in Scioto Sandstone Using CO_2

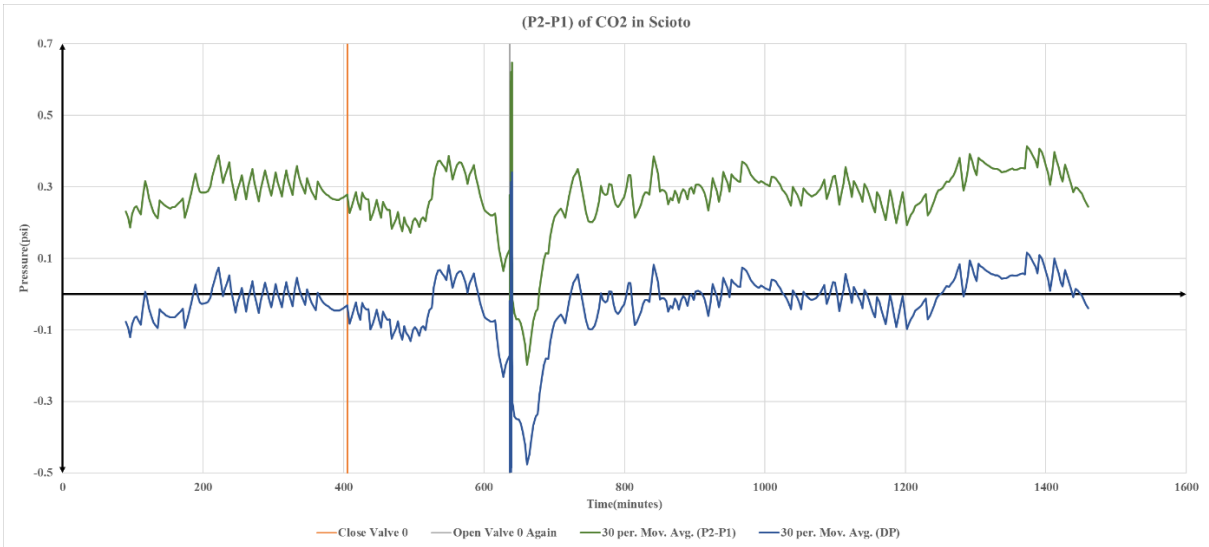

Figure 38 Pressure Difference Change in Scioto Sandstone Using CO_2

When comes to carbon dioxide, things become a little different. The fluctuation in this test (actually, all tests using carbon dioxide as displacing gas) is much more severe than other experiments. The Joule-Thomson effect[149] and hydraulic shock may cause the fluctuation when injecting gas into the system and after opening the valve again, since the compressed gas going through a narrow nozzle and the pressure changed suddenly, the temperature change will cause pressure change in a short time. Under 293.15K, 101.325 KPa, the Joule-Thomson coefficient of carbon dioxide is 10.9055 K/MPa. Under 293.15 K, 2026.5 kPa, the Joule-Thomson coefficient of carbon dioxide is 11.2065 K/MPa. If we take 11 K/MPa as the Joule-Thomson coefficient at 295.15 K, 275.79 kPa (40 psi), as per 0.6 psi (0.004 MPa) pressure drop, we will get 0.045 K temperature drop. This is plausible in theory. What we observed from the pressure gauge on the CO_2 gas tank is that once the pressure regulator was opened and set to a fixed value, say, 40 psi, it will have a vibration around one psi about every half minute, regardless of attaching the gas tank to any other devices. It means the pressure on the gauge would vary between 40.3 psi (or higher) to 39 psi (or lower) in one cycle. When reaching the minimum point, say, 39 psi, it will go back to 40.3 psi in the next

cycle again. This vibration always occurs when using CO_2 as a displacing gas and does not happen in other gas tanks. Later figures will also present this phenomenon. To prevent the scattering point being spread in the whole picture, we will take the moving average of the CO_2 pressure data.

Due to the feature mentioned above about the CO_2 gas tank, it resembles a huff-n-puff process. Just like nitrogen flooding mentioned in section 3.2.1, the general trend of carbon dioxide in the system is decreasing with time due to the unsteady flow. During the shutdown period of closing valve 0, we see the pressure in Compartment 2 is still decreasing. This decrease can be taken as the CO_2 is adsorbing onto the pore wall and the carbon dioxide in the bulk phase would convert into adsorbed phase. In Figure 38, we can see that from around 100 minutes to 400 minutes, the average pressure difference is basically steady. After opening the valve again at around 640 minutes, the pressure difference takes around 100 minutes to become steady again.

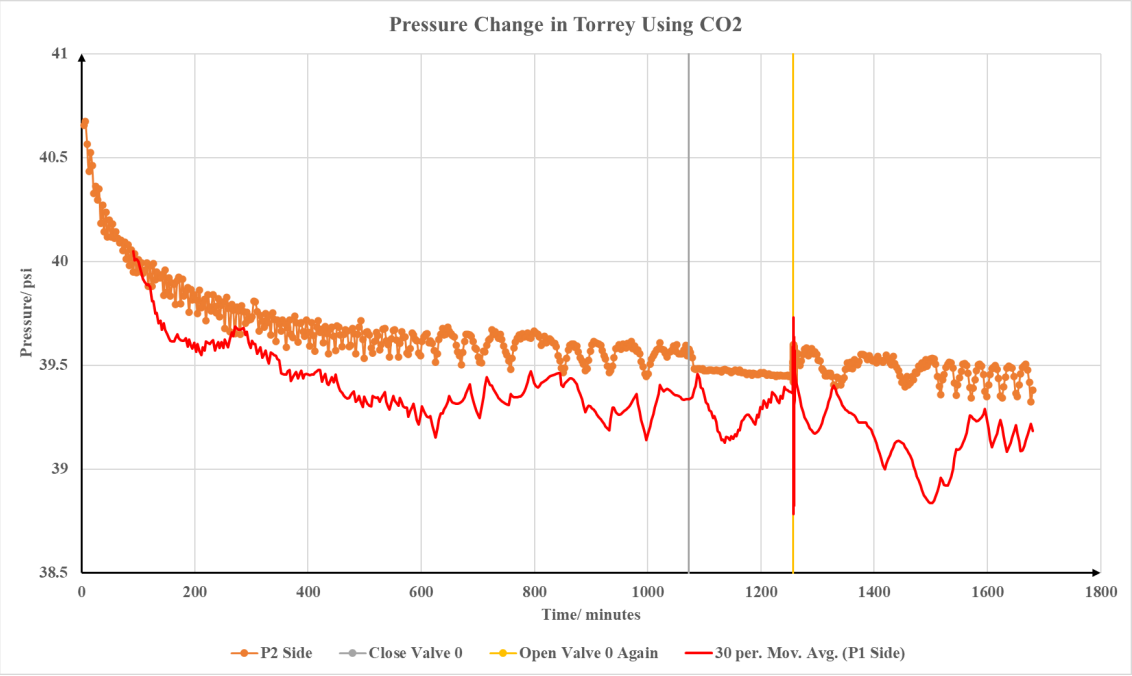

Figure 39 Pressure Change in Torrey Sandstone Using CO_2

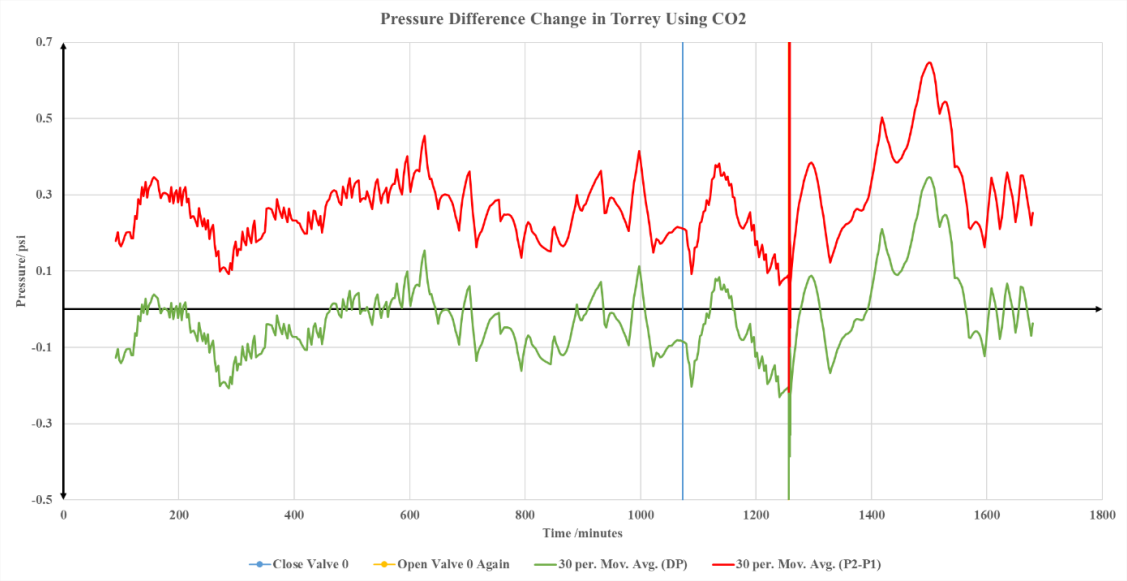

Figure 40 Pressure Difference Change in Torrey Sandstone Using CO_2

The general trend in Figures 39 and 40 are similar to those of Figures 37 and 38. And the pressure decreasing trend in Torrey Sandstone becomes steady faster than in Scioto. This is also caused by the higher permeability of Torrey Sandstone. The only difference is the period after opening valve again. At the moment of opening the valve again, in both Figure 37 and Figure 39 we have observed the pressure increasing in P1 side and pressure decreasing in P2 side. But after that, in Scioto Sandstone, we observed the pressure in P1 have a sharp increase, whereas in Torrey we observed a decrease in P1. For this phenomenon, one reason is that the pressure regulator may lose its accuracy after using it for a long time. Another reason is the smaller permeability core, Scioto, has more microscale or nanoscale pores. These pores have a larger specific surface area and can absorb more CO_2 on them. Thus, when the pressure decreases, more adsorbed carbon dioxide will be released from the pore wall and contribute to the flux in the pores, thus we can see a higher increase in the Scioto core. But the decrease in Torrey is not well understood. We speculate that this is a pressure regulator issue at the moment. The fluctuation in moving average curves is the result of the periodical behavior of the gas regulator. Since the periodical behavior does not strictly follow

the 30 seconds fixed frequency, there would be fluctuation even with moving average.

3.2.3 Methane Test

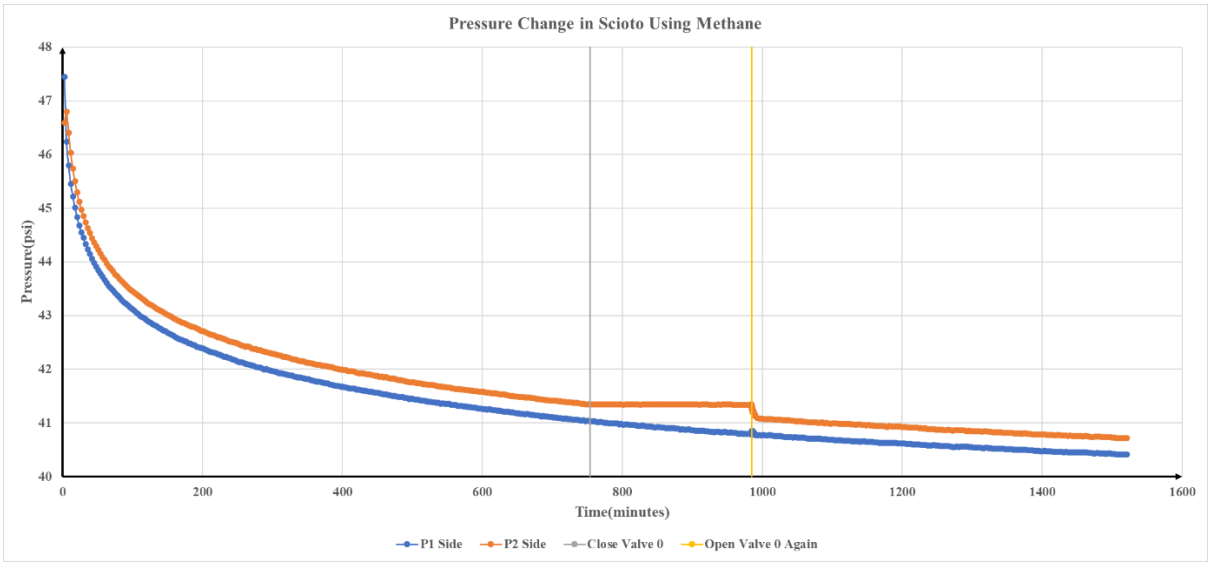

Figure 41 Pressure Change in Scioto Sandstone Using Methane

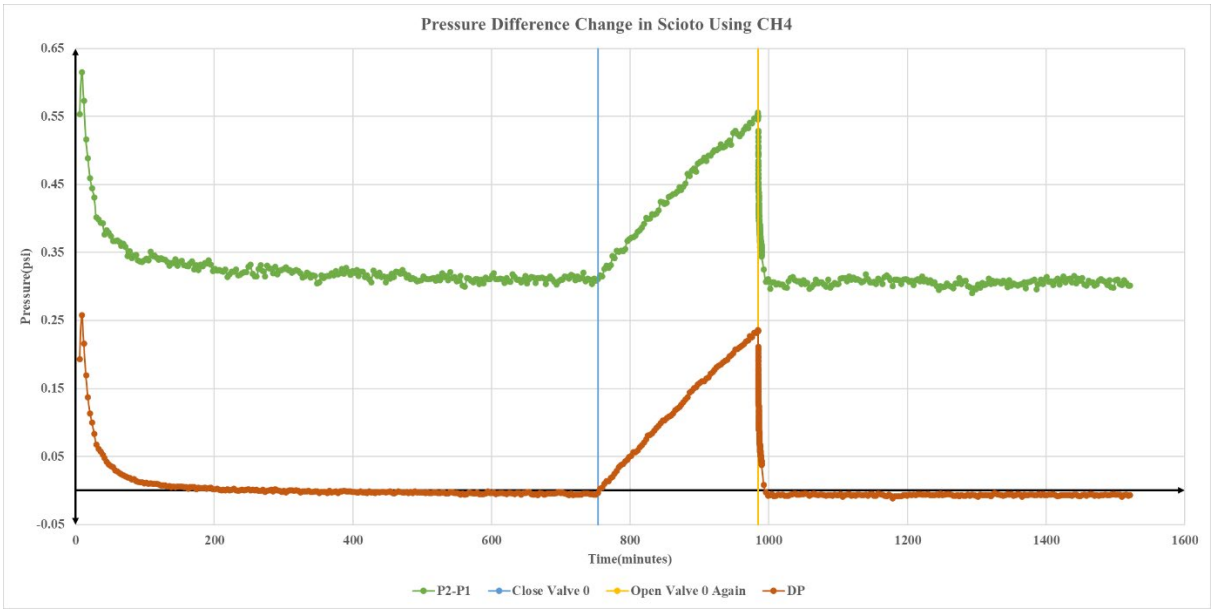

Figure 42 Pressure Difference Change in Scioto Sandstone Using Methane

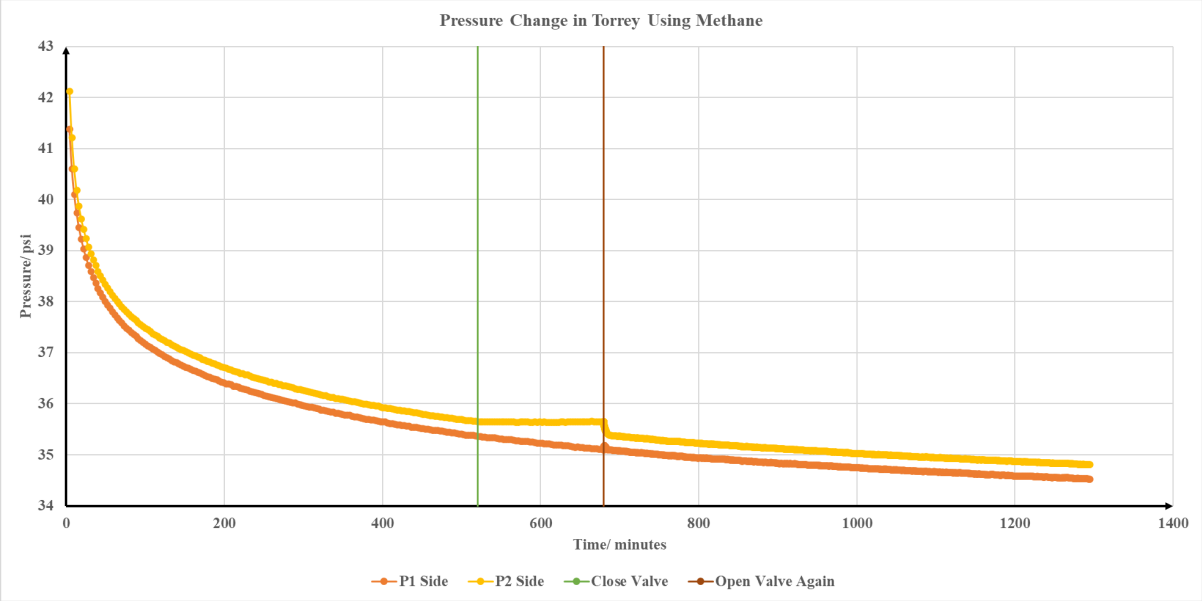

Figure 43 Pressure Change in Torrey Sandstone Using Methane

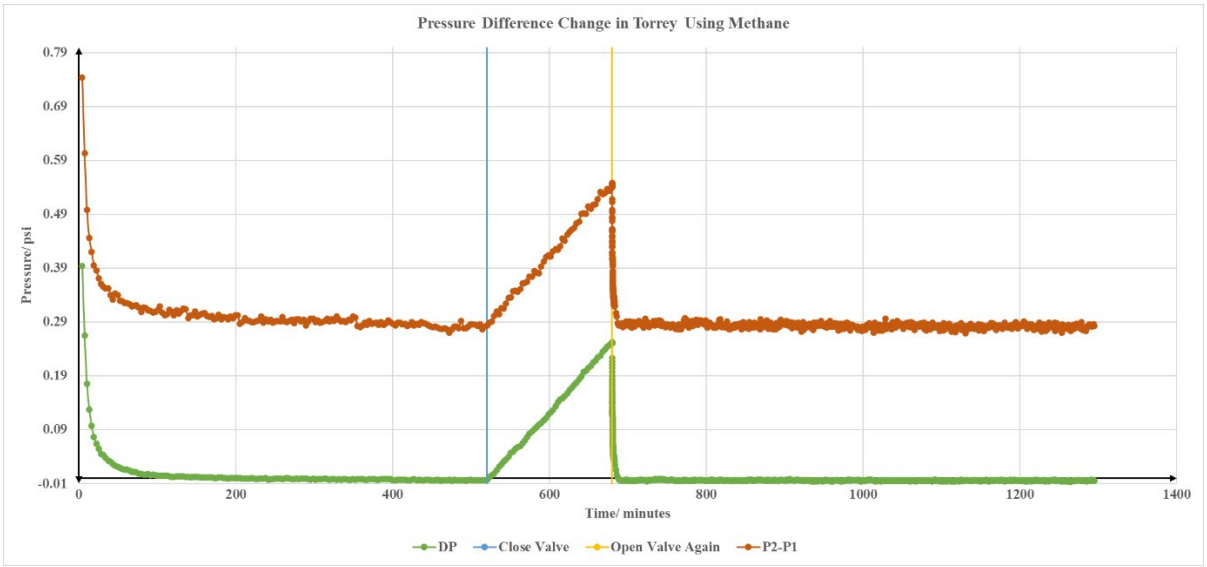

Figure 44 Pressure Difference Change in Torrey Sandstone Using Methane

The methane behavior in the two cores is similar to that of nitrogen. The curves are much smoother in the methane groups. This is the result of making the outlet (plastic tube) just touch the water surface in the beaker. Still, the flow gets close to steady in the Torrey Sandstone faster than in the Scioto Sandstone. The general trend for the three gases in the core is always decreasing when there is only a single component in the system. The pressure change is not the result of mass transfer. In the next part we will discuss the result of coupled gas behavior in the cores.

3.3 Coupled Gases Without-Core Test

3.3.1 Nitrogen-Methane Test

In single gas with core test, we find that the pressure would decrease with time. The pressure square has a linear relationship with the natural logarithm of time. Therefore, the pressure decreasing trend would always occur in the displacing gas side, regardless of what composition of the gas, with or without cores. The time when open Valve 0 again can have effect on how much pressure

will decrease after that. Because the rate of decrease in P1 depends on the time at which valve 0 is opened, and that time varied from one experiment to the next, and because the manual setting of valve 8 may have varied from one experiment to the next, the magnitude of this effect can be small relative to the effect of coupled gases in some tests but large in others, which is difficult to eliminate and access the magnitude of it in the system. So here we should make an assumption that all pressure decrease in coupled gas system is due to the coupled gas effect, rather than the pressure decrease caused by single gas behavior. This assumption should be applied and effective in both 3.3 and 3.4 part.

Here we should clarify several terminologies: Time 0 means the time when open Valve 0 at the moment when the pressure at circulating side (Compartment 1) equals to that in the Compartment 2. Real-time pressure means the all the pressure variation with time compared to the pressure at time 0. It is calculated by $P_{RT} = P_t - P_0$. Normalized pressure $P_{Norm,t}$ is another pressure variation calculation method, which is calculated by the following equation:

$$P_{Norm,t} = \frac{P_t - P_0}{P_0} \tag{3.1}$$

Here P_t is at any given time after the experiment start the pressure at that time. P_0 is the pressure at time 0.

In this section, as we described the experiments procedure in Section 2.3, one of the gases is circulating at Compartment 1 side, and the other kind of gas is saturating in Compartment 2. This is much like a preparation process for the next section but without core. The pressure at the circulation side and the stagnant side are the same, or at least, very close to each other. This is to eliminate the pressure difference between two sides and thus eliminate convection. Therefore, once the valve between the compartments is opened, there is only diffusion at first. And in case of no core between them, the permeability of the system is very high. So even if there are two gases at different sides, they can communicate their pressure response very quickly. In this situation, we

tend to regard the two compartments as a whole. In the picture, this will embody the overlap of the curves on each other. To observe what is happening in the system, we could focus on the pressure change of one side.

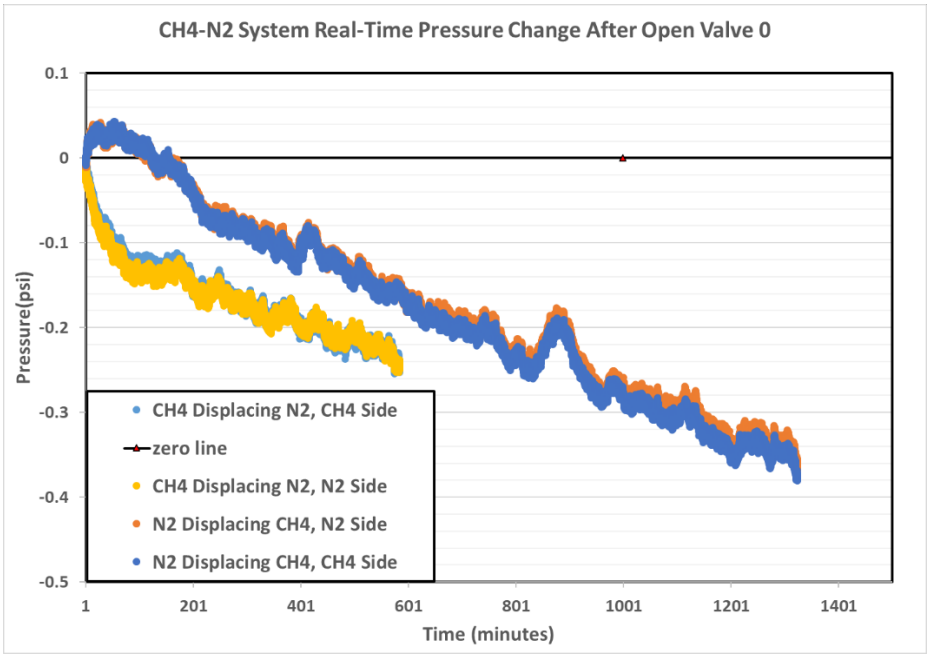

Figure 45 Real-Time Pressure Response of CH_4-N_2 System without Cores

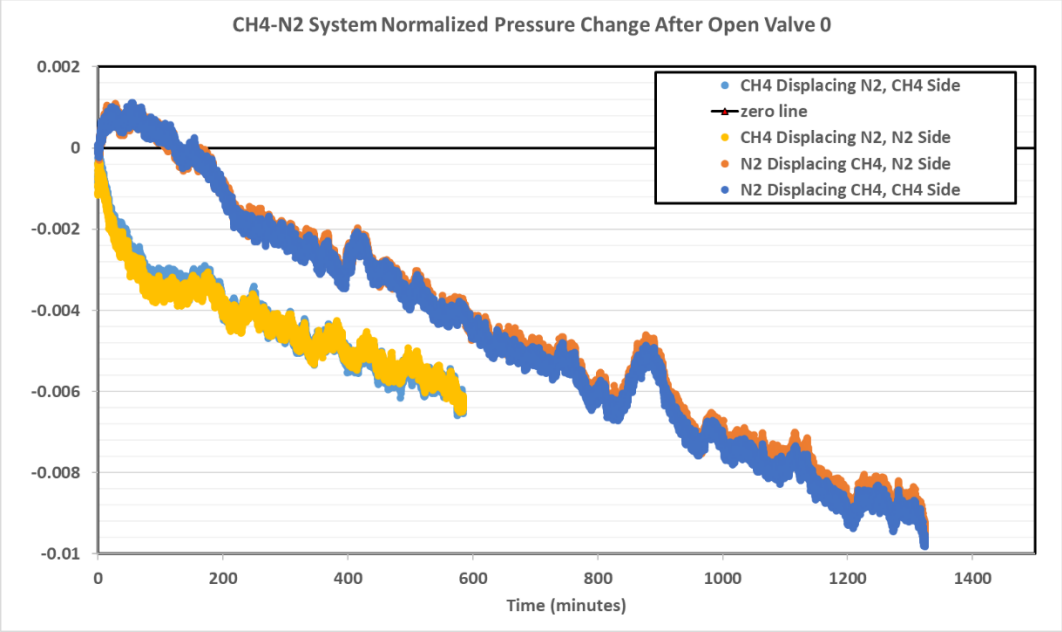

Figure 46 Normalized Pressure Response of CH_4-N_2 System without Cores

In the methane-nitrogen system, the molecular weight of methane is lower than that of nitrogen. Therefore, methane is lighter and moves faster than nitrogen when there is no core between them. When nitrogen is the displacing gas and methane is displaced gas, nitrogen is heavier and thus the total flux is from lighter gas side (methane) to heavier gas side (nitrogen). But notice here the barycenter is on the heavier substance (nitrogen) side and it moves towards the lighter substance side. In this case, the heavier component would drag the lighter substance against its concentration gradient. Thus, we can see the pressure in the system (deep blue and orange curves) increases first. The reason is the heavier component is the dominate substance and can affect the pressure response. And then it reaches the maximum value at around 50 minutes followed by decreasing, creating a bump on the picture, because it reaches the diffusion barrier at this point. The concentration of nitrogen in Compartment 2 increases and its concentration gradient decreases, making the driving

force for the nitrogen decreasing. Further, the drag effect decreases, and more methane comes to the circulation side than nitrogen comes into Compartment 2. Therefore, the total system gains less substance in than lose substance flowing out. If we use the equation A-22 in Appendix, we will find the methane has a concentration of 0.5 in Compartment 1 at around 205 minutes. This is the point where the pressure becomes the same as the initial condition. The following trend is much like the process what we observe in section 3.2.1, decreasing again. Notice this phenomenon is totally different than all the similar experiments introduced in the literature review section. This is not a step gas change process and we do not have a porous medium between the gases. The direct gas change in our experiment is much like attaching a fixed volume gas with the same pressure when the gas is flowing in the tube under a fixed pressure gradient.

When the gases are reversed, things are totally different. But the reasons are the same. If we choose methane as displacing gas and nitrogen as displaced gas, we will get an inversed-dune shaped curves at first 200 minutes. We still have faster diffusing methane, but we have heavier nitrogen who wants to diffuse out of the dead end (Compartment 2). Methane is dragged by the much heavier nitrogen. Therefore, we can say the total net flux for the first 200 minutes is towards the circulation side (Compartment 1) and thus the pressure in the system would go down quickly. When the time is over 200 minutes, we found the general trend is to follow the single gas flooding mode.

The reason why the peak absolute value and the valley absolute value are not the same is because of the drag effect and the diffusion speed. The resistance compensates for the fast diffusion of methane. Therefore, the absolute value of peak value is smaller than the absolute value of valley value.

3.3.2 Nitrogen-Carbon Dioxide Test

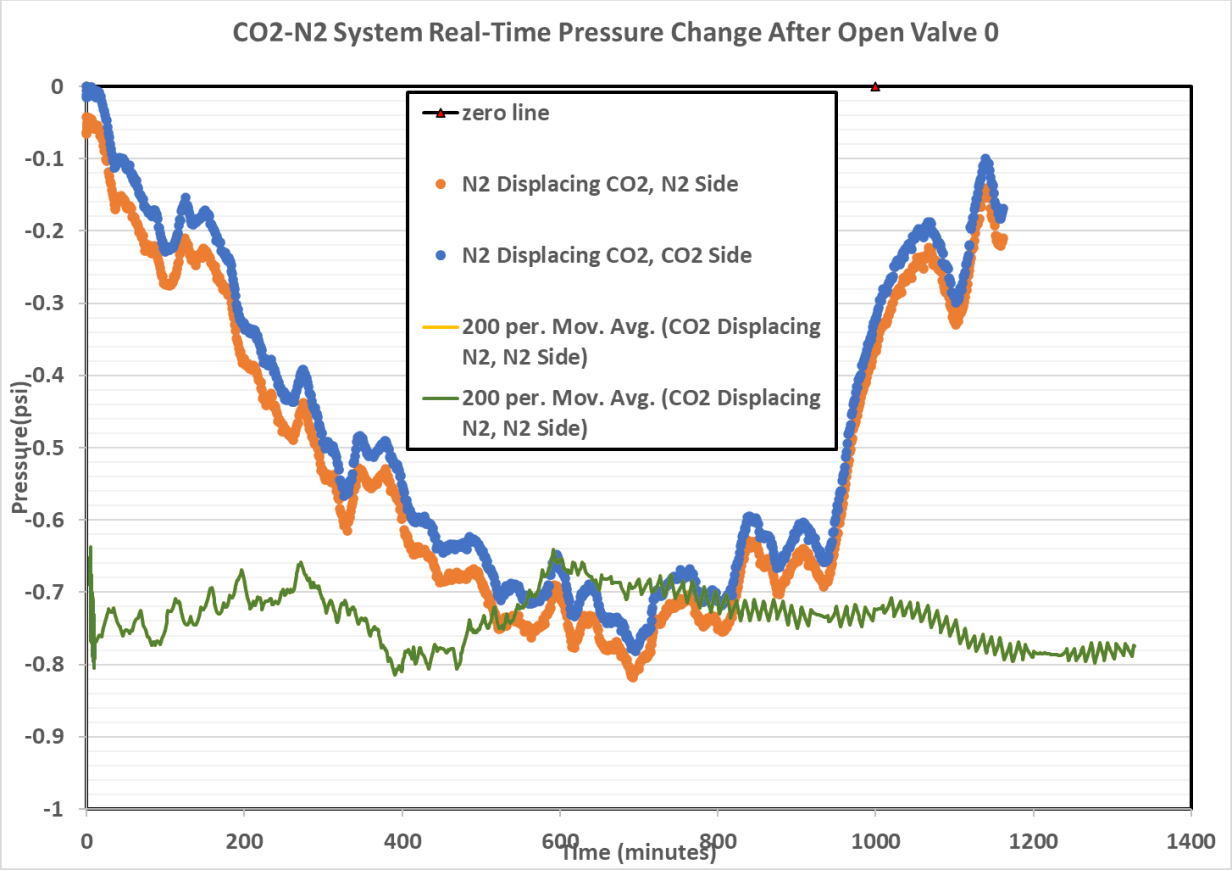

Figure 47 Real-Time Pressure Response of CO_2-N_2 System without Cores

In the CO_2-N_2 system, the diffusion barrier and non-equimolar diffusion are more obvious. Nitrogen is lighter than carbon dioxide. Therefore, nitrogen has a faster diffusion speed. From the blue curve and orange curve in the graph, we can see at first 700 minutes, the net flux in the circulation system is towards the circulation side (Compartment 1) due to the movement of barycenter towards Compartment 1. The heavier carbon dioxide bulk drags the nitrogen against its concentration gradient, the friction between carbon dioxide and nitrogen molecules slows down the nitrogen molecules and even pushes them back together with carbon dioxide molecules. But at the same time, the faster diffusing nitrogen is moving towards the dead end, where its concentration

is low. Therefore, the drag effect is actually the competition between the molecular flux, which is the diffusion direction of lighter molecules, and the movement of barycenter, which usually locating at the heavier component. At first, the barycenter is moving slowly, but it is more dominant. As more nitrogen comes into the dead end and CO_2 bulk is moving into the circulation side and finally totally replaced by nitrogen, the mass starts to build up in the system (after 700 minutes). Thus, we can observe the reverse diffusion and the diffusion barrier. After 700 minutes, the net flux direction turned to the dead end (Compartment 2) side and thus the pressure is building up. Based on the accuracy of the transducers, the pressure fluctuations within 0.1 psi scale were not significant, which can be taken as noise.

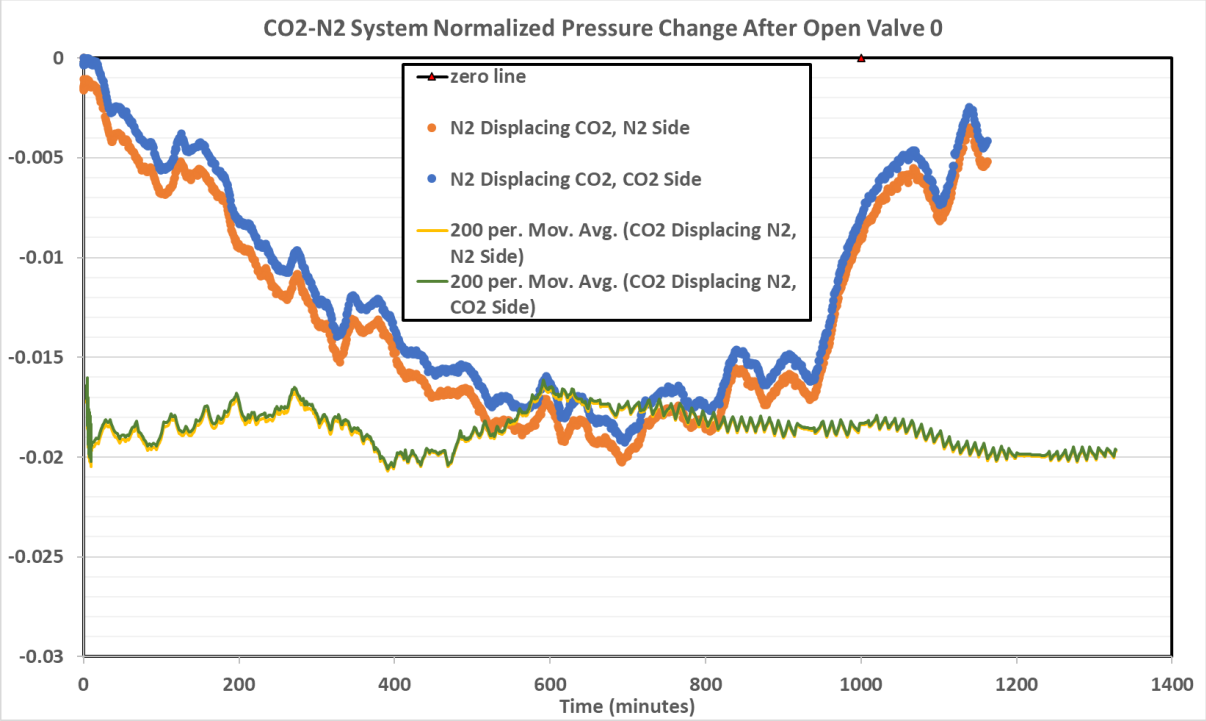

Figure 48 Normalized Pressure Response of CO_2-N_2 System without Cores

When we reverse the gases, as we talked before, the output mode of carbon dioxide regulator is

much like huff-n-puff. Therefore, at the moment of opening the valve between two compartments, there are pressure differences established and varying quickly and repeatedly. This will lead to a result that the nitrogen will quickly deplete and replaced by carbon dioxide. Therefore, we can infer that after several cycles, there is mainly carbon dioxide inside the system, both in circulation side and dead end. In Figure 47 and 48, we can see the CO_2 displacing behavior curves are almost flat without much vibration. The flat trend without decreasing is combined the mechanism of CO_2 circulating (Figure 37-40 show the decreasing trend) with little or no supply of nitrogen from dead end. This indicates the huff-n-puff of CO_2 has become a steady flow in the whole system. In general, we are focusing more on the trend rather than the fluctuations in a certain period. We want to see whether mass is building up in the system or not.

3.3.3 Methane-Carbon Dioxide Test

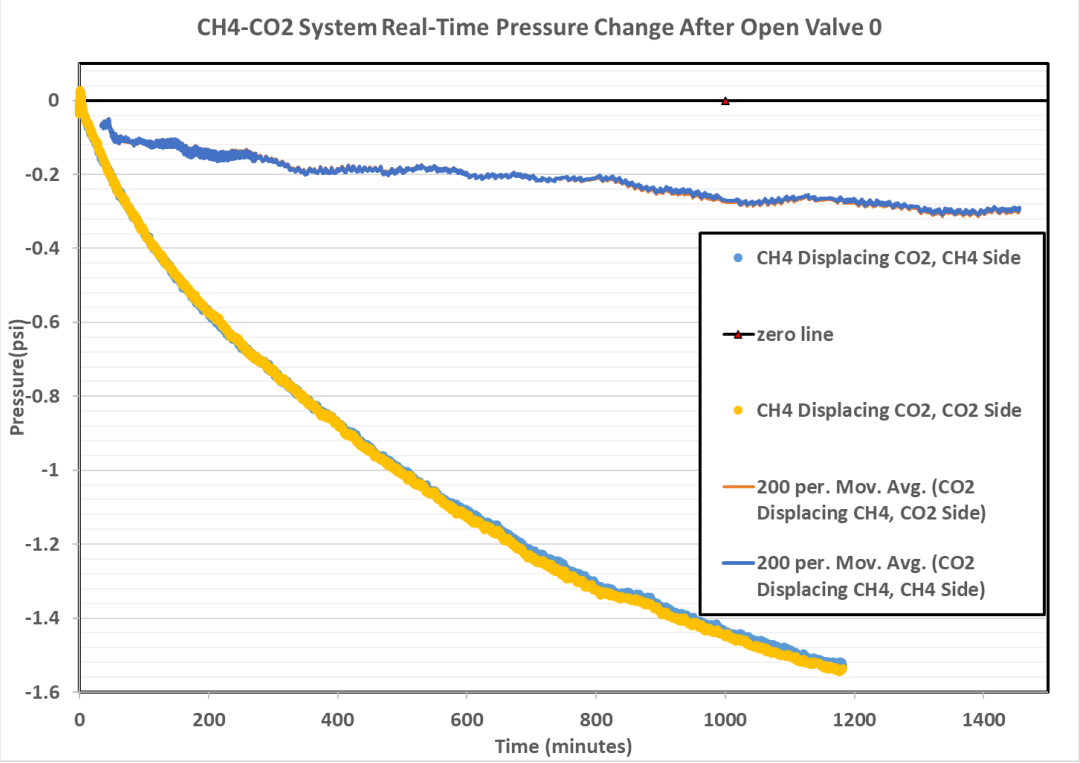

Figure 49 Real-Time Pressure Response of CO_2-CH_4 System without Cores

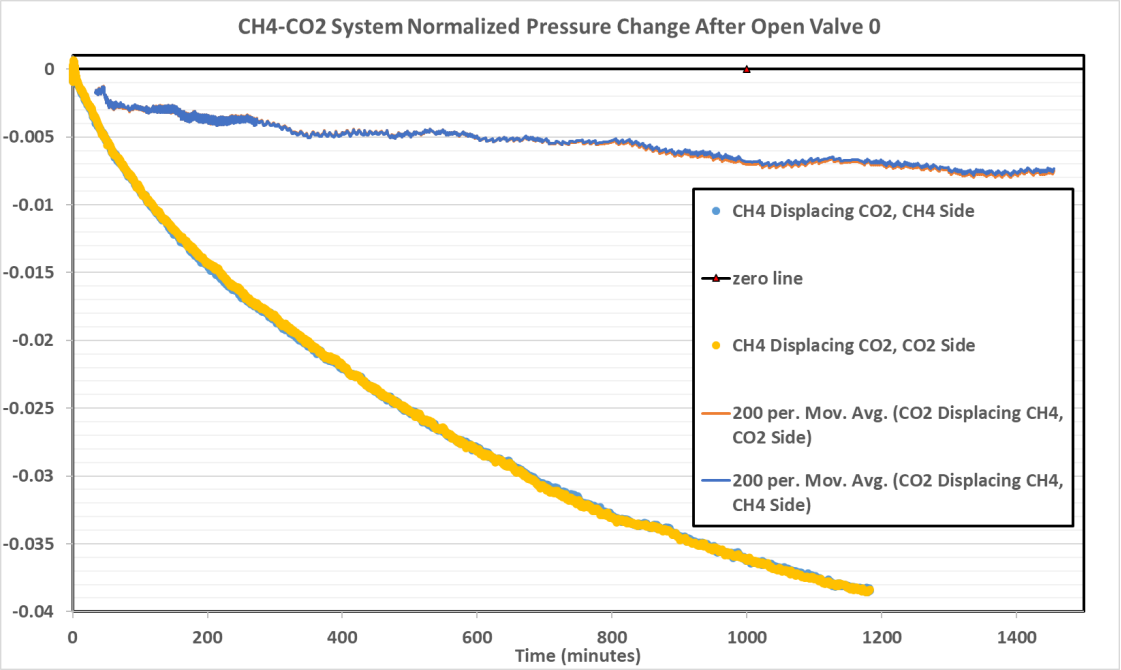

Figure 50 Normalized Pressure Response of CO_2-CH_4 System without Cores

In the CH_4-CO_2 system, we first look into the situation using CH_4 as displacing gas. In this scenario, we could find the general trend of this process is smoothly decreasing. In the first ten minutes, there is a little bump, up to 0.001 psi. And then the pressure is always decreasing. Within 1200 minutes, the pressure decreases to nearly 1.6 psi, which is similar to the single gas flow in the system of methane. The little bump in the first ten minutes can be taken as the open valve effect. It is too small to affect the following decreasing trend of the circulation side. If we compared the CO_2-CH_4 system with the CO_2-N_2 system, we could find there is no diffusion barrier and reverse diffusion in the CO_2-CH_4 system. Here we didn't observe the bounce back of the curve. Since the pressure at the circulation side is always decreasing, the mass is losing from the system and this process is controlled by heavier carbon dioxide.

Whereas using carbon dioxide as displacing gas, as we talked earlier, the system is under huff-n-puff mode and the dead end is full of CO_2 after several cycles. Therefore, the smooth decreasing

of pressure reveals the carbon dioxide behavior when using it as the displacing gas and is similar to single gas operating in the system. But since methane diffuses faster than nitrogen in binary condition, we do not see the flat trend showing in Figure 44 and 45, due to no supply of methane from dead end.

In general, the dominant factor which affects the pressure change at the beginning of countercurrent flow is the molecular weight. The heavier component tends to drag lighter component. After that, the concentration gradient changes and the driving force changes. This will result in pressure trend change.

3.3.4 Overview of the Behavior of Gas

3.3.4.1 Nitrogen Behavior

When we investigate the specific gas effect on binary diffusion, we should not only consider the molecular weight difference between molecules, but also the polarity of them. When two gases of different polarities are placed in contact with one another, there may be some degree of intermolecular attraction or repulsion between the two types of molecules. At the same time, quadrupole moment is a measure of the distribution of charge within a molecule, and it reflects the degree to which the molecule is asymmetrical in shape. Gases with a non-zero quadrupole moment can exhibit more complex interactions with other molecules and surfaces, which can influence their diffusion properties. A gas molecule with a non-zero quadrupole moment can experience more complex interactions with surrounding surfaces, such as walls or other gas molecules. These interactions can result in a slower diffusion rate, as the molecule may spend more time near the surface or other molecules before moving away. The magnitude of the quadrupole moment can also affect the degree of these interactions, with larger quadrupole moments generally leading to stronger interactions (C. Graham, J. Pierrus & R.E. Raab, 1989[140]; A G Shashkov et al., 1979[[141]; Jagiello and Kenvin et al. 2020[142])

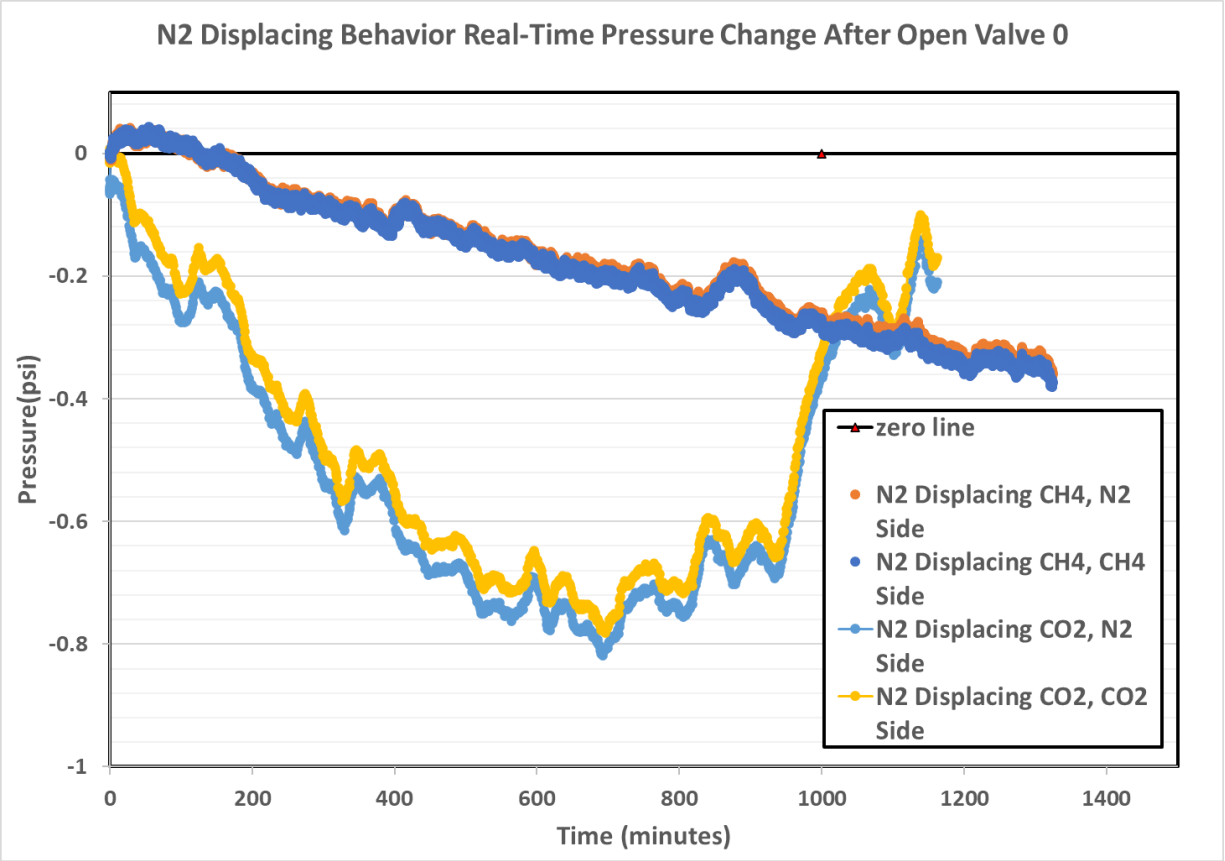

Figure 51 N_2 Displacing Behavior, Real-Time Pressure Change

As we have shown in section 2.2.3, the polarity of nitrogen is the smallest among the three gases, and it has the second largest quadrupole moments and molecular weight. Therefore, we can infer from Figure 51 and 52 that the interaction between nitrogen and methane is weaker than that of nitrogen and carbon dioxide. The molecular weight of nitrogen is between methane and carbon dioxide. Therefore, when we use nitrogen as a displacing gas, it can push methane back and be pushed back by carbon dioxide. The result is, when it pushes the methane, the mass tends to be conserved in the system, therefore the pressure in the system will increase. When the diffusion barrier is reached, we do not see pressure increase anymore. At this time, the lighter gas molecules will dominate the net flux direction of the system. We can then observe the pressure decreasing in the system, since the lighter methane diffuses to the circulation side and being taken away. At this

time the pressure response in the system is much like the single gas behavior. When the carbo dioxide is used as displaced gas in Compartment 2, the CO_2 has heavier molecular weight. Thus, CO_2 will drag the nitrogen out. Therefore, the pressure decreases at first. When the CO_2 is almost depleted, it cannot prevent the nitrogen entering Compartment 2. Thus, we observe the pressure bounce back again.

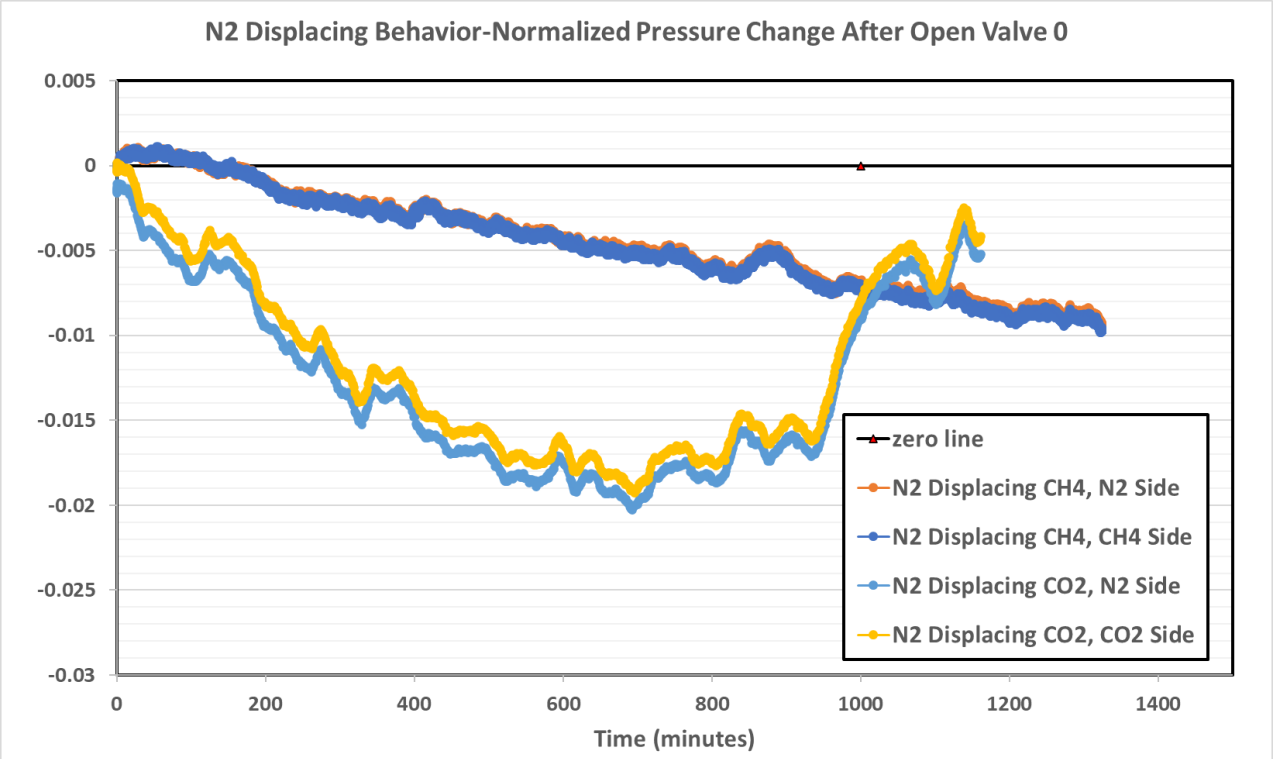

Figure 52 N_2 Displacing Behavior-Normalized Pressure Change

3.3.4.2 Carbon Dioxide Behavior

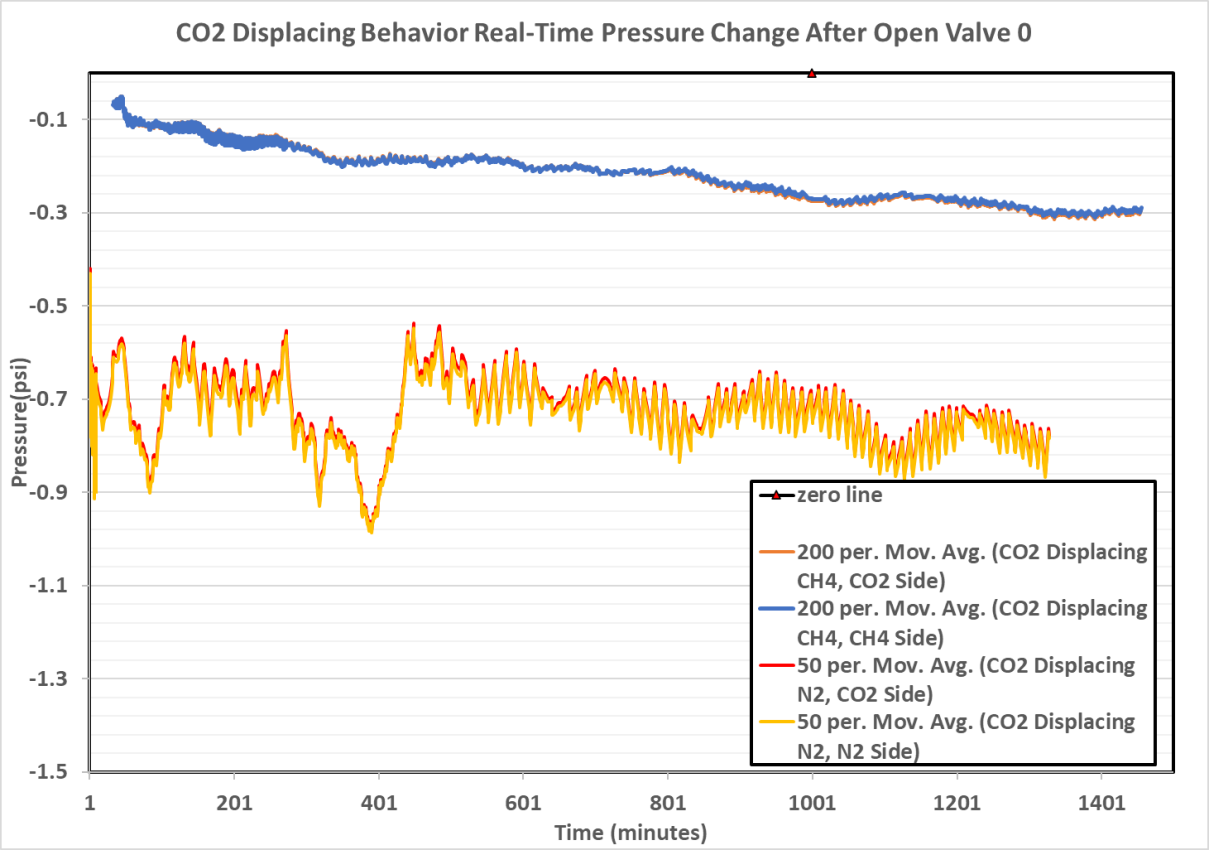

Figure 53 CO_2 Displacing Behavior, Real-Time Pressure Change

As we discussed before, the carbon dioxide displacing mode is much like a huff-n-puff mode. The general decreasing trend is actually the embodiment of the CO_2 behavior in a circulating side. But for the displaced gases, the decreasing amount for nitrogen is higher than methane. In this case we consider the reason is the time when we open the valve between compartments are different. The moment when we open the valve and use nitrogen as the displaced gas is much closer to the plateau stage than using methane as the displaced gas. Therefore, the curve of CO_2-N_2 group is flatter than CO_2-CH_4 group. The pressure at plateau stage is lower than the viscous flow stage (see Figure 37 and 39). Thus, the CO_2-N_2 group becomes steady at a lower pressure level.

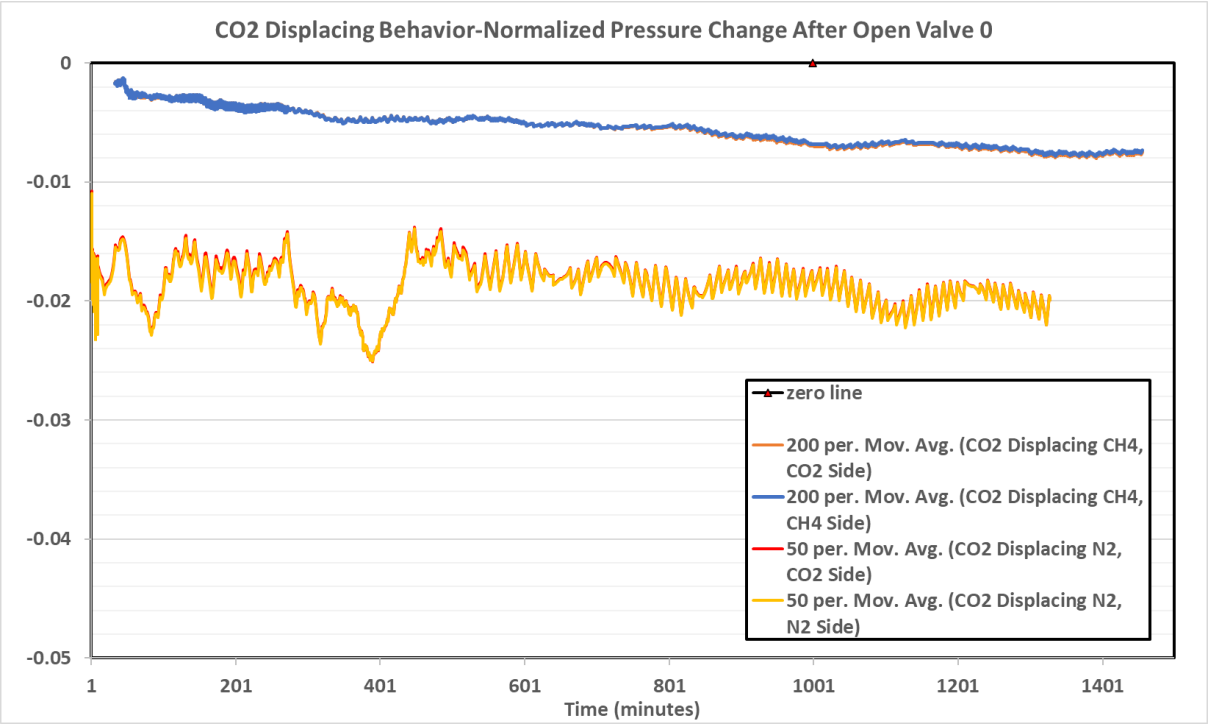

Figure 54 CO_2 Displacing Behavior-Normalized Pressure Change

3.3.4.3 Methane Behavior

When using methane as displacing gas, first we all know the molecular weight of methane is lower than nitrogen and carbon dioxide. Therefore, the drag effect now is showing in the system. CO_2 has a larger molecular weight than nitrogen, which means the drag effect of CO_2 is more powerful than nitrogen and prevents the methane coming into Compartment 2 more effectively. Thus, we can see the decreasing speed of CH_4-CO_2 system is faster than CH_4-N_2 system.

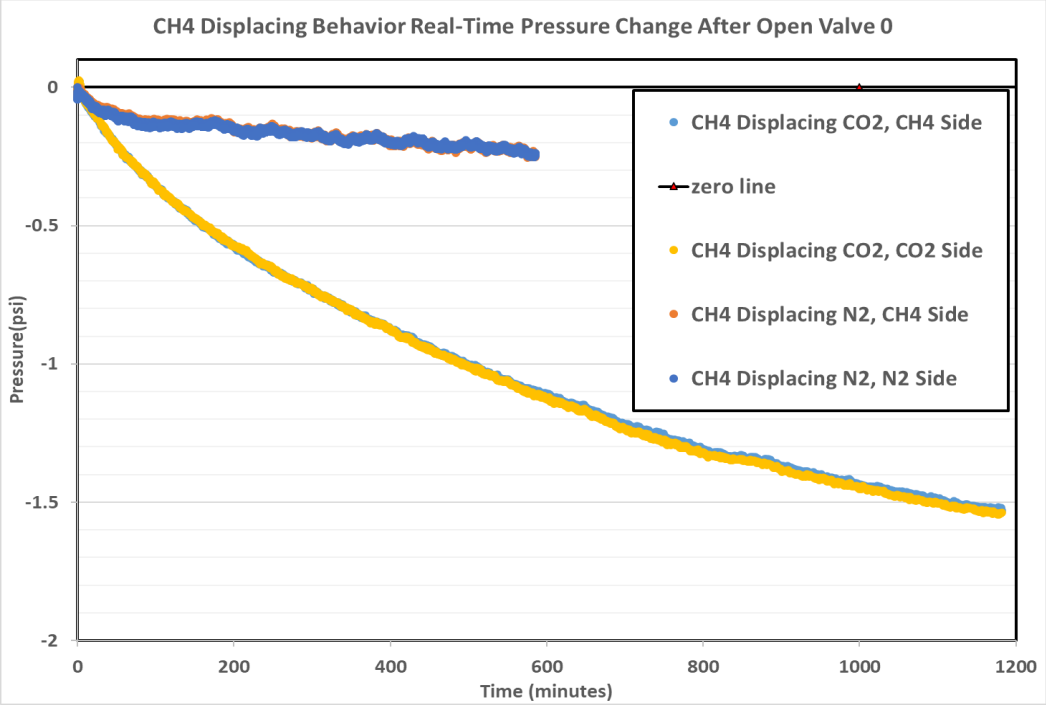

Figure 55 CH_4 Displacing Behavior, Real-Time Pressure Change

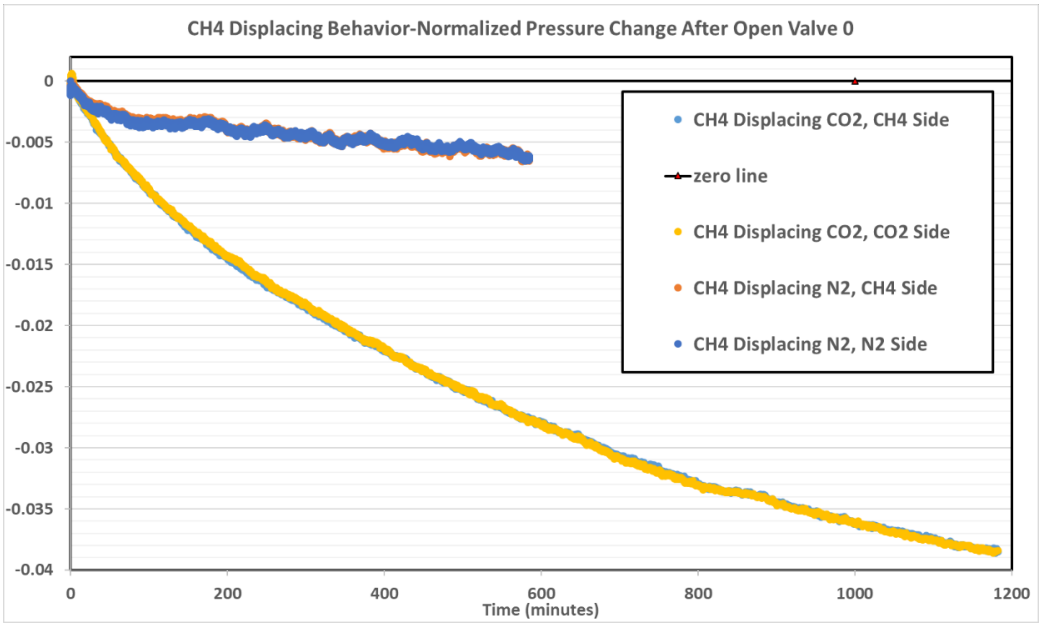

Figure 56 CH_4 Displacing Behavior-Normalized Pressure Change

3.4 Coupled Gases Countercurrent Diffusion Test with Cores

With the control group presented in section 3.2 and 3.3, we now focus on the core effect on the gas's countercurrent diffusion. First, we can look at the experiment procedure from the diagram below. The graph is randomly selected from one of the experiments.

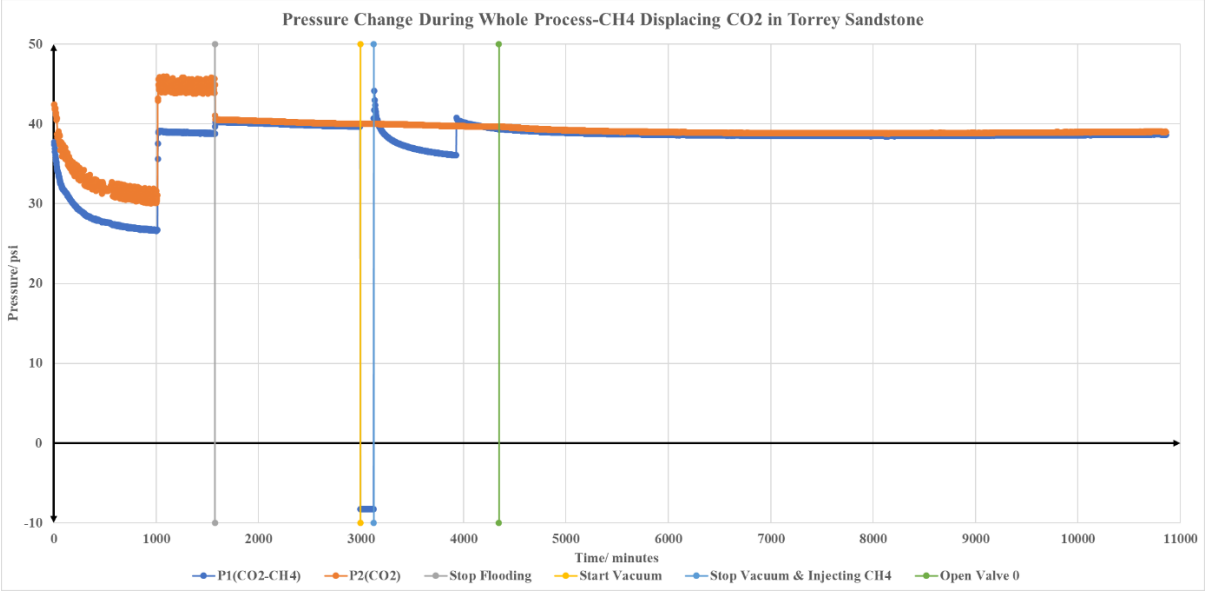

Figure 57 Pressure Change During Whole Process-CH_4 Displacing CO_2 in Torrey Sandstone

In Figure 57, we present a pressure change during the whole experiment process in two compartments. The time 0 here is the time when injecting Gas 2 into the system (We didn't record the pressure increase data when injecting the gas into the system. So only pressure decreasing period was presented). In this specific picture, Gas 2 is carbon dioxide and is being injected from Compartment 2 side. The core used here is Torrey Sandstone. At around 100 minutes, we found the pressure in the system decreased too much, thus we increased the pressure at the pressure regulator. Then we flood the system for another 600 minutes. The grey line shows the time when we stop injecting CO_2 into the system and close both Valve 5 and Valve 7. After this, we let the

system come to equilibrium, and wait for about 1400 minutes. During this period, no gas flows through the core and so there is no pressure difference. After 3000 minutes, we connected the vacuum at the outlet of Compartment 1 (just near Valve 8) and vacuumed Compartment 1 for 200-300 minutes. Here Compartment 2 and the core has been isolated from Compartment 1. Then we injected methane into Compartment 1 and let it flood until the pressure was stable. Notice at this time Compartment 1 is separated from the core holder and Compartment 2, therefore during this time the pressure in Compartment 2 (the orange line) and the core holder is constant. At around 3900 minutes, we find the pressure in Compartment 1 is lower than that in the core, so we adjust the pressure regulator to increase the pressure at methane side and let it equal to the pressure in the core to eliminate the pressure difference. At around 4300 minutes, we open Valve 0, which is located between Compartment 1 and the core. This is the time that the differential pressure transducer shows 0 pressure difference at the two side of the core. We make this to let the diffusion happen. Notice before opening Valve 0 Compartment 2 is connected to the core holder. Then we observe the pressure change both in Compartment 1 and Compartment 2, as well as the pressure difference at the two sides of the core (DP). The procedure we show here is much the same as other experiments we have done. The most important thing is to make sure the circulation side has the same pressure as in the core before opening Valve 0.

Here we should clarify one thing: In almost all the gas-pair tests, no matter what core we used, the pressure difference between the two sides of the core is nearly zero and the general trend for the curve is flat. Let us randomly choose three pictures from the test to show the situation.

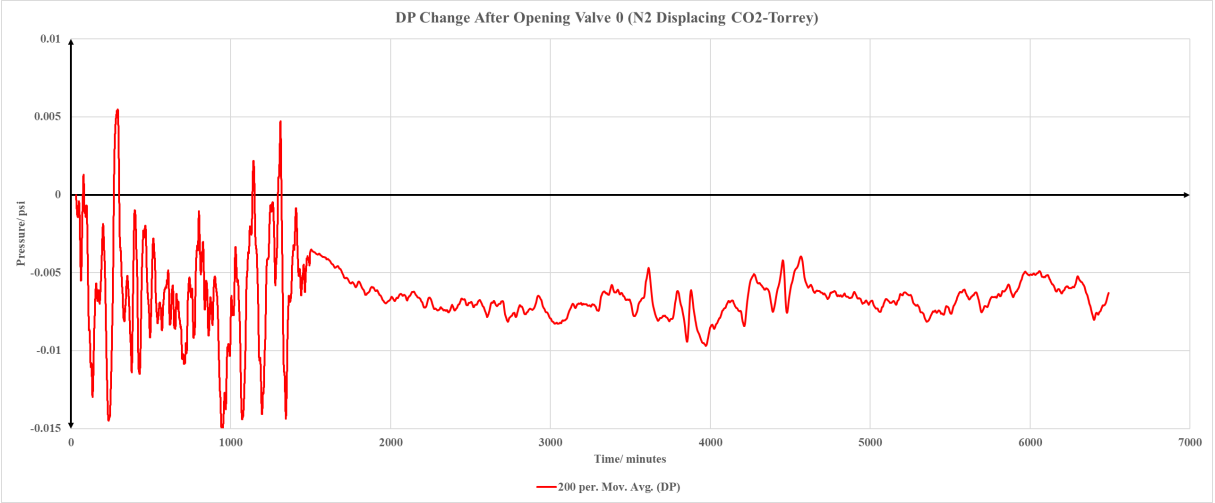

Figure 58 DP Change After Opening Valve 0 Using N_2 Displacing CO_2 in Torrey Sandstone

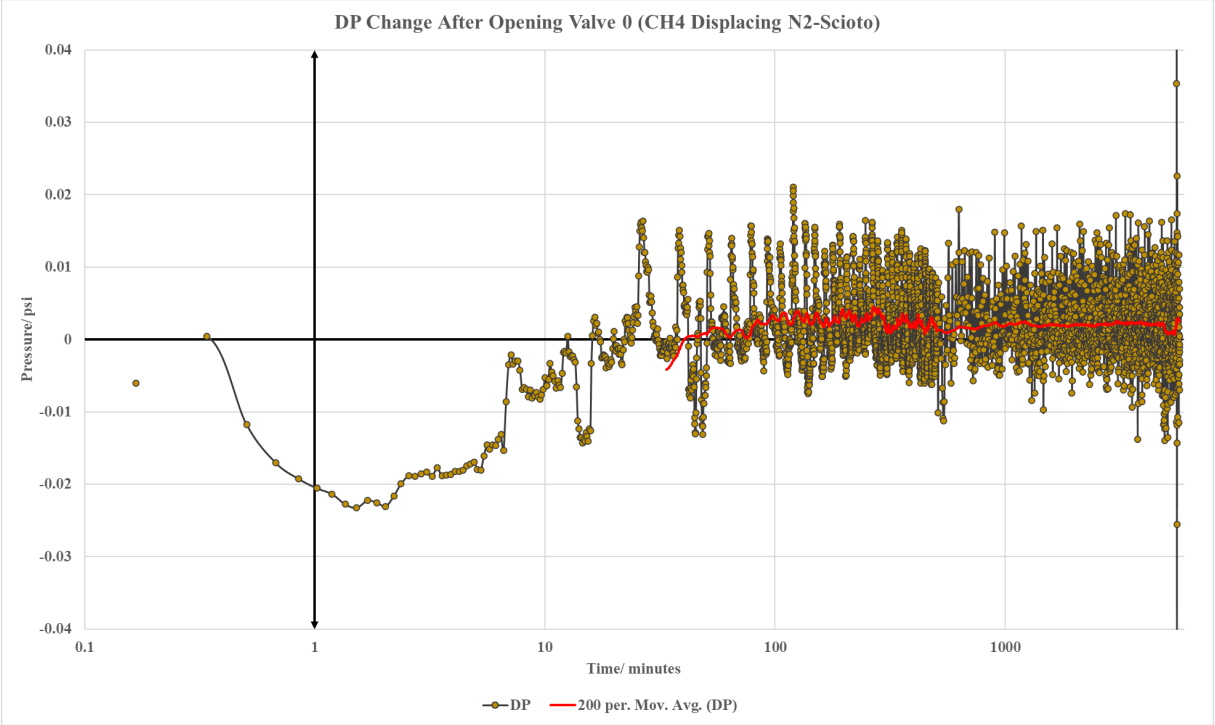

Figure 59 DP Change After Opening Valve 0 Using CH_4 Displacing N_2 in Scioto Sandstone

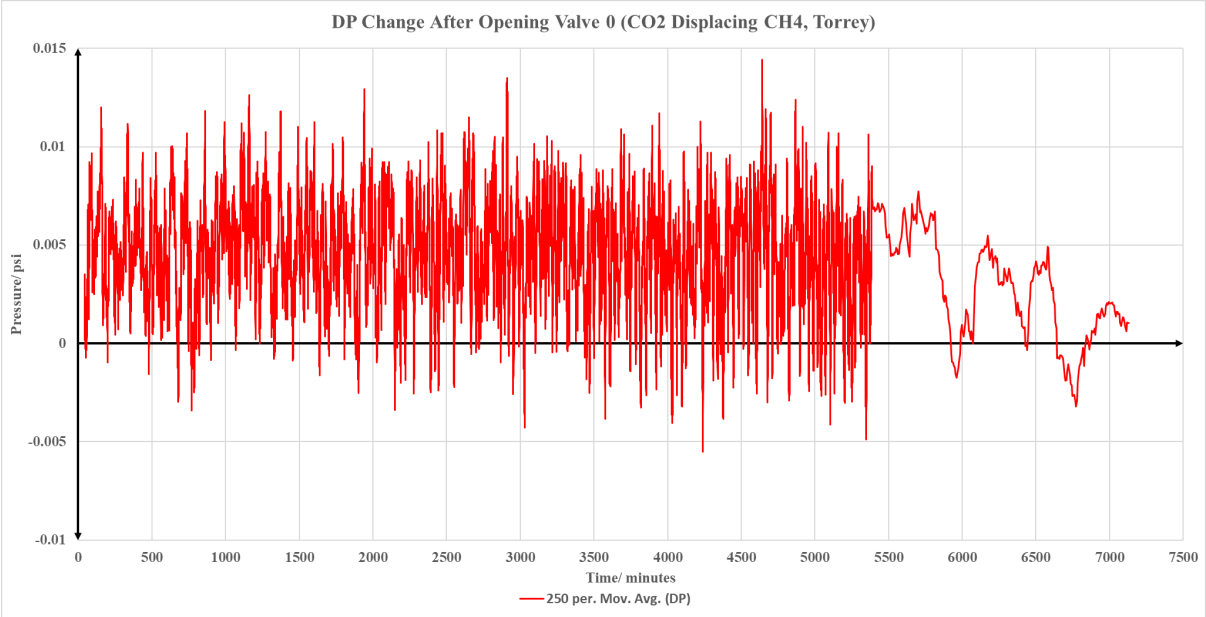

Figure 60 DP Change After Opening Valve 0 Using CO_2 Displacing CH_4 in Torrey Sandstone

The fluctuation in three diagrams is not the same due to the recording frequency of data. In Figure 58, before 1500 minutes, the data was recorded every 10 seconds. After that, the frequency was changed to every 180 seconds. In Figure 59, we take the record every 10 seconds. In Figure 60, we take the record every 10 seconds before 5400 minutes. After that, it was changed to 180 minutes. Notice the time 0 here is the time when opening Valve 0.

From Figure 58 to 60, we can see the sudden change of pressure mainly focusing on the first 100 minutes. Then the curves are still vibrating but within 0.02 psi. This process is much like the situation without the core. And this small change is negligible compared to the pressure change in each compartment. The fluctuations presented in the pictures indicate that the pressure difference change is below the acceptable measure accuracy. If we take the maximum value, 0.02 psi, and divided by 27, the whole measure range of differential pressure regulator, we will get 0.00074, which is 0.07% of the range, which can be taken as noise.

Here we should present the calculated mean free of each gas under the experiment conditions (40 psi, 24 Celsius degrees, based on equation 2.9):

Table 6 Mean Free Path of Three Gases Under Experiment Conditions

	Mean Free Path/ μm
CO_2	0.030746
N_2	0.02527
CH_4	0.023187

The calculated Knudsen Number is showing below based on equation 1.9:

Table 7 Knudsen Number of Gases Under Experiment Condition in Two Cores

	Torrey	Scioto
CO_2	0.051	0.077
N_2	0.042	0.063

CH_4	0.038	0.058

According to section 1.2.1.3, the single phase of the gas, under experiment conditions, are all in Fick's diffusion mode, based on our criteria. Whereas in other standard, the Knudsen number in this range will indicate the flow has slippage effect. In this case, the gas molecules would interact with each other rather than with the pore wall.

Liu (Liu, 2019[129]) tried to find the mechanism of shale gas transport in the real reservoir conditions. They analyzed the sensitivity of a non-linear model of the diffusion of gases in shale matrix. The average pore diameters, surface diffusivity and the pressure of gases were considered for their effect on gas diffusion. When the temperature and the pores size were fixed, the Knudsen number was a constant. Molecular diffusion is the product of Knudsen number and the Knudsen diffusivity., and Knudsen number is inversely proportional to the pressure. The lower the pressure, the higher the Knudsen number. In this case, the Knudsen diffusion keeps the same, but the molecular diffusion becomes more evident. The non-linear diffusivity in shale matrix is a function of gas pressure and pore sizes. Pore sizes could have a complex distribution in the underground space. The characteristics of gas flow can be divided into four regimes: viscous flow, slippage flow, transition flow, and free molecular flow. When the pore size is small, there are obvious effects of temperature and pressure on the flow regimes. Bigger pore sizes and high gas pressure mean higher non-linear diffusivity. But this behavior is not consistent with the change of pore sizes. As the pore sizes decrease, the trend that non-linear diffusivity decreases with the decrease of pressure is going to vanish. In the end, with the pressure decreasing, the non-linear diffusivity may increase. On the other hand, surface diffusion may reinforce this phenomenon: When the pressure of gas and the pore sizes are small, the surface diffusion contributes a lot to the total diffusion. If the porosity is fixed, as the pore size decreases, the specific surface area would increase, thus more surface diffusion would occur due to the gas adsorption. Therefore, the surface diffusion cannot be neglected in shales where micro-scale and nano-scale pores are the main characteristic. The

Langmuir isothermal adsorption indicates the concentration of adsorbed gas would decrease with the pressure, and this would cause the surface diffusion decrease. Under high pressure conditions, the surface can be negligible. In this case, although the concentration of adsorbed gas is high, the viscous flow is dominant. Therefore, the total diffusion is affected by the combined result of pore sizes, gas pressure and surface diffusion.

As the pressure increases, the viscosity of gases increases, and the diffusion caused by viscous flow decreases. Other than that, the change of pressure of gas would cause the related real gas parameter Z to change, which in turn further changes the viscous flow, Knudsen diffusion and surface diffusion. The real gas effect would promote the gas transmission under lower pressure and set resistance at high pressure. As the pressure goes up in the organic matter, the Knudsen diffusion, surface diffusion and molecular diffusion would decrease, but the viscous flow and the slippage effect would increase. These two factors combined will cause the total diffusivity to increase. In the inorganic pores, however, the Knudsen diffusion would not change due to the constant porosity, tortuosity and the pore sizes, and no gases were adsorbed in them. Besides, the molecular diffusion and the Knudsen diffusion would have little contribution to the total diffusion. Thus, we can conclude that the main difference between the transport in shale reservoir and traditional gas reservoir is the flow in nano-scale pores of the organic matter in shale.

Du (Du, 2018[130]) explored the mechanism of using carbon dioxide to displace methane in shale or tight reservoirs. They found at the beginning of displacement, carbon dioxide would continuously diffuse into the matrix from outside, and methane diffuse from inside the matrix to the outside. At this time, carbon dioxide would have competitive adsorption with methane. Therefore, the adsorbed methane would become free methane inside the core and carbon dioxide doing the opposite. The free methane inside the pore and the fractures increases the resistance of the transport and injecting of carbon dioxide, resulting in the dispersion of carbon dioxide when transporting in the reservoir. Under low pressure conditions, the adsorption amount of methane on shale decreases, then carbon dioxide can diffuse into micropores and nanopores and replace the

methane in them. But competitive adsorption does not affect the flow of carbon dioxide in the reservoir too much—it just lowers the transport speed and increases the length of mass transfer region. There is no separation happening inside the core. Under high pressure conditions, however, as the adsorption of methane increased, more carbon dioxide needed to diffuse into the pores in order to replace the adsorbed methane. The competitive adsorption began to impact on the transport of carbon dioxide obviously in the reservoir. The separation effect appears in the system. The existence of unmovable regions is the main difference between the higher pressure and lower pressure condition using carbon dioxide to displace methane in shale. This unmovable region enables carbon dioxide more time to displace methane, which means it is hard for CO_2 to displace methane under high pressure conditions. It also lowers the transport speed of carbon dioxide significantly by prolonging the length of mass transfer area and increasing the diffusion coefficient. The adsorption rate of these two gases would increase with pressure increasing and decrease with temperature decreased. When other parameters are fixed, the ranking of adsorption rate of these gases in shale is CO_2>CH_4>N_2.

3.4.1 Nitrogen-Methane Test

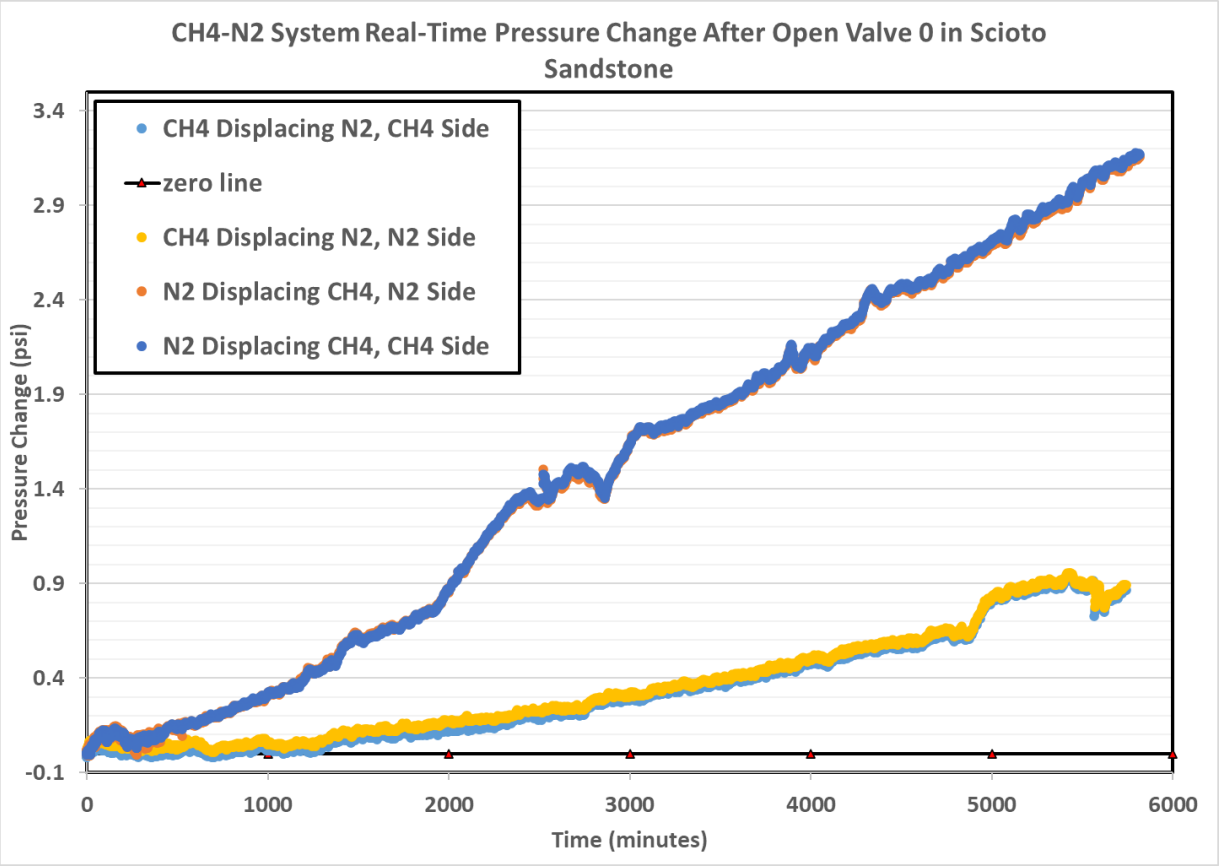

Figure 61 CH_4-N_2 System Real-Time Pressure Change After Open Valve 0 in Scioto Sandstone

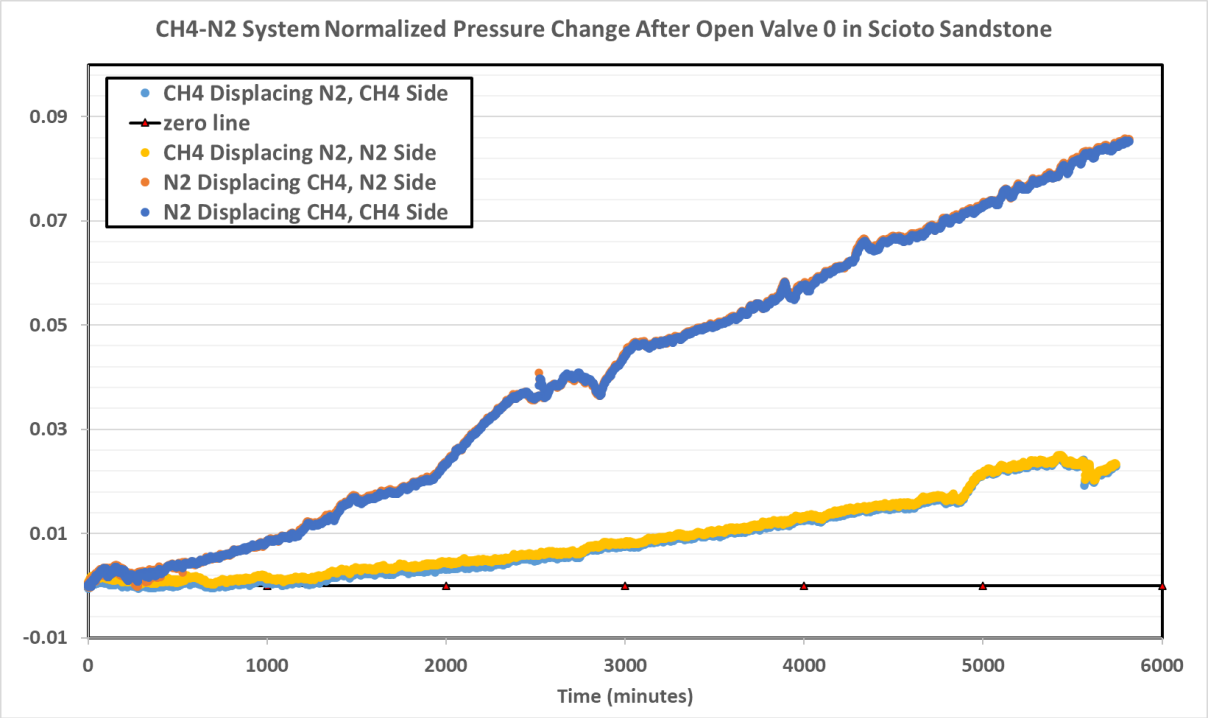

Figure 62 CH_4-N_2 System Normalized Pressure Change After Open Valve 0 in Scioto Sandstone

In the Scioto Sandstone, we found the pressure in methane-nitrogen system is building up. This is totally different from what we observe when there is no core in the system. Thus, we can confirm the core plays a role in the isobaric countercurrent diffusion. First, let us look at the deep blue and orange curves. As we have talked in Figure 58 to 60, the pressure difference between two sides of the core is nearly zero. Therefore, here we can see the two curves overlap each other. At first 200 minutes, we can see a small bump with a pressure increasing to 0.16 psi. This process is similar to the no-core condition. But this was different from the bump in Figure 30, since the pressure increasing in Figure 61 in first 200 minutes was 2 times of that in Figure 30. And the temperature in this experiment varied within 1 Celsius degree, and all the data were corrected to 24 Celsius. In this case, we can say this bump is very unlikely caused by pressure transducers or temperature change. This bump is beyond the minimum accuracy range of the transducer. But we cannot exclude the existence of the possibility of pressure difference before opening the valve. After that,

the pressure is building up in the system, which means materials are accumulating inside the system. At time 0, we open Valve 0 to let the circulated nitrogen touch the core, and also touch the methane inside the pores. The molecular weight of methane and size is lower than that of nitrogen. Therefore, methane will diffuse faster than nitrogen. And methane is an adsorbable gas, at least more likely to be adsorbed on the pore wall than nitrogen. At the beginning of the diffusion, the methane in free phase diffuses towards the circulation side under the concentration gradient. Therefore, the concentration as well as the pressure of methane in free phase decreases. With the nitrogen diffuses into the pore space, although slower than methane diffusing out, will gradually diffuse further into Compartment 2. In this case, the partial pressure of methane would decrease due to the above mentioning reasons and cause the methane in adsorbed phase to desorb from the pore wall. The mean free path of methane and nitrogen are much smaller than the pore diameter, therefore the main interaction is between the two kinds of molecules. Therefore, with more methane desorbed from the pore walls but are dragged or stuck by nitrogen molecules, combined with nitrogen continuously diffuse into the pore space and Compartment 2, the molecules entering into the system is more than the molecules diffuse out of the system. Thus, the pressure is building up. As we have analyzed before, the heavier gas always dominates at the beginning of the diffusion. Therefore, the characteristics of nitrogen will greatly affect the pressure behavior in the system.

If we use equation 2.19 to calculate how much weight in gram of methane was needed in the system to increase 1 psi, we can assume that the pressure buildup was just caused by methane, and the mole of nitrogen kept constant. Assume we increased the pressure in the system from 40 psi (275790.3 Pa) to 41 psi (282685.0 Pa) in a closed system. The temperature was 24 Celsius degrees (297.15 K). The molar mass of methane is 16 g/mol, and 28 g/mol for nitrogen. The volume of the system was 156 cubic centimeters, including dead volume. The calculation result is 0.006965 g, which is 0.000435 mol of methane. Which means as long as there was 0.006965 g methane entering the system or desorbing from the wall and not taken away, the pressure will build up for 1 psi. This is comparable to the adsorption isotherm data shown in Figure 80.

Now we can focus on the yellow and light blue curves. These two curves represent using methane at circulating side and nitrogen in the core & Compartment 2. In this case, methane is the displacing gas in the circulation side. Methane is more likely to adsorb on to the pore wall. However, the nitrogen would drag the methane molecules when they diffuse out of the cores. And this drag-effect would largely decrease the diffusion speed into the core and Compartment 2. Therefore, the pressure buildup when using methane displacing nitrogen is much slower than the reverse one. In both cases, surface diffusion would occur during the adsorption of methane on the pore walls, due to the change of methane concentration on the surface. In methane displacing nitrogen experiment, the comprehensive effect of Fick diffusion and surface diffusion as well as the adsorption of methane make the methane enter the system more quickly than nitrogen diffusing out, but at a slower speed. Because methane molecules would tend to capture the vacant point on the pore wall driven by concentration gradient at the surface. This would create additional flux towards Compartment 2. This also creates pressure building up in the system. Notice all of the conclusions are based on the experiment time scale. If we extend the observing time, say 14000 minutes or longer, we may find the pressure will decrease in the end, following the trend presented from Figure 33 to Figure 44. The reason will be explained in the appendix.

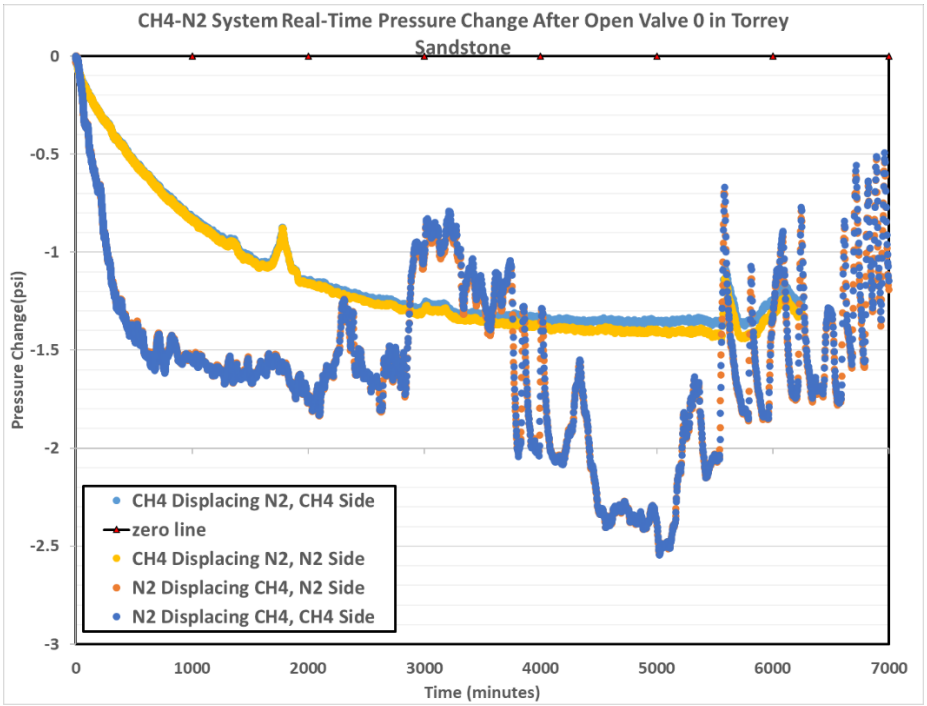

Figure 63 CH_4-N_2 System Real-Time Pressure Change After Open Valve 0 in Torrey Sandstone

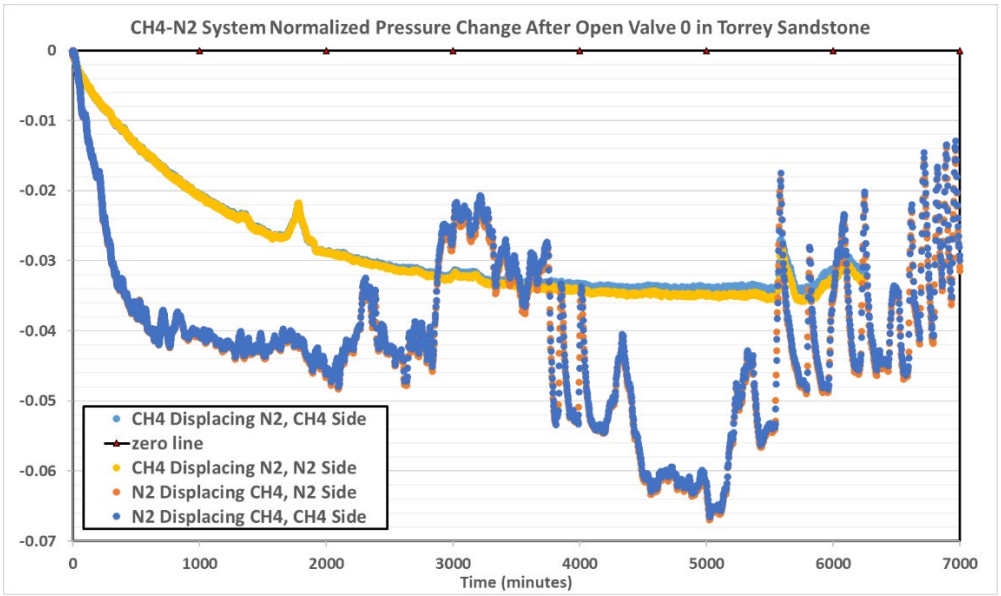

Figure 64 CH_4-N_2 System Normalized Pressure Change After Open Valve 0 in Torrey Sandstone

The nitrogen-methane displacing behavior is different in Torrey Sandstone. The pressure did not build up in both tests. First, we should be clear that the fluctuation in the nitrogen displacing curves is due to the pressure change of water level at the outlet of Valve 8. The add and vaporization of water would affect the pressure at the outlet. The decreasing trend shows the mass flowing in is less than flowing out.

In Torrey Sandstone, we did not observe a bump at the very beginning of the experiment. And we find the pressure decreasing in methane displacing nitrogen mode is lower than that in the reverse group (the methane displacing nitrogen group has less pressure decrease in the same time interval). This is different from the no-core situation as well as in Scioto core. This is due to the different pore sizes. Methane is still under the dragging of nitrogen molecules. The movement of barycenter is from core to the circulation side at first when using methane as displacing gas, which is contradictory to the direction of total diffusion flux. Just like what we have analyzed before: at first, the system was dominated by heavier nitrogen, but the faster diffusion of methane as well as the adsorption of methane on the surface slow down the process of nitrogen diffusion. This resistance is exerted on both kinds of gas molecules. But in general, the nitrogen molecules have the decisive mass flux contribution. The larger pores in Torrey Sandstone could let the two kinds of molecules have more interaction than in Scioto and provide more space for them to move. And in the reversed group, methane diffuses to the circulation side faster, and increases the total flux together with the surface diffusion flux. The nitrogen presented in the system reduced the partial pressure of methane. This will lead to the desorption of methane from the porous media. Thus, the increased flux due to the desorption of methane creates more pressure reduction since more mass is flowing out. The total mechanism in Torrey core combines Fick's diffusion, surface diffusion and sorption. In larger pores, the methane in the free phase can quickly flow out from the circulation side. More methane comes out than nitrogen comes in. Therefore, the pressure decreases faster in Torrey core. In both Scioto and Torrey conditions, we did not see pressure bouncing back to the zero line. This indicates the accumulating or depleting outcome for the core effect.

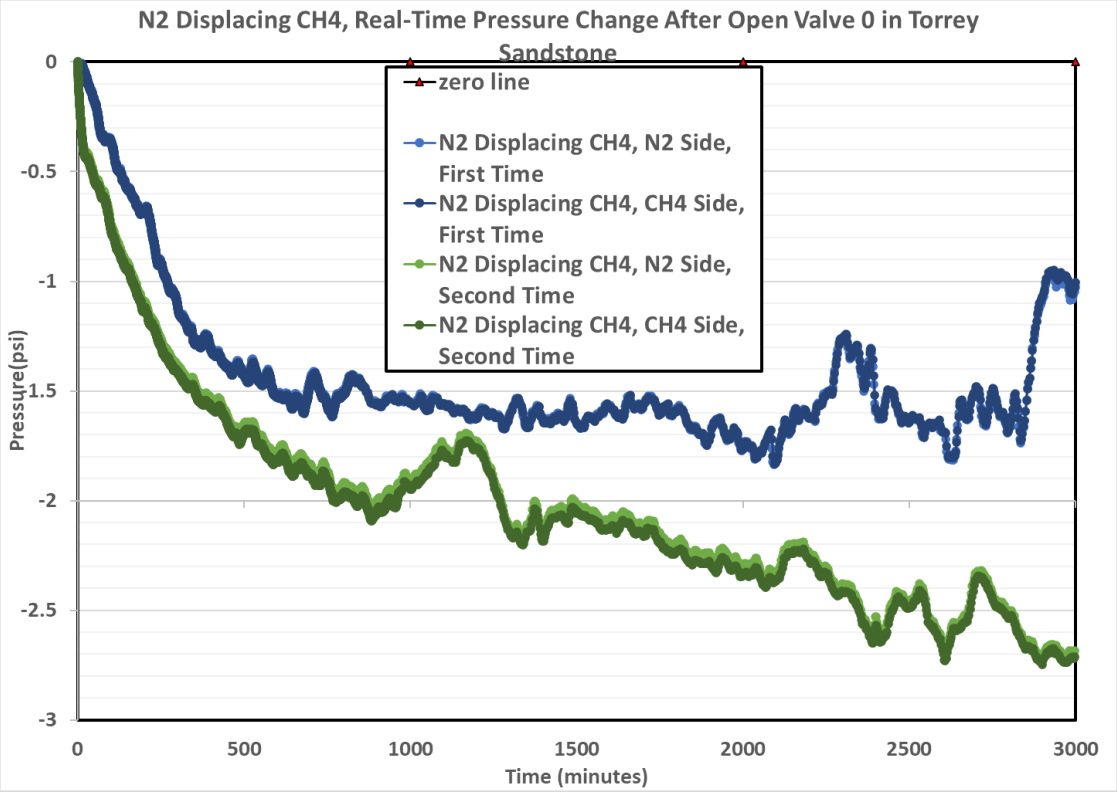

Figure 65 Repeatability Test, Using N_2 Displacing CH_4 in Torrey Sandstone

In Figure 65, we put a repeat test of nitrogen displacing methane. This is to make sure the result of each result we get from the experiment is repeatable and the occur of general trend is not random. Although there may exist some differences in the repeated group test, this is not challenging the result of each experiment and the trend. We would like to investigate the mass flow in or out during the whole process rather than certain moments. We select only one group of results from the same experiments, since we care more about the trend rather than the specific value. And the sampling frequency is different from each other. Therefore, we don't take average calculation in our discussion of results.

3.4.2 Nitrogen-Carbon Dioxide Test

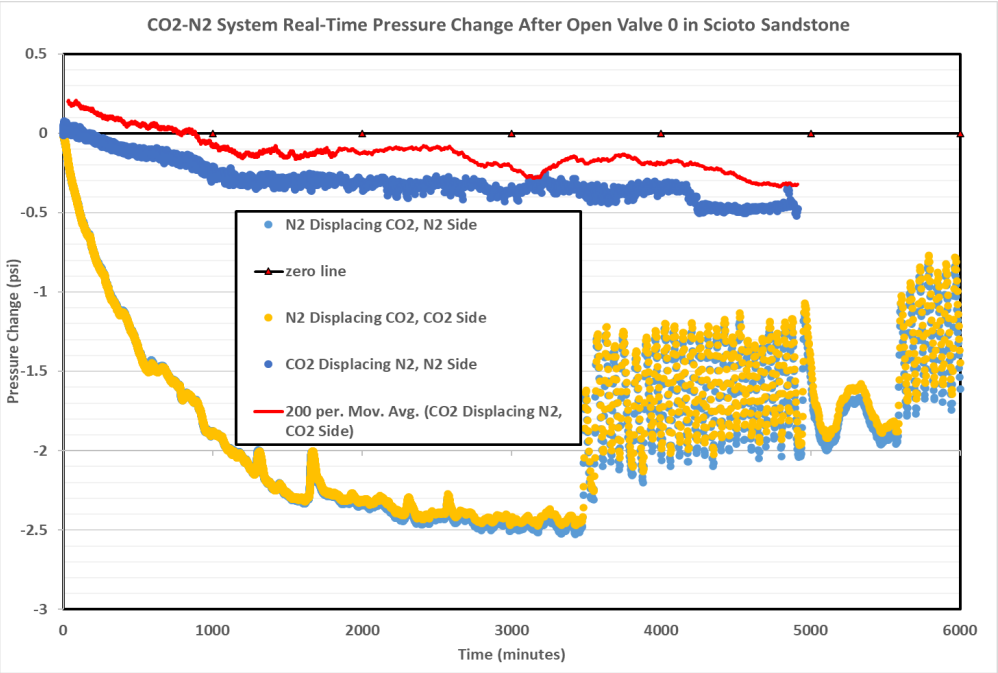

Figure 66 CO_2-N_2 System Real-Time Pressure Change After Open Valve 0 in Scioto Sandstone

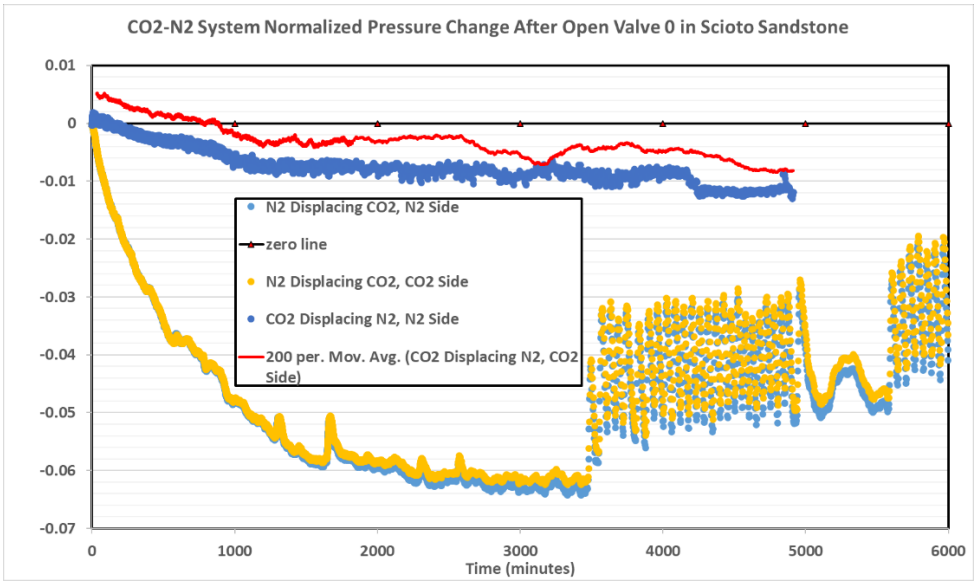

Figure 67 CO_2-N_2 System Normalized Pressure Change After Open Valve 0 in Scioto Sandstone

When carbon dioxide is present in the system, no matter in the circulation side or in the core, the general pressure trend is always decreasing. Eight curves in both Figures 66 and 67 indicate the mass in the system is under net flux towards the outside of system. The severe fluctuation of nitrogen displacing carbon dioxide curves (yellow and light blue one) after 3500 minutes is due to adding water in the beaker at the outlet. But the general trend of the period after 3500 minutes is moving upward. This is similar to what we observed during the no-core experiment. In nitrogen displacing carbon dioxide group, the carbon dioxide is adsorbed on the pore wall and occupies all space in the pore and Compartment 2. When Valve 0 was opened, CO_2 dominated the net flux in the system. CO_2 bulk tends to move towards the circulation side and prevent some of the nitrogen molecules entering the pore space, through both the drag effect in free space and the CO_2 adsorption layer. The diffusion barrier occurs at around 3000 minutes, which is much later than the no-core situation. This is the result of porous media, since less nitrogen molecules can directly contact with carbon dioxide molecules in the nanoscale pores. As most of the carbon dioxide coming into the circulation side and taken away by the flow of nitrogen, the slope of the pressure

curve is decreasing. After 3000 minutes, the diffusion of nitrogen reaches its diffusion barrier. As concentration of CO_2 inside the system decreases as time goes by, nitrogen starts to flow into the core and Compartment 2 much easier than before. At this time, the mass flowing in surpasses the mass flowing out. Therefore, the pressure after 3000 minutes begins to bounce back.

Now let us look at the CO_2 displacing nitrogen situation (deep blue and red curve). The deep blue curve shows a good filter effect of the core, since the vibration at CO_2 side (the so-called "huff-n-puff" cycle behavior of CO_2 pressure regulator) does not affect the pressure in Compartment 2 much (no severe vibration, just smooth change). In this case, CO_2 will try to enter the pores under its concentration gradient and tend to adsorb onto the pores. But since the nitrogen diffuses much faster than carbon dioxide, it will drag carbon dioxide molecules, too. Therefore, it will slow down the diffusion as well as the adsorption of CO_2. The decrease of pressure when CO_2 displacing N_2 is much slower than the reverse one. Since nitrogen doesn't tend to adsorb onto the pore wall (compared to carbon dioxide), there is no competitive adsorption in the core. At first, CO_2 is hard to enter the pores due to its large molecular weight. But this "huff-n-puff" mode could provide pressure difference and finally, convection. This means carbon dioxide molecules could enter the porous media and Compartment 2 under pressure gradient, and then flow out with nitrogen molecules at "puff" stage. In this case, the concentration of carbon dioxide would increase in the free phase in the system. But since the pores are small (compared to no core conditions), the pressure decreases at a lower speed. The general trend is dominated by the carbon dioxide injection, and the pressure change follows the behavior of carbon dioxide.

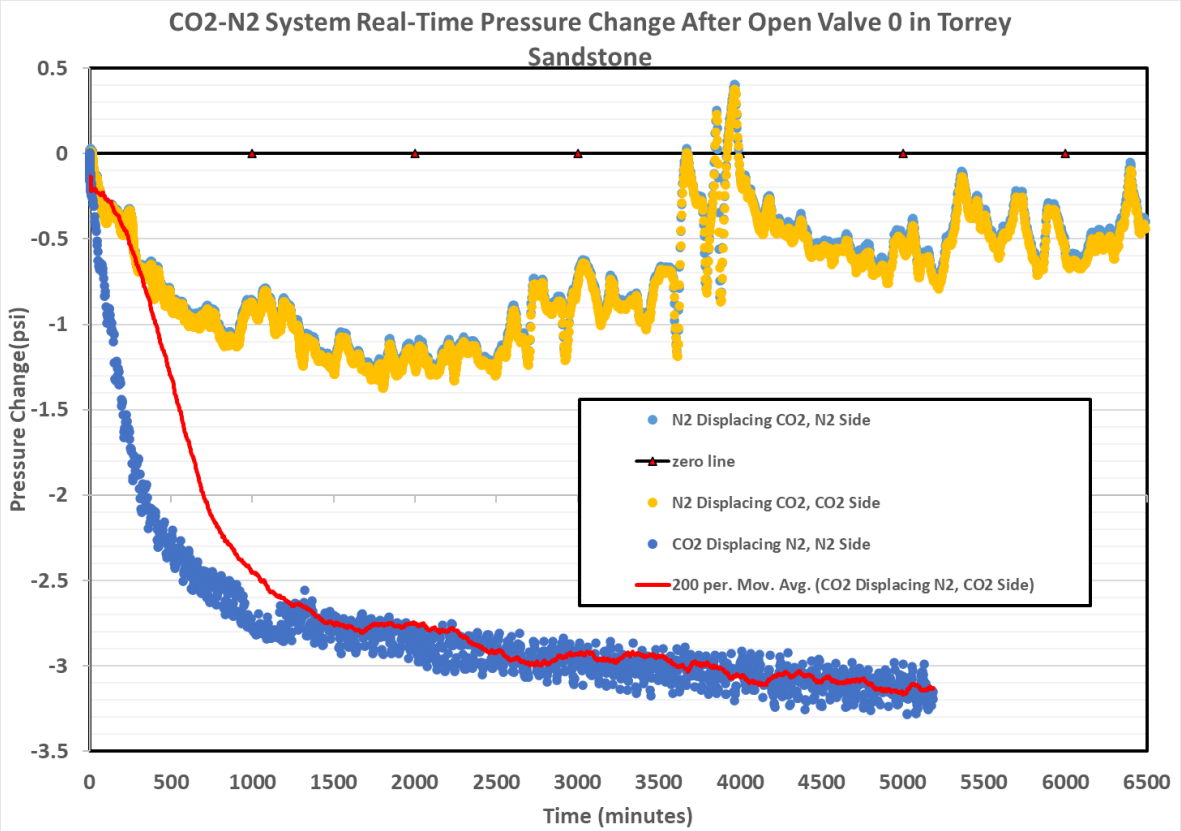

Figure 68 CO_2-N_2 System Real-Time Pressure Change After Open Valve 0 in Torrey Sandstone

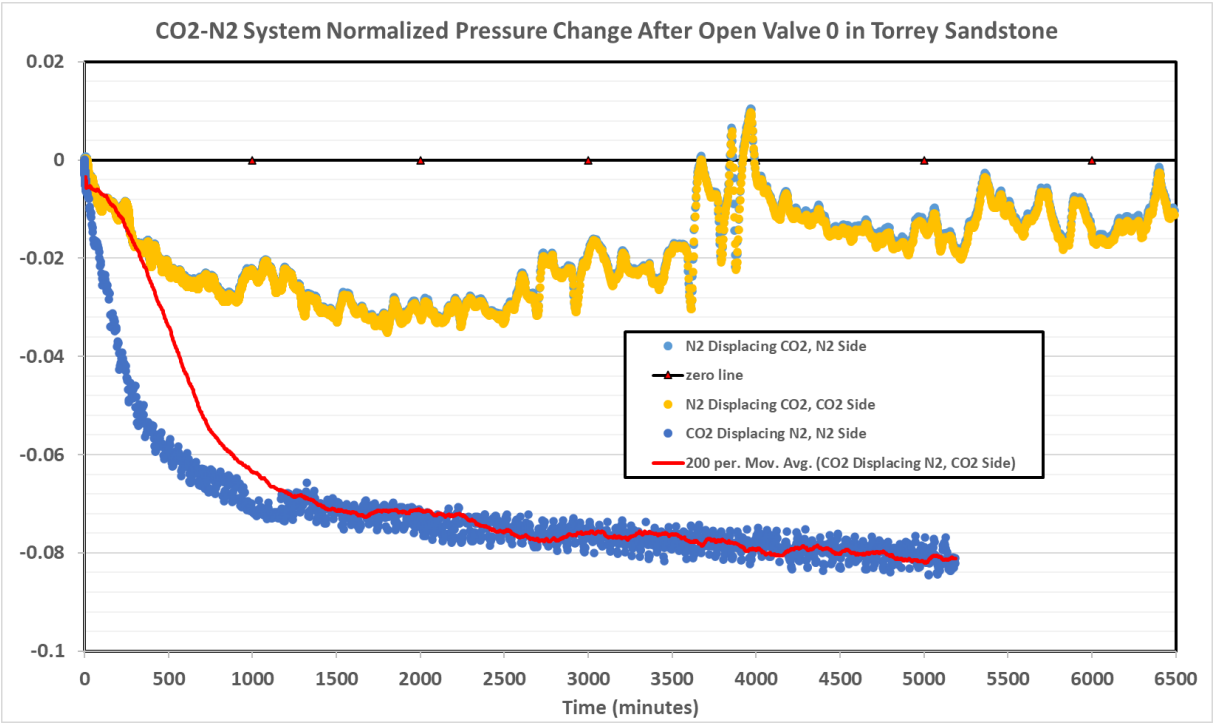

Figure 69 CO_2-N_2 System Normalized Pressure Change After Open Valve 0 in Torrey Sandstone

In Torrey core, we observed something different with the situation in Scioto Sandstone. But there was also something similar. Similar points are the trend and the behavior of the two systems: First, both groups have their pressure lower than the initial pressure in the end. Second, the N_2 displacing CO_2 curves (yellow and light blue one) display the diffusion boundary and reverse diffusion, which is similar to that in Scioto Sandstone and no-core condition. The only difference is the decreasing speed and the decreasing amount in Torrey Sandstone is reversed, compared to the situation in Scioto Sandstone. Since the pore size of Torrey Sandstone is larger, the effect of adsorption layer is less obvious than in the Scioto core. Therefore, as we can see in the red and deep blue curves, the pressure decreases very fast at first 1000 minutes, and then the slope becomes much smaller. This is because Torrey Sandstone has a larger pore diameter and CO_2 enters the pore space much easier. And CO_2 would adsorb on the pore wall. Simultaneously, the nitrogen molecules in the core and Compartment 2 would diffuse faster and get less resistance from the CO_2 adsorption layer and

CO_2 in free phase. During this process, the fast depletion of nitrogen is the main contributor for the fast-decreasing trend, and this process should be combined with the adsorption of carbon dioxide on the pore wall. After 1000 minutes, most of the nitrogen in Compartment 2 is replaced by CO_2, then the pressure behavior is much like using CO_2 solely in the system, whose pressure decreases much slower. Whereas the behavior of N_2 displacing CO_2 showing in yellow and light blue curves is similar to the reason explained in Scioto core. At the beginning stage the CO_2 would diffuse towards the circulation side. But since the pore size is larger, this process does not last as long as in Scioto core. When the CO_2 in the pore is almost depleted, the nitrogen from the circulation side starts to massively diffuse into the core. This process lasts for 3500 minutes. At the same time, the CO_2 desorbed from the pore wall would continuously enter the pore. From 3500 minutes to 4000 minutes, the vibration of pressure was due to the water level change at the outlet of Valve 8. But this didn't affect the pressure trend in general. Since Torrey core has larger pore sizes than Scioto, we can see it reached pressure boundary earlier than in Scioto core. The pressure bounces back at around 2000 minutes, which is earlier than in the Scioto core, but much later than no-core condition. The moving average in the red line shows the pressure at carbon dioxide side when using it to displace nitrogen, which is deviating from the deep blue line (pressure nitrogen side). Notice here the moving average method was adopted, and the actual vibration is much more severe than the moving average shows. As we talked before, the carbon dioxide regulator behavior was much like huff-n-puff mode, therefore the vibration was severe. This deviation does not affect the general trend of pressure decreasing, and this will create pressure differences between the two sides of the core, which will introduce convection.

3.4.3 Methane-Carbon Dioxide Test

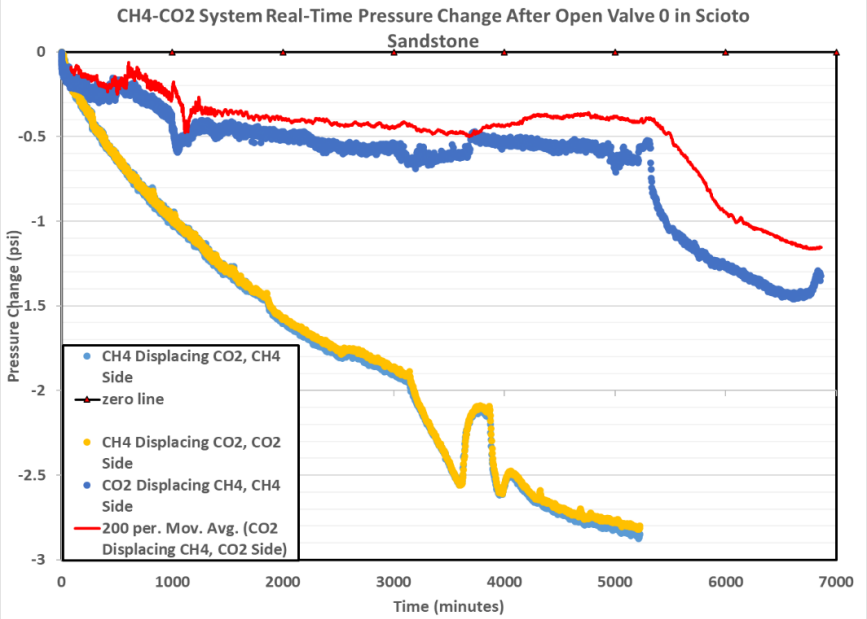

Figure 70 CH_4-CO_2 System Real-Time Pressure Change After Open Valve 0 in Scioto Sandstone

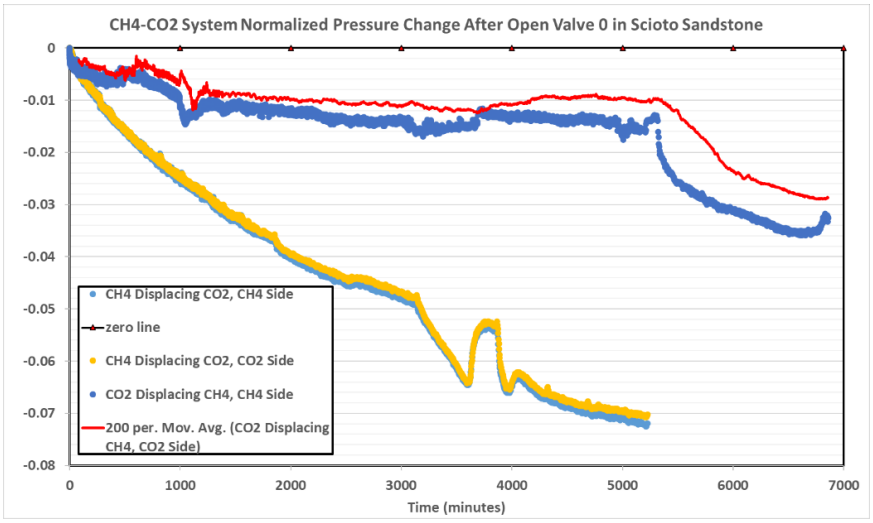

Figure 71 CH_4-CO_2 System Normalized Pressure Change After Open Valve 0 in Scioto Sandstone

The CH_4-CO_2 system behavior in Scioto core is similar to the situation of no-core condition. But the decreasing speed is much slower in the core. In this case, both CO_2 and CH_4 can absorb on the pore walls. Some scholars have declared before that the adsorption rate of carbon dioxide is higher than that of methane. Therefore, competitive adsorption would occur on the pore wall during the countercurrent diffusion. Let us look at the yellow and light blue curves first. These two curves represent the pressure response at the two sides of the core when using methane to displace carbon dioxide. The decreasing of pressure is generally smooth during the whole process. CO_2 is more likely to attach to the pore walls than methane. And the CO_2 molecules in free phase cause a huge resistance for methane molecules to enter the core. The CO_2 adsorption layer creates additional resistance for methane molecules to diffuse in. At the beginning, the CO_2 bulk movement dominates the total flux. The CO_2 enters Compartment 1 and is quickly taken away by the flood of methane. In this case, the pressure response measuring in two compartments basically show the methane pressure decreasing similar to no-core condition in Compartment 1 and the decrease mole fraction of CO_2 with little supplement of methane coming from the circulation side. Generally speaking, the pressure decrease caused by CO_2 flowing out of the system is larger than the pressure builds up caused by the adsorption of methane and the methane diffusing into the system. And since methane was dragged by carbon dioxide molecules, the pressure at this time behaved like unsteady single gas flow. If the observation is longer, we may see pressure bounce back after the carbon dioxide was depleted.

The deep blue and red curves show the process of CO_2 displacing methane. In this case, the CO_2 will have competitive adsorption with methane on the pore walls. The CO_2 will quickly adsorb onto the pore wall and create additional surface flux in nearby regions, which further lowers the methane flux in the pores. And the quick adsorption of CO_2 in the pore space increases the mass flowing in the system, but does not increase the pressure, because they are all in adsorbed phase. Therefore, at first 5000 minutes, this was a process combining the “huff-n-puff” from carbon dioxide side, and the competitive adsorption between two kinds of gas molecules. During the puff process, the pressure at Compartment 1 would decrease and some of the carbon dioxide and

methane molecules will be driven to Compartment 1 under pressure gradient. And in the next cycle, more carbon dioxide would be injected into the core and Compartment 2. After 5000 minutes, the pressure decreased suddenly. This is caused by the accomplishment of competitive adsorption and the depletion of methane. So, it represents the carbon dioxide single component behavior.

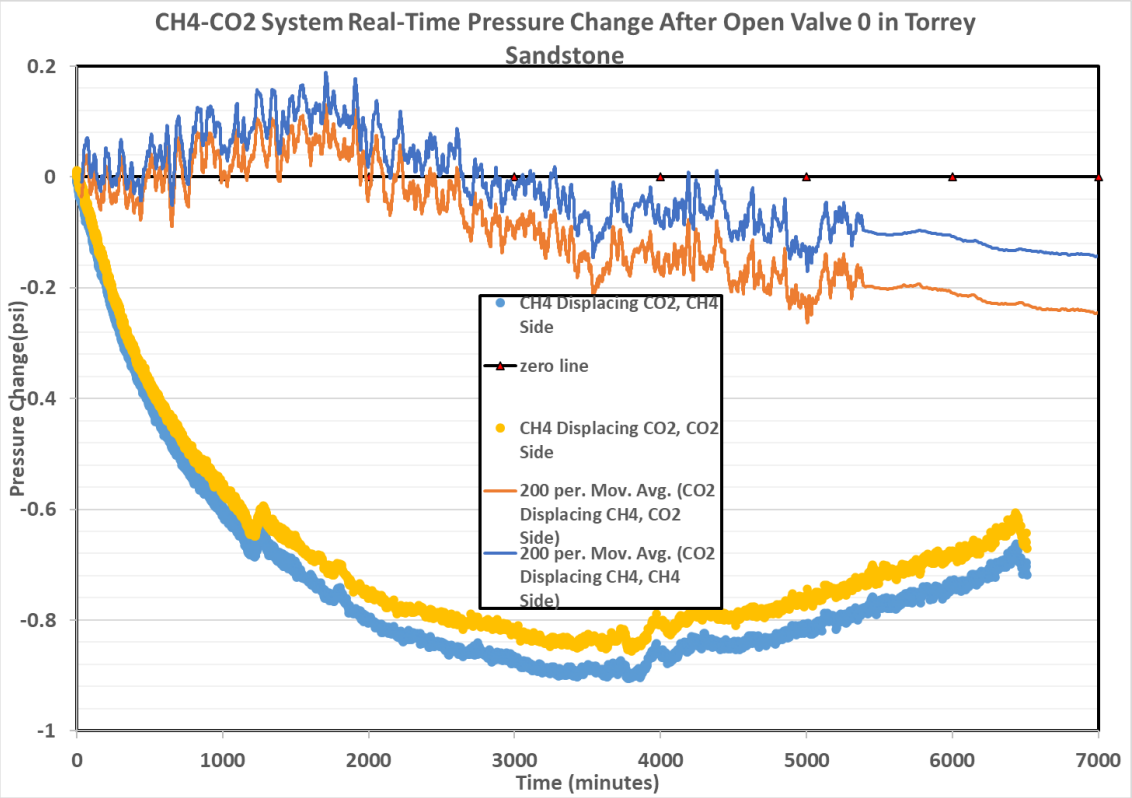

Figure 72 CH_4-CO_2 System Real-Time Pressure Change After Open Valve 0 in Torrey Sandstone

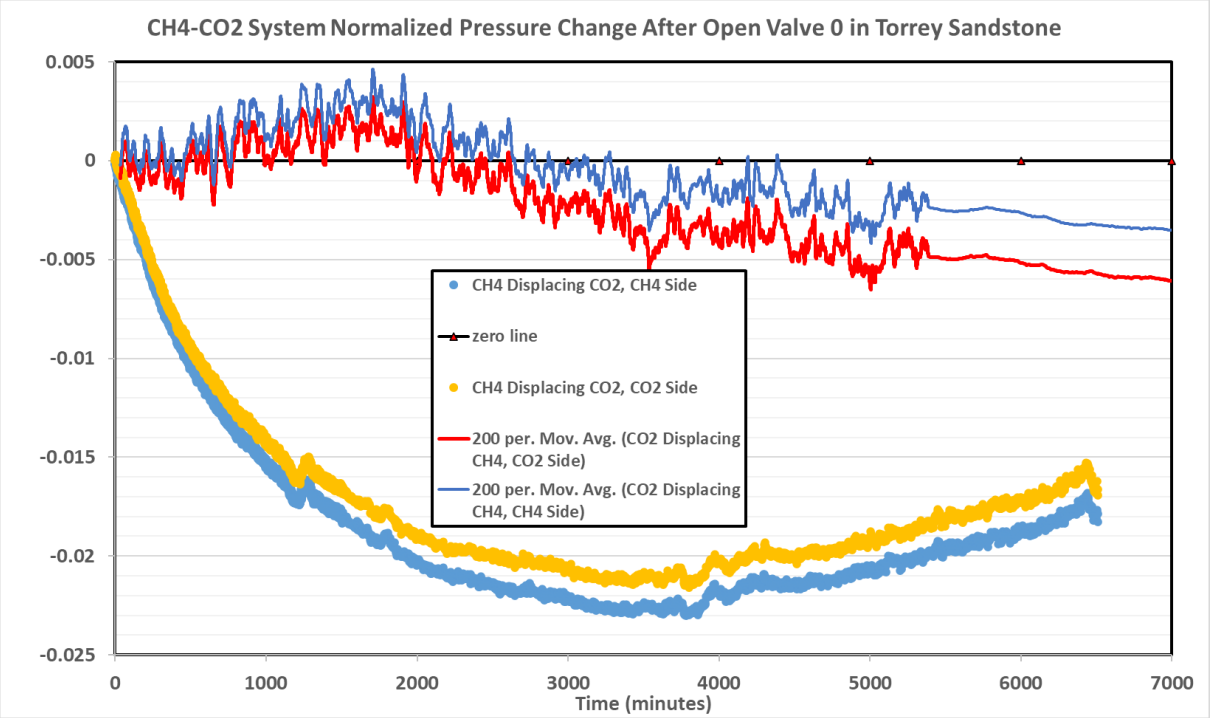

Figure 73 CH_4-CO_2 System Normalized Pressure Change After Open Valve 0 in Torrey Sandstone

The methane-carbon dioxide pair has the highest consistency among the three groups. The decreasing trend in this group is always similar: pressure of CO_2 displacing CH_4 groups always decreases slower than CH_4 displacing CO_2 groups, with or without a core. Here we only introduce the difference in Torrey core. First thing is we observe a pressure increase in CO_2 displacing CH_4 experiment. This "bump" started at around 500 minutes and finished at around 2000 minutes. The pressure increase in the system means the mass flows in is more than the mass flowing out. Since the Torrey Sandstone has larger permeability and average pore size, this will create additional space for the diffusion of molecules along the concentration gradient. At first 500 minutes, the pressure does not change much. This is considered to be a stalemate stage, which means the pressure decrease caused by methane diffusing towards the circulation side is offset by the pressure increase caused by the CO_2 diffusing into the core and Compartment 2. When enough CO_2

molecules come into the pore space, it will have competitive adsorption with the methane molecules to capture the absorb point on the pore wall. During this stage, CO_2 molecules diffuse into the pore structures with the help of surface diffusion. And with more methane molecules are displaced by CO_2 molecules, they are dragged by the CO_2 molecules diffusing in and have a reverse diffusion against its own concentration gradient. Thus, we can see the pressure is building up in the system. After the surface diffusion is finished, the methane adsorption layer is replaced by CO_2 adsorption layer, the drag effect decreases and cannot prevent the methane molecules diffusing into the circulation side. After the 3000 minutes point, we can see the pressure decrease and follow the behavior of CO_2 flooding in the system. The decreasing trend after 2000 minutes is the CO_2 unsteady flow.

In methane displacing CO_2 experiment, we observed a pressure bounce back at around 3700 minutes. This phenomenon is also similar to the previous experiment. CO_2 is heavier and its bulk diffusion dominates the total flux before 3700 minutes. More CO_2 diffuses out than methane diffuses inside the core. As the supplement from the adsorption layer of CO_2 and the CO_2 inside Compartment 2 is depleted, methane starts to flow into the pore and Compartment 2, which means the mass flux flowing out of the system is decreasing. Methane starts to accumulate in the pore space and Compartment 2 as well as forming a new adsorption layer of methane. Thus, we can see the pressure bounce back.

3.4.4 Overview of the Gas Behavior

3.4.4.1 Nitrogen Behavior

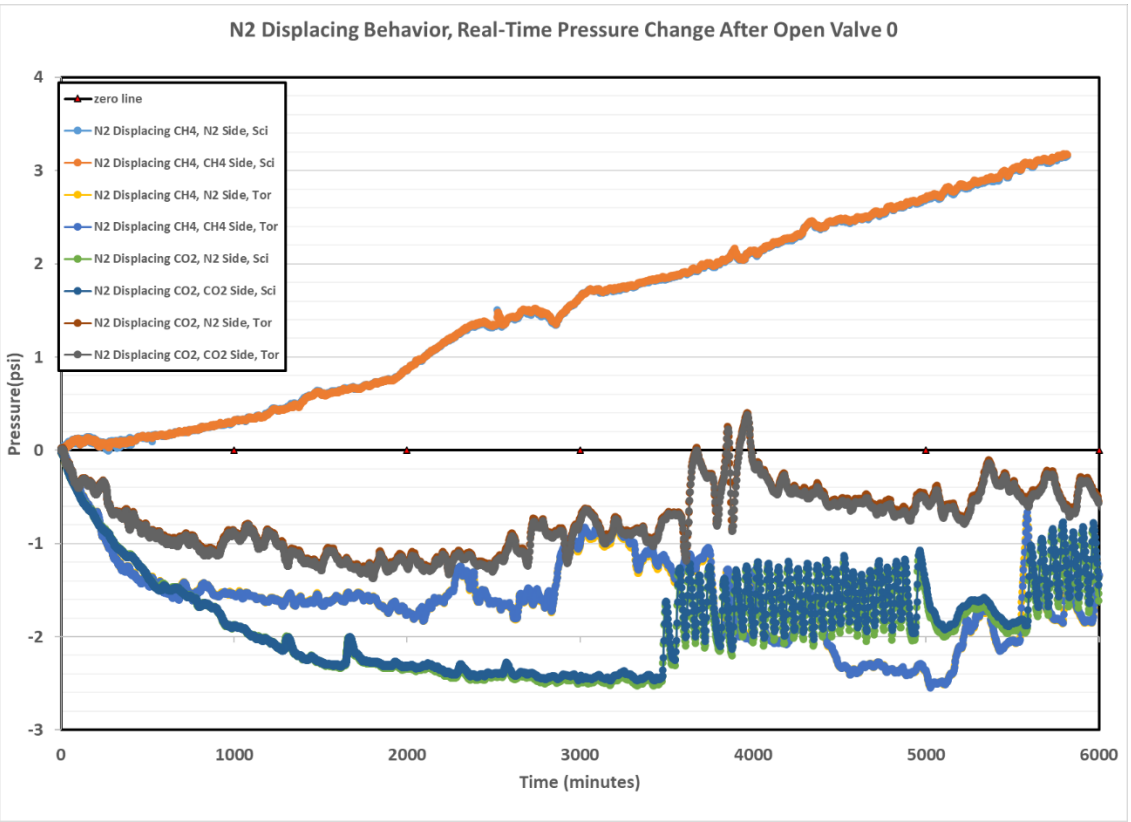

Figure 74 N_2 Displacing Behavior, Real-Time Pressure Change After Open Valve 0

The molecular weight of nitrogen is in between methane and carbon dioxide. Therefore, for the gas diffusion at the beginning, nitrogen should push methane and be pushed by carbon dioxide. This phenomenon is more obvious in the smaller permeability core (Scioto). But in Figure 74 and 75, we found that the behavior of nitrogen displacing methane in Torrey Sandstone seems not to behave like this. We think this is caused by the change of permeability of the core. Since Torrey

has a larger pore size, the interaction between molecules is more than that in smaller pores. From Figure 74 and 75, we can see the impact of permeability on nitrogen displacing carbon dioxide is obvious: pressure decreases more in lower permeability core, but the time of reaching the minimum point is later than higher permeability core. This is because the lower permeability core has a smaller pore size but a larger specific surface area. This will absorb more gas. And in nitrogen displacing carbon dioxide mode, we observed pressure bounce back. But there was no such behavior in nitrogen displacing methane. According to the result in single gas behavior, this pressure bounce back cannot reach original level (0 line) since the pressure at Compartment 1 side is always decreasing.

Notice the pressure change in Figure 74 is different from those changes in Figure 33. Since in Figure 33, there is only nitrogen in the system and the pressure decreases 2 psi in 1000 minutes. Then it comes close to steady state. But in Figure 74, the pressure decreases much slower than single gas conditions and this is reflected in the time of reaching steady state. Moreover, the decreasing amounts are not the same, either. In nitrogen displacing methane in Scioto core, the pressure even builds up. Therefore, the change of time scale and the decreasing amount of pressure both illustrate the situations shown in Figure 33 and Figure 74 are definitely not the same thing. So as in Figure 35.

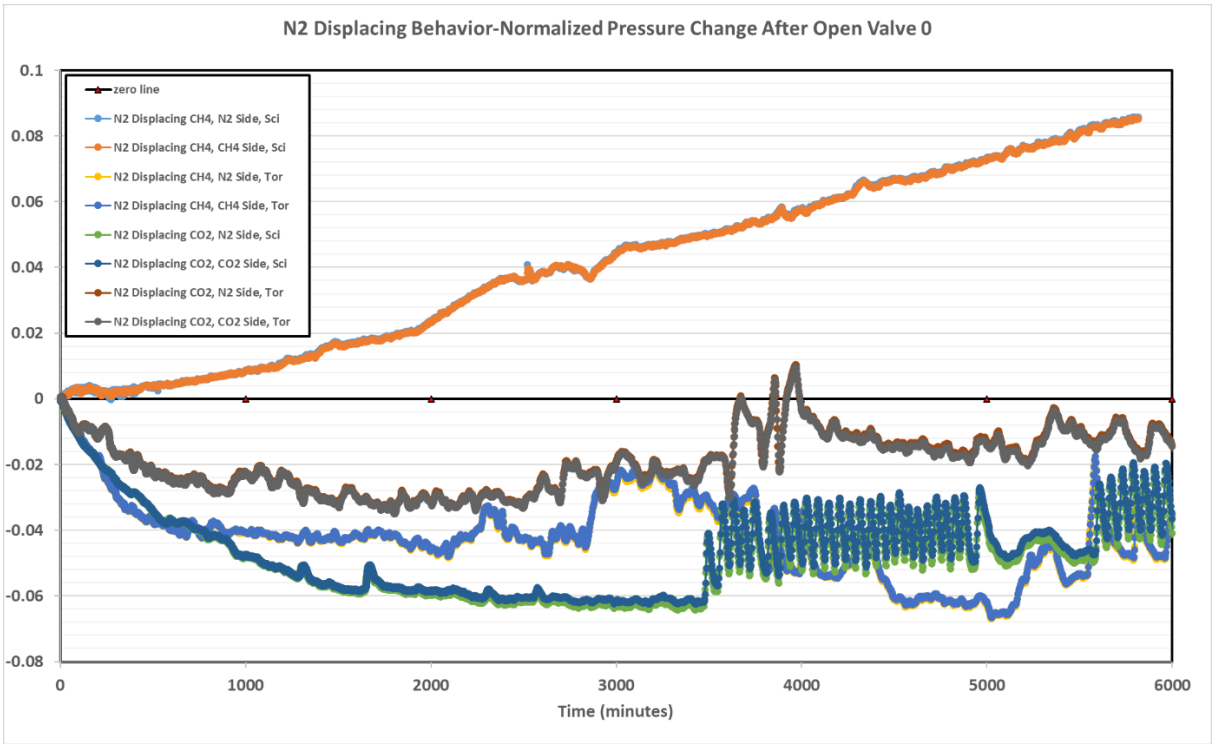

Figure 75 N_2 Displacing Behavior-Normalized Pressure Change After Open Valve 0

3.4.4.2 Carbon Dioxide Behavior

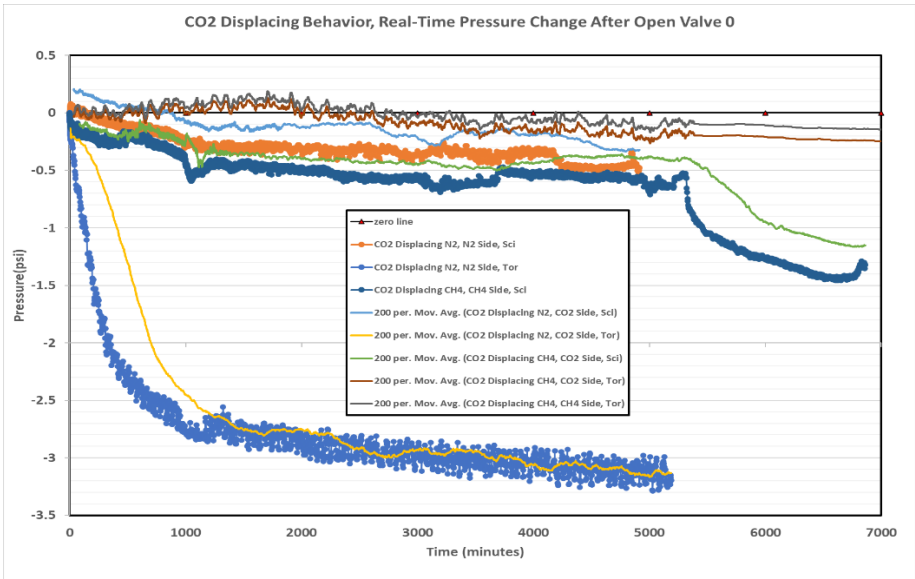

Figure 76 CO_2 Displacing Behavior, Real-Time Pressure Change After Open Valve 0

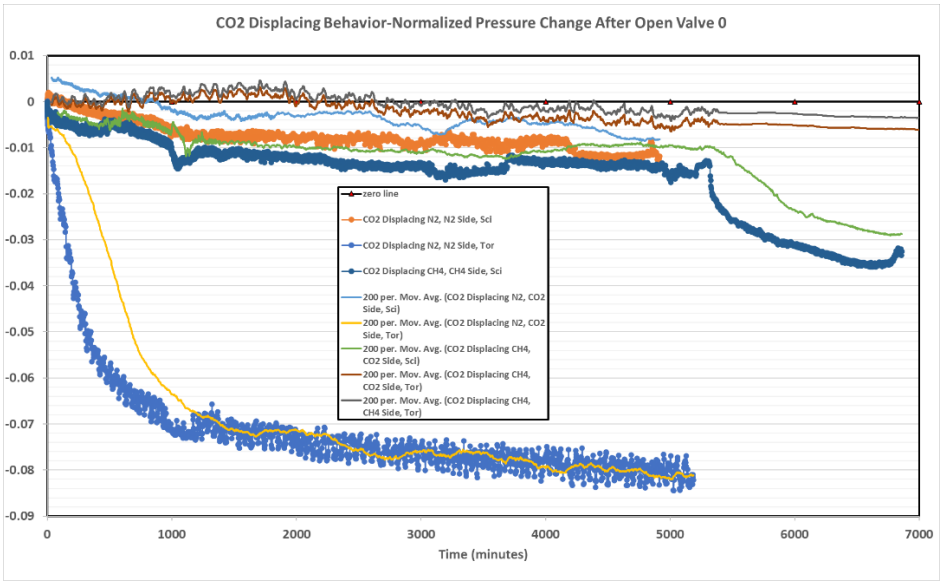

Figure 77 CO_2 Displacing Behavior-Normalized Pressure Change After Open Valve 0

CO_2 is the heaviest gas molecules among the three gases. Therefore, it will push the other two in the beginning. But it also has the largest adsorption ability. The adsorption of CO_2 on the pore wall will increase the mass entering the system but not reflecting in pressure. Therefore, as we can see from Figure 76 and 77, the trends of these experiment results are all decreasing, which means the mass flow into the system is less than the mass flowing out. Since if we use carbon dioxide as displacing gas, it is much heavier than the other two gases and hard to enter the pores. The main method it enters the system is through the pressure gradient created by the periodically increasing pressure cycle due to the gas regulator. And each cycle it will bring some of the displaced gas out of the system. Therefore, it will show a decreasing trend for most cases because the pressure cycle is the dominate factor and the pressure decreasing cannot be ignored. And since nitrogen is not adsorbed on the pore wall, it will get out of the system easier than methane.

Compared with Figure 35 and 37, the pressure decrease in carbon dioxide displacing nitrogen in Scioto core group from around 800 minutes to the end of the experiment is comparable to the situations in Figure 35 and 37, but the fast-decreasing speed showing in the first 800 minutes in Figure 76 is totally different from Figure 35 and 37, since there is no such behavior in single gas mode. The fast-decreasing trend should be caused by the combination of adsorption of carbon dioxide on the pores as well as the diffusion of nitrogen. Of course, we cannot ignore the “huff-n-puff” pressure releasing mode on carbon dioxide gas regulator. This behavior may contribute to the fast depletion of nitrogen in the core and Compartment 2.

3.4.4.3 Methane Behavior

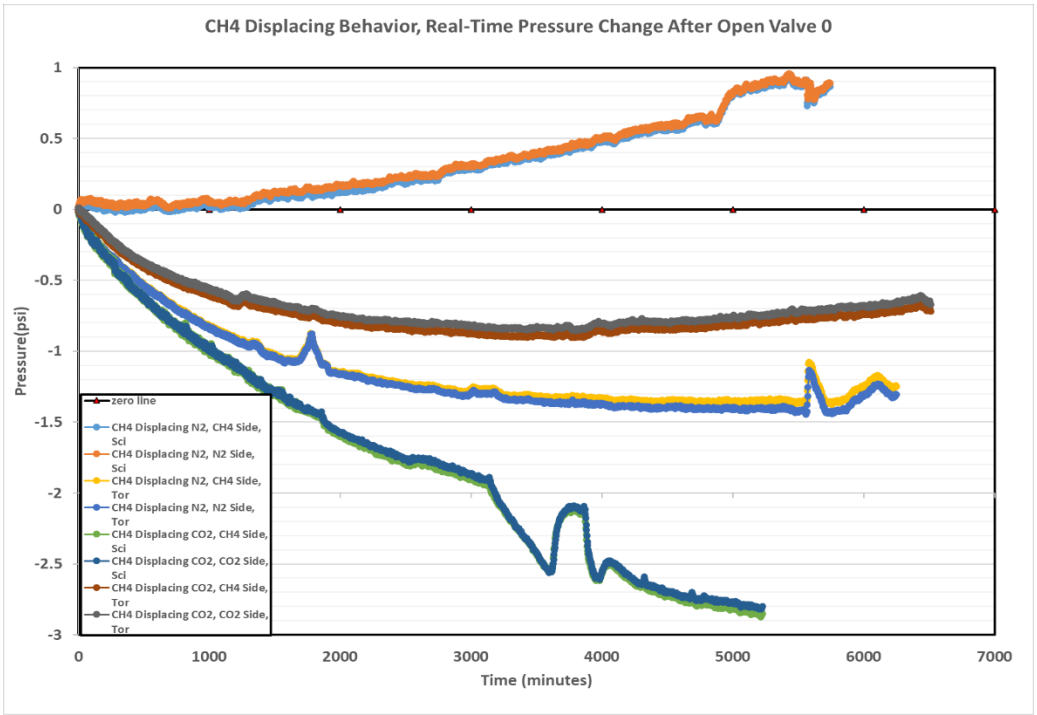

Figure 78 CH_4 Displacing Behavior, Real-Time Pressure Change After Open Valve 0

Methane is the lightest among the three gases. Therefore, it has the fastest diffusion speed, but also the most easily to be dragged. In Scioto core, we find a more pressure change than in Torrey core. Since larger pores can have more space for the movement of molecules. At this time, the heavier component is dominating the total flux. But the drag effect from lighter components is also worth noticing here. Thus, in Torrey core, we find the pressure is always decreasing, but not so fast as in Scioto core. In Scioto core, we find the trend for methane displacing nitrogen is totally different. Here we think the reason is methane is much easier to absorb on the pore wall than nitrogen, and it quickly diffuses into the system, which will lead to the mass accumulation in the system. In methane displacing CO_2 experiment, CO_2 is more likely to be absorbed on the pore surface, and CO_2 is much heavier than methane, thus the CO_2 is dominating the pressure change in this case. If

we compare the pressure decreasing speed in Figure 39, we found that in single gas experiments, the pressure decreases much faster than what Figure 78 is showing. And in single gas experiments, the pressure will never bounce back (increase again). Therefore, the pressure behavior shown in Figure 39 could not be first order effect.

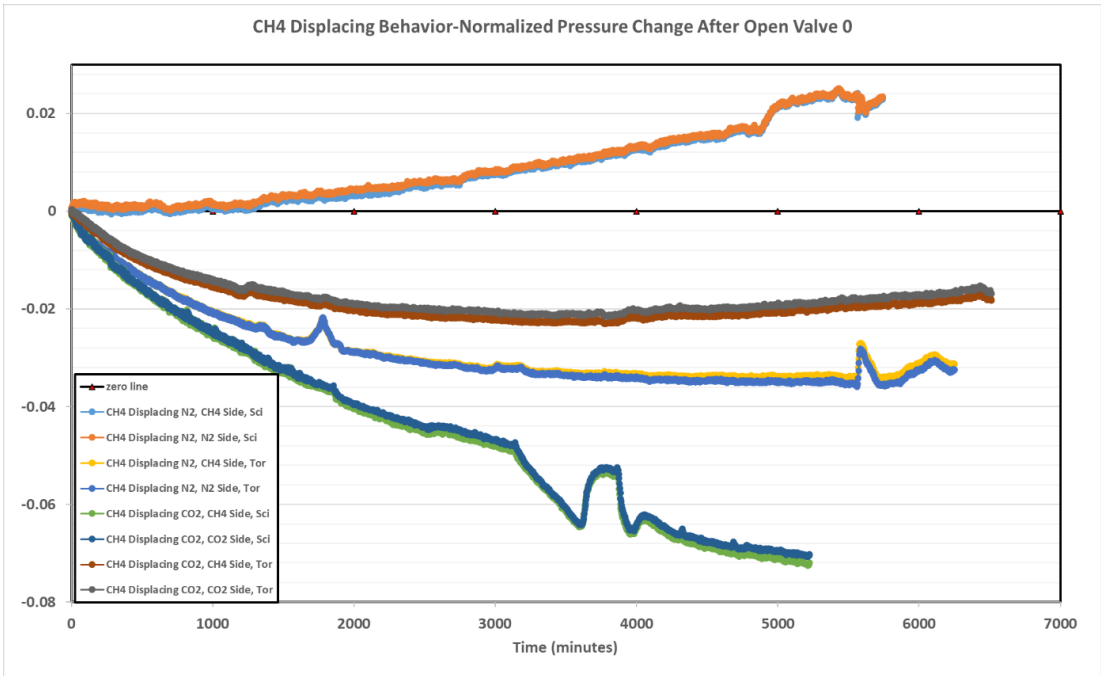

Figure 79 CH_4 Displacing Behavior-Normalized Pressure Change After Open Valve 0

In general, the pressure response in porous media is the combination result of different mechanisms, such as surface diffusion, molecular diffusion, adsorption, and may have Knudsen diffusion. In order to verify the pressure caused by corresponding factors, we need to further develop the experiment. For example, to verify the Knudsen diffusion impact, we can use shale cores to carry out the experiment. The smaller the pore size, the larger the Knudsen number is. And thus, we can eliminate the impact of molecular diffusion, which means molecules would tend to hit the wall

rather than hit each other. This requires the cores to have permeability at Nano-Darcy scale. If the shale is going to be used, then the organic matter factor could also be checked. On the other hand, if we want to explore the adsorption impact, we should measure the gas adsorption isotherm on the cores. To better observe the pressure behavior under molecular diffusion, we can use high permeability cores, like in Darcy scale sandstone to further prove the competitive mechanism. The pressure building up or decrease presented in this thesis is observed in limited time and condition. Therefore, within a limited time scale, we try to analyze these factors one by one. If the observing time goes longer, the conclusions may be different.

In case of adsorption, we found it played a role in the pressure response with the adsorbable gas, such as carbon dioxide. This phenomenon was also verified by previous scholars. Fujii et al. (Fujii et al., 2009[134]) measured the adsorption isotherm for carbon dioxide on Kimachi Sandstone at 33, 40 and 50 Celsius degrees, respectively. They found the mass of the core sample increased at atmosphere pressure. And the sorption capacity increased with pressure applied and decreased with the increase of temperature. At the same time, the swelling effect would change the pore structure and affect the adsorbing capacity of carbon dioxide. But they didn't mention the function of organic matter in the core.

Bashier (Bashier, 2018[135]) tested the adsorption isotherm of methane on Scioto Sandstone and Bandera Sandstone. They set the pressure up to 1250 psi under constant 23 Celsius degrees. Below shows the isotherm for methane on Scioto core:

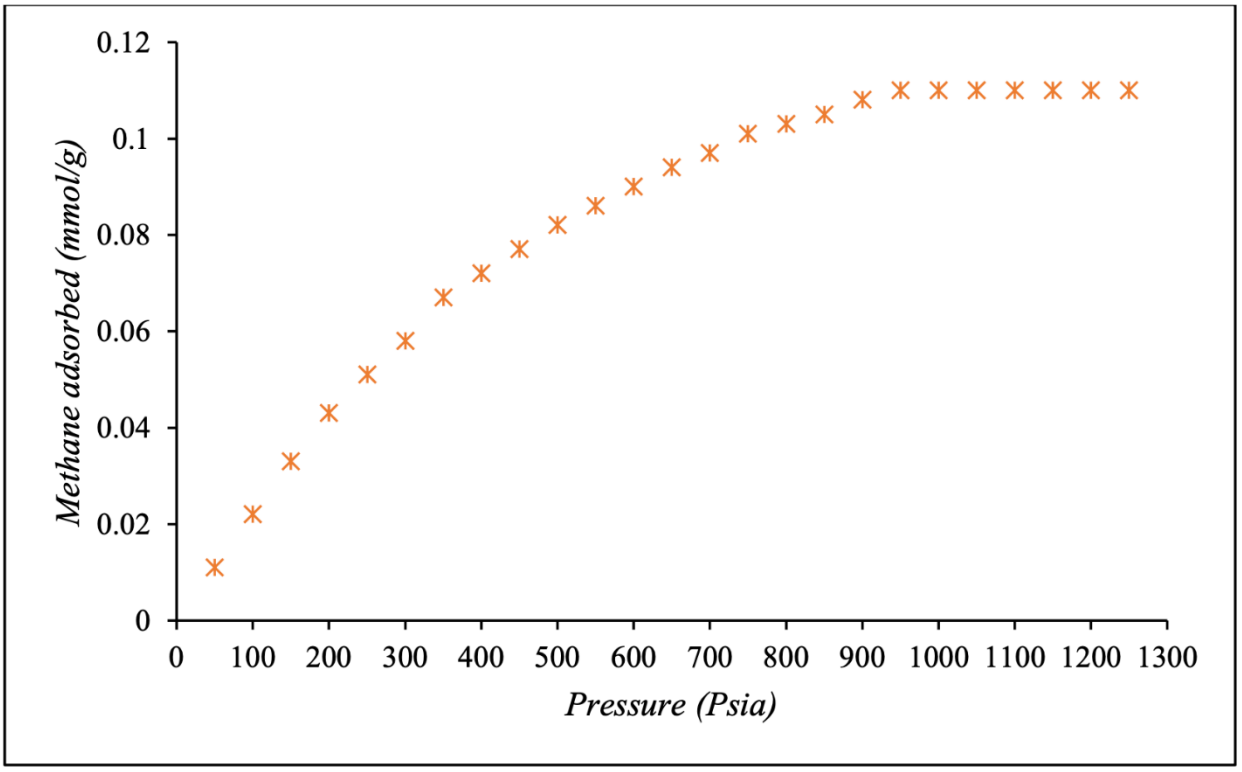

Figure 80 Methane Adsorption Isotherm in Scioto Sandstone[135]

The equilibrium and saturation pressure are the key control factors for the interaction between methane and pore wall. The potential force created during this process will cause an increase of adsorption at low pressure and completely fill the pores with methane molecules. The pore sizes, surface area and the mineral components of the sandstone would all affect the adsorption behavior. Although there is no organic material in sandstone, the clay minerals could also provide additional surface area for the adsorption of methane. Compared the adsorption capacity of carbon dioxide and that of methane, carried by Hasan et al. (Hasan et al., 2017[136]), they found in sandstones, the adsorption capacity of methane is lower than that of carbon dioxide. Thus, in sandstone, we can still have competitive adsorption in the pores. What's more, the adsorption layer of methane would interact with the molecules in the void space, therefore the combined mechanism is more complex.

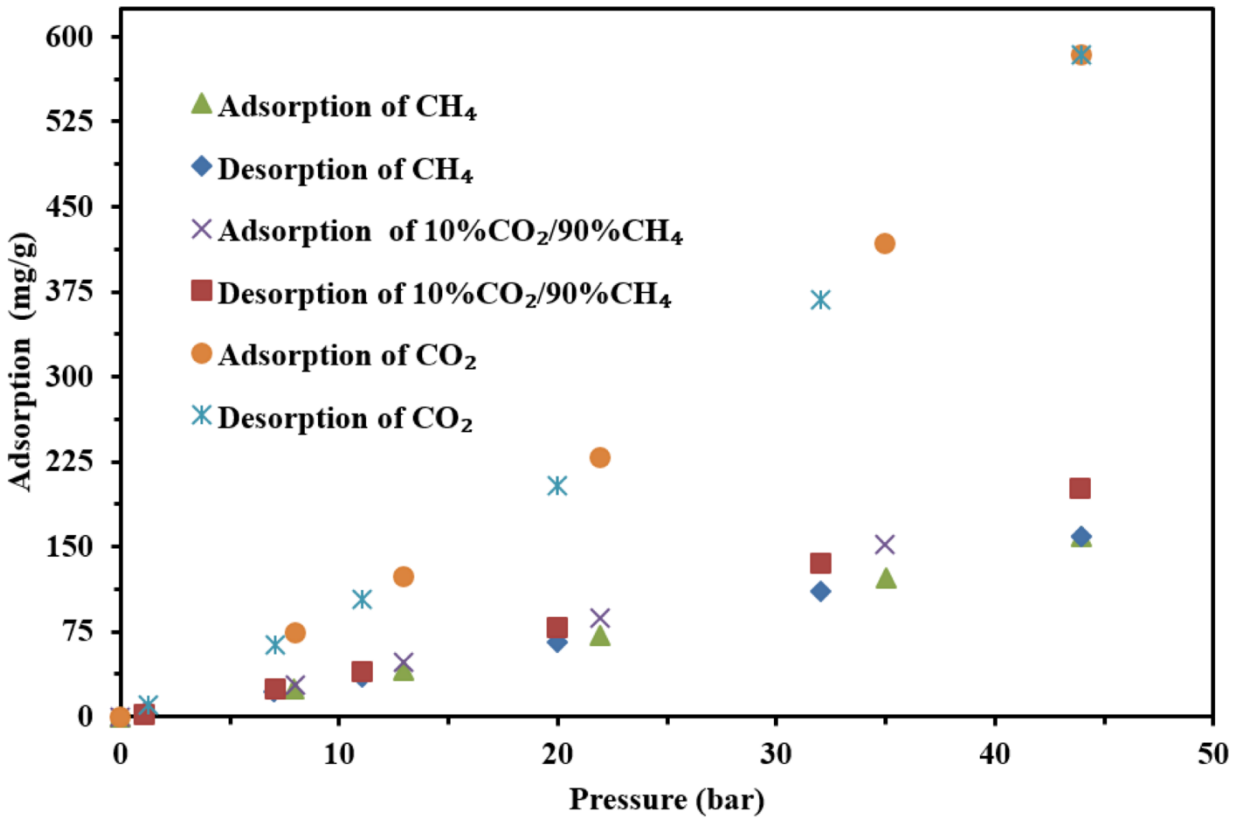

Figure 81 Adsorption/Desorption of CH_4, CO_2 and 10%CO_2-90%CH_4 mixture on shale at 100 Celsius[136]

Li et al. (Li et al., 2019[137]) and Xu et al. (Xu et al., 2022[138]) both confirmed the adsorption of nitrogen in sandstones was belong to H3 types. The low permeability sandstones had a large pore volume. And the pore volume was positively proportional to the specific surface area. The adsorption capacity of nitrogen is the lowest among the three gases mentioned before. Therefore, the possibility of blocking the pore by nitrogen molecules is also the lowest.

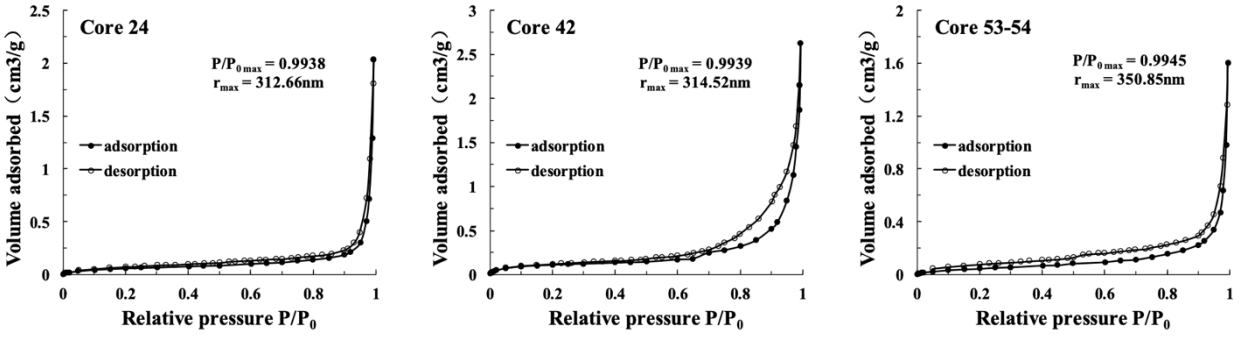

Figure 82 Nitrogen Adsorption and Desorption Isotherm in Sandstone (by Li et al. [137])

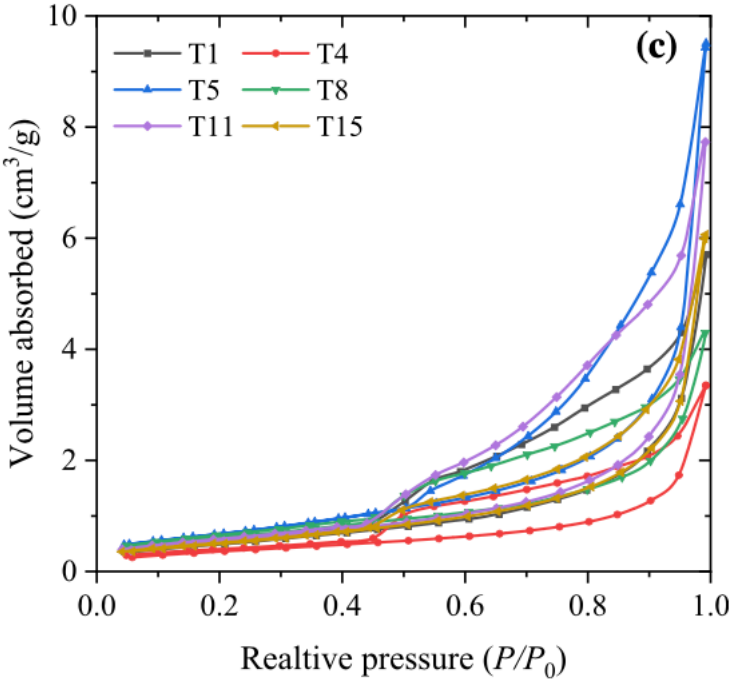

Figure 83 Nitrogen Adsorption and Desorption Isotherm in Sandstone (by Xu et al. [138])

Different color lines in Figure 81 mean different sandstone cores.

4. Conclusions and Recommendations

In this thesis, we look back at what the other scholars have been doing in their research activities on countercurrent diffusion. Our work is based on their design mechanism and thought and extend the experiment condition to fit the realistic procedure in the field. We observe the pressure change with time during the countercurrent diffusion by using two different permeability cores and three kinds of gases (nitrogen, carbon dioxide, and methane) to mimic the cyclic gas injection process of Enhanced Gas Recovery process in the field. Our object is to see whether we can achieve mass storage or mass depletion under specific conditions. So far, we find single gas operating in the system would not trigger diffusion flux in the system. The mass transfer in no-core binary diffusion is dominated by the heavier component. The total pressure change at the beginning stage is affected by heavier bulk movement direction, and later will be affected by lighter components. In binary countercurrent diffusion with core experiments, we have the following conclusion: First, we did not observe obvious pressure difference at the two sides of the core. The DP curves stabilized at zero line for most of the time. The permeability of the core will have an impact on the countercurrent diffusion. This impact is exerted by the pore size and the specific surface area. Organic matters should also play a role in this process, but we do not investigate this factor. Another important conclusion is the gas sort, which is a dominant factor in all cases. Their molecular weight, polarity, adsorption characteristics would determine the velocity of mass bulk moving and the diffusion speed. What we have found is that although the lighter molecules may have faster diffusion speed, in most cases the mass flux direction is dominated by the heavier component. The drag effect, the adsorption rate of heavier component greatly influences the flow direction, and thus influences the pressure response. But the gas itself is not the only factor affecting the mass transfer rate, we must consider the pore effect on the gases, too. And we also confirm using CO_2 as a displacing gas can effectively deplete the methane inside the porous media. Meanwhile, the CO_2 itself can be stored inside the pore by adsorption process, which is a win-win

process in both Enhanced Gas Recovery and CCUS processes.

In this research, we mainly explore the impact of permeability and different gases on the diffusion of gas in porous media. There are, of course, many other parameters need to be considered in the research of relevant experiments, such as different temperature (Yang et al., 1982[131]), different pressure, different flow rate, presence of organic matter and/or water in the porous media and even multicomponent gases diffusion (saturate the core with more than one kind of gas), etc. These factors are also important but not shown in this research. At the same time, due to the equipment and the space limited in the lab, we do not have a real-time gas chromatograph connected at the outlet of the system to monitor the component change as time goes by. And the observation time for some of the experiments is not long enough, limited by the storage memory of the computer. Therefore, some phenomena will be missed for this reason. In future works, one could consider these factors and further develop the theory over the non-steady state diffusion process.

References

[1] Outlook for energy (2023-01-10) ExxonMobil. Available at: https://corporate.exxonmobil.com/energy-and-innovation/outlook-for-energy (Accessed: January 30, 2023).

[2] Energy Outlook: Energy Economics: Home (2023-01-30) bp global. bp global. Available at: https://www.bp.com/en/global/corporate/energy-economics/energy-outlook.html (Accessed: January 30, 2023).

[3] IPCC. Sixth Assessment Report Synthesis Report Outline. Report of the Scoping Meeting for the IPCC Sixth Assessment Report Synthesis Report (Singapore 21 – 23 October 2019)

[4] IEA (2022-11-10) World energy outlook 2022 – analysis, IEA. Available at: https://www.iea.org/reports/world-energy-outlook-2022 (Accessed: February 1, 2023).

[5] Stevens, P. (2012) The Shale Gas Revolution: Developments and changes. London: Chatham House.

[6] Gong, B. (2020) "The development and implication of nature gas market in the context of the Shale Revolution," Shale Energy Revolution, pp. 19–36. Available at: https://doi.org/10.1007/978-981-15-4855-0_2.

[7] O'Sullivan, F. and Paltsev, S. (2012) "Shale gas production: Potential versus actual greenhouse gas emissions," Environmental Research Letters, 7(4), p. 044030. Available at: https://doi.org/10.1088/1748-9326/7/4/044030.

[8] Wang, S. (2018) "Shale Gas Exploitation: Status, problems and Prospect," Natural Gas Industry B, 5(1), pp. 60–74. Available at: https://doi.org/10.1016/j.ngib.2017.12.004.

[9] Kinnaman, T.C. (2011) “The economic impact of shale gas extraction: A review of existing studies,” Ecological Economics, 70(7), pp. 1243–1249. Available at: https://doi.org/10.1016/j.ecolecon.2011.02.005.

[10] Wang, Q. and Li, R. (2017) “Research status of Shale Gas: A Review,” Renewable and Sustainable Energy Reviews, 74, pp. 715–720. Available at: https://doi.org/10.1016/j.rser.2017.03.007.

[11] Melikoglu, M. (2014) “Shale Gas: Analysis of its role in the Global Energy Market,” Renewable and Sustainable Energy Reviews, 37, pp. 460–468. Available at: https://doi.org/10.1016/j.rser.2014.05.002.

[12] Burnham, A. et al. (2011) “Life-cycle greenhouse gas emissions of shale gas, natural gas, coal, and petroleum,” Environmental Science & Technology, 46(2), pp. 619–627. Available at: https://doi.org/10.1021/es201942m.

[13] Curtis, J.B. (2002) “Fractured shale-gas systems,” AAPG Bulletin, 86. Available at: https://doi.org/10.1306/61eeddbe-173e-11d7-8645000102c1865d.

[14] Holditch, S. (2006) “Tight Gas Sands,” Journal of Petroleum Technology, 58(6). Available at: https://doi.org/10.2118/103356-ms.

[15] Sakhaee-Pour, A., Bryant, S.L. (2014) Effect of pore structure on the producibility of tight-gas sandstones. AAPG Bulletin; 98 (4): 663–694. doi: https://doi.org/10.1306/08011312078

[16] Spencer, C.W. (1985) "Geologic Aspects of Tight Gas Reservoirs in the Rocky Mountain Region." J Pet Technol 37: 1308–1314. doi: https://doi.org/10.2118/11647-PA

[17] Clarkson, C.R. R., Nobakht, M., Kaviani, D., and Ertekin. T. "Production Analysis of Tight-Gas and Shale-Gas Reservoirs Using the Dynamic-Slippage Concept." (2012) SPE J. 17: 230–

242. doi: https://doi.org/10.2118/144317-PA

[18] Aguilera, R. (2010) "Flow Units: From Conventional to Tight Gas to Shale Gas Reservoirs." Paper presented at the Trinidad and Tobago Energy Resources Conference, Port of Spain, Trinidad, June 2010. doi: https://doi.org/10.2118/132845-MS

[19] Naik G.C. (2004) Tight Gas Reservoir–an Unconventional Natural Energy Source for the Future, pp. 1-32.

[20] Zhang, T., Sun, S. and Song, H. (2018) "Flow mechanism and simulation approaches for Shale Gas Reservoirs: A Review," Transport in Porous Media, 126(3), pp. 655–681. Available at: https://doi.org/10.1007/s11242-018-1148-5.

[21] Wu, K. et al. (2014) "Apparent permeability for gas flow in shale reservoirs coupling effects of gas diffusion and desorption," Proceedings of the 2nd Unconventional Resources Technology Conference [Preprint]. Available at: https://doi.org/10.15530/urtec-2014-1921039.

[22] Shabro, V., Torres-Verdin, C. and Javadpour, F. (2011) "Numerical simulation of shale-gas production: From pore-scale modeling of slip-flow, Knudsen diffusion, and Langmuir desorption to reservoir modeling of compressible fluid," All Days [Preprint]. Available at: https://doi.org/10.2118/144355-ms.

[23] Hu Y. et.al. (2013) "Physical simulation on gas percolation in tight sandstone" Petroleum Exploration and Development. DOI: 10.11698/PED.2013.05.10.

[24] Yang X., Fu L. (2012) "Accumulation mechanism of tight sandstone gas reservoir and its exploration prospects," Fault-Block Oil & Gas Field, 19(3): 302-306.

[25] Fu H., Tang D., Xu H., et al. (2012) "Characteristics of tight sandstone reservoir and

accumulation process of gas pool," Fault-Block Oil & Gas Field, 19(1): 47-50.

[26] Yang X. (2018) "Tight Sandstone Gas Reservoir Effectiveness and Hydrocarbon Forming Regularity of Es4 in Ji Yang Depression," A Dissertation Submitted for the Degree of Doctor of Engineering in China University of Petroleum (East China).

[27] Moridis, G.J., Blasingame, T.A. and Freeman, C.M. (2010) "Analysis of mechanisms of flow in fractured tight-gas and shale-gas reservoirs," All Days [Preprint]. Available at: https://doi.org/10.2118/139250-ms.

[28] Dong X. (2019) "Study on microscopic migration rule and flow mechanism of shale gas" A Dissertation Submitted to China University of Mining & Technology in Partial Fulfillment of the Requirement for the Master of Engineering.

[29] Bing Z. (2018) "Research on Evaluation Method of Basin-scale Tight Gas Sands Resources-Illustrated by the Case of North America," A Thesis Submitted to the Northeast Petroleum University.

[30] Law, B.E., Pollastro, R.M. and Keighin, C.W. (1986) "Geologic characterization of low-permeability gas reservoirs in selected wells, Greater Green River Basin, Wyoming, Colorado, and Utah," Geology of Tight Gas Reservoirs [Preprint]. Available at: https://doi.org/10.1306/st24459c13.

[31] Wu, K. et al. (2016) "A model for multiple transport mechanisms through nanopores of shale gas reservoirs with real gas effect–adsorption-mechanic coupling," International Journal of Heat and Mass Transfer, 93, pp. 408–426. Available at: https://doi.org/10.1016/j.ijheatmasstransfer.2015.10.003.

[32] Li, D. et al. (2014) "Effect of Knudsen diffusion and Langmuir adsorption on pressure transient response in tight- and shale-gas reservoirs," Journal of Petroleum Science and

Engineering, 124, pp. 146–154. Available at: https://doi.org/10.1016/j.petrol.2014.10.012.

[33] Zhou, M.Q. (2021) “Research on Huff and Puff of Shale Gas CO_2 Injection,” A Dissertation Submitted to Chongqing University in Partial Fulfillment of the Requirement for the Master of Engineering.

[34] Li C., Zhu S. (2015) “Diffusion Is Not the Production Mechanism of Shale Gas”, Xinjiang Petroleum Geology. 1001-3873（2015）06-0719-05. DOI:10.7657/XJPG20150615

[35] IEA. CCUS https://www.iea.org/fuels-and-technologies/carbon-capture-utilisation-and-storage

[36] Melzer S.L. (2012) “Carbon Dioxide Enhanced Oil Recovery (CO_2 EOR): Factors Involved in Adding Carbon Capture, Utilization and Storage (CCUS) to Enhanced Oil Recovery,” A report in CO_2 Consultant and Annual CO_2 Flooding Conference.

[37] Vega, B. and Kovscek, A.R. (2010) “Carbon dioxide (CO_2) sequestration in oil and gas reservoirs and use for enhanced oil recovery (EOR),” Developments and Innovation in Carbon Dioxide (CO_2) Capture and Storage Technology, pp. 104–126. Available at: https://doi.org/10.1533/9781845699581.1.104.

[38] Hasan, M.M.F. et al. (2015) “A multi-scale framework for CO_2 Capture, utilization, and sequestration: CCUS and CCU,” Computers & Chemical Engineering, 81, pp. 2–21. Available at: https://doi.org/10.1016/j.compchemeng.2015.04.034.

[39] Liu, H.J., Were P., Li, Q., Gou, Y., Hou, Z. (2017) "Worldwide Status of CCUS Technologies and Their Development and Challenges in China", Geofluids, vol. 2017, Article ID 6126505, 25 pages. https://doi.org/10.1155/2017/6126505

[40] Bachu, S. (2016) “Identification of oil reservoirs suitable for CO_2 -EOR and CO_2 storage

(CCUS) using reserves databases, with application to Alberta, Canada," International Journal of Greenhouse Gas Control, 44, pp. 152–165. Available at: https://doi.org/10.1016/j.ijggc.2015.11.013.

[41] Liu, H.J. et al. (2017) "Worldwide status of CCUS Technologies and their development and challenges in China," Geofluids, 2017, pp. 1–25. Available at: https://doi.org/10.1155/2017/6126505.

[42] Rodeny W., Menefee, A., Clarens, A. (2016) "Environmental Life Cycle Analysis of Water and CO_2-Based Fracturing Fluids Used in Unconventional Gas Production". Environmental Science & Technology.

[43] Chapiro, G. and Bruining, J. (2015) "Combustion enhance recovery of Shale Gas," Journal of Petroleum Science and Engineering, 127, pp. 179–189. Available at: https://doi.org/10.1016/j.petrol.2015.01.036.

[44] Ettehadtavakkol, A., Lake, L.W. and Bryant, S.L. (2014) "CO_2-Eor and storage design optimization," International Journal of Greenhouse Gas Control, 25, pp. 79–92. Available at: https://doi.org/10.1016/j.ijggc.2014.04.006.

[45] Núñez-López, V. and Moskal, E. (2019) "Potential of CO_2-EOR for near-term decarbonization," Frontiers in Climate, 1. Available at: https://doi.org/10.3389/fclim.2019.00005.

[46] F. Gozalpour, S., Ren R. and Tohidi B. (2005) "CO_2 EOR and Storage in Oil Reservoir". Oil & Gas Science and Technology - Rev. IFP, 60 3 537-546. DOI: https://doi.org/10.2516/ogst:2005036

[47] Du Y., Pang F., Chen K., Lin T., Chen X., Wang R. (2019) Experiment of Breaking Shale Using Supercritical Carbon Dioxide Jet. Earth Science.,44(11).

https://doi.org/10.3799/dqkx.2019.221

[48] Hou B., Song Z., Jia J., et al. (2018) "Experimental investigation on mechanical properties of tight sandstone under the effect of SC-CO_2". China Offshore Oil and Gas, 30(5):109—115.

[49] Hajj, E.I. et al. (2013) Carbonate Reservoir Interaction with Supercritical Carbon Dioxide. International Petroleum Technology Conference.

[50] Wilkins, R., Menefee, A.H. and Clarens A.F. (2016) "Environmental Life Cycle Analysis of Water and CO_2-Based Fracturing Fluids Used in Unconventional Gas Production" Environmental Science & Technology 50 (23), 13134-13141. https://doi.org/10.1021/acs.est.6b02913

[51] Syah, R.; Alizadeh, S.M., Nurgalieva, K.S.; Grimaldo Guerrero, J.W.; Nasution, M.K.M.; Davarpanah, A.; Ramdan, D.; Metwally, A.S.M. (2021) "A Laboratory Approach to Measure Enhanced Gas Recovery from a Tight Gas Reservoir during Supercritical Carbon Dioxide Injection". Sustainability, 13, 11606. https://doi.org/10.3390/su132111606

[52] Wang, L. et al. (2015) "Comparison of enhanced coalbed methane recovery by pure N_2 and CO_2 Injection: Experimental Observations and Numerical Simulation," Journal of Natural Gas Science and Engineering, 23, pp. 363–372. Available at: https://doi.org/10.1016/j.jngse.2015.02.002.

[53] Zhou, F., Hussain, F. and Cinar, Y. (2013) "Injecting pure N_2 and CO_2 to coal for enhanced coalbed methane: Experimental observations and numerical simulation," International Journal of Coal Geology, 116-117, pp. 53–62. Available at: https://doi.org/10.1016/j.coal.2013.06.004.

[54] Liu, D., Li, Y., Yang S., and Agarwal R.K., (2021) CO_2 sequestration with enhanced shale gas recovery, Energy Sources, Part A: Recovery, Utilization, and Environmental Effects, 43:24, 3227-3237, DOI: 10.1080/15567036.2019.1587069

[55] Louk, K. et al. (2017) “Monitoring CO_2 storage and enhanced gas recovery in unconventional shale reservoirs: Results from the Morgan County, Tennessee injection test,” Journal of Natural Gas Science and Engineering, 45, pp. 11–25. Available at: https://doi.org/10.1016/j.jngse.2017.03.025.

[56] Tosun İ. (2019) Fundamental mass transfer concepts in engineering applications. Boca Raton: Taylor & Francis, a CRC title, part of the Taylor & Francis imprint, a member of the Taylor &Francis Group, the academic division of T&F Informa, plc. https://books.google.ca/books?id=6PycDwAAQBAJ&lpg=PP1&ots=4Bl04W_Bex&dq=Fundamental%20mass%20transfer%20concepts%20in%20engineering%20applications&lr&pg=PR3#v=onepage&q=Fundamental%20mass%20transfer%20concepts%20in%20engineering%20applications&f=false

[57] Thirumaleshwar, M. (2006) Fundamentals of Heat and Mass Transfer. Pearson.

[58] Song, H. et al. (2016) “Unifying diffusion and seepage for nonlinear gas transport in Multiscale Porous Media,” Chemical Physics Letters, 661, pp. 246–250. Available at: https://doi.org/10.1016/j.cplett.2016.06.073.

[59] Bird, R. B., Stewart, W. E., and Lightfoot, E. N. (2002) Transport Phenomena, 2nd ed., New York: John Wiley & Sons.

[60] Marrero T. R. and Mason, E. A. (1972) "Gaseous Diffusion Coefficients", Journal of Physical and Chemical Reference Data 1, 3-118 https://doi.org/10.1063/1.3253094

[61] Kestin, J., Knierim, K., Mason, E. A., Najafi, B.S., Ro, T., and Waldman, M. (1984) "Equilibrium and Transport Properties of the Noble Gases and Their Mixtures at Low Density", Journal of Physical and Chemical Reference Data 13, 229-303 https://doi.org/10.1063/1.555703

[62] Rahmanian, M.R., Aguilera, R. and Kantzas, A. (2011) "A new unified diffusion-viscous flow model based on pore level studies of tight gas formations," All Days [Preprint]. Available at: https://doi.org/10.2118/149223-ms.

[63] Wan, Y. et al. (2015) "An experimental investigation of diffusivity and porosity anisotropy of a Chinese gas shale," Journal of Natural Gas Science and Engineering, 23, pp. 70–79. Available at: https://doi.org/10.1016/j.jngse.2015.01.024.

[64] Mezedur, M.M., Kaviany, M. and Moore, W. (2002) "Effect of pore structure, randomness and size on effective mass diffusivity," AIChE Journal, 48(1), pp. 15–24. Available at: https://doi.org/10.1002/aic.690480104.

[65] Qiao, J. et al. (2021) "Pore-scale heterogeneity of tight gas sandstone: Origins and impacts," Journal of Natural Gas Science and Engineering, 96, p. 104248. Available at: https://doi.org/10.1016/j.jngse.2021.104248.

[66] Javadpour, F., Singh, H., Rabbani, A., Babaei, M., and Enayati.S., (2021) "Gas Flow Models of Shale: A Review," Energy & Fuels. 35 (4), 2999-3010. https://doi.org/10.1021/acs.energyfuels.0c04381

[67] Zhong, Y. et al. (2019) "Experimental and numerical analyses of apparent gas diffusion coefficient in Gas Shales," Fuel, 258, p. 116123. Available at: https://doi.org/10.1016/j.fuel.2019.116123.

[68] Chen, J. et al. (2017) "The effect of Knudsen diffusion and adsorption on shale transport in nanopores," Advances in Mechanical Engineering, 9(9), p. 168781401772185. Available at: https://doi.org/10.1177/1687814017721858.

[69] Kim, C. et al. (2016) "Diffusion characteristics of nanoscale gas flow in shale matrix from Haenam Basin, Korea," Environmental Earth Sciences, 75(4). Available at:

https://doi.org/10.1007/s12665-016-5267-4.

[70] Kuila, U., Prasad M. and Kazemi, H., (2013) "Assessing Knudsen flow in gas-flow models of shale reservoirs," CSEG Recorder https://csegrecorder.com/assets/pdfs/2013/2013-05-RECORDER-Assessing_Knudsen_Flow.pdf

[71] Li, J., Cai, C. and Li, Z.-H. (2021) "Knudsen diffusion differs from Fickian Diffusion," Physics of Fluids, 33(4), p. 042009. Available at: https://doi.org/10.1063/5.0048978.

[72] Tsong, T. (2001) "Mechanisms of surface diffusion," Progress in Surface Science, 67(1-8), pp. 235–248. Available at: https://doi.org/10.1016/s0079-6816(01)00026-0.

[73] Wu, K. et al. (2015) "A model for surface diffusion of adsorbed gas in nanopores of Shale Gas Reservoirs," All Days [Preprint]. Available at: https://doi.org/10.4043/25662-ms.

[74] Wu, K. et al. (2016) "A unified model for gas transfer in nanopores of shale-gas reservoirs: Coupling pore diffusion and surface diffusion," SPE Journal, 21(05), pp. 1583–1611. Available at: https://doi.org/10.2118/2014-1921039-pa.

[75] Kapoor, A., Yang, R.T., and Wong C., (1989) Surface Diffusion, Catalysis Reviews—Science and Engineering, 31:1-2, 129-214, DOI: 10.1080/01614948909351350

[76] Ehrlich, G. and Stolt, K. (1980) "Surface diffusion," Annual Review of Physical Chemistry, 31(1), pp. 603–637. Available at: https://doi.org/10.1146/annurev.pc.31.100180.003131.

[77] Yang, B. et al. (2016) "Measurement of the surface diffusion coefficient for adsorbed gas in the fine mesopores and micropores of Shale Organic matter," Fuel, 181, pp. 793–804. Available at: https://doi.org/10.1016/j.fuel.2016.05.069.

[78] Qu, Z.G. et al. (2020) "Pore-scale investigation on coupled diffusion mechanisms of free and

adsorbed gases in nanoporous organic matter," Fuel, 260, p. 116423. Available at: https://doi.org/10.1016/j.fuel.2019.116423.

[79] Wang, J. et al. (2016) "Apparent permeability prediction of organic shale with generalized lattice Boltzmann model considering surface diffusion effect," Fuel, 181, pp. 478–490. Available at: https://doi.org/10.1016/j.fuel.2016.05.032.

[80] Xu, B., Qin, H. and Chen, L. (2022) "Investigation of Molecular Mean Free Path, molecular kinetic energy, and molecular polarity affecting Knudsen diffusivity along pore channels," Separations, 9(5), p. 130. Available at: https://doi.org/10.3390/separations9050130.

[81] Hamdan, M.H. and Sawalha, K.D. (1996) "Dusty gas flow through Porous Media," Applied Mathematics and Computation, 75(1), pp. 59–73. Available at: https://doi.org/10.1016/0096-3003(95)00104-2.

[82] Rezaveisi, M., Javadpour, F. and Sepehrnoori, K. (2014) "Modeling chromatographic separation of produced gas in Shale Wells," International Journal of Coal Geology, 121, pp. 110–122. Available at: https://doi.org/10.1016/j.coal.2013.11.005.

[83] Long, H. et al. (2021) "Adsorption and diffusion characteristics of CH_4, CO_2, and N_2 in micropores and mesopores of bituminous coal: Molecular dynamics," Fuel, 292, p. 120268. Available at: https://doi.org/10.1016/j.fuel.2021.120268.

[84] Xu, R. (2022) "Flow capacity characterization of unconventional natural gas bearing rocks using digital rock physics: A comparison between advection and diffusion," Journal of Petroleum Science and Engineering, 215, p. 110624. Available at: https://doi.org/10.1016/j.petrol.2022.110624.

[85] Remick, R.R. and Geankoplis, C.J. (1973) "Binary diffusion of gases in capillaries in the transition region between Knudsen and Molecular Diffusion," Industrial & Engineering

Chemistry Fundamentals, 12(2), pp. 214–220. Available at: https://doi.org/10.1021/i160046a012.

[86] Novák, M. and Schneider, P. (1990) “Pressure changes during unsteady-state diffusion of gases in porous catalyst pellets: An experimental study,” Applied Catalysis, 66(1), pp. 209–217. Available at: https://doi.org/10.1016/s0166-9834(00)81639-5.

[87] Novák, M. et al. (1988) “Dynamics of non-isobaric diffusion in porous catalysts,” Chemical Engineering Science, 43(2), pp. 185–193. Available at: https://doi.org/10.1016/0009-2509(88)85030-9.

[88] Ehrhardt, K., Klusáček, K. and Schneider, P. (1988) “Finite-difference scheme for solving dynamic multicomponent Diffusion Problems,” Computers & Chemical Engineering, 12(11), pp. 1151–1155. Available at: https://doi.org/10.1016/0098-1354(88)87036-4.

[89] Čapek, P. et al. (1997) “Gas transport in porous media under dynamic conditions,” Catalysis Today, 38(1), pp. 31–38. Available at: https://doi.org/10.1016/s0920-5861(97)00036-9.

[90] Arnošt, D. and Schneider, P. (1995) “Dynamic transport of multicomponent mixtures of gases in porous solids,” The Chemical Engineering Journal and the Biochemical Engineering Journal, 57(2), pp. 91–99. Available at: https://doi.org/10.1016/0923-0467(94)02900-8.

[91] Yang, J. et al. (2005) “Gas phase transport, adsorption and surface diffusion in a porous glass membrane,” Catalysis Today, 104(2-4), pp. 344–351. Available at: https://doi.org/10.1016/j.cattod.2005.03.069.

[92] Tuchlenski, A., Uchytil, P. and Seidel-Morgenstern, A. (1998) “An experimental study of combined gas phase and surface diffusion in porous glass,” Journal of Membrane Science, 140(2), pp. 165–184. Available at: https://doi.org/10.1016/s0376-7388(97)00270-6.

[93] Santiago, C.J.S. and Kantzas, A. (2017) “Chromatographic separation and liquid drop-out in unconventional gas reservoirs,” Journal of Petroleum Science and Engineering, 159, pp. 553–563. Available at: https://doi.org/10.1016/j.petrol.2017.09.049.

[94] Soukup, K., Schneider, P. and Šolcová, O. (2008) “Wicke–Kallenbach and Graham's diffusion cells: Limits of application for low surface area porous solids,” Chemical Engineering Science, 63(18), pp. 4490–4493. Available at: https://doi.org/10.1016/j.ces.2008.06.020.

[95] Soukup, K., Schneider, P. and Šolcová, O. (2008) “Comparison of Wicke–Kallenbach and Graham's diffusion cells for obtaining transport characteristics of porous solids,” Chemical Engineering Science, 63(4), pp. 1003–1011. Available at: https://doi.org/10.1016/j.ces.2007.10.032.

[96] Krishna, R. (2016) “Investigating the validity of the Knudsen diffusivity prescription for mesoporous and macroporous materials,” Industrial & Engineering Chemistry Research, 55(16), pp. 4749–4759. Available at: https://doi.org/10.1021/acs.iecr.6b00762.

[97] Čapek, P. et al. (1997) “Gas transport in porous media under dynamic conditions,” Catalysis Today, 38(1), pp. 31–38. Available at: https://doi.org/10.1016/s0920-5861(97)00036-9.

[98] Hejtmánek, V. et al. (1998) “Dynamics of pressure build-up accompanying multicomponent gas transport in porous solids: Inert Gases,” Chemical Engineering Journal, 70(3), pp. 189–195. Available at: https://doi.org/10.1016/s1385-8947(98)00095-3.

[99] Hejtmánek Vladimír et al. (1999) “Dynamics of pressure build-up accompanying multicomponent gas transport in porous solids: Adsorbable gases,” Chemical Engineering Journal, 74(3), pp. 171–179. Available at: https://doi.org/10.1016/s1385-8947(99)00078-9.

[100] Van Den Broeke, L.J.P. and Krishna, R. (1995) “Experimental verification of the Maxwell-stefan theory for Micropore Diffusion,” Chemical Engineering Science, 50(16), pp.

2507–2522. Available at: https://doi.org/10.1016/0009-2509(95)00102-b.

[101] Santiago, C.J.S. and Kantzas, A. (2018) "Investigating the effects of gas type and operation mode in enhanced gas recovery in unconventional reservoirs," Journal of Natural Gas Science and Engineering, 50, pp. 282–292. Available at: https://doi.org/10.1016/j.jngse.2017.12.001.

[102] Krishna, R. (1993) "Problems and pitfalls in the use of the Fick formulation for intraparticle diffusion," Chemical Engineering Science, 48(5), pp. 845–861. Available at: https://doi.org/10.1016/0009-2509(93)80324-j.

[103] Chen, Y.D. and Yang, R.T. (1992) "Predicting binary fickian diffusivities from pure-component Fickian diffusivities for surface diffusion," Chemical Engineering Science, 47(15-16), pp. 3895–3905. Available at: https://doi.org/10.1016/0009-2509(92)85138-2.

[104] Zhukovskii, N.E. (1900) Uber Den hydraulischen stoss in Wasserleitungsrohren. St. Petersbourg. 8th series (in German), 9 (5): 1–71

[105] Zhang, Z. et al. (2020) "Effects of instantaneous shut-in of high production gas well on fluid flow in tubing," Petroleum Exploration and Development, 47(3), pp. 642–650. Available at: https://doi.org/10.1016/s1876-3804(20)60081-7.

[106] Marić, I. (2005) "The Joule–Thomson effect in natural gas flow-rate measurements," Flow Measurement and Instrumentation, 16(6), pp. 387–395. Available at: https://doi.org/10.1016/j.flowmeasinst.2005.04.006.

[107] Perry, J.H. and Herrmann, C.V. (1935) "The Joule–Thomson effect of methane, nitrogen, and mixtures of these gases," The Journal of Physical Chemistry, 39(9), pp. 1189–1196. Available at: https://doi.org/10.1021/j150369a003.

[108] Sigmund, P.M. (1976) “Prediction of molecular diffusion at reservoir conditions. part 1-measurement and prediction of binary dense gas diffusion coefficients,” Journal of Canadian Petroleum Technology, 15(02). Available at: https://doi.org/10.2118/76-02-05.

[109] Yang, S. (2018) Fundamentals of Petrophysics. Springer-Verlag Berlin An.

[110] Li, Z. et al. (2015) “Numerical and experimental study on gas flow in nanoporous media,” Journal of Natural Gas Science and Engineering, 27, pp. 738–744. Available at: https://doi.org/10.1016/j.jngse.2015.09.014.

[111] Liu, H.-H. and Zhang, J. (2020) “An efficient laboratory method to measure the combined effects of Knudsen diffusion and mechanical deformation on shale permeability,” Journal of Contaminant Hydrology, 232, p. 103652. Available at: https://doi.org/10.1016/j.jconhyd.2020.103652.

[112] McGivern, W.S. and Manion, J.A. (2021) “Binary diffusion coefficients for methane and fluoromethanes in Nitrogen,” Journal of Chemical & Engineering Data, 66(8), pp. 3047–3056. Available at: https://doi.org/10.1021/acs.jced.1c00161.

[113] Piszko, M. et al. (2019) “Diffusivities of binary mixtures consisting of carbon dioxide, methane, and propane by dynamic light scattering,” Journal of Chemical & Engineering Data, 65(3), pp. 1068–1082. Available at: https://doi.org/10.1021/acs.jced.9b00495.

[114] Ellis, C. S. and Holsen, J. N. (1969) “Diffusion Coefficients for He-N_2 and N_2-CO_2 at Elevated Temperatures,” Industrial & Engineering Chemistry Fundamentals 1969 8 (4), 787-791. DOI: 10.1021/i160032a030

[115] Huang W., Liu D., Sun J., et al. (2020) Shale gas seepage and diffusion law in micro-nano pore. Science Technology and Engineering, 20(14): 5583-5588

[116] Sander, R. et al. (2020) "CH_4, CO_2, N_2 diffusion in Bowen Basin (Australia) coal: Relationship between sorption kinetics of coal core and crushed coal particles," Journal of Natural Gas Science and Engineering, 81, p. 103468. Available at: https://doi.org/10.1016/j.jngse.2020.103468.

[117] Liu, J., Li, S. and Wang, Y. (2019) "Molecular dynamics simulation of diffusion behavior of CH_4, CO_2, and N_2 in mid-rank coal vitrinite," Energies, 12(19), p. 3744. Available at: https://doi.org/10.3390/en12193744.

[118] Yu, S., Bo, J. and Qu, M. (2018) "Molecular dynamic simulation of self- and transport diffusion for CO_2/CH_4/N_2 in low-rank coal vitrinite," Energy & Fuels, 32(3), pp. 3085–3096. Available at: https://doi.org/10.1021/acs.energyfuels.7b03676.

[119] Cui, X., Bustin, R.M. and Dipple, G. (2004) "Selective Transport of CO_2, CH_4, and N_2 in Coals: Insights from modeling of Experimental Gas Adsorption Data," Fuel, 83(3), pp. 293–303. Available at: https://doi.org/10.1016/j.fuel.2003.09.001.

[120] Shi, Q. (2021) "Molecular dynamics simulation of diffusion and separation of CO_2/CH_4/N_2 on Mer Zeolites," Journal of Fuel Chemistry and Technology, 49(10), pp. 1531–1539. Available at: https://doi.org/10.1016/s1872-5813(21)60095-6.

[121] Sun, F. et al. (2019) "Transport behaviors of real gas mixture through nanopores of Shale Reservoir," Journal of Petroleum Science and Engineering, 177, pp. 1134–1141. Available at: https://doi.org/10.1016/j.petrol.2018.12.058.

[122] Yuan, W. et al. (2014) "Experimental study and modelling of methane adsorption and diffusion in Shale," Fuel, 117, pp. 509–519. Available at: https://doi.org/10.1016/j.fuel.2013.09.046.

[123] Dang W. (2018) Study on adsorption diffusion behavior and control mechanism of shale

gas. China University of Geosciences (Beijing). DOI: 10.27,493/d.cnki.gzdzy.2018.000,184

[124] Šolcová, O., Šnajdaufová, H. and Schneider, P. (2001) "Multicomponent counter-current gas diffusion in porous solids: The graham's-law diffusion cell," Chemical Engineering Science, 56(17), pp. 5231–5237. Available at: https://doi.org/10.1016/s0009-2509(01)00149-x.

[125] Šolcová, O. and Schneider, P. (2003) "Multicomponent counter-current gas diffusion: Determination of transport parameters," Applied Catalysis A: General, 244(1), pp. 1–9. Available at: https://doi.org/10.1016/s0926-860x(02)00499-4.

[126] Perrot, P. (2008) A to Z of thermodynamics. Oxford: Oxford University Press.

[127] Holman, J.P. (1988) Thermodynamics. New York, NY: McGraw-Hill.

[128] Levine, I.N. (2017) Physical Chemistry. Boston: McGraw-Hill.

[129] Liu J. (2019) "Study on Shale Gas Multi-Scale Transport Characteristics and Flow Consistency Mechanism," A Dissertation Submitted to China University of Mining & Technology in Partial Fulfillment of the Requirement for the Doctor of Philosophy.

[130] Du X.. (2018) "Dynamic Study of the Displacement of Adsorbed CH_4 on Shales by Injecting CO_2," A Thesis Submitted to Chongqing University in Partial Fulfillment of the Requirement for the Doctor's Degree of Engineering.

[131] Yang, R.T. and Liu, R.T. (1982) "Gaseous diffusion in porous solids at elevated temperatures," Industrial & Engineering Chemistry Fundamentals, 21(3), pp. 262–268. Available at: https://doi.org/10.1021/i100007a012.

[132] Perkins, T.K., and O.C. Johnston. "A Review of Diffusion and Dispersion in Porous

Media." SPE J. 3 (1963): 70–84. doi: https://doi.org/10.2118/480-PA

[133] Cunningham, R.E. (1980) “Diffusion in gases and porous media.” New York: Plenum Press.

[134] Fujii, T. et al. (2009) “Measurements of CO_2 sorption on rocks using a volumetric technique for CO_2 Geological Storage,” Energy Procedia, 1(1), pp. 3715–3722. Available at: https://doi.org/10.1016/j.egypro.2009.02.170.

[135] Bashir, H.B. (2018) Methane adsorption into sandstones and its role in gas recovery from Depleted Reservoirs. thesis.

[136] Hasan, M. et al. (2017) “Enhanced Gas Recovery (EGR) methods and production enhancement techniques for Shale & Tight Gas Reservoirs,” Day 4 Thu, April 27, 2017 [Preprint]. Available at: https://doi.org/10.2118/188090-ms.

[137] Li, X. et al. (2019) “Fractal characterization of nanopore structure in shale, tight sandstone and mudstone from the Ordos Basin of China using nitrogen adsorption,” Energies, 12(4), p. 583. Available at: https://doi.org/10.3390/en12040583.

[138] Xu, S. et al. (2022) “Fractal analysis of pore structure differences between shale and sandstone based on the nitrogen adsorption method,” Natural Resources Research, 31(3), pp. 1759–1773. Available at: https://doi.org/10.1007/s11053-022-10056-5.

[139] Thermodynamics graphical homepage - urieli - updated (6/22/2015). Available at: https://www.ohio.edu/mechanical/thermo/

[140] C. Graham, J. Pierrus & R.E. Raab (1989) Measurement of the electric quadrupole moments of CO2, CO and N2, Molecular Physics, 67:4, 939-955, DOI: 10.1080/00268978900101551

[141] A G Shashkov et al., 1979 J. Phys. B: Atom. Mol. Phys. 12 3619. https://iopscience.iop.org/article/10.1088/0022-3700/12/21/019/meta

[142] Jagiello, J., et al. (2020). "Exploiting the adsorption of simple gases O-2 and H-2 with minimal quadrupole moments for the dual gas characterization of nanoporous carbons using 2D-NLDFT models." Carbon 160: 164-175.

[143] https://www.biologyonline.com/dictionary/diffusion

[144] Matthew Balhoff, Chapter 7 - Component transport in porous media, Editor(s): Matthew Balhoff, Developments in Petroleum Science, Elsevier, Volume 75, 2022. https://doi.org/10.1016/B978-0-323-99235-0.00001-4

[145] Ho, C. K., & Webb, S. W. (2006). Gas Transport in Porous Media. Springer London, Limited.

[146] Dake, L. P. (2001). Fundamentals of Reservoir Engineering. Elsevier.

[147] Al-Hussainy, R., & Crawford, P. B. (1965). The Flow of Real Gases Through Porous Media. In Proceedings of Fall Meeting of the Society of Petroleum Engineers of AIME. https://doi.org/10.2118/1243-a

[148] Schlichting, H., & Gersten, K. (2003). Boundary layer theory: With 22 tables. Springer.

[149] Roebuck J.R.; Murrell T.A.; Miller E.E.: The Joule-Thomson Effect in Carbon Dioxide. J. Am. Chem. Soc. 64 (1942) 400-411

Appendix A

In order to explain why there is always a pressure decreasing at the circulation side, we should introduce the knowledge of gas seepage [146]. Our equipment setting is generally made of gas source (pressure is constant), lines, core, and compartments. Gas source can be taken as a closed circle boundary gas reservoir with fixed pressure. All the lines and cores can be taken as the formation. The producing end can be taken as a production well. When we analyze the pressure response, we can start from the radius direction. After we open the gas regulator on the gas tank and wait for the pressure response to reach the outlet of the system, we can take this process as an unsteady well testing period, which all gas well should experience after starting to produce. The whole process can be taken as natural depletion of the gas reservoir. The pressure build up is not shown in the pictures after the regulator is opened, but we can explain it first: When the gas enters the pipelines, the gas density would increase and the collision frequency between molecules also increases. Then the pressure would increase along the lines and finally reach the outlet (well bottom). Before the pressure response from the well bottom (producing end, outlet) reach the reservoir boundary (pressure source, gas tank), the flow in the system is unsteady, which can be characterized by the following equation:

$$\frac{dP}{dt} \neq constant \tag{A-1}$$

Here P is pressure at any point except at the pressure source (gas tank) in MPa, and t is time in ks. The gas seepage continuity equation can be written as:

$$-\nabla \cdot (\rho V) = \frac{\partial(\rho\phi)}{\partial t} \tag{A-2}$$

Here ρ is gas density in kg/m^3. V is gas seepage velocity in m/ks. ϕ is porosity. If we rewrite it into Cartesian coordinate system, we can have:

$$-\frac{\partial(\rho V_x)}{\partial x} - \frac{\partial(\rho V_y)}{\partial y} - \frac{\partial(\rho V_z)}{\partial z} = \frac{\partial(\rho\phi)}{\partial t} \tag{A-3}$$

And we also have real gas equation of state:

$$pV' = ZnRT \tag{A-4}$$

Where p is the absolute pressure of gas in MPa. V' is the gas volume in m^3. T is temperature in

Kelvin. n is the amount of substance in kmol. R is the gas factor in 0.008314 $MPa \cdot m^3/(kmol \cdot K)$. Z is compressibility factor. Combined with $n = \frac{m}{M_g}$, where m is gas mass in kg and M_g molar mass is in kg/kmol, we can calculate the density of gas as:

$$\rho = \frac{m}{V'} = \frac{M_g}{RT}\frac{p}{Z} \quad \text{A-5}$$

Assume the gas flow in the system obey Darcy's law, we have the equation of motion as:

$$V = -\frac{K}{\mu}\nabla p \quad \text{A-6}$$

Here K is permeability in D, and μ is gas viscosity in $mPa \cdot s$. If we write equation A-6 into Cartesian coordinate, we have:

$$V_x = -\frac{K}{\mu}\frac{\partial p}{\partial x} \quad \text{A-7}$$

So as in y and z direction. According to equation A-5 and A-7, assume the formation is thermostatic, we have:

$$-\frac{\partial(\rho V_x)}{\partial x} = \frac{KM_g}{RT}\frac{\partial}{\partial x}\left(\frac{p}{\mu Z}\frac{\partial p}{\partial x}\right) \quad \text{A-8}$$

Hussainy (Hussainy & Crawford, 1965[147]) defined a concept of pseudo-pressure, which is:

$$\psi = 2\int_{p_0}^{p}\frac{p}{\mu Z}dp \quad \text{A-9}$$

Here, ψ is pseudo pressure in $MPa^2/(mPa \cdot s)$, p_0 is reference pressure in MPa. Then we have:

$$d\psi = 2\frac{p}{\mu Z}dp \quad \text{A-10}$$

Combine equation A-10 and equation A-8, we have:

$$-\frac{\partial(\rho V_x)}{\partial x} = \frac{KM_g}{2RT}\frac{\partial^2\psi}{\partial x^2} \quad \text{A-11}$$

Similarly, we have equation in y and z direction, they are:

$$-\frac{\partial(\rho V_y)}{\partial y} = \frac{KM_g}{2RT}\frac{\partial^2\psi}{\partial y^2} \quad \text{A-12}$$

$$-\frac{\partial(\rho V_z)}{\partial z} = \frac{KM_g}{2RT}\frac{\partial^2\psi}{\partial z^2} \quad \text{A-13}$$

The summation of equation A-11, A-12 and A-13 is:

$$-\frac{\partial(\rho V_x)}{\partial x} - \frac{\partial(\rho V_y)}{\partial y} - \frac{\partial(\rho V_z)}{\partial z} = \frac{KM_g}{2RT}\nabla^2\psi \quad \text{A-14}$$

Combine equation A-14 and A-3, we can have:

$$\frac{KM_g}{2RT}\nabla^2\psi = \frac{\partial(\rho\phi)}{\partial t} \quad \text{A-15}$$

Since the compressibility of gas molecules is much higher than that of rock, we usually ignore the compressibility of rock when calculating, thus equation A-15 can be transformed into:

$$\frac{KM_g}{2RT}\nabla^2\psi = \phi\frac{\partial\rho}{\partial t} \quad \text{A-16}$$

Based on gas compressibility factor $c_g = \frac{d\rho}{\rho d\rho}$, according to equation A-5, we have:

$$\frac{\partial\rho}{\partial t} = \rho\frac{d\rho}{\rho d\rho}\frac{\partial p}{\partial t} = c_g\rho = c_g\frac{\mu M_g}{RT}\frac{p}{\mu Z}\frac{\partial p}{\partial t} = c_g\frac{\mu M_g}{2RT}\frac{\partial\psi}{\partial t} \quad \text{A-17}$$

Combine equation A-17 and A-16, we have:

$$\nabla^2\psi = \frac{\mu\phi c_g}{K}\frac{\partial\psi}{\partial t} \quad \text{A-18}$$

Here we define $\eta = \frac{K}{\mu\phi c_g}$, then we have:

$$\nabla^2\psi = \frac{1}{\eta}\frac{\partial\psi}{\partial t} \quad \text{A-19}$$

Equation A-19 is the real gas seepage differential equation and can be applied to any pressure condition (as long as in gas phase, not in supercritical condition).

Now let's assume that there is a gas reservoir with a constant thickness h and is homogeneous everywhere. The inner boundary is a well with constant production rate (since Valve 8 is fixed, this condition is achieved). The outer boundary is at an infinite distance. Under the initial condition, the whole system is in equilibrium. When the production begins (open Valve 7 means open outlet, and open Valve 1 or Valve 5 means open gas source), the flow in the formation is planar radial flow. A figure can illustrate the situation. The well radius is r_w, and the thickness of the reservoir is h. All parameters with subscript SC mean the ground condition (since in real reservoir, the pressure at wellhead is different from that at the well bottom).

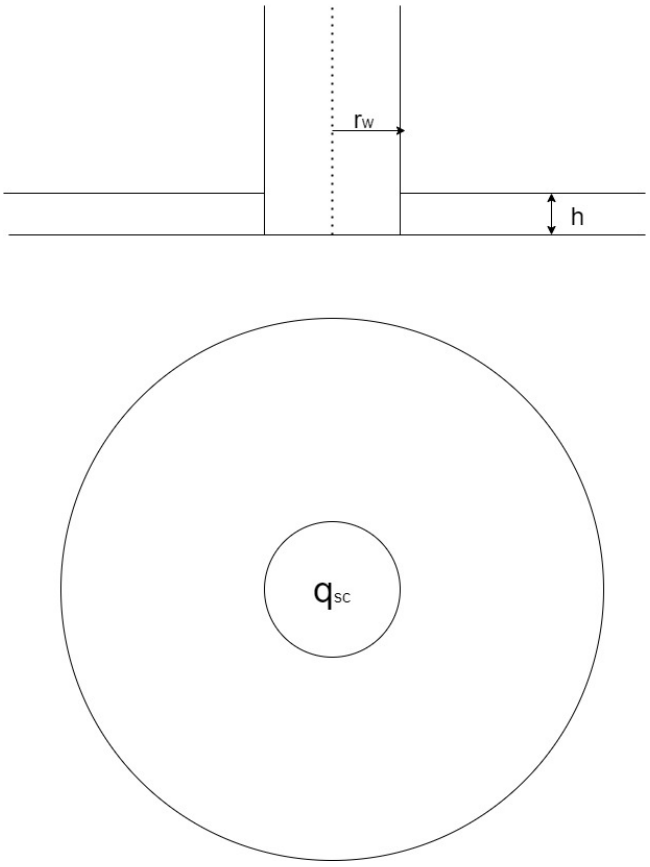

Figure 84 An Infinite Large Circular Gas Reservoir

Then we can develop the model according to equation A-19:

$$\frac{1}{r}\frac{\partial}{\partial r}\left(r\frac{\partial \psi}{\partial r}\right)=\frac{1}{\eta}\frac{\partial \psi}{\partial t}$$

$$\psi\,|r\to\infty=\psi_i$$

$$\lim_{r\to 0}\left(r\frac{\partial \psi}{\partial r}\right)=\frac{q_{sc}p_{sc}\mathrm{T}}{\pi KhT_{sc}Z_{sc}} \qquad \text{A-20}$$

$$\psi\,|t=0=\psi_i$$

Here ψ_i is the pseudo pressure at initial condition in $MPa^2/(mPa\cdot s)$, and q_{sc} is the production rate of the gas well at ground pressure. r is radius in m. Solve A-20, we can get:

$$\psi(r,t)=\psi_i-\frac{q_{sc}p_{sc}\mathrm{T}}{2\pi KhT_{sc}Z_{sc}}Ei\left(\frac{r^2}{4\eta t}\right) \qquad \text{A-21}$$

If we use logarithmic function to represent exponential integral, we will have:

$$\psi(r,t) = \psi_i - \frac{q_{sc}p_{sc}\mathrm{T}}{2\pi KhT_{sc}Z_{sc}} ln(\frac{4\eta t}{\gamma r^2}) \quad \text{A-22}$$

Where $\gamma = e^{0.57721\ldots} \approx 1.781$. Then, if we consider skin factor s, the pseudo pressure at the well bottom can be expressed as:

$$\psi_{wf} = \psi_i - \frac{q_{sc}p_{sc}\mathrm{T}}{2\pi KhT_{sc}Z_{sc}} ln(\frac{4\eta t}{\gamma r_w^2} + 2s) \quad \text{A-23}$$

Equation A-21, A-22 and A-23 are based on Darcy's flow regime. Let

$$a_t{}' = \frac{p_{sc}\mathrm{T}}{2\pi KhT_{sc}Z_{sc}} ln(\frac{4\eta t}{\gamma r_w^2} + 2s) \quad \text{A-24}$$

Then equation A-23 can be transformed into:

$$\psi_i - \psi_{wf} = a_t{}' q_{sc} \quad \text{A-25}$$

The term $a_t{}'$ is a Darcy flow term at unsteady flow regime and is a function of time.

In equation A-22, we can see the pressure at a given point in the gas well (we take the production well as an example, which corresponds to the outlet in our experiment), the pressure will decrease with the time goes by. So, in theory, there will be no steady state in this system. The pressure will decrease but in a slower mode as time goes by. If the production rate is fixed (the openness of Valve 8 is fixed), the square of bottomhole pressure has a linear relationship with the logarithm of time. When there is no core in the system, the basic theory is the same. The difference between two situations is just in no core condition, the reaching of steady state is quicklier than those situations with cores. Meanwhile, it reaches steady state (smaller slope in pressure-time figures) quicklier in larger permeability pores than in smaller pores. For the same kind of gas, if we keep the choke (Valve 8) at the same position, this means the q_{sc} should be the same, or production rate keeps the same, as long as the initial pressure are the same, and thus we can know the decreasing speed should be the same in the same core. But in different cores, or using different gases, the decreasing speed could be different. This value can be calculated based on equation A-22. But since we don't have needle valve or the mass flow controller to precisely adjust the flow rate, we have to keep the valve position the same in each experiment. Then we can present the relationship between pressure square and the natural logarithm of time:

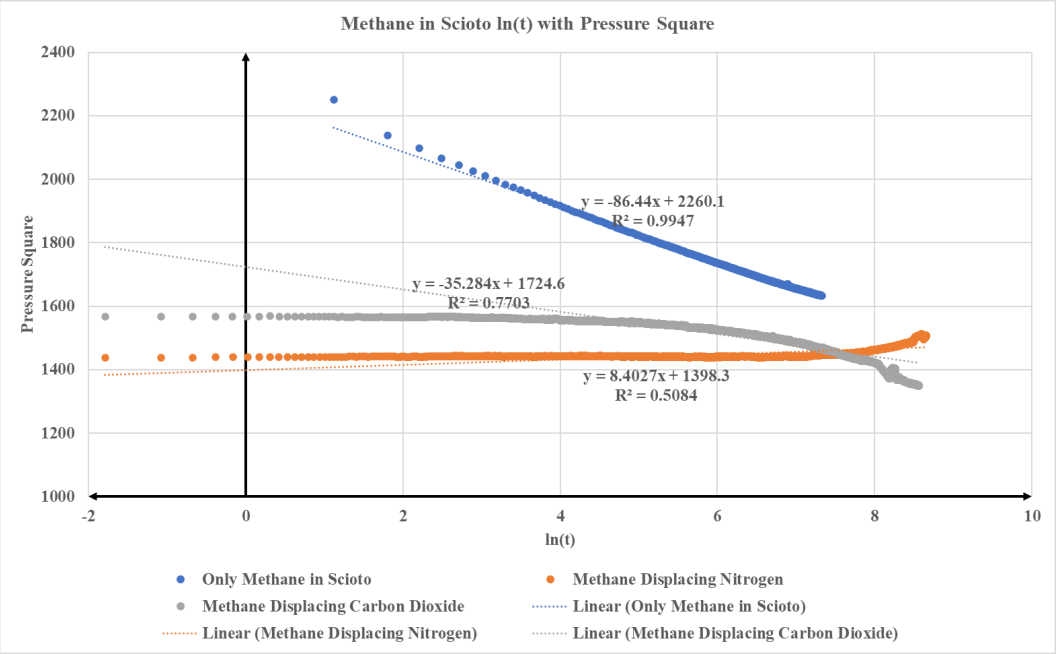

Figure 85 Methane Displacing Behavior in Scioto ln(t) with Pressure Square

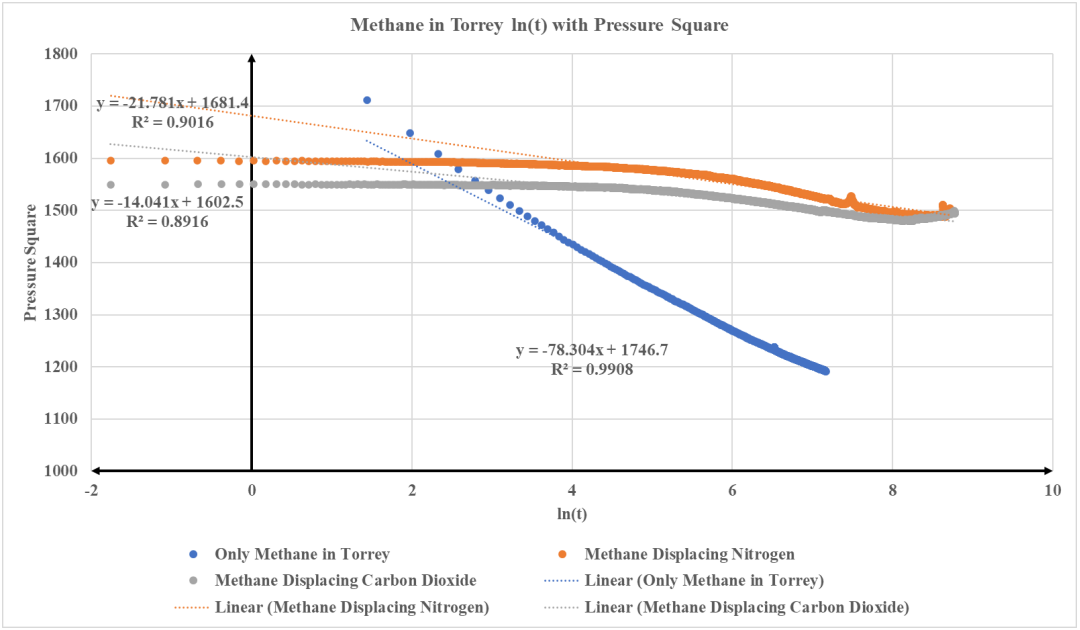

Figure 86 Methane Displacing Behavior in Torrey ln(t) with Pressure Square

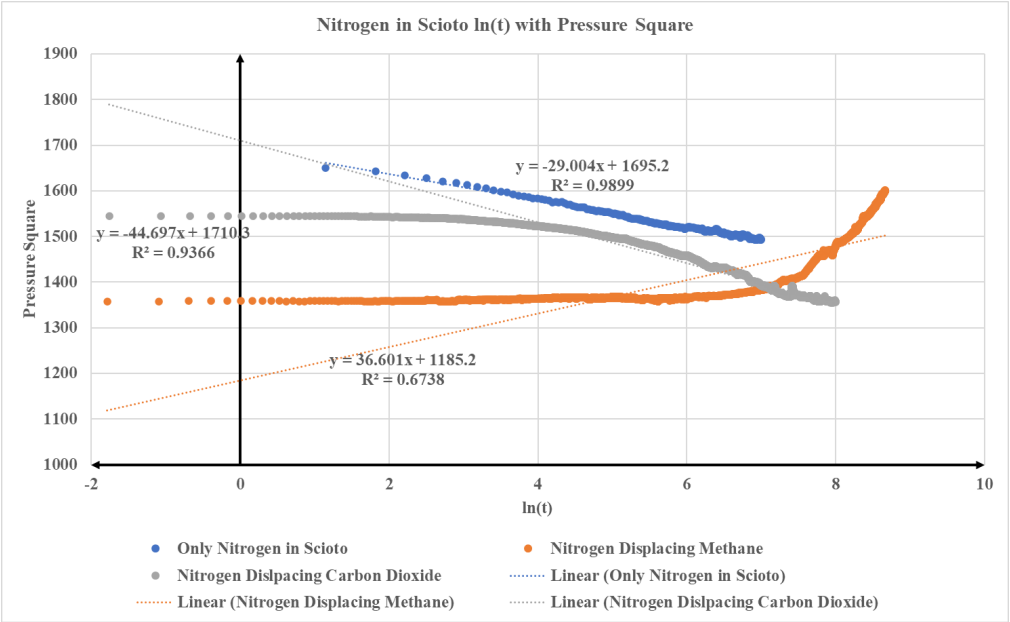

Figure 87 Nitrogen Displacing Behavior in Scioto ln(t) with Pressure Square

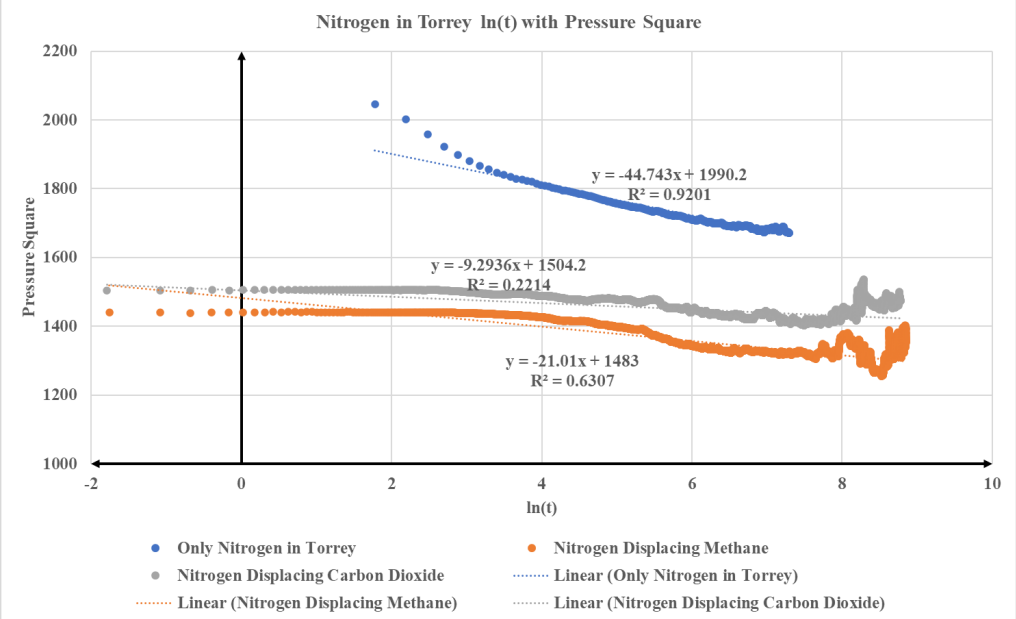

Figure 88 Nitrogen Displacing Behavior in Torrey ln(t) with Pressure Square

As we talked before, the pressure difference before we opened Valve 0 was 0 at the two sides of the core. And after Valve 0 was opened, the pressure difference was almost 0 across the whole experiment. But at the same time, the pressure is changing on the two sides. This means there is no convection and diffusion happened. If there was convection, the pressure difference cannot be zero. So, the countercurrent diffusion began from Valve 0 and moved towards the core and finally reached Compartment 2. But there is no way to know where it happens exactly. But since the pressure is not stable, diffusion should happen in this pressure changing process.

Figures 85 to 88 are the proof of the unsteady flow in the system and what happened in the countercurrent diffusion. Here we should clarify that the unit in Figure 85 to 88 is different from the unit applied in the appendix part, especially equation A-22. The pressure is in psi and the time is in minutes in the figures. If we modified the parameter in the pressure term and the time term in equation A-22, we would get the equation for the figure. But the relationship between pressure square and natural logarithm of time is still available. From the slope and the intercept, we can know the basic parameters in the flow system. And since carbon dioxide displacing behavior had a periodical behavior, we did not present the carbon dioxide displacing behavior in the figures. The linear regression result in methane groups (blue lines) are better than nitrogen groups, because we put the producing end (a plastic tube) into a beaker with water to see whether there was gas coming out in nitrogen groups, and we didn't take such measure in methane groups. But in both groups, the linear regression results show highly consistent with equation A-22. The pressure decay shown in blue lines is not avoidable if the gas is flooding in the system. This can be taken as the depletion of gas reservoir process driven by its own elastic potential energy.

If the pressure decreasing in the first 1000 minutes in Figure 33 is the same thing as those in Figure 74, both the orange and grey curves in Figures 87 and 88 should overlap with the corresponding blue line, at least the slope should be the same, according to equation A-22. But both nitrogen and methane test behavior (grey lines and orange lines) did not show a similar behavior with blue lines in the graphs. This implies something else could happen and contribute to this. The flat trend at

the beginning 54 minutes in methane groups shows the mass is conserved in the system, or the exchange rate of mass flowing in is equal to mass flowing out, which is totally different from the blue lines. In this case, we suspect that the diffusion could happen instead of unsteady flow.

For the solution of equation 1.13 (Fick's second law), the boundary condition for it at the interface of two substance is $c_A = c_{A0}$ and at infintely far is $c_A = 0$. The initial condition for substance A in substance B is $c_A = 0$. Then we can have the solution:

$$\frac{c_A}{c_{A0}} = 1 - erf\frac{z}{\sqrt{4\mathcal{D}_{AB}t}} \quad \text{A-42}$$

Here z is diffusion distance in cm and t is time in second. And its interfacial flux is:

$$N_{Az0} = c_{A0}\sqrt{\frac{\mathcal{D}_{AB}}{\pi t}} \quad \text{A-43}$$

And here $\mathcal{D}_{AB}$ is influenced by equation 1.11 and 1.12. The tortuosity of the porous media could influence the diffusion coefficient, and thus influence the equilibrium time. In the binary countercurrent diffusion experiments, after Valve 0 was opened, the gas at the two sides of the valve will contact first, but in the lines. Since the line between Valve 0 and the core holder is short and the concentration of Gas 1 at Compartment 1 is always 1, the Gas 2 on the right-hand side of Valve 0 would quickly diffuse to the other side of the valve. And then the gas at the right-hand side of the valve would be replaced by Gas 1. And then Gas 1 would touch the core. Then the diffusion coefficient would decrease due to the tortuosity of the porous media. Then Gas 1 would interact with Gas 2 in the pores. Finally reach Compartment 2. From Figure 85 to 88, we can see the pressure square behavior is not close to single gas flooding mode. Thus, we can say the system is not reaching equilibrium within the observation time.

Appendix B

In this section, we will present the temperature change in all binary gas with core experiments.

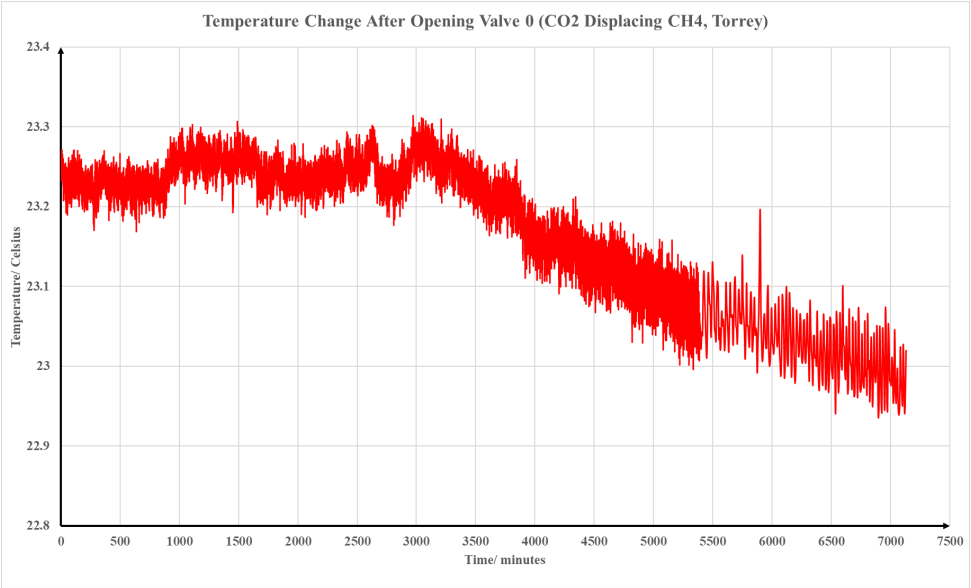

Figure 89 CO_2 Displacing CH_4 in Torrey Temperature Change

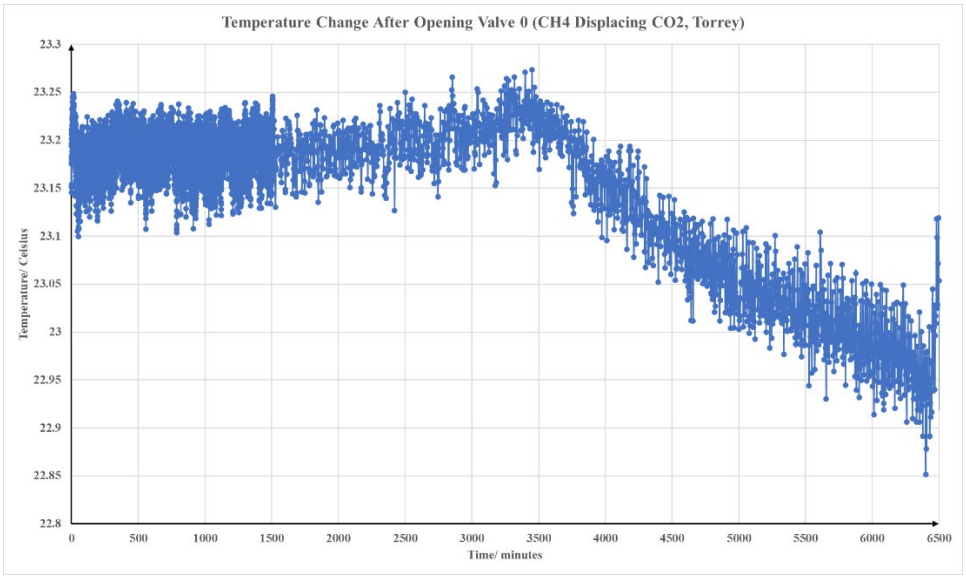

Figure 90 CH_4 Displacing CO_2 in Torrey Temperature Change

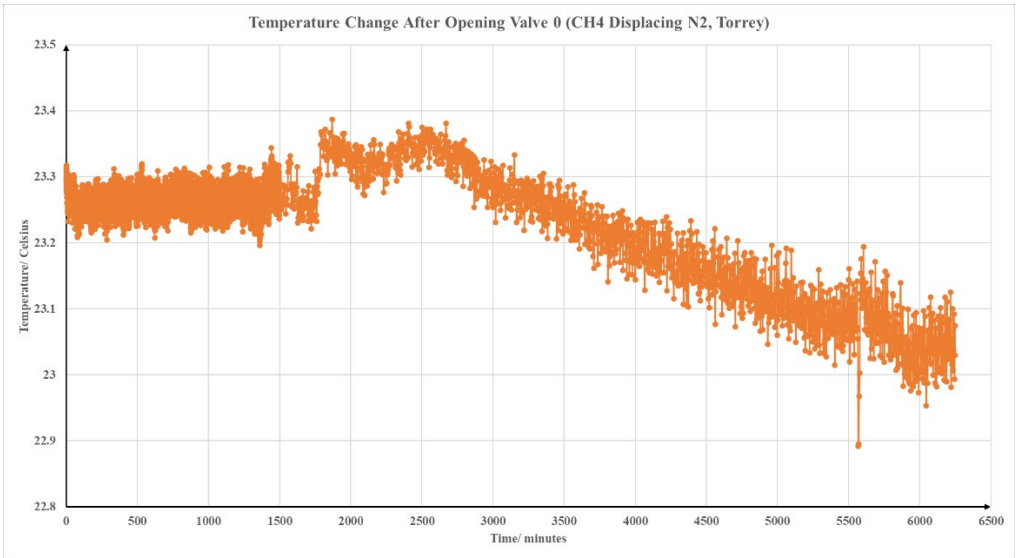

Figure 91 CH_4 Displacing N_2 in Torrey Temperature Change

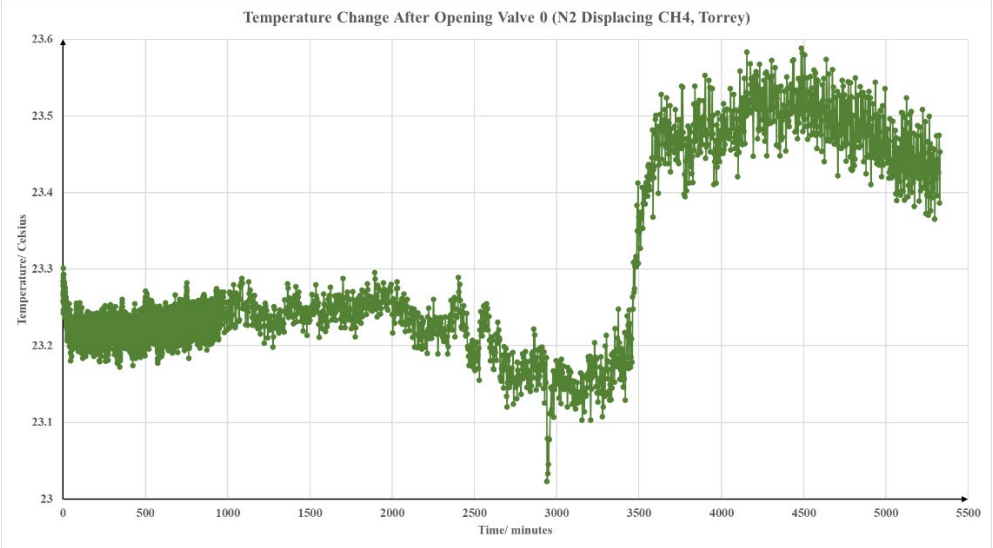

Figure 92 N_2 Displacing CH_4 in Torrey Temperature Change

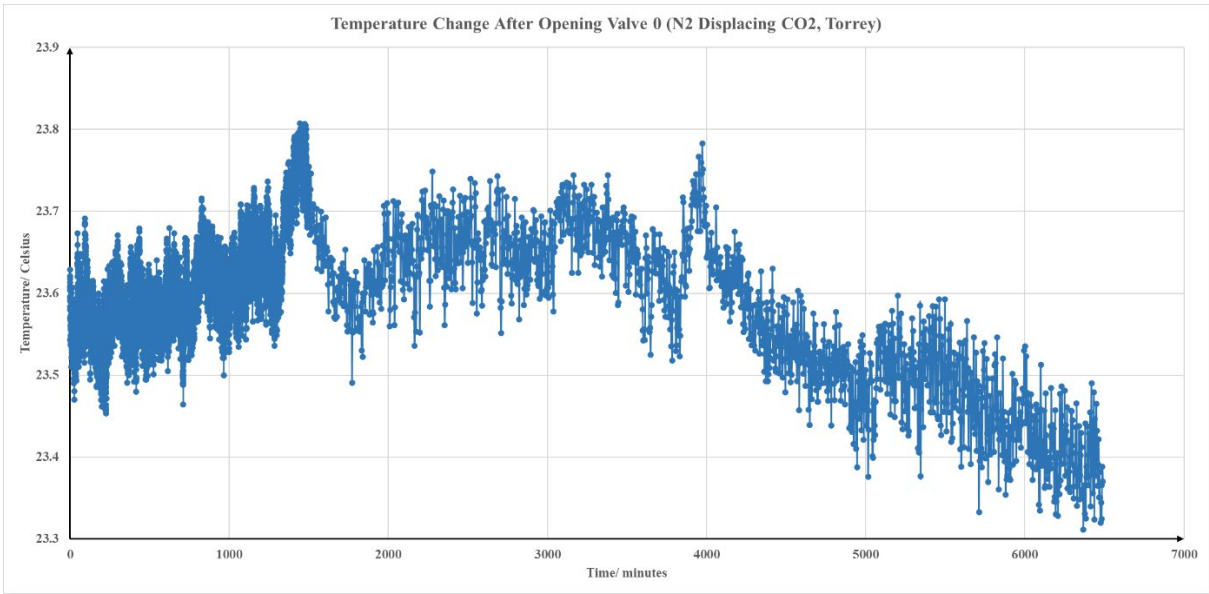

Figure 93 N_2 Displacing CO_2 in Torrey Temperature Change

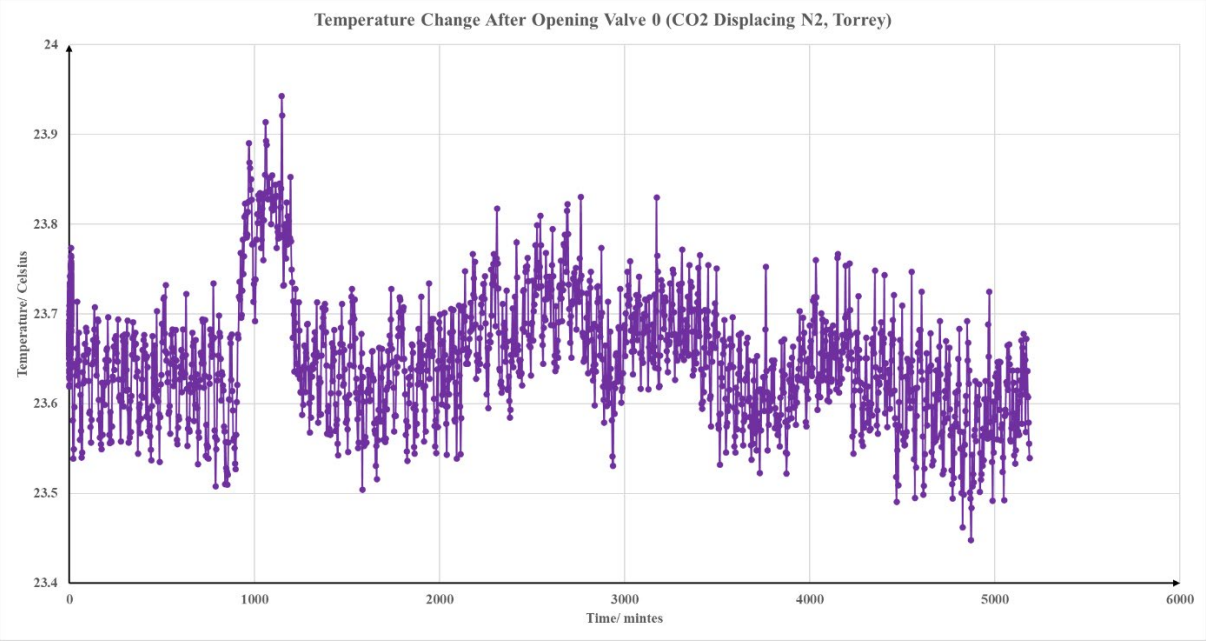

Figure 94 CO_2 Displacing N_2 in Torrey Temperature Change

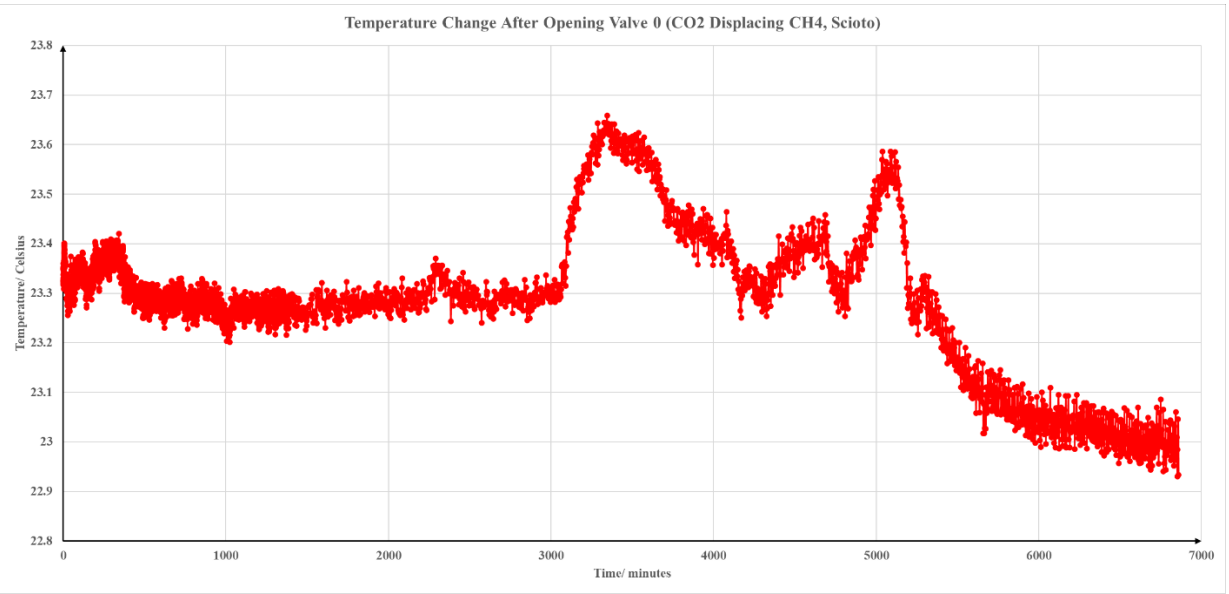

Figure 95 CO_2 Displacing CH_4 in Scioto Temperature Change

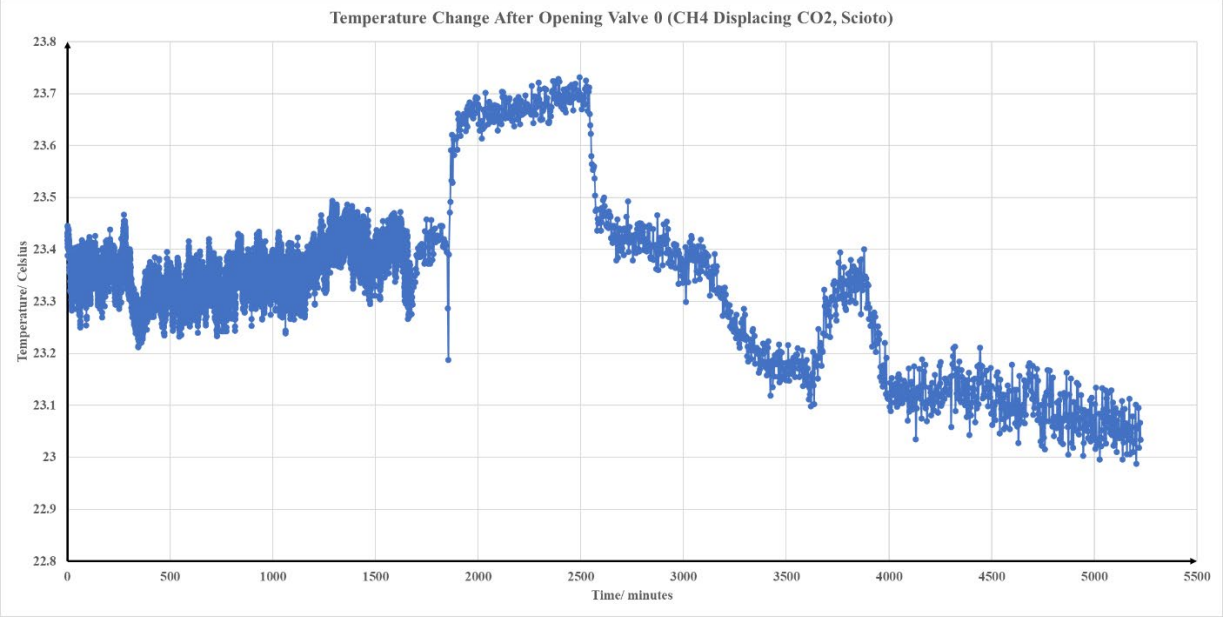

Figure 96 CH_4 Displacing CO_2 in Scioto Temperature Change

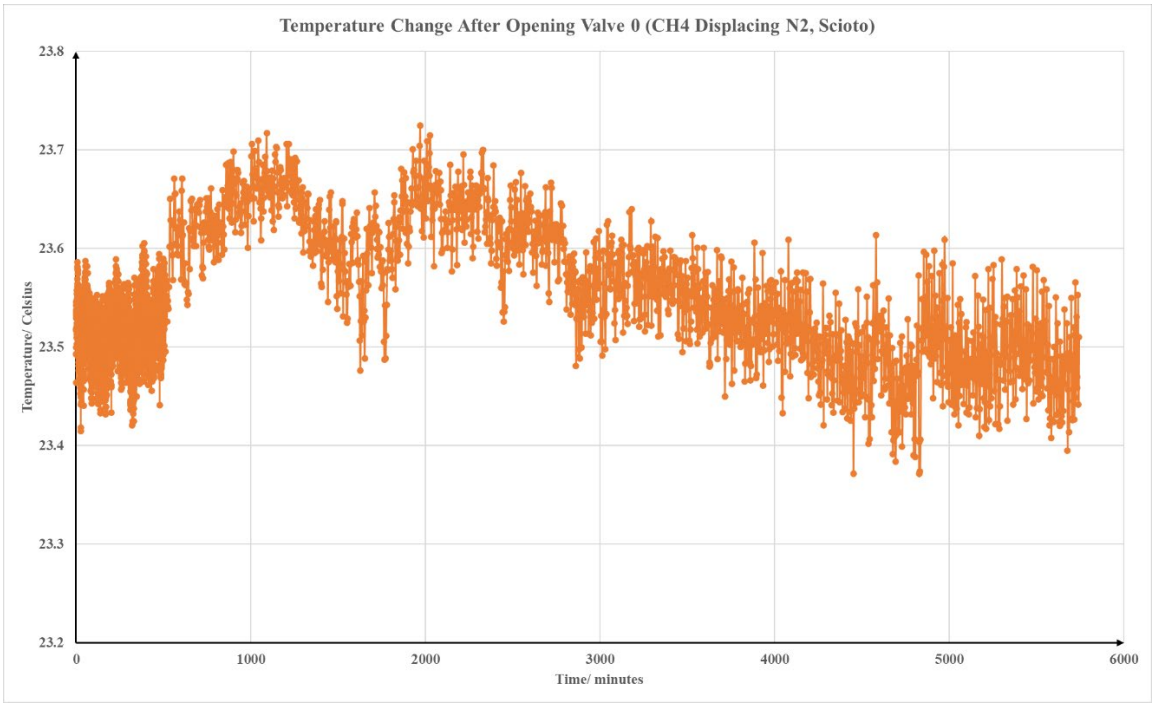

Figure 97 CH_4 Displacing N_2 in Scioto Temperature Change

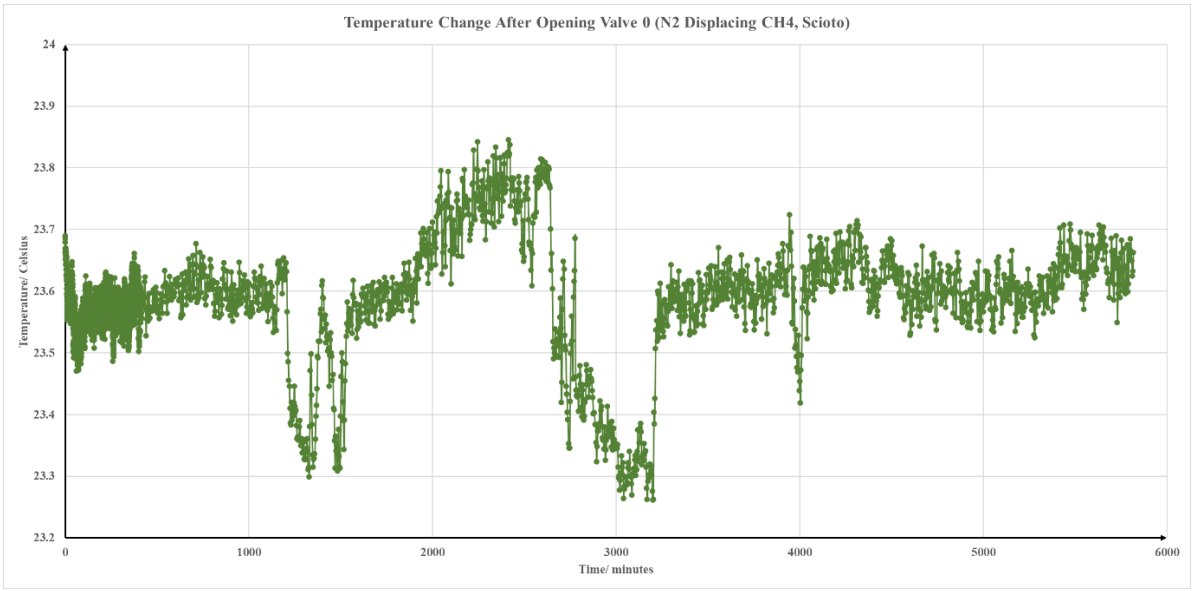

Figure 98 N_2 Displacing CH_4 in Scioto Temperature Change

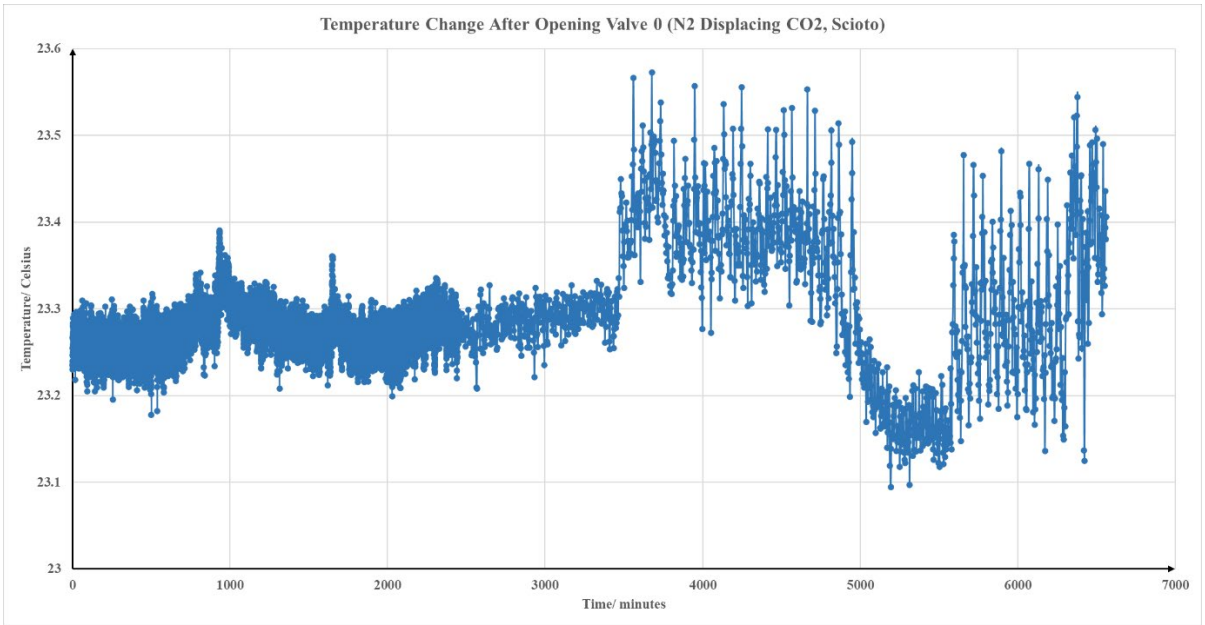

Figure 99 N_2 Displacing CO_2 in Scioto Temperature Change

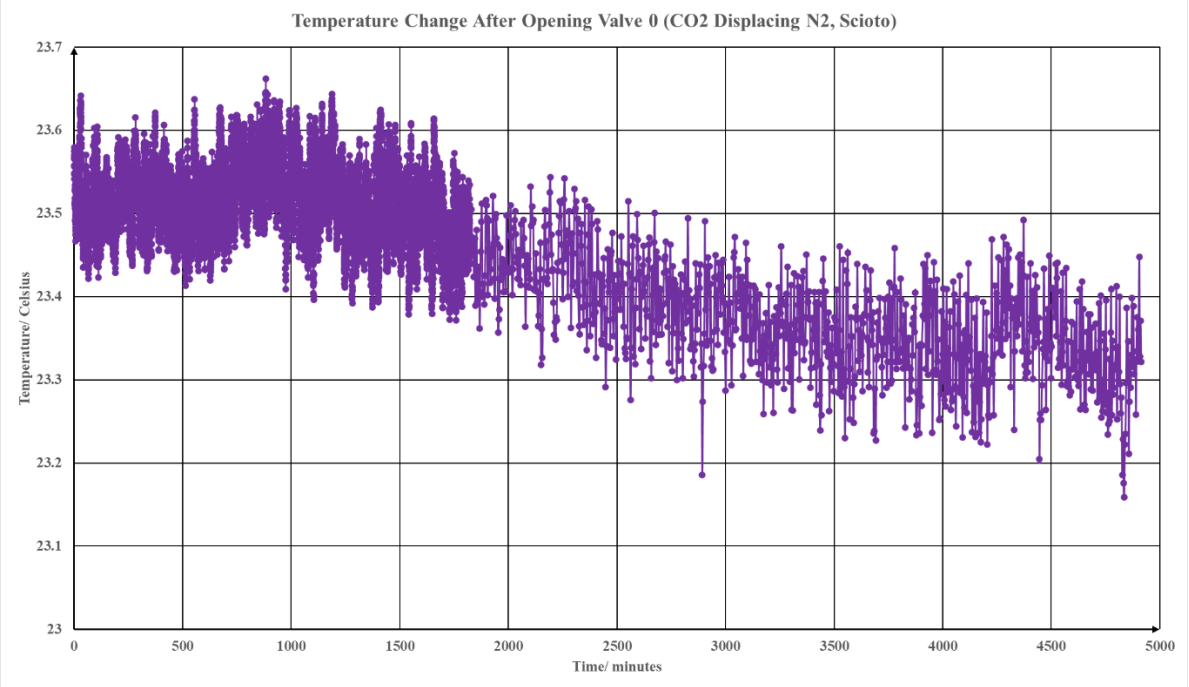

Figure 100 CO_2 Displacing N_2 in Scioto Temperature Change